The Understanding and Development of Rhodium-Catalysed Asymmetric Cross-Coupling Reactions



Lucy van Dijk

University of Oxford

A thesis submitted for the degree of

Doctor of Philosophy

2021

Declaration

This thesis describes work carried out in the Chemistry Research Laboratory, Oxford, between May 2017 and December 2020 under the supervision of Prof. Stephen Fletcher, excluding April to June 2020 when the Chemistry Research Laboratory was closed due to the COVID-19 pandemic. Research carried out at Jealott's Hill International Research Centre between June and August 2019 under the supervision of Dr. Liz Jones (Syngenta), and computational research supervised by Prof. Robert Paton (Colorado State University) is also described.

This thesis is a result of my own work, except when stated otherwise, and has not been submitted for any other degree at this or any other university.

Lucy van Dijk

Acknowledgements

I've been fortunate to have many wonderful mentors. First, I would like to thank Steve for giving me the opportunity to conduct this research, and for always being available to discuss problems, ideas or to just have a chat. I'm grateful to Rob Paton for all his support in my research and professional endeavours. I would like to thank my industrial supervisor and trusted mentor Liz Jones; I always appreciate her advice and input. I also enjoyed working with Paul Cox while at Syngenta. I'm indebted to the NMR group at Oxford, thanks to Prof. Tim Claridge, and Dr. Nader Amin. My research is funded by the EPSRC Synthesis for Biology and Medicine program, thank you to Prof. Martin Smith, Dr. Lara Lourenço Venda and all the other SBM staff and students for their support.

All the Fletcher group members, past and present, have made this journey more successful and enjoyable than it could possibly have been without them. To name just a few; Alex, Chus, Elias, Michael, Mireia, Nisha, Reece, Rob, Sedef, Sourabh, and in particular Wieland – thank you all for the valuable conversations, whether they were discussions while scribbling on a fumehood sash or laughs over a pint in the pub.

I want to thank my partner Diarmuid for his endless support through encouraging advice, a silly laugh, or a comforting hug - he always knows which is needed.

I'm extremely lucky to have sisters who double as best friends, and I am forever grateful to Sophie and Poppy. Thanks also to Poppo, and to all my family for their love and support. Although they may not understand its contents, I couldn't have produced this thesis without the lessons my parents taught me. To thank them for their unconditional love, their support and everything else, I would like to dedicate this thesis to my parents, Jan and Ingrid van Dijk.

Abstract

This thesis examines the understanding and development of Rh(I)-catalysed cross-couplings with arylboronic acids. Our group has previously developed an asymmetric Rh-catalysed Suzuki-Miyaura cross-coupling of racemic allylic halides and boronic acids. Based on a combination of experimental and computational studies, a mechanism is proposed for this highly enantioselective transformation. The first step in the catalytic cycle is irreversible transmetalation. Oxidative addition can happen *via syn*- or *anti*-pathways and, in cases where a diastereomeric starting material is used, the diastereoselectivity is set in this irreversible step. The stereochemistry of the product is set by reductive elimination from a η^3 Rh-complex formed from both allyl halide enantiomers. This study has led to a better understanding of our group's method and we believe it will contribute towards the broader understanding of Rh-allyl chemistry and of asymmetric reactions with racemic substrates in general.

Attempts to significantly expand our group's Rh-catalysed asymmetric Suzuki-Miyaura method, with a particular focus on forming quaternary stereocentres, are next presented. These involve the use of substrates with unsymmetric allyl units which introduces regioselectivity issues. Inspired by our mechanistic insights, these regioselectivity issues can be solved by employing enantioenriched substrates in a regiodivergent transformation.

In the final chapter, a regioselective Rh-catalysed hydroarylation of cyclobutenes is discussed. This carbometallation method can be used to synthesise biologically relevant cyclobutane products. Our group, and likely others, will continue to explore the potential and limitations of transition-metal catalysed cross-couplings with cyclobutenes.

Overall, this thesis examines the mechanism of Rh-catalysed asymmetric Suzuki-Miyaura transformations with racemic substrates and details the development of a Rh-catalysed regiodivergent Suzuki-Miyaura reaction along with a Rh-catalysed regioselective hydroarylation.

List of Abbreviations

APCI	atmospheric pressure chemical ionisation
approx.	approximate
aq.	aqueous
Ar	aryl
ATR	attenuated total reflection
au	atomic unit(s) (Hartree)
BBN	borabicyclo[3.3.1]nonane
BINAP	2,2’-bis(diphenylphosphino)-1,1’-binaphthyl
bis	bidentate or doubly coordinated
Bn	benzyl
Boc	*tert*-butyloxycarbonyl protecting group
br./l.	branched to linear ratio
calcd	calculated
Cbz	carboxybenzyl protecting group
cm^{-1}	inverse centimetre(s)
cod	cyclooctadiene
COSY	correlation spectroscopy
d	doublet or days (depending on context)
dba	dibenzylideneacetone
DCE	dichloroethane
dd	doublet of doublets
d.r.	diastereomeric ratio
DFB	difluorobenzene
dt	doublet of triplets
DFT	density functional theory
DMAP	4-dimethylaminopyridine
DME	dimethyl ether
DMF	dimethylformamide
DMSO	dimethyl sulfoxide
dppf	1,1'-bis(diphenylphosphino)ferrocene
DTBM	3,5-di-*tert*-butyl-4-methoxyphenyl
DyKAT	dynamic kinetic asymmetric transformation

E	energy
ECP	effective core potential
ee	enantiomeric excess
EI	electron ionisation
eq.	equivalent(s)
ESI	electrospray ionisation
Et	ethyl
eV	electronvolt(s)
Fig.	figure
g	gram(s)
GC	gas chromatography
GCMS	gas chromatography–mass spectrometry
h	hour(s)
H	enthalpy
HDMS	bis(trimethylsilyl)amine
HPLC	high-performance liquid chromatography
HRMS	high resolution mass spectrometry
HSQC	heteronuclear single quantum coherence
Hz	hertz
^{i}Pr	isopropyl
IR	infrared spectroscopy
J	coupling constant
K	kelvin or equilibrium constant (depending on context)
k	rate constant
kcal	kilocalories
KIE	kinetic isotope effect
LRMS	low resolution mass spectrometry
M	molar
m	multiplet
m	meta
Me	methyl
mg	milligram(s)
MHz	megahertz

min	minute(s)
mL	millilitre(s)
mmol	millimole(s)
mol	mole(s)
MTBE	methyl *tert*-butyl ether
^{n}Bu	butyl
nm	nanometre(s)
NMR	nuclear magnetic resonance
NOESY	nuclear overhauser effect spectroscopy
^{n}Pr	normal propyl
p	pentet (quintet)
p	para
Ph	phenyl
PhAc	acetophenone
pin	pinacol ester
PMB	*p*-methoxybenzyl
ppm	parts per million
q	quartet
qh	quasi harmonic
rot.	rotameric
r.r.	regioisomeric ratio
RRHO	rigid-rotor/harmonic-oscillator
R_t	retention time
rt	room temperature
s	singlet (NMR) or strong (IR) (depending on context)
S	entropy
sec	seconds
SegPhos	4,4’-Bi-1,3-benzodioxole-5,5’-diylbis(diphenylphosphane)
SFC	supercritical fluid chromatography
t	triplet
^{t}Bu	*tert*-butyl
td	triplet of doublets
Tf	triflyl

THF	tetrahydrofuran
TMB	trimethoxybenzene
TMS	tetramethylsilane
TOF	time-of-flight
Tol	tolyl
TS	transition structure
Ts	tosyl
UPC^2	ultra-performance convergence chromatography
UV	ultra-violet
w	weak
wt.	weight
w/w	weight by weight
xylyl	3,5-dimethylphenyl
ZPE	zero-point energy
δ	chemical shift
σ	Hammett substituent constant
ν	wavenumber
°C	degrees Celsius
ΔG	free energy difference
$\Delta G^{\ddagger}$	activation energy
$\Delta\Delta G^{\ddagger}$	difference in energy between two TS
µL	microliters
λ_{max}	maximum wavelength

Table of Contents

CHAPTER 1: AN INTRODUCTION TO CATALYTIC ASYMMETRIC SUZUKI-MIYAURA CROSS-COUPLINGS 1

1. The Importance of the Suzuki-Miyaura Coupling 1

2. Palladium-Catalysed Asymmetric Suzuki-Miyaura Couplings 2
2.1 Palladium-Catalysed Asymmetric Csp^2-Csp^2 Suzuki-Miyaura Couplings 2
2.2 Palladium-Catalysed Asymmetric Csp^2-Csp^3 Suzuki-Miyaura Couplings 6
2.3 Palladium-Catalysed Asymmetric Csp^3-Csp^3 Suzuki-Miyaura Couplings 8

3. Nickel-Catalysed Asymmetric Suzuki-Miyaura Couplings 9
3.1 Nickel-Catalysed Asymmetric Csp^2-Csp^3 Suzuki-Miyaura Couplings 9
3.2 Nickel-Catalysed Asymmetric Csp^3-Csp^3 Suzuki-Miyaura Couplings 11
3.3 Photoredox Dual Catalysis in Asymmetric Suzuki-Miyaura Couplings 12

4. Rhodium-Catalysed Asymmetric Suzuki-Miyaura Couplings 12
4.1 Rhodium-Catalysed Asymmetric Suzuki-Miyaura Couplings with Non-Chiral Substrates 12
4.2 Rhodium-Catalysed Asymmetric Suzuki-Miyaura Couplings with Racemic Substrates 14

5. Other Transition Metal-Catalysed Asymmetric Suzuki-Miyaura Couplings 17
5.1 Iridium-Catalysed Asymmetric Suzuki-Miyaura Couplings 17
5.2 Copper-Catalysed Asymmetric Suzuki-Miyaura Couplings 18
5.3 Iron-Catalysed Asymmetric Suzuki-Miyaura Couplings 19
5.4 Cobalt-Catalysed Asymmetric Suzuki-Miyaura Couplings 20

6. Conclusions and Thesis Outline 21

CHAPTER 2: A MECHANISTIC INVESTIGATION OF RHODIUM-CATALYSED ASYMMETRIC SUZUKI-MIYAURA COUPLINGS WITH RACEMIC ALLYL HALIDES 23

1. Introduction 23
1.1 Mechanism of Rh-catalysed Asymmetric Additions 23
1.2 Mechanism of Asymmetric Allylic Addition Reactions with Racemic Substrates 24
1.3 Project Aim 26

2. Results and Discussion 30
2.1 Understanding the Active Catalytic Species 30
2.2 Eliminating Some Mechanistic Proposals 31
2.3 Natural Abundance ^{13}C Kinetic Isotope Effects 32
2.4 Transmetalation 36
2.5 DFT Calculations 39
2.6 Reaction Kinetics 42
2.7 Arylation with Heterocyclic Allyl Chlorides 50
2.8 Arylation with Diastereomeric Allyl Chlorides 56

3. Conclusions 58

CHAPTER 3: RHODIUM-CATALYSED REGIODIVERGENT SUZUKI-MIYAURA COUPLINGS TO FORM QUATERNARY STEREOCENTRES 61

1. Introduction 61
1.1 Quaternary Stereocentres 61
1.2 Preparation of Asymmetric Quaternary Stereocentres in Cyclic Molecules 62
1.3 Project's Initial Aims 64

2. Results and Discussion, Part I **66**
2.1 Preliminary Investigation of Rh-Catalysed Asymmetric Arylation to form Quaternary Stereocentres 66
2.2 Asymmetric Allylic Arylation of 'Pseudo-Symmetrical' Disubstituted Substrates 67
2.3 Understanding the Stability of Allyl Halides 68
2.4 Selection of a Suitable Model Substrate 69
2.5 Optimisation of the Rh-Catalysed Asymmetric Arylation with a Racemic Substrate 73
2.6 Scope of the Rh-Catalysed Asymmetric Arylation with a Racemic Substrate 78
2.7 Considering the Mechanism of this Rh-Catalysed Asymmetric Arylation 78

3. Results and Discussion, Part II **80**
3.1 Regiodivergent Reactions with Enantioenriched Substrates 80
3.2 Preparation of Enantioenriched Allylic Substrates 81
3.3 Preliminary Results for the Rh-Catalysed arylation of Enantioenriched Allylic Substrates 82

4. Conclusions **85**

5. Future Directions **86**
5.1 Regiodivergent Reactions on Racemic Mixtures 86
5.2 Regiodivergent Reactions with Enantiopure Substrates 87
5.3 Rh-Catalysed Suzuki-Miyaura Cross-Coupling in Natural Product Synthesis 89
5.4 Rh-Catalysed Suzuki-Miyaura Cross-Coupling with Acyclic Substrates 90

CHAPTER 4: REGIOSELECTIVE SYNTHESIS OF CYCLOBUTANES *VIA* RHODIUM CATALYSED CARBOMETALLATION 93

1. Introduction **93**
1.1 The Importance of Cyclobutanes 93
1.2 Synthesis of Cyclobutanes 94
1.3 Enantioselective Synthesis of Cyclobutanes *via* Rhodium Catalysed Carbometallation 95
1.4 Project Aim 99

2. Results and Discussion **100**
2.1 Spirocyclic Cyclobutene Synthesis 100
2.2 Optimisation of the Hydroarylation of Spirocyclic Cyclobutenes 100
2.3 Scope of the Hydroarylation of Spirocyclic Cyclobutenes 103
2.4 Application to the Target Synthesis of a Biologically Active Cyclobutane 105
2.5 Mechanism of the Hydroarylation of Spirocyclic Cylobutenes 106

3. Conclusions **108**

4. Future Directions **108**

SUPPLEMENTARY INFORMATION 111

1. Instrumentation, Methods and Materials **111**

2. Supplementary Information for Chapter 2 **114**
2.1 Preliminary NMR Spectroscopic Experiments 114
2.2 Preliminary Mechanistic Experiments 117
2.3 Transmetalation Competition Experiments 119
2.4 ^{13}C Kinetic Isotope Effect 121
2.5 Reaction Kinetics 124
2.6 Arylation with Heterocyclic Allyl Chlorides 141
2.7 General Information on Computational Methods 151
2.8 Computed Kinetic Isotope Effects 151
2.9 Energies of Optimised Structures 153

3. Supplementary Information for Chapter 3 **157**

3.1 Synthesis of Allylic Alcohols 157
3.2 Synthesis of Allylic Substrates 168
3.3 Rhodium-Catalysed Allylic Arylation with Arylboronic Acids 177
3.4 Computational Details 186

4. Supplementary Information for Chapter 4 **189**
4.1 Cyclobutene Starting Materials Synthesis 189
4.2 Cyclobutane Synthesis *via* Rh-Catalysed Hydroarylation 193
4.3 Deuterium Labelling Study 211

REFERENCES 212

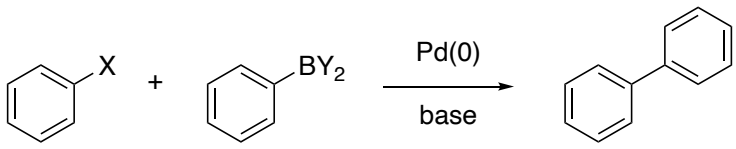
Chapter 1: An Introduction to Catalytic Asymmetric Suzuki-Miyaura Cross-Couplings

This chapter is based around the following publications;

- F. W. Goetzke, L. van Dijk, S. P. Fletcher, Catalytic Asymmetric Suzuki-Miyaura Coupling Reactions. in *Organoboron Compounds*, I. Marek, Ed. *Wiley: Chichester* (2019).
- J. González, L. van Dijk, F. W. Goetzke, S. P. Fletcher, Highly Enantioselective Rhodium-Catalyzed Cross-Coupling of Boronic Acids and Racemic Allyl Halides*. Nat. Protoc.,* 14, 2972, (2019).

1. The Importance of the Suzuki-Miyaura Coupling

The Suzuki-Miyaura Csp^2-Csp^2 transition metal catalysed cross-coupling between arylboronic acids and aryl halides is widely used across industry and academia (Scheme 1).[1] This robust C-C bond forming method displays predictable chemoselectivity, high functional group tolerance and uses reagents which are often commercially available and easy to handle. These desirable features enable its use in the rapid parallel synthesis of compounds in automated array formats.[2] Arylboronic acids are particularly attractive reagents as they are generally air stable, and readily available.[3] The Suzuki-Miyaura cross-coupling is one of the most powerful organic synthetic C-C bond forming methods and its significant impact has been recognised by the Nobel committee.[4]



X = halide or pseudohalide
Y = OH, alkoxyl or alkyl

Scheme 1. The Suzuki-Miyaura cross-coupling.

However, the widespread use of the Suzuki-Miyaura Csp^2-Csp^2 cross-coupling has led to an over-representation of flat, biaryl molecules in drug discovery programmes.[5] It has been

shown that candidates with increased saturation and a greater numbers of chiral carbon centres have a higher probability of success in drug discovery.[6,7] In order to enable the investigation of these desirable three-dimensional scaffolds, asymmetric variants of the Suzuki-Miyaura transition metal catalysed cross-coupling between boronic nucleophiles and pseudo halides coupling partners have been developed to enantioselectively synthesise chiral molecules.[8] Stereospecific transition metal catalysed Suzuki-Miyaura cross-couplings are also commonly employed to generate enantioenriched stereogenic centres,[9,10] but in this chapter, we will focus on enantioselective transition metal catalysed Suzuki-Miyaura cross-couplings.

2. Palladium-Catalysed Asymmetric Suzuki-Miyaura Couplings

2.1 Palladium-Catalysed Asymmetric Csp^2-Csp^2 Suzuki-Miyaura Couplings

The first asymmetric variants of the Suzuki-Miyaura reaction developed were Pd-catalysed Csp^2-Csp^2 cross-couplings to form axially chiral biaryl products. Atropisomers are stereoisomers that are conformationally restricted by a high barrier to rotation and can display axial chirality. This structural motif is found in natural products and is also essential in organic synthetic chemistry, as it is the origin of chirality in many privileged chiral ligand classes which are routinely used in asymmetric reactions (Fig. 1).

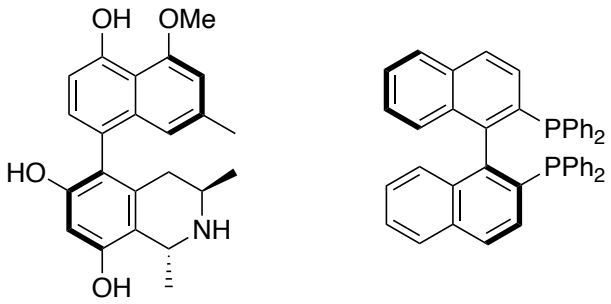


Figure 1. Atropisomers displaying axial chirality. Natural product Korupensamine A and privileged ligand BINAP.

The groups of Buchwald and Cammidge independently developed the first asymmetric variants of the Suzuki-Miyaura coupling to form axially chiral products (Fig. 2).[11,12] Cammidge developed a Pd-catalysed coupling of aryl halides and arylboronates to enantioselectively

synthesise binaphthalene-derived products (Fig. 2a).[11] Buchwald's coupling of aryl bromides and boronic acids allowed for the use of phosphonate in the ortho position of the aryl halide which enables the synthesis of new axially chiral ligands (Fig. 2b).[12]

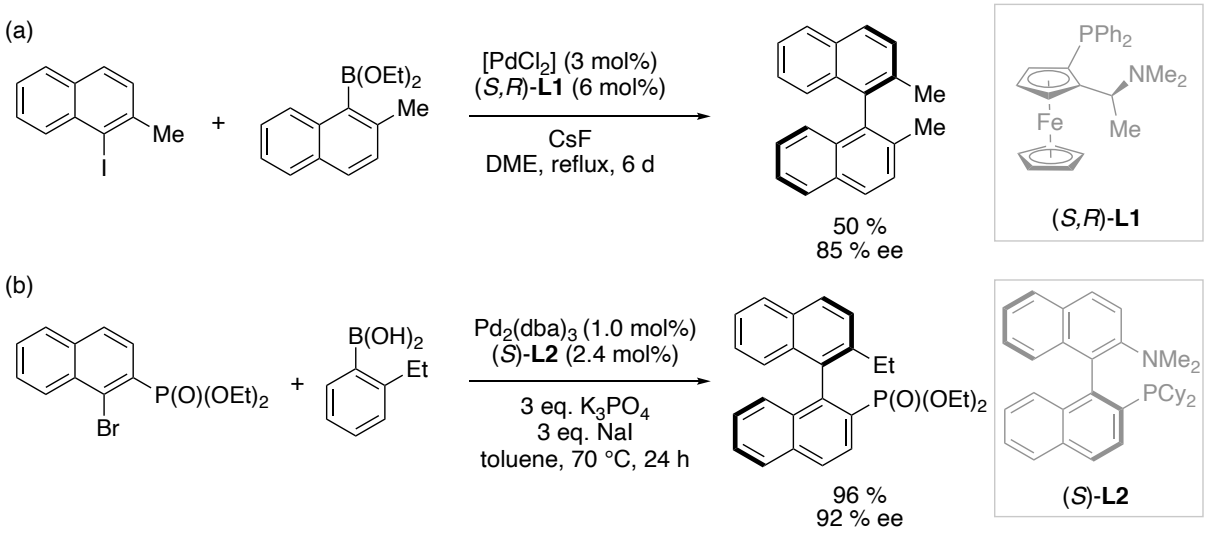


Figure 2. (a) Cammidge[11] and (b) Buchwald's[12] seminal publications on asymmetric Suzuki-Miyaura cross-coupling transformations.

Over the last 20 years, these Pd-catalysed asymmetric Csp^2-Csp^2 Suzuki-Miyaura cross-couplings to form axially chiral biaryl products have been further developed, with many different chiral ligands and aryl coupling partners employed.[13] Their application has been demonstrated in the total synthesis of atropisomeric natural products, including the synthesis of Korupensamine A (shown in Fig. 1),[14] and in the synthesis of axially chiral biaryl ligands.[15] The generally accepted mechanism of these reactions involves oxidative addition of the halide or pseudo-halide species to yield an Pd-aryl complex which then undergoes transmetalation with the arylboronic coupling partner (Fig. 3).[16] Subsequent enantiodetermining reductive elimination releases the atropisomeric product.[17]

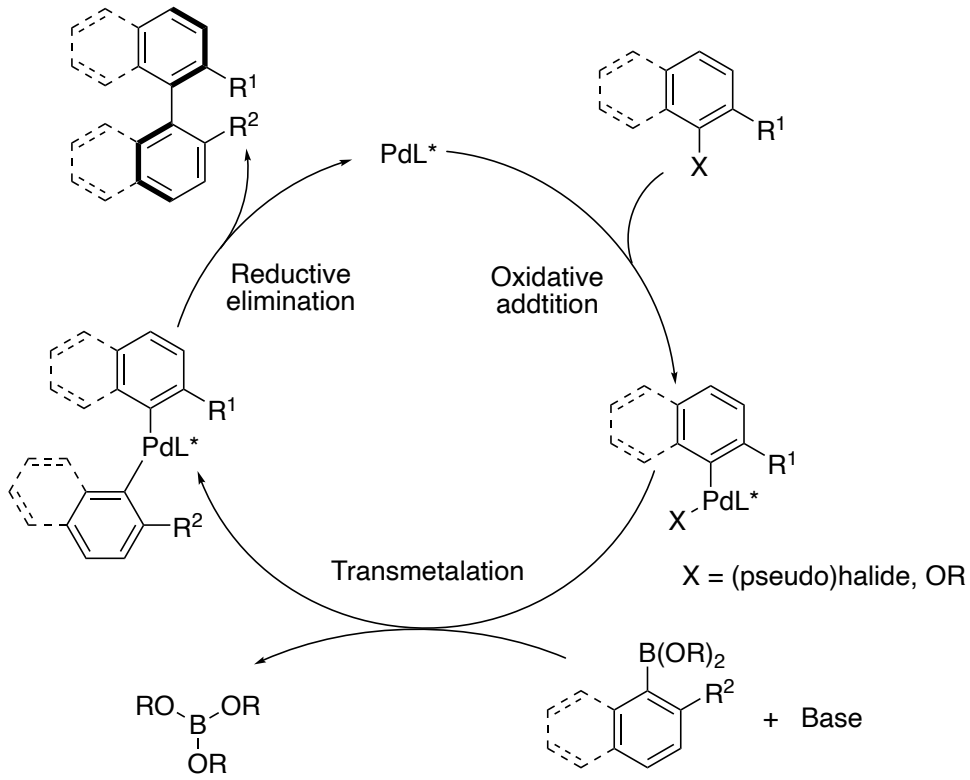


Figure 3. Catalytic cycle for Pd-catalysed asymmetric Csp^2-Csp^2 Suzuki-Miyaura cross-coupling.

Pd-catalysed asymmetric Csp^2-Csp^2 Suzuki-Miyaura cross-couplings which operate *via* dynamic kinetic asymmetric transformations (DyKATs) have also been developed. DyKATs enable the use of racemic cross-coupling partners and both enantiomers of the racemate are converted into an enantioenriched product. This generally occurs *via* one of the two general mechanistic paradigms shown in Fig. 4.[18] Diastereomeric intermediates can be formed from each enantiomer of the starting material, which can interconvert (Fig. 4a) and one intermediate reacts faster than the other to give the major enantiomer of the product. Alternatively, the two enantiomers of the starting material form a common intermediate after reaction with the catalyst and the stereochemistry of the product is set in the subsequent reaction (Fig. 4b).

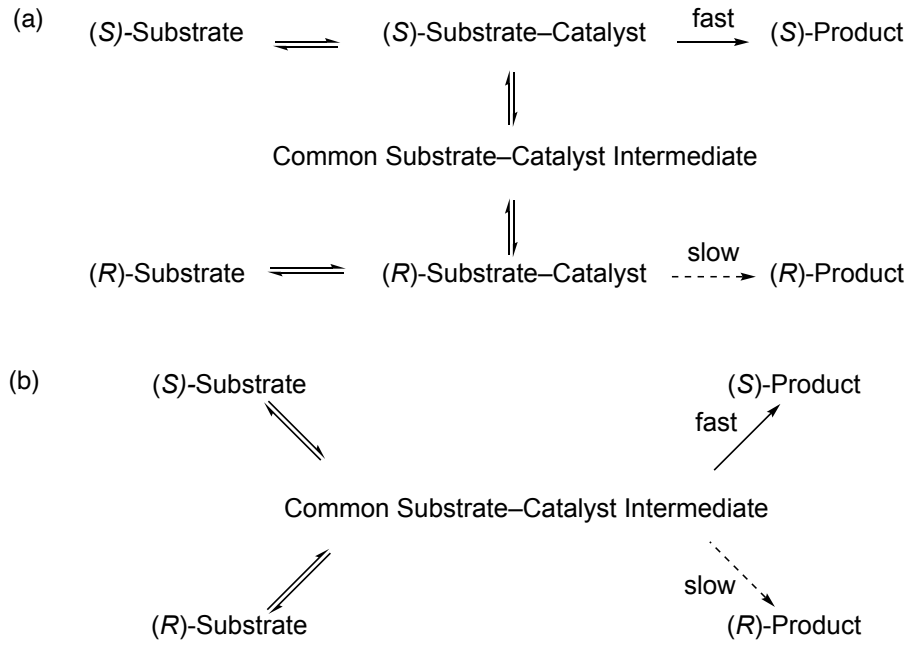


Figure 4. Schematic representation of (a) type 1 DyKAT and (b) type 2 DyKAT.

Lassaletta and co-workers have reported a Pd-catalysed DyKAT employing racemic aryl triflate coupling partners (Fig. 5).[19] The palladacycle intermediate formed after oxidative addition of both enantiomers of the starting material is configurationally liable, which is the key factor enabling this DyKAT. Reductive elimination results in the enantioenriched axially chiral product.

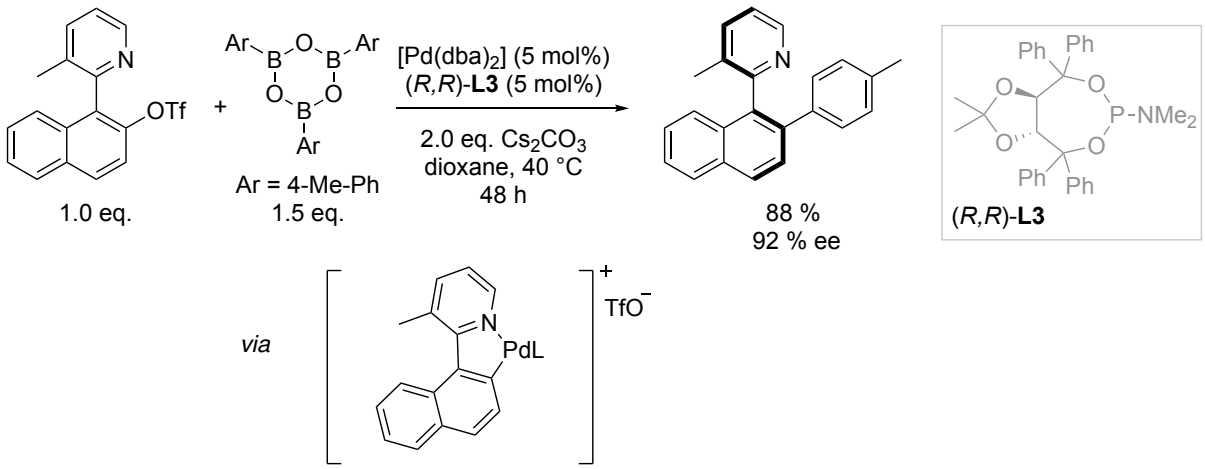
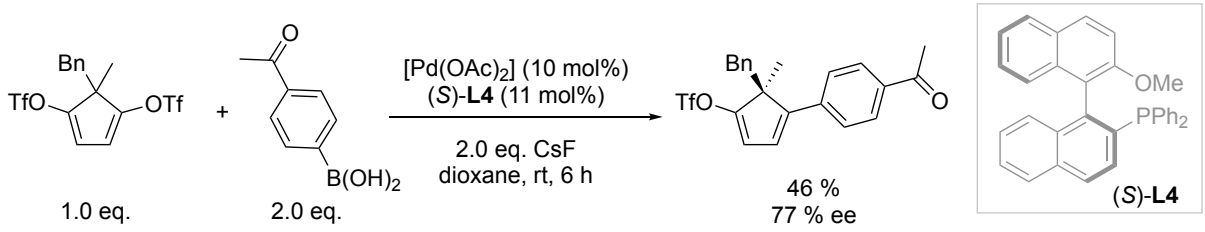


Figure 5. Pd-catalysed asymmetric Csp^2-Csp^2 cross-coupling which operates *via* a DyKAT mechanism.[19]

In an alternative Pd-catalysed asymmetric Csp^2-Csp^2 Suzuki-Miyaura cross-coupling strategy, *meso*-compounds can be exploited through desymmetrisation to access chiral molecules. For example, Willis *et. al.* reported the Pd-catalysed desymmetrisation of bistriflate *meso*-

compounds to reveal a point chiral quaternary stereocentre in the biaryl product (Scheme 2).[20]



Scheme 2. Pd-catalysed asymmetric Csp^2-Csp^2 cross-coupling which operates *via* desymmetrisation.[20]

2.2 Palladium-Catalysed Asymmetric Csp^2-Csp^3 Suzuki-Miyaura Couplings

As previously mentioned, small molecules with increased saturation have a higher probability of success in drug discovery.[6,7] Therefore, the asymmetric synthesis of Csp^3 hybridised chiral centres is highly desirable to selectively access these scaffolds. This can be achieved using catalytic asymmetric Suzuki-Miyaura cross-couplings employing Csp^3 hybridised nucleophiles or electrophiles. The use of Csp^3 hybridised coupling partners introduces additional challenges such as facile β-hydride elimination.[21]

We have seen that Pd can catalyse Csp^2-Csp^2 cross-couplings to form chiral biaryl products, but it can also catalyse the formation of Csp^3 stereocentres *via* asymmetric Suzuki-Miyaura cross-couplings. This has been demonstrated by Miyaura and co-workers in their enantioselective cross-coupling of aryl and vinyl bromides with Csp^3 hybridised allyl potassiumtrifluoroborates where they achieved good branched to linear selectivity in the acyclic products (Fig. 6a).[22] Subsequently, a mechanistic study showed rate-determining transmetalation is followed by fast reductive elimination, with no indication of isomerisation of the Pd-complex occurring prior to reductive elimination.[23] However, Morken and co-workers later developed an intramolecular variant of this aryl-allyl cross-coupling transformation (Fig. 6b) where they propose rapid Pd-allyl isomerisation prior to the enantiodetermining reductive elimination.[24]

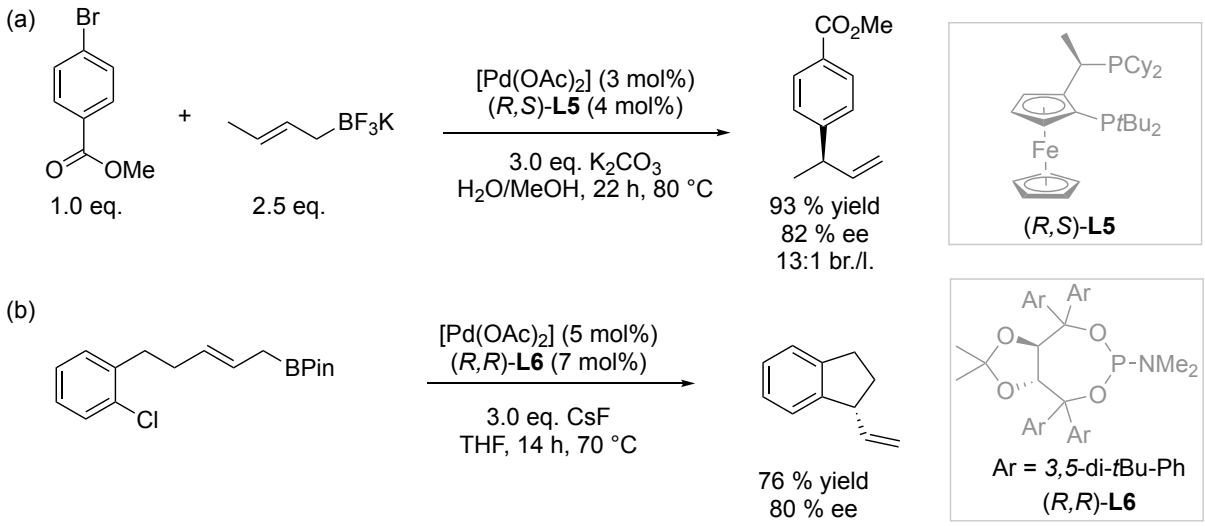


Figure 6. Pd-catalysed asymmetric Csp^2-Csp^3 cross-coupling (a) developed by Miyaura and co-workers.[22] (b) intramolecular variant developed by Morken and co-workers.[24]

Morken and co-workers have also developed Pd-catalysed cross-coupling methods for the desymmetrisation of 1,1-diborylalkanes to generate asymmetric boronate-substituted Csp^3 stereocentres. In the proposed mechanism, the transmetalation of one of the two enantiotopic boronate substituents is stereodetermining (Fig. 7a).[25] Along with aryl halides, vinyl bromide electrophilic coupling partners can also be employed in this transformation.[26] Boronates are useful synthetic handles for further functionalisation, as demonstrated by the synthesis of (*R*)-tolterodine and natural product arenolide (Fig. 7b).[25,27]

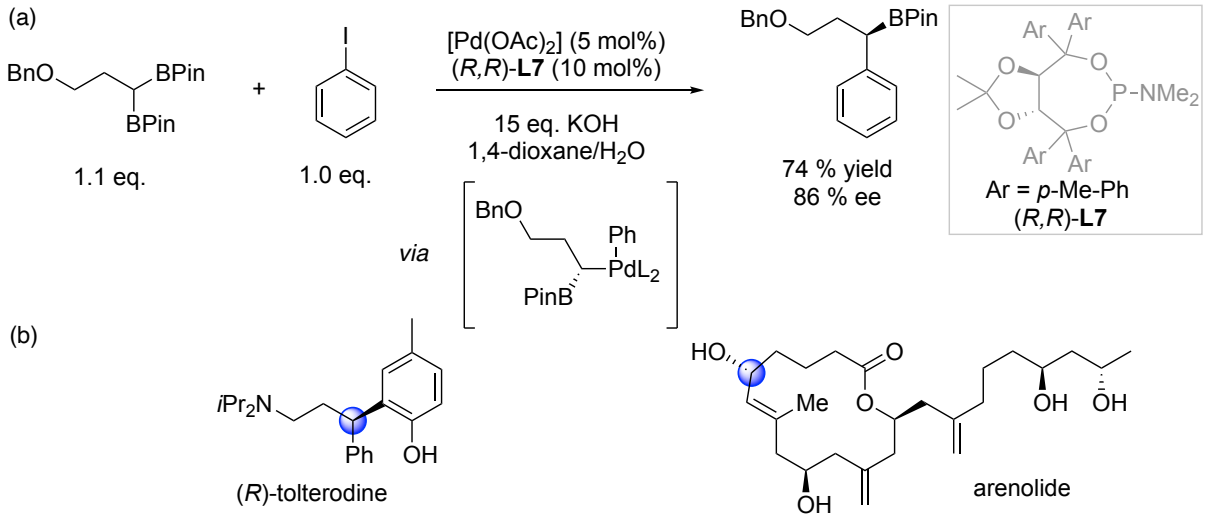


Figure 7. (a) Morken and co-worker's Pd-catalysed enantiotopic-group-selective coupling used in the total synthesis of (*R*)-tolterodine.[25] (b) structure of drug (*R*)-tolterodine[25] and natural product arenolide.[25,27]

Tang and co-workers recently reported the cross-coupling of racemic α-bromo carboxamides with arylboronic acids (Fig. 8).[28,29] Using a sterically hindered ligand (**L8**) is key to preventing a second transmetalation event which would lead to the undesired homocoupled aryl-aryl product. This method was applied to the asymmetric synthesis of the dopamine receptor agonist (*R*)-SKF 38393 (Fig. 8).

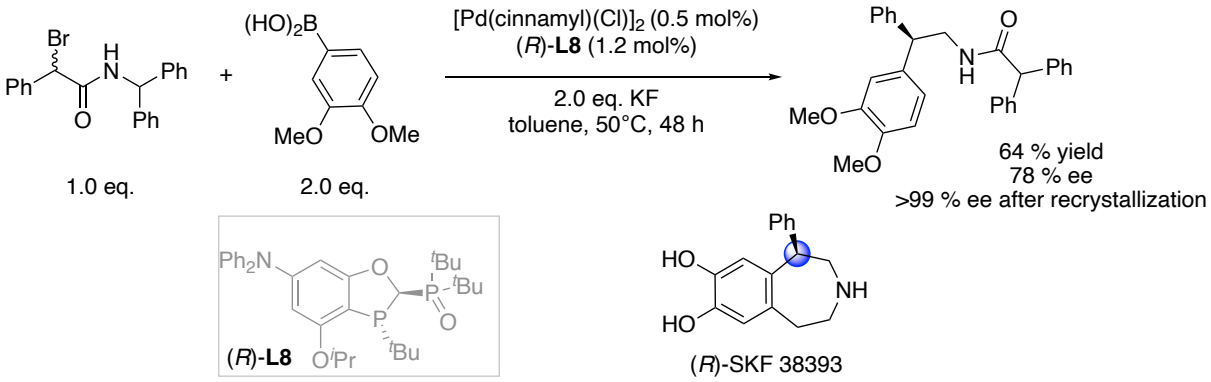


Figure 8. Tang and co-worker's Pd-catalysed asymmetric synthesis of α-aryl carboxamides.[29]

2.3 Palladium-Catalysed Asymmetric Csp^3-Csp^3 Suzuki-Miyaura Couplings

Along with Csp^2-Csp^3 cross-coupling protocols, Morken and co-workers have also reported Pd-catalysed asymmetric Csp^3-Csp^3 Suzuki-Miyaura cross-couplings. Here, allylboronic acid pinacol esters are coupled with allylic carbonates to enantioselectively generate chiral products (Fig. 9a).[30] Branched or linear allyl carbonates can be employed suggesting a common π-allyl Pd intermediate is generated from oxidative addition of the both enantiomers of racemic branched electrophiles. Subsequent transmetalation of the allylboronic coupling partner generates a bis-π-allyl-Pd complex which undergoes reductive elimination to yield the product. This method has been extended to enable the construction of quaternary stereocentres (Fig. 9b).[31] Here, the use of caesium fluoride is essential to avoid the formation of a 1,3-diene *via* elimination of the allyl carbonate. The utility of this method is demonstrated in the concise synthesis of natural product (*R*)-cuparenone (Fig. 9b).

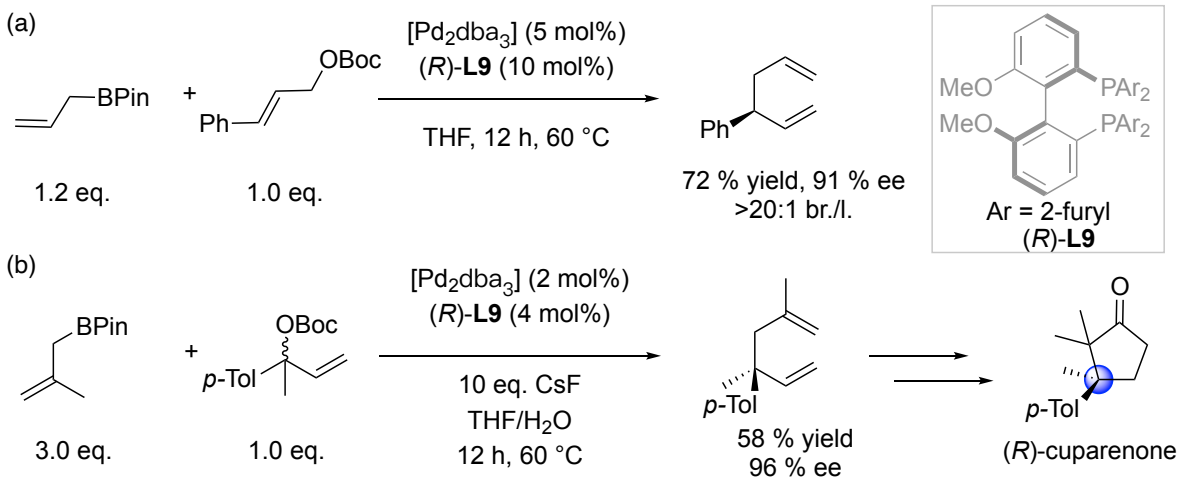


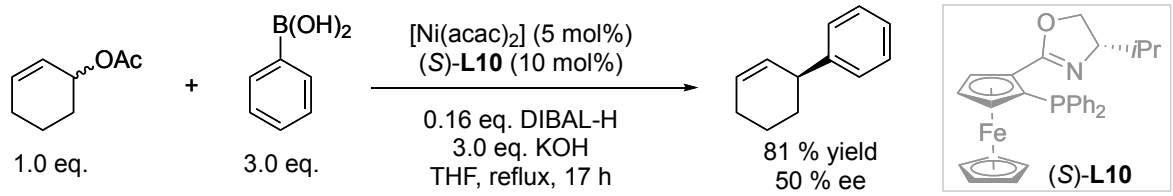
Figure 9. (a) Morken and co-worker's asymmetric Pd-catalysed Csp^3-Csp^3 coupling.[30] (b) Application in the total synthesis of (*R*)-cuparenone.[31]

3. Nickel-Catalysed Asymmetric Suzuki-Miyaura Couplings

Aside from palladium, other transition metals have also been demonstrated to catalyse asymmetric Suzuki-Miyaura cross-couplings. Nickel is a cheaper, more abundant alternative to palladium and it is an excellent tool for the coupling of some challenging electrophiles and alkyl nucleophiles.[32]

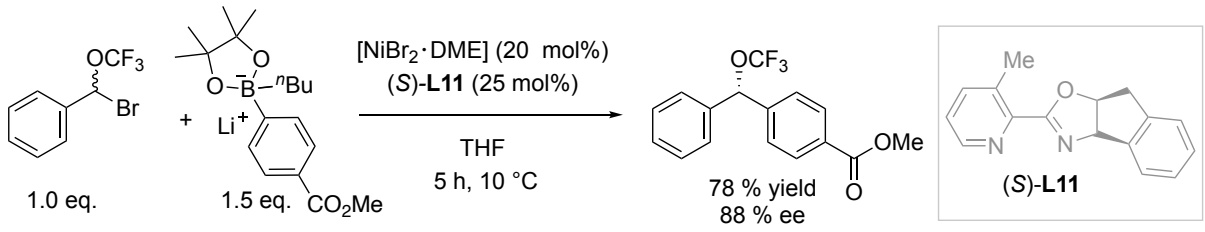
3.1 Nickel-Catalysed Asymmetric Csp^2-Csp^3 Suzuki-Miyaura Couplings

Uemura and co-workers reported a Ni-catalysed coupling of racemic allyl acetates and arylboronic acids (Scheme 3).[33] Low enantioselectivity was observed but, published over 20 years ago, this early example demonstrated the potential for Ni-catalysed asymmetric cross-coupling with racemic substrates.



Scheme 3. Early example of a Ni-catalysed Csp^2-Csp^3 cross-coupling developed by Uemura and co-workers.[33]

Since then, other groups have developed enantioconvergent Ni-catalysed Csp^2-Csp^3 cross-couplings with practically useful levels of enantioinduction.[34] For example, Shen and co-workers developed an enantioselective cross-coupling with racemic secondary benzyl bromides (Scheme 4).[35] Here, lithium organoborate nucleophiles were used to enable transmetalation at the reduced temperature required to achieve good enantioselectivity.



Scheme 4. Ni-catalysed Csp^2-Csp^3 cross-coupling developed by Shen and co-workers.[35]

The Fu group has developed many Ni-catalysed cross-couplings. In their enantioconvergent arylation of racemic α-chloro-amides with arylboron nucleophiles, excellent enantioselectivities and yields were achieved (Fig. 10a).[36] Later, they reported a cross-coupling employing arylboronic nucleophiles with a tethered olefin. In this cascade reaction, transmetalation is followed by Ni-catalysed cyclisation of the tethered olefin *via* β-migratory insertion. Subsequent coupling with the alkyl bromide generates the 2,3-dihydrobenzofuran products (Fig. 10b).[37] The practical utility of this method was demonstrated by the synthesis of the core of drug candidate fasiglifam (Fig. 10b).

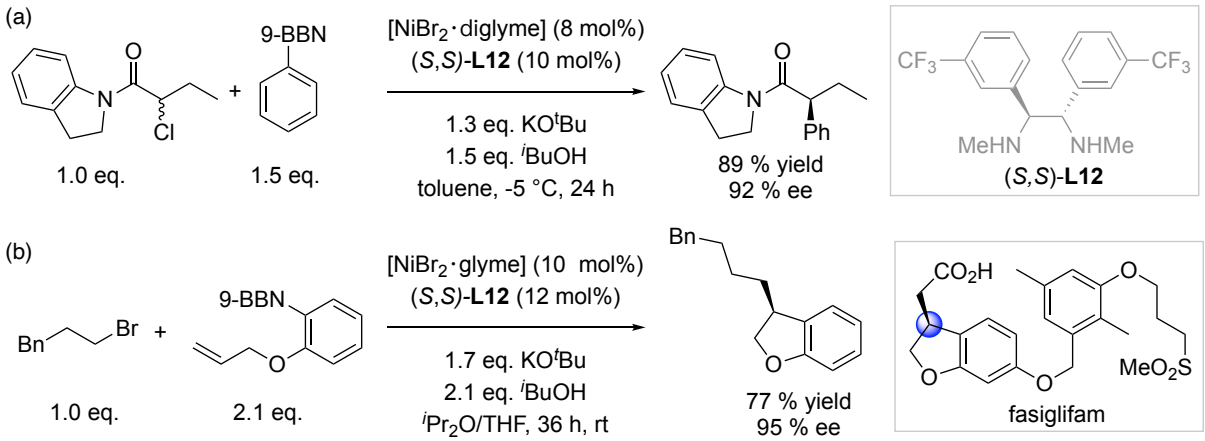


Figure 10. Ni-catalysed Csp^2-Csp^3 cross-couplings developed by the Fu group.[36,37]

3.2 Nickel-Catalysed Asymmetric Csp^3-Csp^3 Suzuki-Miyaura Couplings

Along with Csp^2 hybridised aryl nucleophilic coupling partners, the Fu group[38] and others[39,40] have also developed cross-coupling methods using alkylboron nucleophiles (Fig. 11). In these Ni-catalysed asymmetric reactions, a directing group is required in the alkyl halide coupling partner. The examples shown in Figure 11 use aryl[38] and sulfonyl[41] directing groups, but a wide range of directing groups can be employed[42,43] including amines,[44] and amides.

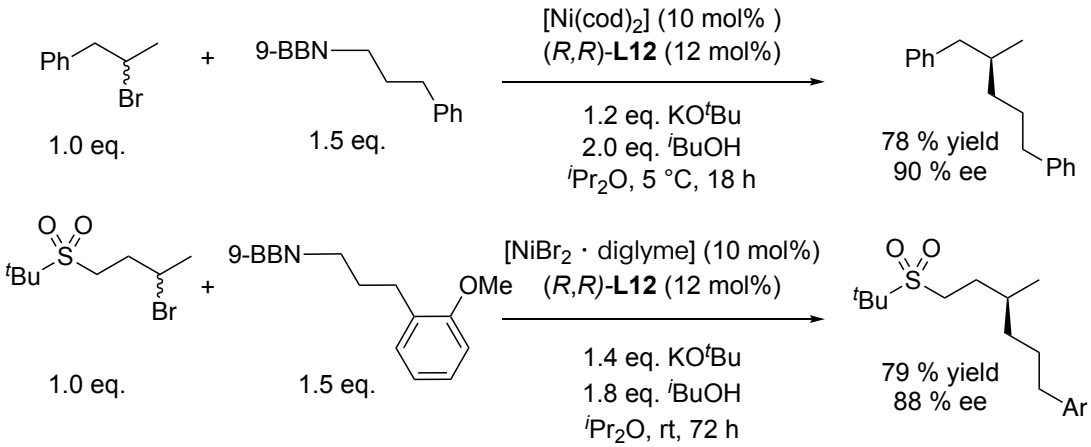


Figure 11. Ni-catalysed Csp^3-Csp^3 cross-couplings developed by the Fu group.[38,41]

These asymmetric Csp^3-Csp^3 cross-couplings operate *via* the general mechanistic scheme shown in Figure 12. Transmetalation is followed by a single electron transfer mediated oxidative addition of the racemic alkyl halide. Reductive elimination generates the alkyl-alkyl coupling product.

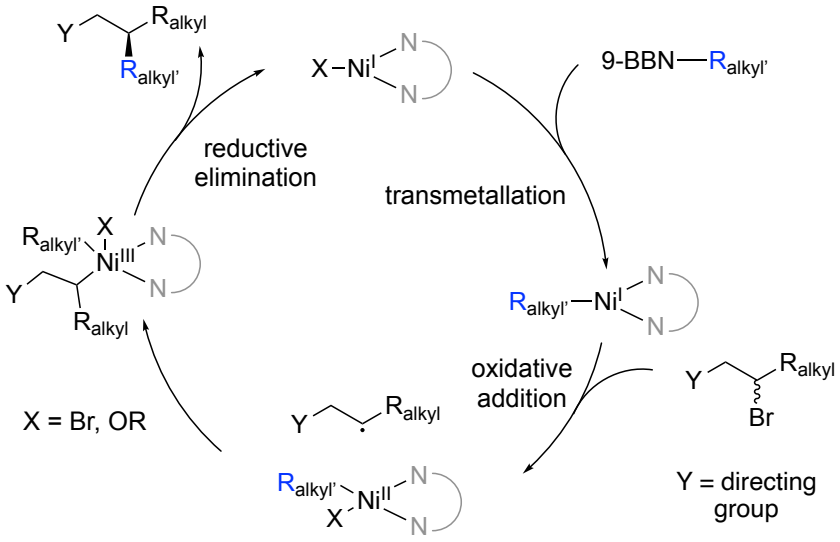
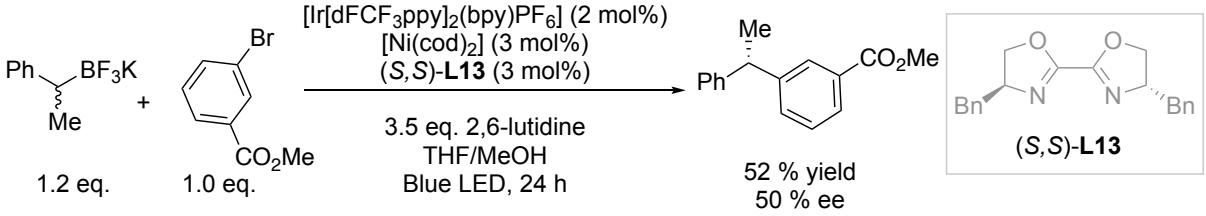


Figure 12. General mechanism for Ni-catalysed Csp^3-Csp^3 cross-couplings developed by the Fu group.

3.3 Photoredox Dual Catalysis in Asymmetric Suzuki-Miyaura Couplings

Molander and co-worker's reported the use of photoredox catalysis to enable cross-coupling reactions with Csp^3-hybridised nucleophiles (Scheme 5).[45,46] In this dual catalytic system, irradiation with blue LED light excites the Ir photocatalyst which can then activate the racemic secondary benzyltrifluoroborates by single electron transfer, and Ni catalyses the cross-coupling with an arylbromide. The enantioselectivity in these transformations is moderate but highlights the potential for future work using photoredox dual catalysis in asymmetric Suzuki-Miyaura cross-couplings.



Scheme 5. Molander and co-worker's asymmetric coupling employing photoredox catalysis.[45]

4. Rhodium-Catalysed Asymmetric Suzuki-Miyaura Couplings

Rh-catalysis has been employed for asymmetric Csp^2-Csp^3 Suzuki-Miyaura cross-couplings and provides complementary reactivity to that which we have already examined for Pd and Ni.

4.1 Rhodium-Catalysed Asymmetric Suzuki-Miyaura Couplings with Non-Chiral Substrates

As previously discussed, desymmetrisation of *meso*-compounds can be used to access enantioenriched arylated products. Lautens and co-workers have reported the Rh-catalysed addition of arylboronic acids to allylic dicarbonates which proceeds with excellent enantio- and regiocontrol (Fig. 13a).[47] They proposed the formation of a 1,2 σ-enyl Rh-intermediate (shown in Fig. 13a) which could reductively eliminate to give the major regioisomer observed. They suggest that the rate of isomerisation to the potential 1,4 σ-enyl isomeric Rh-complex is slow, enabling excellent regiocontrol. However, they acknowledge that mechanistic study is required and that either transmetalation or ionisation could plausibly be the first step in the

catalytic cycle. Later, they showed that the alternative regioisomer can be accessed by modification of the reaction conditions used, albeit with reduced regiocontrol (Fig. 13b).[48]

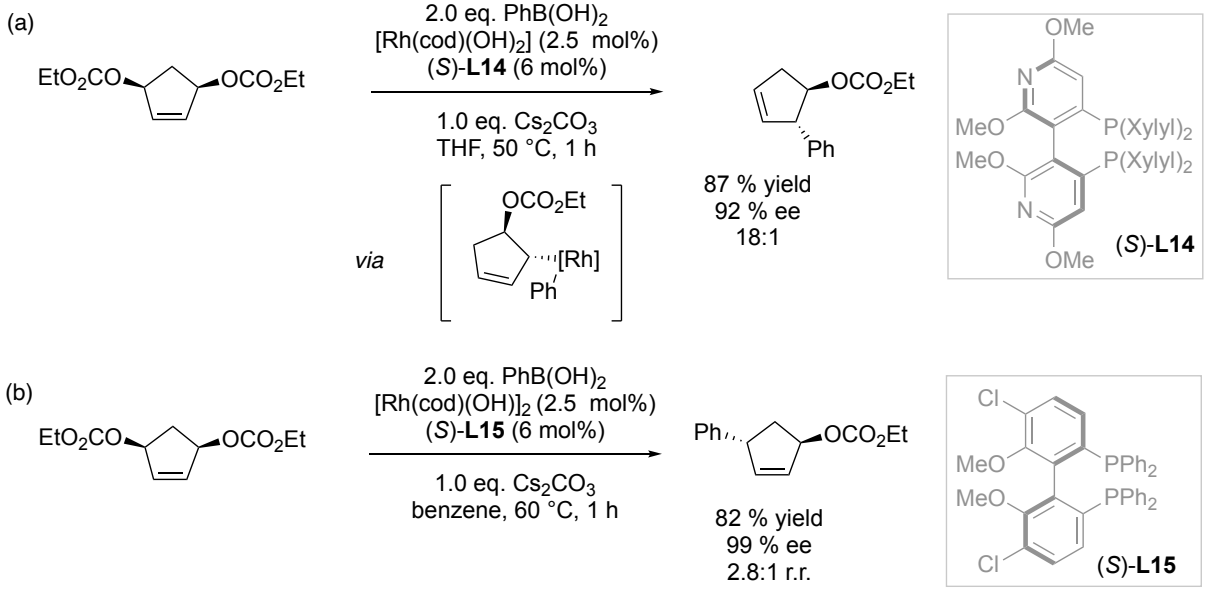
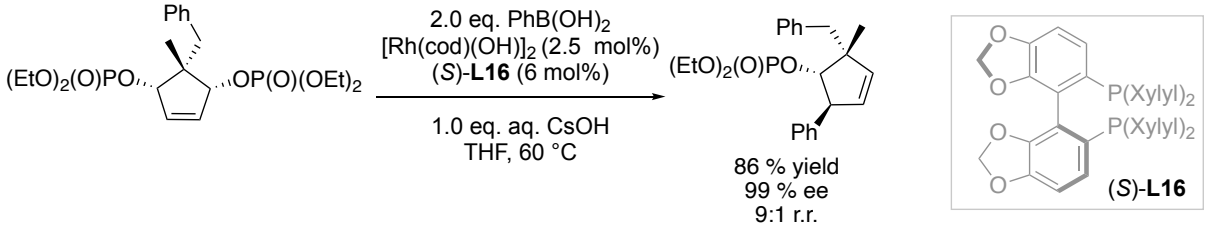


Figure 13. (a) The Lautens group's Rh-catalysed desymmetrisation of *meso*-dicarbonates[47] (b) conditions used to access the alternative regioisomer.[48]

Our group recently reported a related Rh-catalysed desymmetrisation of *meso*-bisphosphates to access quaternary stereocentre containing products (Scheme 6).[49] This arylation proceeds with excellent enantiocontrol for a range of aryl and heteroaryl boronic acids.



Scheme 6. Fletcher and co-worker's Rh-catalysed desymmetrisation strategy to access quaternary stereocentres.[49]

The Lautens group have also developed a Rh-catalysed desymmetrisation of acyclic *cis*-allylic dicarbonates by addition of arylboronic acids (Fig. 14a).[50] Lewis acidic zinc triflate is necessary to promote good conversions and enantioselectivity. Murakami and co-workers reported a desymmetrisation of cyclic and acyclic *cis*-allylic diols (Fig. 14b).[51] Interestingly, arylboroxines

are employed in this transformation which they observed form a boronic ester cycle with the unprotected diol substrate (shown in Fig. 14b).

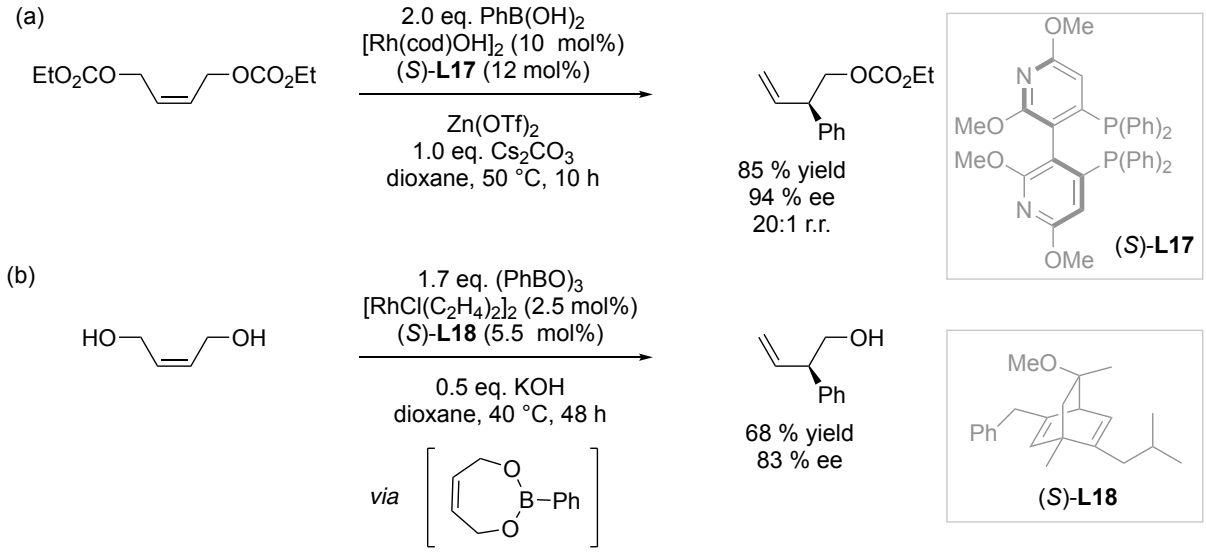
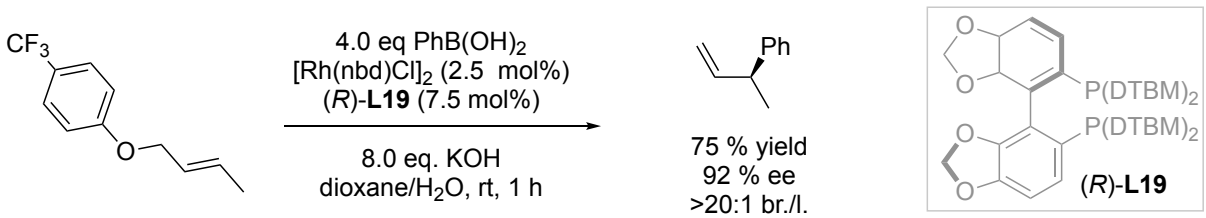


Figure 14. (a) The Lautens group's desymmetrisation of acyclic dicarbonates[50] (b) The Murakami group's desymmetrisation of acyclic diols.[51]

Oi and co-workers have reported a Rh-catalysed cross-coupling of acyclic allylic ethers with arylboronic acids (Scheme 7).[52] This coupling proceeds with excelled regio- and stereocontrol.



Scheme 7. Oi group's regio and enantioselective coupling with linear substrates.[52] DTBM= 3,5-di-^{t}Bu-4-MeO-C_6H_2

4.2 Rhodium-Catalysed Asymmetric Suzuki-Miyaura Couplings with Racemic Substrates

Our group has developed a Rh-catalysed asymmetric arylation of racemic cyclic allylic halides with arylboronic acids (Fig. 15a).[53] A range of arylboronic acids can be used in this highly enantioselective Csp^2-Csp^3 Suzuki-Miyaura cross-coupling, along with heteroaryl and vinylboronic acids.[54] The coupling of heterocyclic partners is particularly relevant for pharmaceutical and agrochemical applications.[1,55] Although pyridinylboronic acids cannot be

employed directly, good yields and enantioselectivities can be achieved using 2-chloropyridine boronic acids (Fig. 15b).[54]

Our group has reported a number of racemic allyl halides which can be employed in this transformation, including heterocyclic and bicyclic electrophilic coupling partners.[54,56] With racemic, diastereomeric substrates excellent enantio- and diastereoselectivity can be achieved (Fig. 15c).[56]

Attempts to significantly further expand the scope of this transformation are discussed in Chapter 3 and the mechanism of these enantioselective Rh-catalysed cross-coupling reactions with racemic substrates will be discussed in Chapter 2.

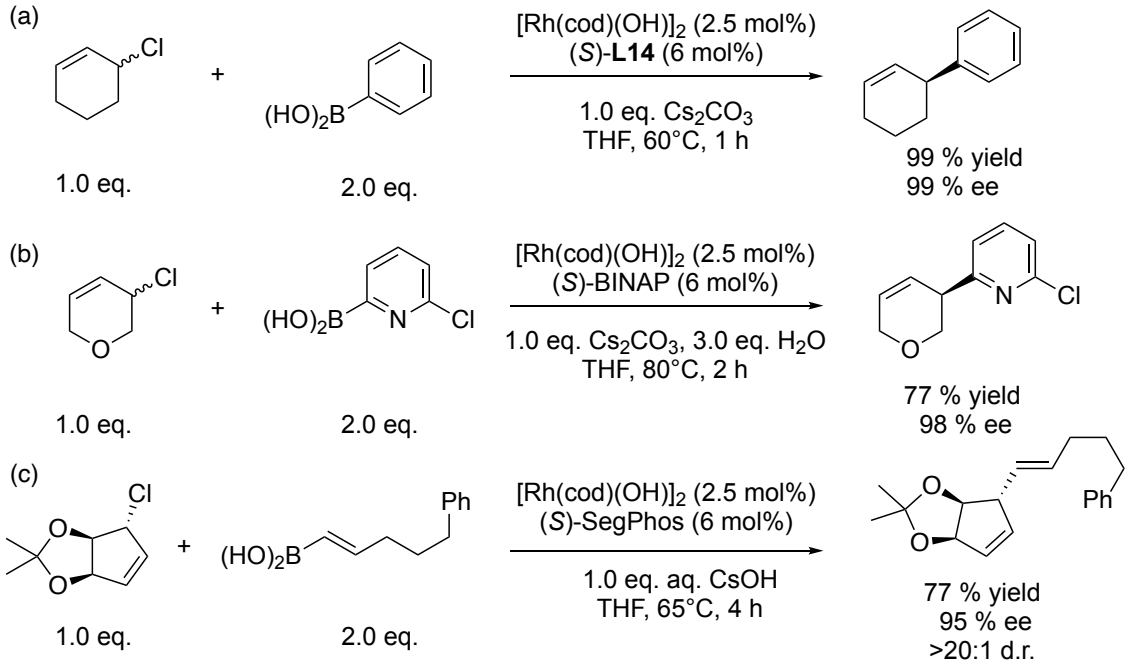


Figure 15. (a) Fletcher and co-worker's Rh-catalysed asymmetric Suzuki-Miyaura cross-coupling of cyclic allylic halides with arylboronic acid[53] (b) example displaying the use of heterocyclic coupling partners in this transformation[54] (c) a diastereoselective example with vinylboronic acid.[56]

Our group previously reported the Rh-catalysed coupling of a piperidinyl allyl chloride with 4-bromophenylboronic acid using Cs_2CO_3 as a base and heating to 80 °C (Fig. 16a).[54] The coupling product formed in this reaction is a key intermediate in Merck's process route to the oncology drug niraparib.[57] In order to demonstrate the practical utility of our Rh-catalysed method, this

transformation was optimised for gram scale synthesis.[58] It was found that the use of the corresponding arylboronic ester coupling partner was necessary to obtain reproducible yields. Modification of the reaction conditions by using 4-bromophenylboronic acid pinacol ester along with aqueous CsOH base allowed for the reduction of the temperature and time required to generate the arylated product in good yield and high enantioselectivity (Fig. 16b).[56]

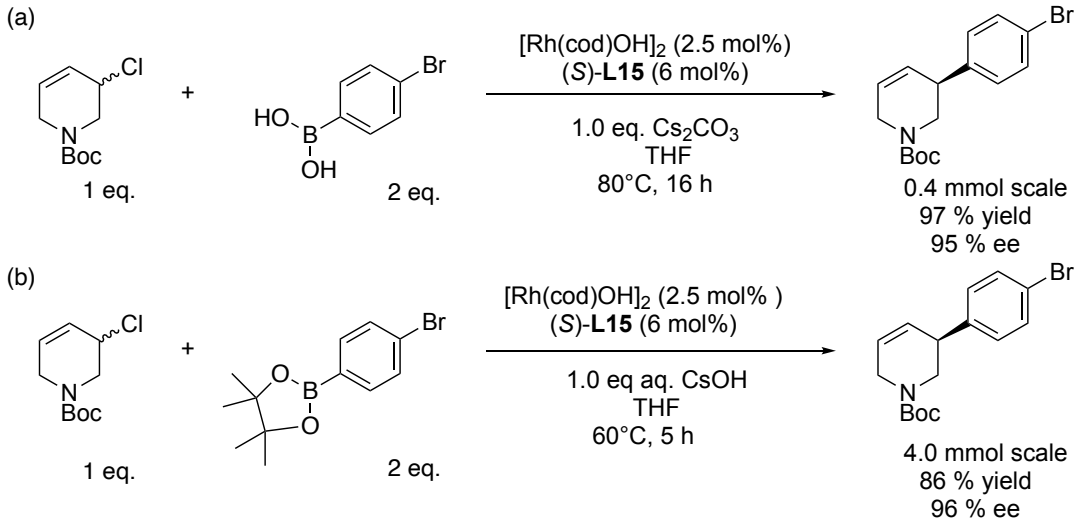


Figure 16. (a) Rh-catalysed cross-coupling on a 0.4 mmol scale.[54] (b) Optimised conditions for reaction on a 4.0 mmol scale.[58]

To demonstrates the application of this method to complex molecule synthesis, our group has exploited this asymmetric Suzuki-Miyaura cross-coupling strategy in the synthesis of a range of complex molecules (Fig. 17). As previously mentioned, the coupling product from the reaction shown in Figure 16 can be used in the synthesis of niraparib.[54] This piperidine-based allyl chloride can also be employed in the synthesis of the drug candidate preclamol and the natural product isoanabasine.[54] The bicyclic allyl chloride coupling partner shown in Figure 15c has been used in a concise total synthesis of the prostaglandin based drug tafluprost.[59]

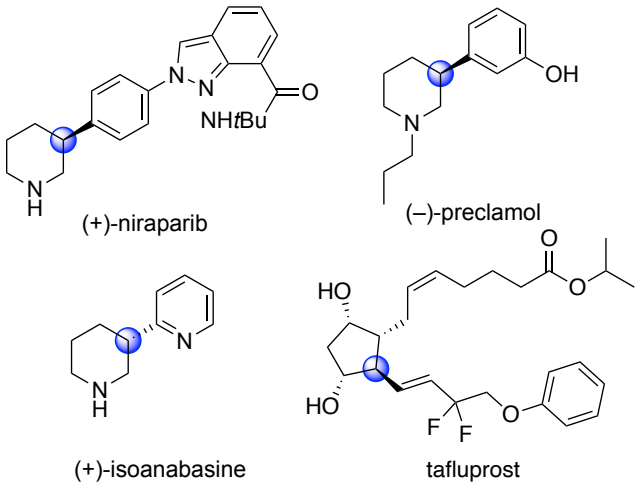


Figure 17. Biologically active compounds which have been synthesised by the Fletcher group using Rh-catalysed asymmetric Suzuki-Miyaura cross-couplings.[54,59]

5. Other Transition Metal-Catalysed Asymmetric Suzuki-Miyaura Couplings

5.1 Iridium-Catalysed Asymmetric Suzuki-Miyaura Couplings

Ir-catalysis is often used in asymmetric allylic substitution reactions.[60] Carreira and co-workers have developed a number of Ir-catalysed cross-couplings of allylic alcohols and boron nucleophiles.[61,62] An acid is required to promote substitution of the alcohol substrate and a flouride is required to activate the boronate (Fig. 18a). They propose that rapid isomerisation of two (η^3-allyl)Ir-intermediates formed enables the use of a racemic starting material.[63] Using this method, the Carreira group have synthesised a number of biologically active complex molecules such as nyasol and hinikiresinol (Fig. 18b).[62]

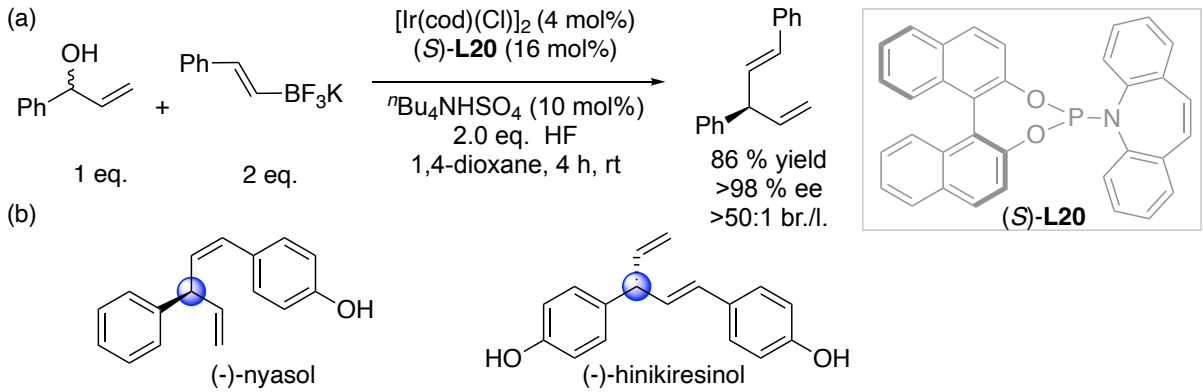
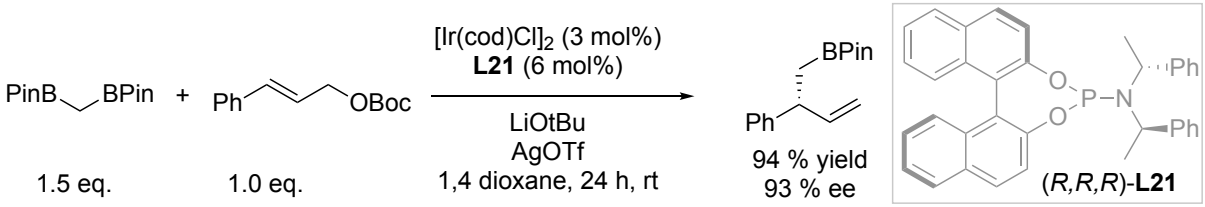


Figure 18. (a) Example of Carreira and co-workers Ir-catalysed asymmetric Csp^2-Csp^3 coupling.[62] (b) Biologically active compounds synthesised using this method.[62]

Ir-catalysis can also be used in asymmetric Csp^3-Csp^3 Suzuki-Miyaura cross-couplings. Niu and co-workers report a regio and enantioselective coupling of allylic carbonates and a diborylmethane reagent (Scheme 8).[64] They proposed that the silver additives assist with the transmetalation step.



Scheme 8. Silver assisted, Ir-catalysed asymmetric Csp^3-Csp^3 Suzuki-Miyaura cross-coupling.[64]

5.2 Copper-Catalysed Asymmetric Suzuki-Miyaura Couplings

Over the last decade, a number of Cu-catalysed asymmetric Suzuki-Miyaura cross-coupling reactions have been reported.[65,66] The Hayashi and Hoveyda groups have both developed asymmetric Cu-catalysed Csp^2-Csp^3 cross-couplings with prochiral allyl phosphates. Along with arylboronic esters (Fig. 19a),[67] vinyl and allenyl boronic esters are also tolerated with minor modifications to the reaction condiditons.[68,69] Substituted allyl phosphates also can be utilised to generate quaternary stereocentre containing products.[70]

Hoveyda and co-workers further extended this work to allow for the use of a diborylmethane reagent in a Csp^3-Csp^3 cross-coupling (Fig. 19b).[71] This method was applied to the synthesis of natural product rhopaloic acid A (Fig. 19b).

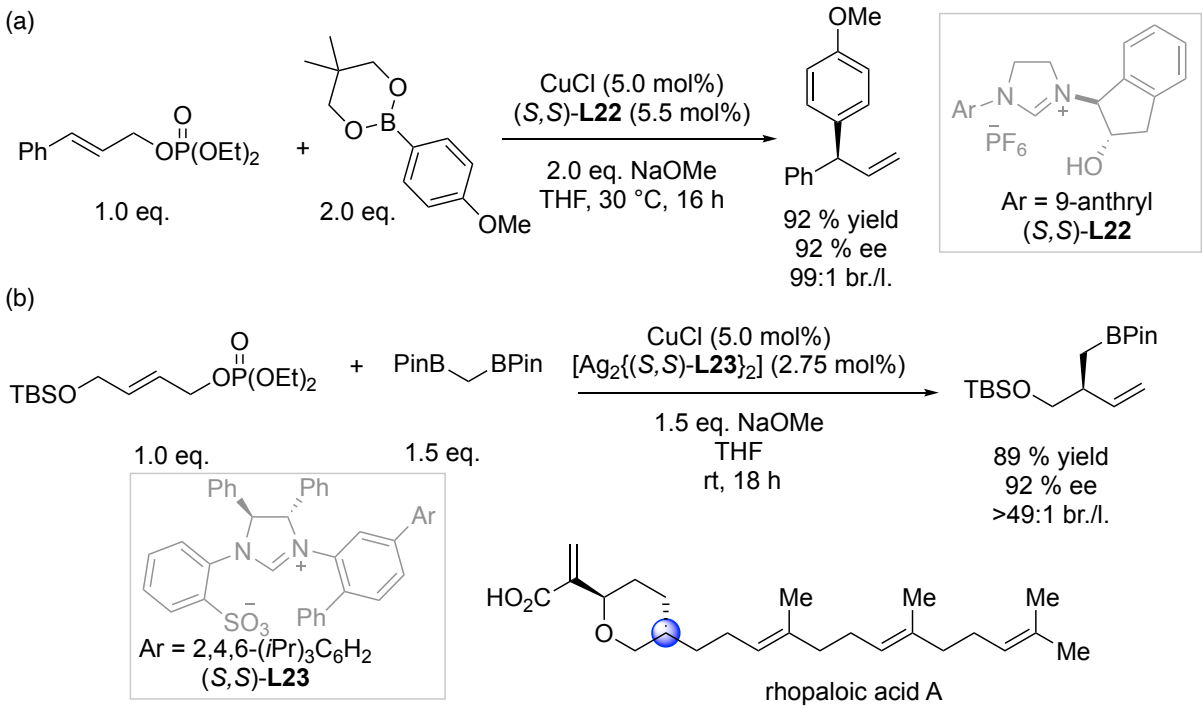
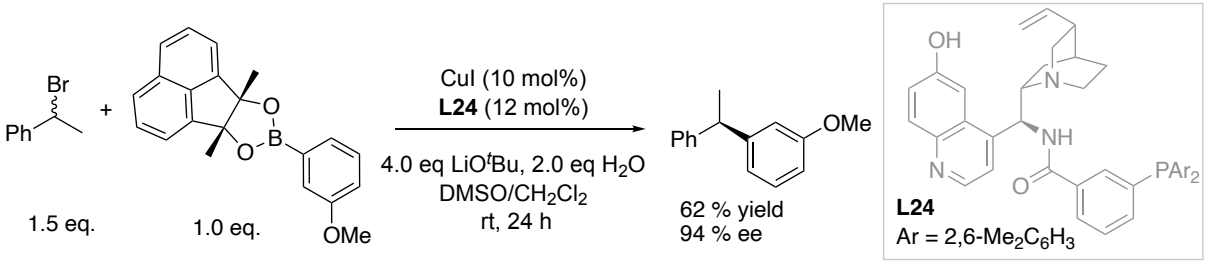


Figure 19. (a) Hayashi and co-workers Cu-catalysed coupling of allyl phosphates and arylboronic esters.[67] (b) Hoveyda and co-workers Cu-catalysed coupling with Csp^3 hybridised organoboron nucleophiles.[71]

Recently, a Cu-catalysed enantioconvergent cross-coupling with alkenyl bromides was reported (Scheme 9).[72] This coupling operates *via* the stereoablative formation of a prochiral alkyl radical from the racemic electrophile. A range of aryl and heteroarylated products can be synthesised in high enantioselectivity and yield using this method.



Scheme 9. Cu-catalysed enantioconvergent radical cross-coupling.[72]

5.3 Iron-Catalysed Asymmetric Suzuki-Miyaura Couplings

In 2019, the first Fe-catalysed asymmetric Suzuki-Miyaura cross-coupling was reported (Fig. 20a).[73] It was shown that racemic α-bromo esters could be coupled with lithium organoboron salts to generate enantioenriched α-aryl products in good yields. Recently, Byers and co-workers reported a Fe-catalysed coupling of racemic benzylic chlorides with arylboronic esters

(Fig. 20b).[74] Although both reports show only moderate enantioselectivity, these will undoubtedly provide inspiration for further investigation of Fe-catalysed asymmetric Suzuki-Miyaura cross-coupling.

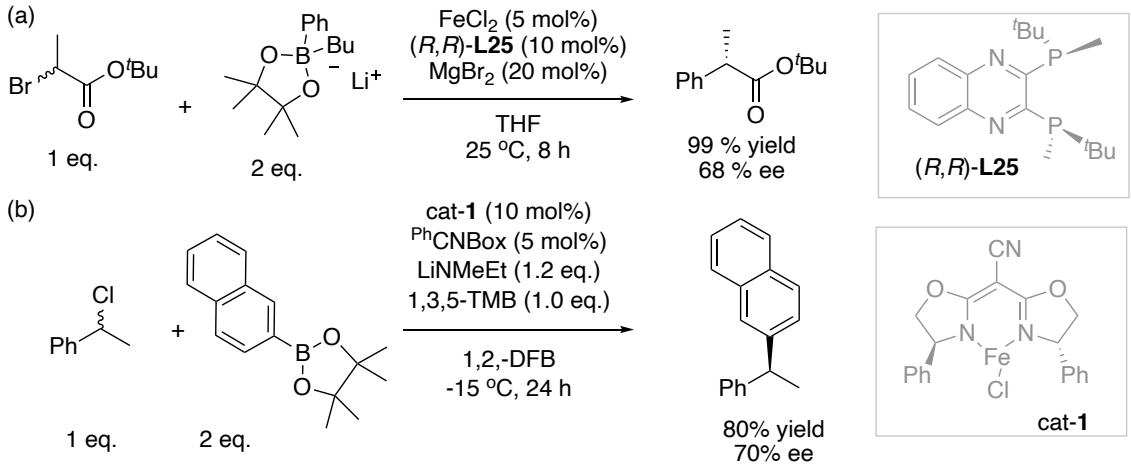
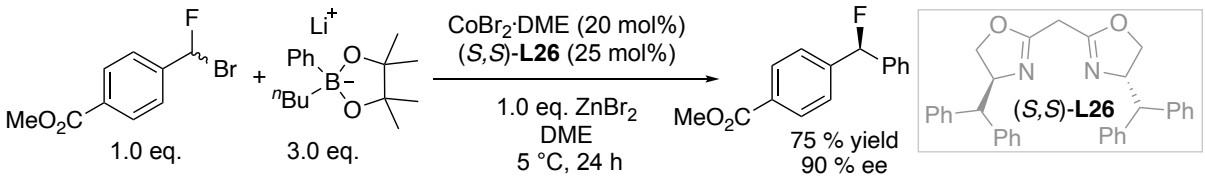


Figure 20. (a) The first Fe-catalysed asymmetric Suzuki-Miyaura cross-coupling.[73] (b) A recent Fe-catalysed asymmetric Suzuki-Miyaura cross-coupling.[74] TMB = trimethoxybenzene, DFB = difluorobenzene.

5.4 Cobalt-Catalysed Asymmetric Suzuki-Miyaura Couplings

As with Fe-catalysed asymmetric cross-couplings, the area of Co-catalysed asymmetric Suzuki-Miyaura cross-couplings is in its infancy. Recently, Shen and co-workers reported the asymmetric Csp^2-Csp^3 cross-coupling of benzyl bromides and lithium arylboronates (Scheme 10).[75] The fluorinated products were accessed with high enantioselectivity disclosing great potential for the further development of Co-catalysed asymmetric Suzuki-Miyaura cross-couplings.



Scheme 10. Co-catalysed asymmetric Suzuki-Miyaura cross-coupling.[75]

6. Conclusions and Thesis Outline

This chapter has given an overview of the asymmetric Suzuki-Miyaura cross-couplings catalysed by a variety of transition metals which have been reported since the seminal publications over 20 years ago.[11,12] This is an active area of research with new innovative and useful methods regularly appearing in the literature. This is highlighted by the fact that since compiling a comprehensive review of the area less than two years ago,[8] many new and exciting reports have emerged. The first Fe- and Co-catalysed procedures for the asymmetric Suzuki-Miyaura cross-coupling have been developed,[73,75] along with many interesting publications with already established transition-metal catalysts for asymmetric Suzuki-Miyaura couplings.[28,29,72]

Our group has continued to expanded our Rh-catalysed asymmetric Suzuki-Miyaura coupling method in recent years.[56,58,59] This highly enantioselective reaction has been shown to tolerate a range of coupling partners, including heterocycles and can be used in the synthesis of complex molecules (section 4.2).[54,59] Understanding the mechanism of this arylation reaction with racemic substrates would enable us to better comprehend its potential and its limitations. It may also aid in the development of new asymmetric cross-coupling reactions with racemic substrates. Investigation of the mechanism of our asymmetric Suzuki-Miyaura coupling method will be explored in detail in Chapter 2 (Fig. 21a). Enantio- and regioselective transformations using substrates with non-symmetric allyl units would greatly expand the scope of this reaction (Fig. 21b), however, controlling selectivity in these reactions poses a significant challenge which will be discussed in Chapter 3.

In general, broadening the scope of asymmetric cross-coupling beyond the commonly used bench-mark substrates would be useful for drug and agrochemical discovery. In particular, cross-coupling reactions involving important pharmacophores such as heterocycles and small structurally defined rings would be useful.[1,76] In Chapter 4, we will discuss a Rh-catalysed

cross-coupling with arylboronic acids which allows for use of cyclobutene coupling partners (Fig. 21c).

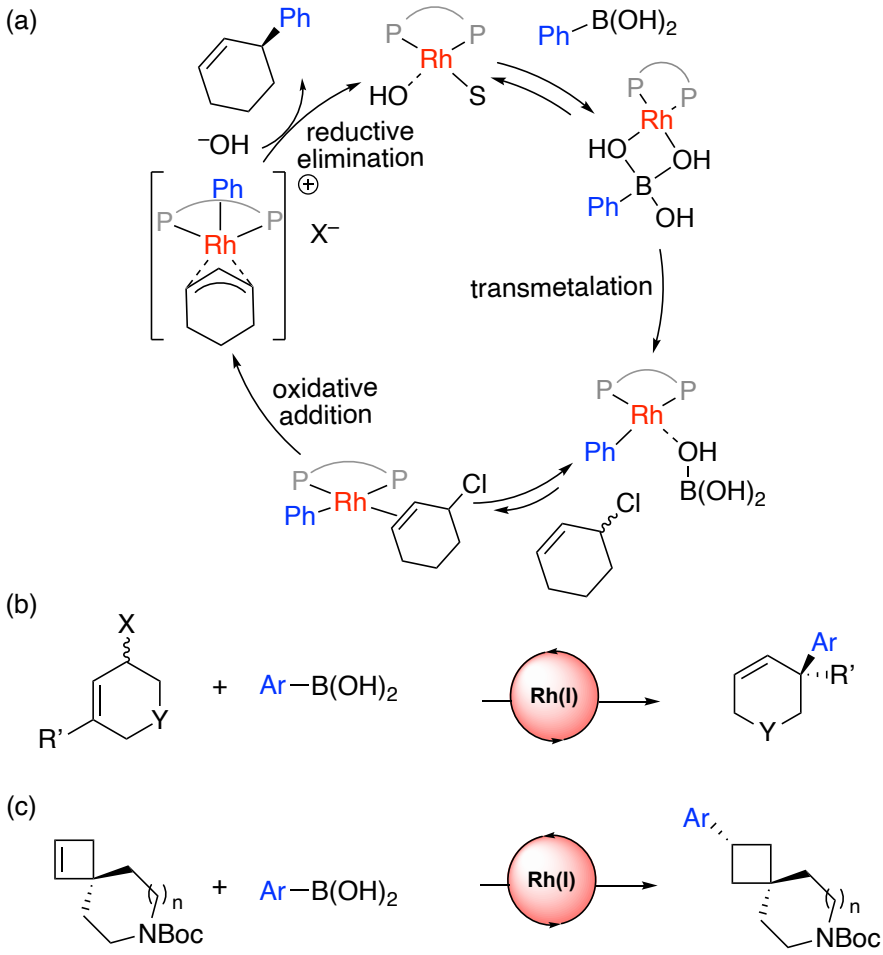


Figure 21. An outline of the work which will be presented in this thesis (a) Proposed mechanism for the Rh-catalysed asymmetric Suzuki-Miyaura cross coupling of racemic allyl halides and arylboronic acids to be discussed in Chapter 2. (b) Efforts to apply this method to the synthesis of quaternary stereocentre containing products, to be discussed in Chapter 3. (c) A Rh-catalysed cross-coupling of arylboronic acids and cyclobutenes to be discussed in Chapter 4.

We anticipate that the broad range of transition metal catalysed reactions described in the literature, and summarised in this chapter, will provide inspiration for future work in the area of asymmetric Suzuki-Miyaura cross-couplings. We look forward to seeing new asymmetric Suzuki-Miyaura methods emerging along with some of the more established methods described finding their place in the medicinal chemist's toolkit for years to come.

Chapter 2: A Mechanistic Investigation of Rhodium-Catalysed Asymmetric Suzuki-Miyaura Couplings with Racemic Allyl Halides

This chapter is based on the following publication.

- L. van Dijk, R. Ardkhean, M. Sidera, S. Karabiyikoglu, O. Sari, T.D.W. Claridge, G.C. Lloyd-Jones, R.S. Paton, S.P. Fletcher, Mechanistic Investigation of Rh(I)-Catalysed Asymmetric Suzuki-Miyaura Coupling with Racemic Allyl Halides, *Nat. Catal,* 4, 284, (2021).

This mechanistic elucidation was a collaborative project. Where experiments or calculations performed by other authors are discussed in this chapter, their contribution is clearly highlighted in the text and additionally acknowledged in the figure captions. S.P.F., L.v.D and M.S. designed the experiments. L.v.D., M.S. and S.K. performed the experiments. L.v.D., R.A., M.S., G.C.L.J., R.P. and S.P.F. analysed the experimental results. R.S.P, L.v.D, R.A. and O.S. conducted and analysed the computational work. T.D.W.C. performed the NMR experiments discussed in sections 2.1 and 2.3. G.C.L.J. derived the pseudo steady-state rate equation.

1. Introduction

1.1 Mechanism of Rh-catalysed Asymmetric Additions

Detailed mechanistic studies on Rh-catalysed asymmetric additions are scarce, particularly in comparison to their Pd-catalysed counterparts. Hayashi and co-workers reported a key study on additions of arylboronic acids to cyclic α,β-unsaturated ketones.[77] Transmetalation is the first step in this catalytic cycle. Subsequently, 2-cyclohexenone inserts into the Rh-aryl bond to form an oxa-π-allyl Rh species which hydrolyses to release the product (Fig. 22). Later, a kinetic study revealed that transmetalation from boron to Rh was the rate-determining step.[78]

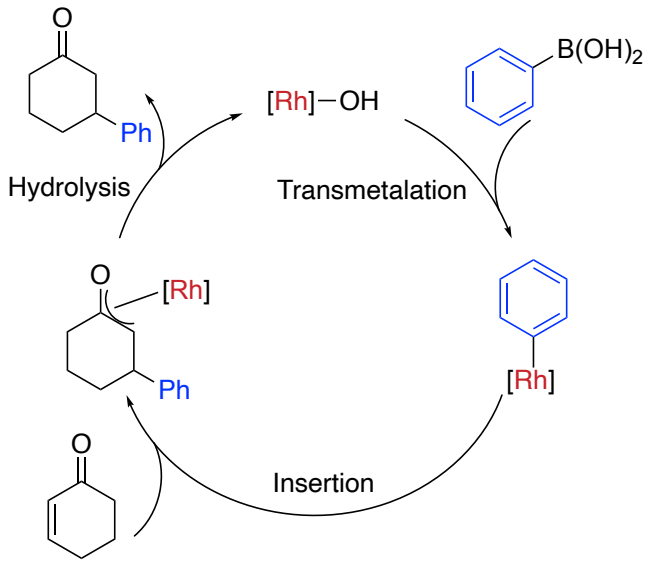


Figure 22. Rh-catalysed 1,4-addition mechanism elucidated by Hayashi and co-workers.[77]

1.2 Mechanism of Asymmetric Allylic Addition Reactions with Racemic Substrates

Asymmetric addition reactions with racemic substrates can operate *via* several different mechanistic pathways to generate enantioenriched products.[79] One such process is dynamic kinetic asymmetric transformation (DyKAT) which involves the formation of a common substrate-catalyst intermediate from both enantiomers of the starting material (as discussed in Chapter 1, section 2.1).[18] Enantioselectivity is achieved when one enantiomer of the product is generated at a significantly higher rate than the other (Fig. 23a). The mechanism of Pd-catalysed DyKATs with racemic electrophiles has been thoroughly investigated.[80] Both enantiomers of the racemic starting material react to form a common intermediate. An outer-sphere addition of a stabilised nucleophile generates the new stereogenic centre. For example, Trost and co-worker's Pd-catalysed asymmetric allylic alkylation operates *via* this mechanism (Fig. 23b).[81] Recently, Li and co-workers reported a Rh-catalysed asymmetric allylic substitution with stabilised nucleophiles which they propose operates *via* an analogous mechanism with a π-allyl-Rh intermediate formed.[82]

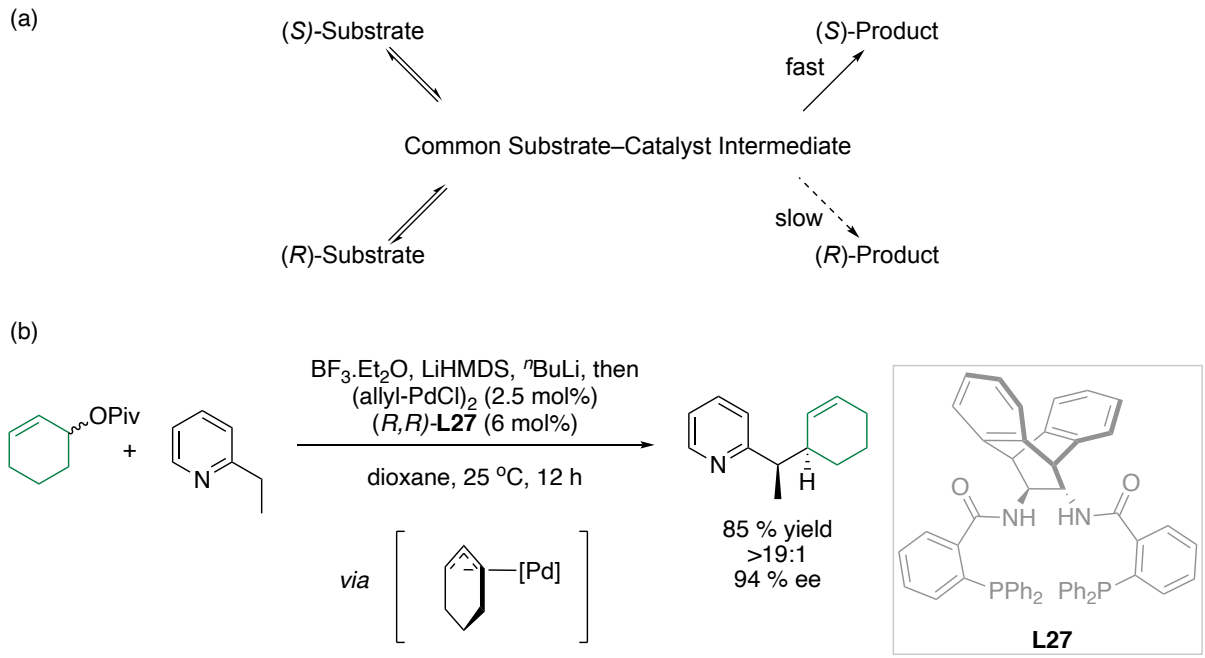


Figure 23. Dynamic kinetic asymmetric transformations (a) General scheme showing the mechanism of type II dynamic kinetic asymmetric transformations (b) Example of a Pd-catalysed DyKAT, Trost and co-worker's asymmetric allylic alkylation of 2-alkylpyridines.[81]

Asymmetric allylic addition reactions with racemic electrophiles can also occur *via* dynamic kinetic resolution. This mechanistic process involves interconversion of the enantiomers of the racemic starting material, and one enantiomer reacts more readily than the other to give the enantioenriched product (Fig. 24a). In contrast to the DyKAT mechanism shown in Fig. 23, Cu-catalysed asymmetric addition of alkylzirconium reagents to racemic allylic substrates operates *via* dynamic kinetic resolution (Fig. 24b).[83,84] The Cu-halide-ligand complex catalyses the addition of the alkylzirconium reagent along with racemisation of the allyl chloride starting material *via* copper mediated reversible formation of an allyl iodide intermediate. The enantiomers of the allyl iodide intermediate can readily interconvert enabling a dynamic kinetic resolution.

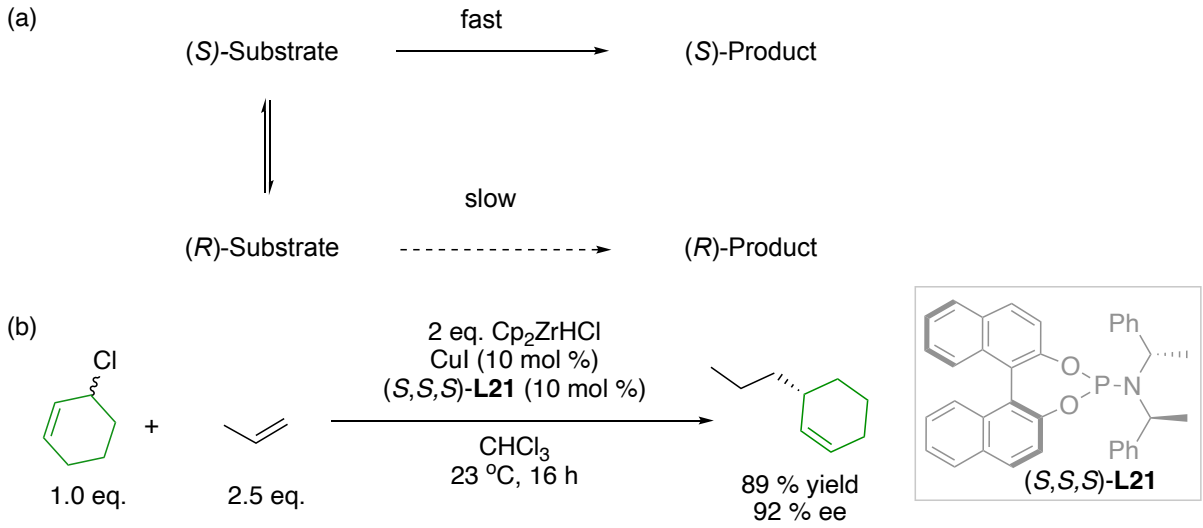


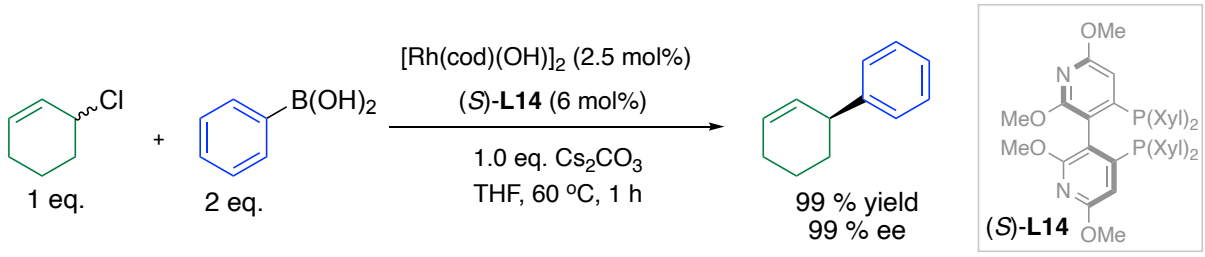
Figure 24. Dynamic kinetic resolution with racemisation of the starting material (a) General scheme showing the mechanism of dynamic kinetic resolutions. (b) An example of a Cu-catalysed dynamic kinetic resolutions; our group's asymmetric allylic alkylation.[83]

Other mechanisms for asymmetric allylic addition reactions with racemic substrates are possible, including direct enantioconvergent processes where both enantiomers of the starting material react *via* different mechanistic pathways to give the same enantioenriched product.[85,86]

1.3 Project Aim

Our group has developed a highly enantioselective Rh-catalysed coupling of boronic acids and racemic allyl halides (Scheme 11 and previously discussed in Chapter 1, section 4.2).[53] In order to gain insight into the mechanism of this reaction, which was previously unknown, we embarked on a mechanistic investigation involving a combination of experimental and computational studies. Along with a comprehension of the mechanism underpinning the Rh-catalysed couplings reactions developed by our group,[53,54,56,58] we hoped to gain further understanding of the limitations and potential of Rh-catalysed asymmetric additions. This study aims to contribute towards a broader understanding of Rh-allyl chemistry and of

asymmetric catalytic reactions with racemic substrates in general.



Scheme 11. Rh(I)-catalysed asymmetric coupling of phenylboronic acid and racemic 3-chlorocyclohex-1-ene.[53]

Rh-catalysed DyKATs are generally much less understood in comparison to their Pd-catalysed counterparts. However, a DyKAT mechanism analogous to that observed in Pd-catalysed asymmetric additions to racemic nucleophiles could be operative here where oxidative addition of both enantiomers of the starting material results in a Rh-allyl species.[82] Transmetalation of that species would be followed by an inner-sphere nucleophilic attack to give the arylated product (Fig. 25a).[87]

Alternatively, the Rh-catalysed arylation here could operate *via* a dynamic kinetic resolution mechanism, involving facile interconversion of starting material enantiomers followed by a stereospecific addition step (Fig. 25b). Other mechanisms are plausible, including direct enantioconvergent processes (Fig. 25c).[85]

Rh-catalysed hydroarylation and Rh-catalysed processes involving diene electrophiles are known.[88,89,90] Another mechanism that could potentially be operative here involves elimination of the allyl halide resulting in a diene intermediate which could then undergo hydroarylation with a Rh-aryl species (Fig. 25d).

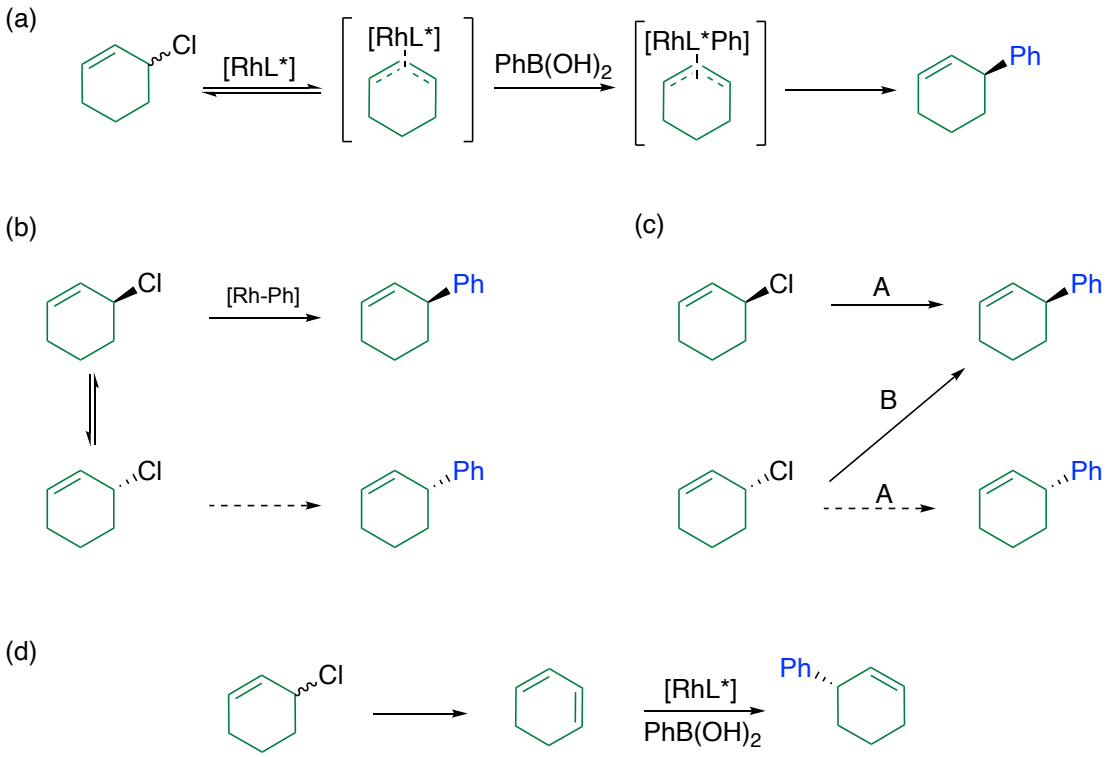


Figure 25. (a) Potential DyKAT mechanism for the transformation under investigation in this study with reversible oxidative addition as the first step. (b) Potential dynamic kinetic resolution mechanism. (c) Potential composite mechanism. (d) Potential mechanism involving elimination to diene followed by hydroarylation.

This chapter will discuss the experimental and computational studies conducted to examine this mechanism which directed us away from the scenarios outlined above and instead, pointed towards the proposed cycle shown in Figure 26. The available evidence is consistent with transmetalation of a monomeric active catalyst (**I**) to give a Rh-aryl species. This is followed by irreversible oxidative addition of both enantiomers of the racemic electrophile (**3**) to generate η^3 Rh-complex (**V**). Subsequently, the stereochemistry of the product (**4**) is set in the enantiodetermining reductive elimination step.

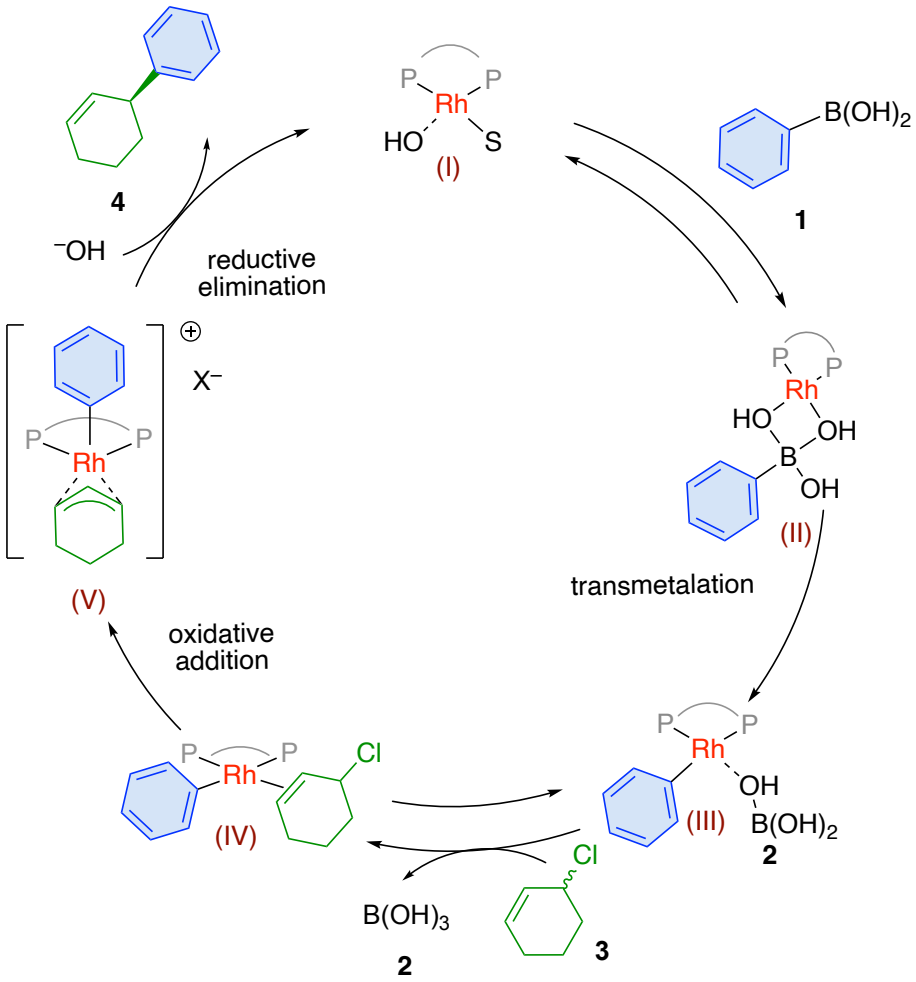


Figure 26. A simplified catalytic cycle showing the proposed mechanism in this work with key steps including transmetalation, oxidative addition and reductive elimination.

2. Results and Discussion

2.1 Understanding the Active Catalytic Species

These experiments were carried out by Dr. M. Sidera, and NMR expert Prof. T.D.W. Claridge.

Dr. Sidera and Prof. Claridge used NMR spectroscopy was used to examine how $[Rh(cod)(OH)]_2$ and (*S*)-Xylyl-P-PHOS ((*S*)-**L14**) react in THF-d_8. Generally, when $[Rh(cod)(OH)]_2$ is used with bisphosphine ligands, *in situ* displacement of cyclooctadiene (cod) with the bisphosphine ligands occurs which can require heating.[91] By comparing our data with literature reports,[77] we identified the formation of pre-catalytic species $[Rh(\mathbf{L14})(OH)]_2$ and the mixed $[Rh_2(cod)(\mathbf{L14})(OH)_2]$ dimer.

As previously observed by Hayashi and co-worker's,[77] Rh-ligand dimer $[Rh(\mathbf{L14})(OH)]_2$ undergoes reaction with phenylboronic acid (**1**) to give a Rh-aryl species. In contrast, when allyl chloride **3** was added to $[Rh(\mathbf{L14})(OH)]_2$, no reaction was observed even upon heating. These observations are not consistent with mechanisms initiated by the allylic electrophile first reacting with a metal-complex (Fig. 25a).[87,92]

In order to gain insight into the active catalytic species, Dr. Sidera measured the ee of the product (**4**) formed while varying the ligand (**L14**) ee.[93] A linear correlation between the enantioenrichment of **L14** and **4** was observed (Fig. 27). This result is consistent with an active catalytic species which is monomeric in Rh and **L14** and provides no evidence for the involvement of high-order aggregates of the catalyst.

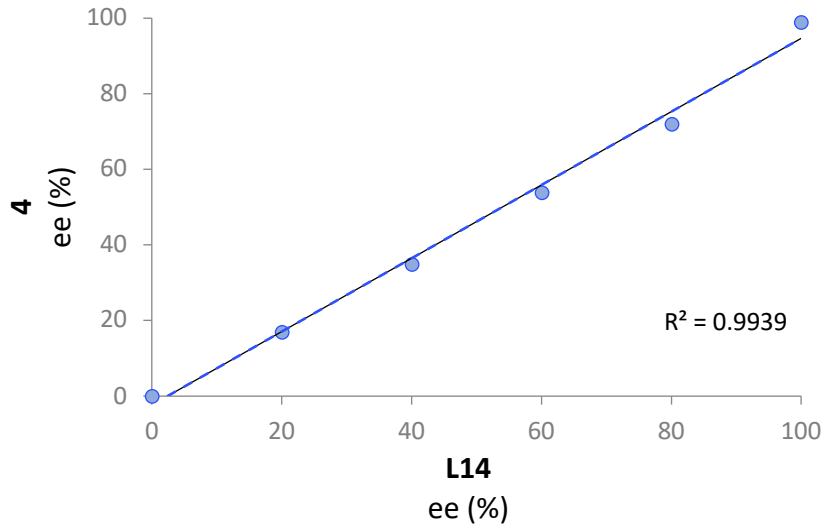


Figure 27. The relationship between the ee of ligand **L14** and product **4**. *Experiments performed by M.S.*

2.2 Eliminating Some Mechanistic Proposals

Some of the mechanistic hypothesis shown in section 1.3 could be easily tested. To test if the reaction could occur *via* the formation of an intermediate diene species by elimination of chloride followed by hydroarylation (Fig. 25d), we used cyclohexa-1,3-diene (**5**) in place of an allyl halide coupling partner and observed no arylated product (Fig. 28a).

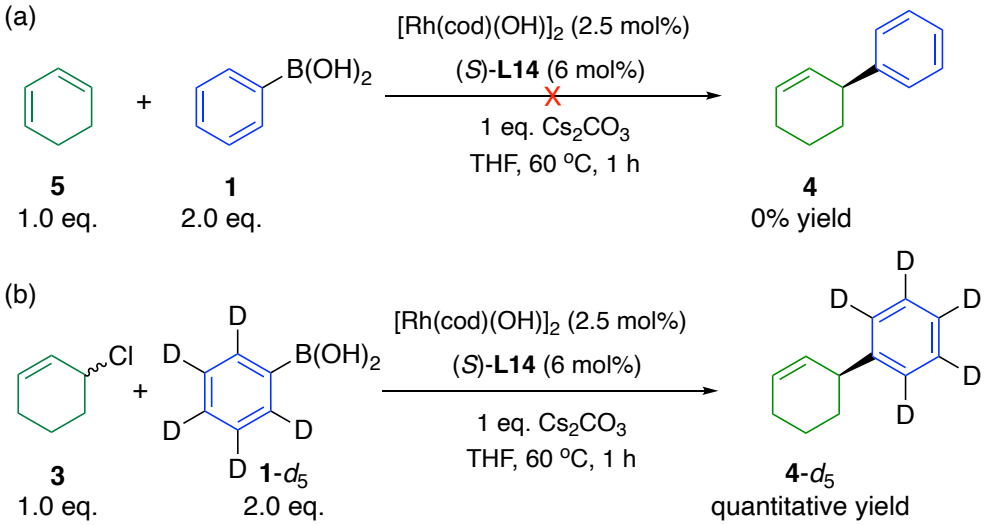


Figure 28. (a) Product **4** is not formed when cyclohexa-1,3-diene (**5**) is used as the starting material. (b) Deuterium labelling experiment using d_5-labelled phenylboronic acid.

A reaction using d_5-phenylboronic acid showed the deuterium labels remained on the phenyl ring (Fig. 28b). As no deuterium was observed on the cyclohexene unit, it rules out

mechanisms involving insertion of the rhodium catalyst into C-H bonds of the aromatic ring.[94] In related Cu-catalysed asymmetric additions (discussed in section 1.2), interconversion of allyl halide enantiomers was observed by NMR spectroscopy.[84] To examine if a similar process was occurring in this Rh-catalysed reaction, we used ^{1}H NMR exchange spectroscopy to attempt to observe exchange between vinylic and allylic protons in **3**. When **3** was subjected to Rh-catalysed arylation with **1**, no exchange between the vinylic and allylic protons in **3** was observed on the NMR timescale suggesting that the allyl chloride enantiomers do not interconvert *via* an S_N2' mechanism or do so at a much slower rate than ^{1}H NMR relaxation rates. As we were unable to observe racemisation on timescales relevant to the reaction, a dynamic kinetic resolution mechanism (Fig. 25b) which requires interconversion of allyl chloride enantiomers appears unlikely here. This does not preclude racemisation happening over the course of the reaction, but it indicates that racemisation is not required for the reaction to occur. However, using this technique interconversion *via* S_N2 mechanism would not be detectable.

2.3 Natural Abundance ^{13}C Kinetic Isotope Effects

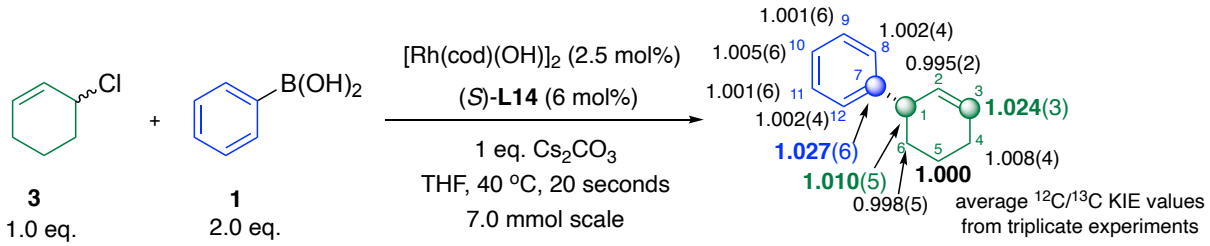
These NMR spectroscopic experiments were carried out by Dr. M. Sidera, and Prof. T.D.W. Claridge. The kinetic isotope effect calculations were carried out by Dr. R. Ardkhean and Prof. R. S. Paton.

The natural abundance ^{12}C/^{13}C kinetic isotope effects (KIE) method developed by Singleton[95,96] has been employed in mechanistic studies of catalytic reactions.[97-104] For these multi-step catalytic mechanisms, any isotope effects observed are the result of isotopic fractionation happening at or before the first irreversible step that involves that reaction component.[105] Typically, the reaction is run to high conversion and the ^{12}C/^{13}C ratio in recovered starting material is examined. However, in our case the isolation of small amounts of starting material at high conversions isn't possible as **3** is too sensitive and volatile to be reliably recovered. We

therefore chose to determine $^{12}C/^{13}C$ ratios generated in product **4** when the reaction is quenched at low conversion. ^{13}C KIEs (K_P) were determined from analysis of the product spectra *via* quantitative measurements of ^{13}C peak intensities obtained from peak deconvolution and were calculated using the formula shown in the equation below.

$$K_P = \frac{\ln(1-F)}{\ln\left(1 - F\left(\frac{R_P}{R_0}\right)\right)}$$

Here, F represents the fractional conversion of starting material to product and R is the carbon peak intensity ratios of the target carbon versus the reference carbon peak (C_5 in all cases). R_P is the peak ratio for the product at low conversion and R_0 is the peak ratio for the fully converted product formed in a reference reaction. Using this method, we observed appreciable KIE at C_7 (1.027 ±0.006), C_3 (1.024 ±0.003) and a smaller, but still significant, KIE at C_1 (1.010 ±0.005) (Scheme 12).



Scheme 12. ^{13}C KIE experimental results, standard errors in parenthesis. *Experiment performed by T.D.W.C.*

For a multi-step catalytic mechanism where only one product is formed, like the one under investigation here, isotope effects are due to isotopic fractionation happening at or before the first irreversible step that involves that reaction component. The ^{12}C fractionation observed at the aryl ipso-carbon (C_7) of the product could be the result of an irreversible reductive elimination, however, as shown in the calculations below (Fig. 29a), this would not explain the KIE observed at C_3. The ^{12}C fractionation observed at C_7 is most likely the result of a KIE in the transmetalation step, as we propose that this step is irreversible (see section 2.4 for evidence

of irreversible transmetalation).

In order to understand the enrichment at C_1 and C_3 in the allyl unit, we enlisted the help of computational chemistry expert Prof. R. S. Paton to calculate the predicted $^{12}C/^{13}C$ KIE that would result from various mechanisms. The values were calculated according to transition state theory applying the Bigeleisen–Mayer equation using scaled vibrational frequencies.[106,107] The most convincing mechanism, as judged by comparing experimental and theoretical results, involves *anti*-oxidative addition followed by reductive elimination.

Within this proposed mechanism, oxidative addition could be reversible or irreversible. If oxidative addition is reversible then reductive elimination is the first irreversible step involving the allyl moiety. The calculated $^{12}C/^{13}C$ KIE that would result from the reductive elimination step in a mechanism with reversible oxidative addition predicts an enrichment in ^{12}C at C_1 but no significant KIE at C_3 (Fig. 29a). We also calculated the equilibrium isotope effect (EIE or fractionation factor) between the Rh-complexes before and after the oxidative addition step. However, no significant enrichment in ^{12}C in the product was predicted as a result of the reversible oxidative addition step (see supplementary table S21 for predicted EIE values). Therefore, the calculated KIE values for a mechanism involving reversible oxidative addition followed by irreversible reductive elimination are not in agreement with experimentally measured KIE values thus ruling out this mechanism (shown in Fig. 29a).

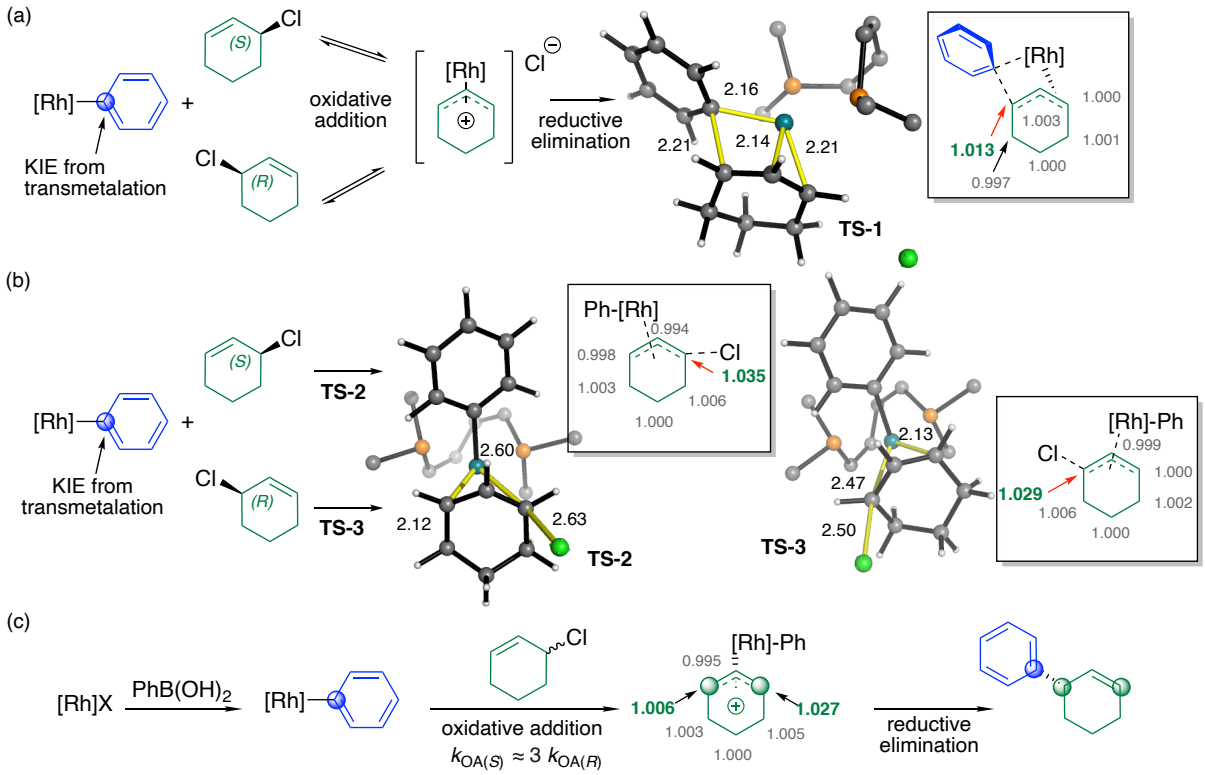


Figure 29. (a) Calculated KIE for reversible *anti*-oxidative addition followed by irreversible reductive elimination. $^{12}C/^{13}C$ KIE that would result from the reductive elimination step shown, along with the reductive elimination TS (b) Calculated KIE for irreversible *anti*-oxidative addition. Oxidative addition TS shown for each enantiomer along with the $^{12}C/^{13}C$ KIE that would result from the irreversible oxidative addition step (c) Combination of elementary KIE, with a ratio of 3.3:1 (*S*):(*R*) oxidative addition, which predicts the experimentally observed ^{12}C enrichment. TS are shown with cropped ligands. Selected distances are shown in Å. *This figure contains calculations performed by R.A. and R.S.P.*

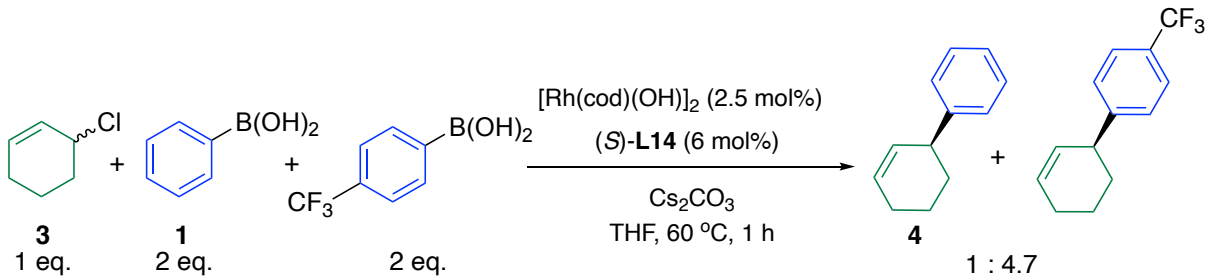
Alternatively, if oxidative addition is irreversible, the calculated KIE with (*S*)-**3** predicts enrichment at C_3, whereas with (*R*)-**3** an enrichment at C_1 is predicted (Fig. 29b). If both enantiomers of **3** undergo an irreversible oxidative addition, the $^{12}C/^{13}C$ ratios generated in product **4** will be a weighted average from the two starting material enantiomers. Our calculations suggest that a 3.3:1 ratio of (*S*)- to (*R*)-**3** undergoing oxidative addition accounts

quantitatively for the experimentally observed KIE (Fig. 29c).

In summary, natural abundance $^{12}C/^{13}C$ KIE are consistent with a mechanism involving irreversible transmetalation, followed by irreversible *anti*-oxidative addition with the two enantiomers of **3** reacting at different rates.

2.4 Transmetalation

Preliminary NMR experiments indicated that transmetalation is the first step in the catalytic cycle (section 2.1). The ^{13}C KIE results indicated that transmetalation is irreversible (section 2.3). However, the results described thus far do not provide insight into the mechanism of transmetalation. Competition experiments with electronically different arylboronic acids can be used to provide further insight into the transmetalation step. A competition experiment was run using equal, excess amounts of phenylboronic acid (**1**) and 4-(trifluoromethyl)phenyl)boronic acid and the ratio of the two arylated products was measured by ^{1}H NMR spectroscopic analysis of the crude reaction mixture after 1 hour (Scheme 13). A 4.7:1 product ratio was observed with phenyl substituted **4** being the minor product formed (Scheme 13). This experiment indicates that the rate of transmetalation is faster for the more electron deficient 4-(trifluoromethyl)phenyl)boronic acid compared to phenylboronic acid.



Scheme 13. Competition experiment between phenylboronic acid and 4-(trifluoromethyl)phenyl)boronic acid.

To further probe the effect of electronics on the transmetalation step, we carried out a series of competition experiments using different *para*- and *meta*-substituted arylboronic acids in competition with phenylboronic acid under conditions analagous to those shown in Scheme 13. The results of this series of experiments revealed a correlation between the ratio of

products obtained and the Hammett constants (σ values) of the substituents on the substituted boronic acid (Table 1).[108] Standard Hammett substituent constants (σ values) are listed in table 1,[108] except in the case of (4-fluorophenyl)boronic acid where σ_p = 0.15 is better parameterised for reactions in non-aqueous media (compared to the standard value of σ_p = 0.06, which was determined in water).[109,110]

Table 1. Results of a series of competition experiment between phenylboronic acid and *para*- and *meta*-substituted arylboronic acids.

	Substitution on arylboronic acid	Hammett constant (σ value)	Ratio of Products (substituted product : **4**)
1	4-MeO	–0.27	0.6 : 1.0
2	4-F	0.15	2.3 : 1.0
3	4-Cl	0.23	3.3 : 1.0
4	3-Cl	0.37	3.8 : 1.0
5	3-Br	0.39	4.4 : 1.0
6	4-CF_3	0.54	4.7 : 1.0

Hammett plots are commonly used to display correlation between σ values and relative rate constants (k_{rel}), which is a kinetic parameter. At this point in the study, we were unable to obtain kinetic data for this system (see section 2.6 later for detailed discussion of the issues encountered). However, making several assumptions, the ratio of products obtained can be used as an approximation of the relative rate (k_{rel}). Assuming that all consumed starting materials are converted to the arylated products only and that the mechanism is the same for all arylboronic acids, we can calculate an approximation for the relative rate (k_{rel}) from the product ratios shown in table 1 and use this to constuct a Hammett plot (Fig. 30).

However, the reaction is pseudo-zero order in boronic acid only at the initial stages of the reaction and later tends towards a positive order (see section 2.6 later for detailed kinetic analysis). Therefore, if product ratios at lower conversions were used, it is likely that the the ρ value obtained from this method of approximation may differ in magnitude, but its sign will remain the same (positive). Therefore, as the approximations required to use the ratio of

products obtained to calculate the relative rate are imprecise, we have not drawn any conclusions from the magnitude of the ρ value in the following plot. However, we can draw conclusions from the positive ρ value observed (see discussion below).

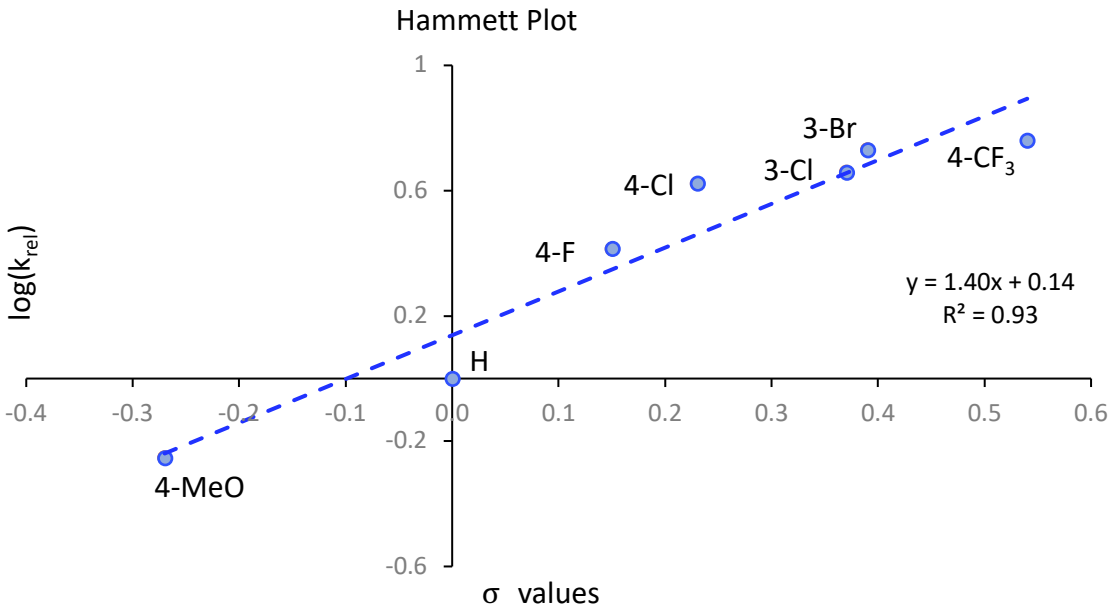
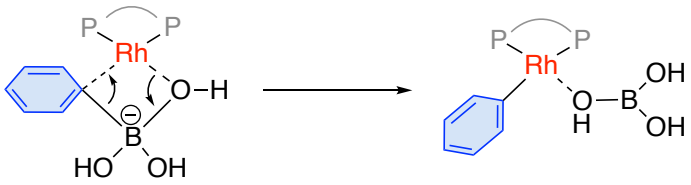


Figure 30. Hammett plot constructed from results of competition experiments with various *meta*- and *para*-substituted arylboronic acids. σ values = Hammett substituent constants, k_{rel} = relative rate.

The Hammett plot revealed a strong positive correlation between the ratio of products obtained and the Hammett constants of the substituents on the boronic acid (positive ρ value).[108] This trend indicates that more electron deficient arylboronic acids transmetalate faster. Their preferential and irreversible entry into the catalytic cycle, leads to the formation of one product in excess (up to 4.7:1 product ratio for (4-(trifluoromethyl)phenyl)boronic acid vs phenylboronic acid, Scheme 13).

Preferential transmetalation with electron deficient boronic acids could be due to increased Lewis acidity of the boron favouring formation of the boronate (Scheme 14). The stochiometric base used in this reaction may aid the formation of this boronate species.[111] Alternatively, or additionally, enhanced ability of the electron poor substrates to stabilise

partial negative charge during transmetalation could promote preferential transmetalation of more electron deficient boronic acids.[112,113]



Scheme 14. Schematic displaying the proposed mechanism of transmetalation.

Density functional theory (DFT) computation revealed an accumulation of negative charge in the aromatic ring in the transmetalation transition structure (TS) (Fig. 31) which is consistent with our experimental observations. Relative to the pre-transmetalation intermediate with a Rh-O-B linkage,[113,114] this elementary step is exergonic by 7.8 kcal/mol, consistent with irreversibility.

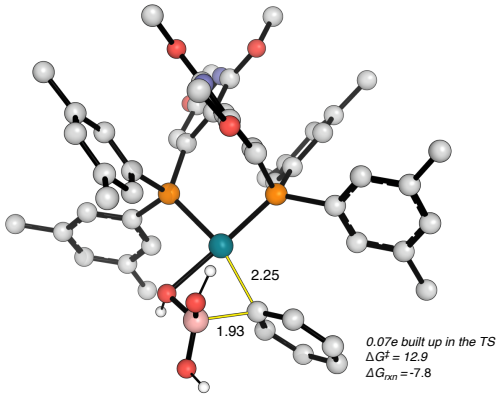


Figure 31. The DFT-computed transmetalation transition structure. ωB97X-D/6-31G(d), LANL2DZ(f). Structure visualised using PyMOL Molecular Graphics System.

2.5 DFT Calculations

Preliminary calculations (not shown) were performed by Dr. O. Sari. These were significantly expanded on by Dr. R. Ardkhean. Later, L. van Dijk finalised this work to produce the end results which are discussed in this section. This work was supervised by Prof. R. S. Paton.

DFT calculations were performed using the ωB97X-D functional.[115] In geometry optimisations, the split-valence 6-31G(d) basis set was used except for Rh where the LANL2DZ(f) (orbital

exponent of 1.35) effective core potential (ECP)/valence double-ζ basis set was used. Single point energy corrections were acquired with an implicit description of the reaction medium by SMD solvent model at the ωB97X-D/6-311+G(d,p) level of theory with the LANL2TZ(f) ECP/valence triple-ζ basis set for Rh. The counterion was not included in the optimisation of complex **V** or in the subsequent reductive elimination transition states. Retaining the chloride anion in an innate ion-pair gives rise to uncertainties regarding the accessible conformations, and accordingly, we have treated these species as infinitely separated ion-pairs.

The Gibbs energy profile shows three key elementary steps – transmetalation, oxidative addition and reductive elimination (Fig. 32). Subsequently, Sunoj and co-workers have independently reported an additional computational investigation of this system which culminates in a similar Gibb's energy profile, further supporting the key conclusions drawn from our DFT calculations.[116]

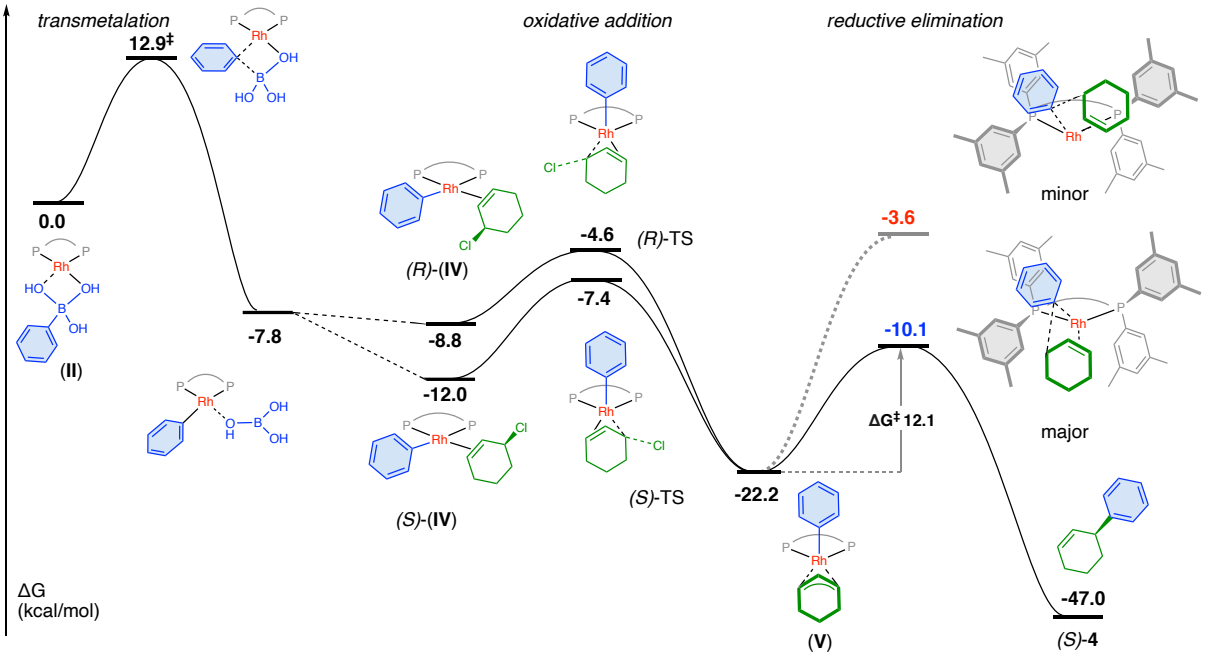


Figure 32. A condensed Gibbs energy profile for transmetalation, oxidative addition and reductive elimination (SMD(THF)-ωB97X-D/6-311+G(d,p), LANL2TZ(f) // ωB97X-D/6-31G(d), LANL2DZ(f)). *This figure combines conclusions drawn from a series of calculations designed, conducted and analysed by R.S.P, L.v.D, and R.A.*

As previously discussed, the transmetalation step is exergonic by 7.8 kcal/mol and therefore predicted to take place irreversibly. Complexation of the Rh-aryl species formed with both enantiomers of allyl chloride **3** leads to Rh-π-olefin complexes (*S*)- and (*R*)-(**IV**). Subsequent oxidative addition is predicted to occur irreversibly. The energy barrier of oxidative addition for (*R*)-**3** is calculated to be higher than that of (*S*)-**3**, which is in qualitative agreement with the natural abundance ^{13}C KIE experiments which suggest that oxidative addition of (*S*)-**3** occurs at a higher rate than oxidative addition of (*R*)-**3** (section 2.3). *Anti*-oxidative addition is predicted with the chloride leaving from the opposite face of the allyl unit to that which the Rh approaches (see Fig. 33 for favoured TS). *Syn*-oxidative addition TSs were also calculated but found to have higher reaction barriers. Oxidative addition of both enantiomers of racemic **3** leads to a common η^3 intermediate (**V**) where the stereochemical information of **3** is lost. This mechanistic feature is key to enabling the use of a racemic electrophile in this reaction.

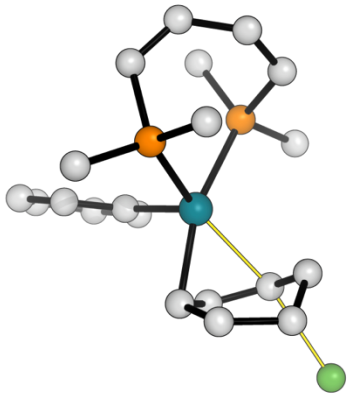


Figure 33. Favoured *anti* S_N2' oxidative addition TS. Structure visualised using PyMOL Molecular Graphics System and shown with cropped ligand.

This common Rh-intermediate (**V**) then undergoes enantiodetermining reductive elimination where the new stereogenic centre is predicted to form irreversibly.[117] There is a large calculated difference in energy between the reductive elimination TSs ($\Delta\Delta G^{‡}$ = 7.2 kcal/mol). This is consistent with both the sense and very high levels of enantioselectivity observed experimentally ((*S*)-**4**, >99% ee). Steric effects between the ligand and allyl fragment lead to

significant differences in key bond distances between the two competing TSs. Analysis of the catalytic pocket highlights the narrow groove imposed by the ligand in which the reductive elimination must take place (Fig. 34).[118] The minor TS displays weaker coordination between alkene and Rh, and is a later TS (i.e. much shorter C-C forming bond compared to the favoured structure). This is consistent with the large energy difference calculated.

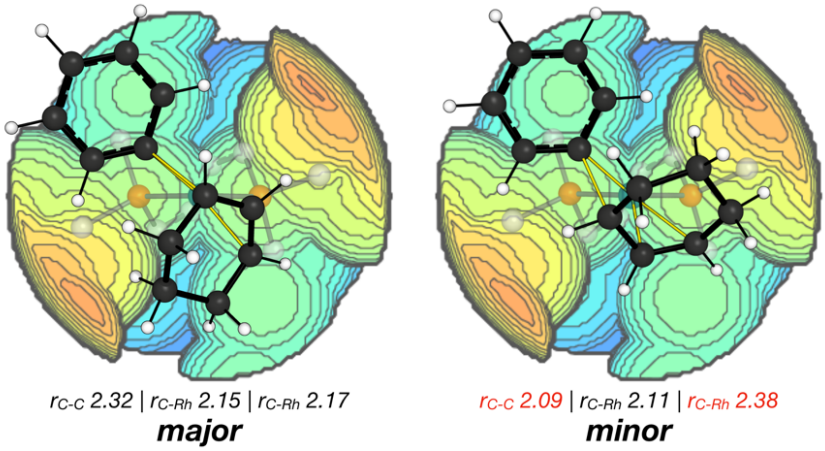


Figure 34. Simplified models showing the origins enantioselectivity. Reductive elimination TSs for **3** with catalytic pocket images generated using SambVca 2.1.52.[118]

2.6 Reaction Kinetics

Kinetic analysis of a reaction can be a powerful tool in mechanistic investigations.[78,119] We first attempted to follow reaction kinetics by *in situ* NMR spectroscopy. However, irreproducible results were obtained which we attribute to lack of stirring. We found that consistent stirring speed was required in order to obtain reproducible results.

Next, we trialled a method involving sampling of a batch reaction. Samples were taken from the reaction at timed intervals, quenched and the concentration of product quantified by ^{1}H-NMR analysis using trimethoxybenzene as an internal standard. We found that monitoring the depletion of starting material was not reliable as the allyl chloride is somewhat volatile. Instead, we decided to measure the production of product which was a more reliable quantitative measure (Fig. 35). The reaction proceeds at a faster rate than was anticipated

and therefore a reduced temperature of 30 °C was used to slow the reaction rate for practical monitoring.

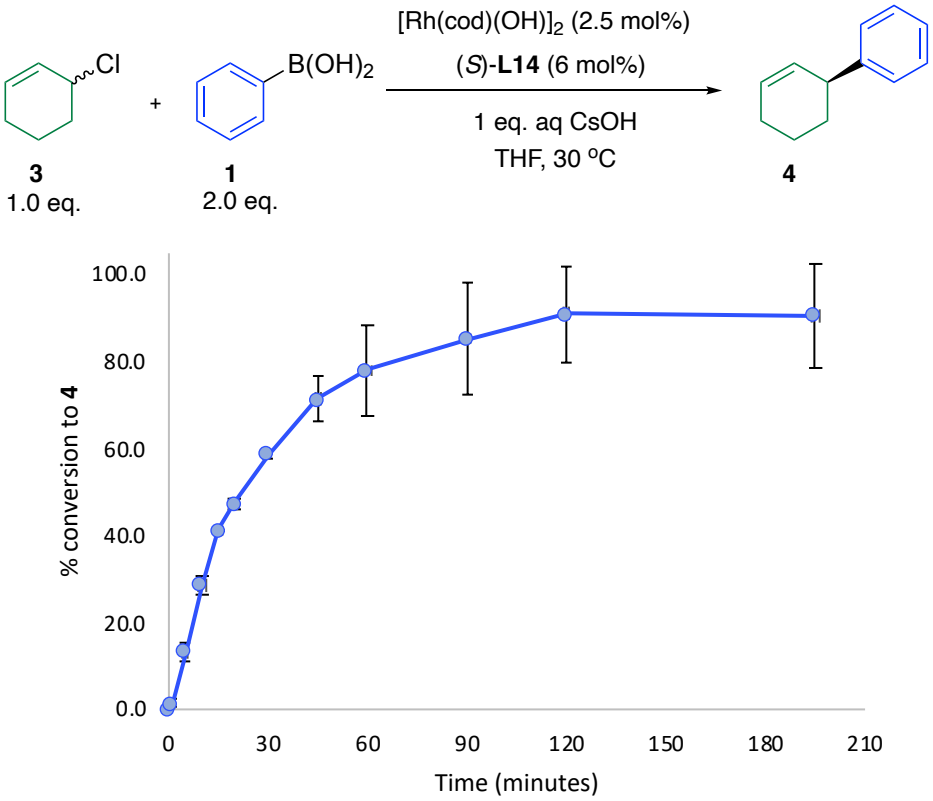


Figure 35. Kinetic data for the Rh-catalysed reaction of phenylboronic acid (**1**) and cyclohexenyl chloride **3**. Average of triplicate experiments shown with standard deviation error bars.

Further issues were encountered while attempting to record meaningful kinetic data using this method. Considerable variation in rates were found between reactions conducted with various commercial sources of (*S*)-**L14** and $[Rh(cod)(OH)]_2$, however kinetic data was found to be reproducible within batches. Using (4-fluoro-3-methylphenyl)boronic acid (**1a**) in place of $PhB(OH)_2$ (**1**) allowed for temporal concentrations to be determined by quantitative ^{19}F NMR using 4,4'-difluoro-1,1'-biphenyl as an internal standard for integration, which proved to be a more reliable analysis technique. Samples were taken at 90-second intervals from the reaction mixtures, over a period of 720 seconds, and all runs were conducted in triplicate.

The kinetics of the Rh-catalysed addition of boronic acid **1a** to **3** were explored under a range of conditions with systematic variation of the total Rh concentration (Fig. 36) and of the initial

concentrations of **3** (Fig. 37a), and of **1a** (Fig. 37b). Experiments examining catalyst inhibition were also performed (Fig. 38).

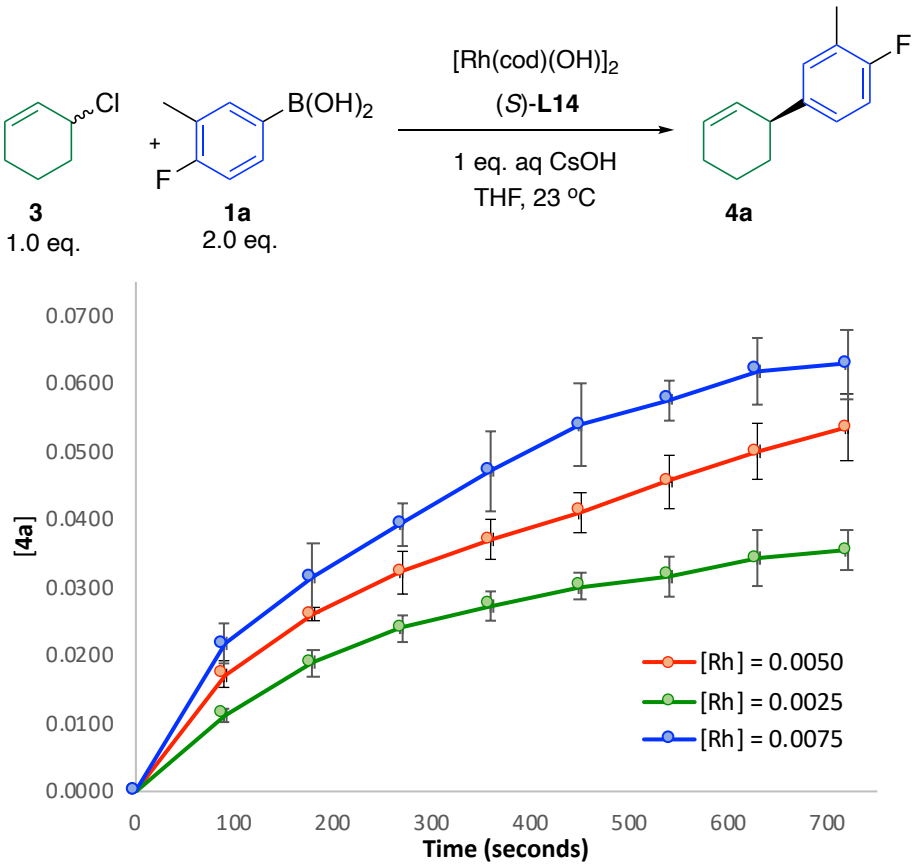


Figure 36. Kinetic data for the Rh-catalysed reaction of (4-fluoro-3-methylphenyl)boronic acid (**1a**) and cyclohexenyl chloride **3** with systematic variation of the total concentration of Rh with $[\mathbf{3}]_0$ = 0.100 M, $[\mathbf{1a}]_0$ = 0.200 M. Average of triplicate experiments shown with standard deviation error bars. Concentrations reported in mol/L.

Reaction kinetic data can be analysed using a number of different techniques.[119] Variable-time normalisation analysis is a visual kinetic analysis method.[120] To find the order in catalyst using this graphical kinetic analysis method, the profiles of reactions run with different catalyst loadings are visualised by plotting the concentration of the product against a normalised time scale, $t[cat]_0^n$ (where t = time, $[cat]_0$ = the initial concentration of catalyst and n is an arbitrary variable). These graphs are then visually compared. Different values for n are tested and the n value that results in curves which overlay gives the order in catalyst.[121] Analysis of the data shown in Figure 36 using this method, indicates that the reaction proceeds with first order

dependence on $[Rh]_{TOT}$ (i.e. when n = 1, the graphs overlay). This analysis method allows direct comparison of several data points across the entire reaction profile. This is particularly useful in cases where the reaction rate is fast and *in situ* monitoring is not available as accurately determining the order *via* extraction of the initial rates would be difficult.[121]

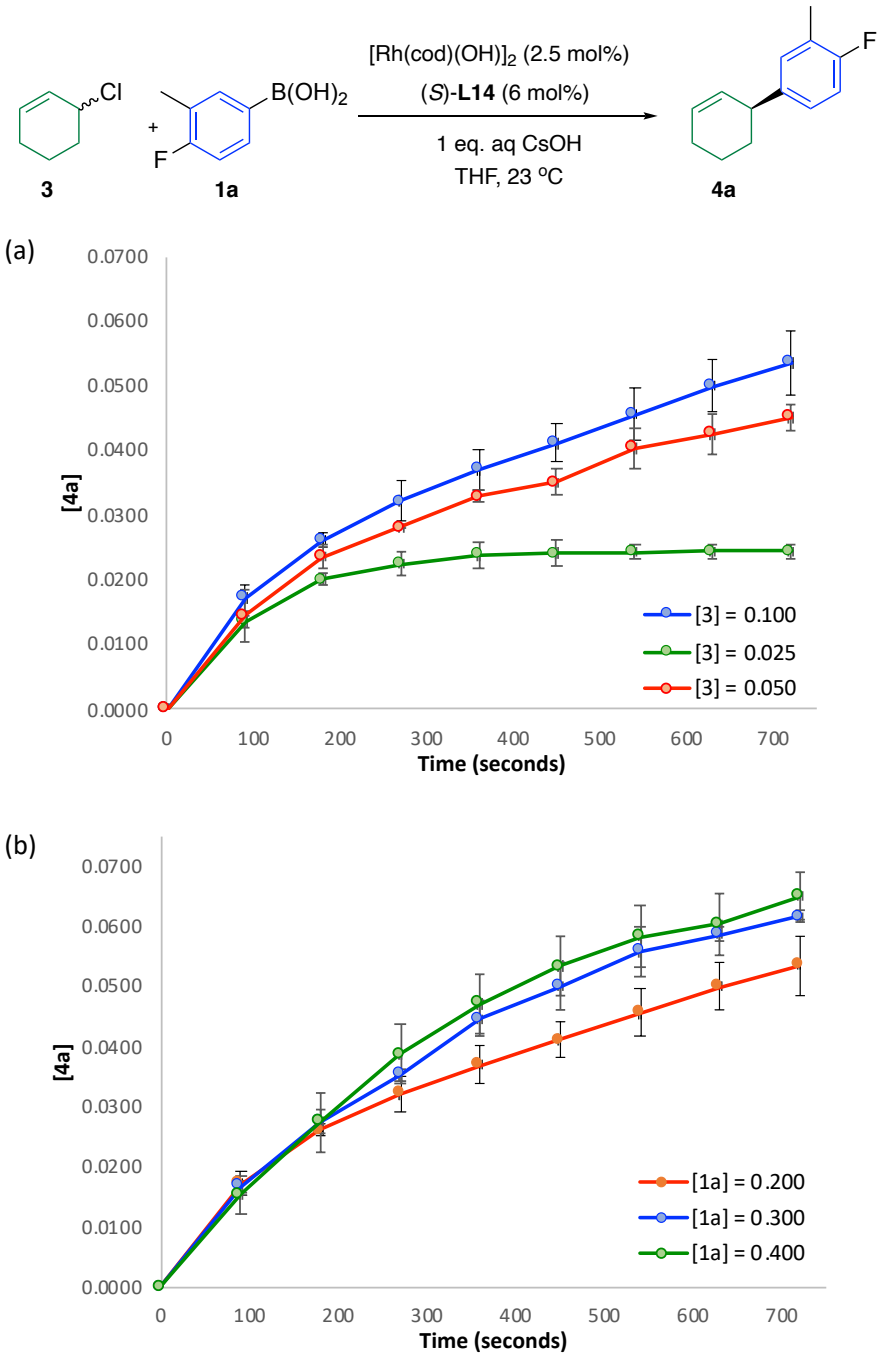


Figure 37. Kinetic data for the Rh-catalysed reaction of **1a** and **3** with systematic variation of the initial concentration of (a) cyclohexenyl chloride **3** ([Rh] = 0.005 M, $[\mathbf{1a}]_0$ = 0.200 M) and (b) (4-fluoro-3-methylphenyl)boronic acid **1a**. ([Rh] = 0.005 M, $[\mathbf{3}]_0$ = 0.100 M). Average of triplicate experiments shown with standard deviation error bars. Concentrations reported in mol/L.

Analysis of the data displayed in Figure 37 revealed that a more complicated relationship was present for these components. When visual kinetic analysis of these plots using variable-time normalisation analysis was attempted, no value for n could be found that allowed the graphs to overlay across all data points. The orders in cyclohexenyl chloride **3** and arylboronate **1a** change over the course of the reaction, with no simple relationships dominant for either component. At this point, we decided that a deriving a kinetic model based on our mechanistic proposal would allow us to better interpret this more complex data. We enlisted the help of reaction kinetics expert Prof. G. C. Lloyd-Jones who derived a pseudo steady-state rate equation based on our proposed mechanism (equation 1, see later).

The kinetic profiles obtained indicate progressive inhibition over the course of the reaction. Inhibition by co-products of the system was investigated. Experiments with exogenous boric acid (**2**) suggest inhibition arises from the accumulation of $Cs[B(OH)_4]$ by-product (Fig. 38). We propose that this co-product (**2**) competes with the arylboronate for coordination to Rh-OH complex (**I**) (K_{inh}, see Fig. 39). Inhibition was also observed in experiments with exogenous caesium chloride (Fig. 38). In this case, we believe that pre-treatment of the system with caesium chloride inhibits the formation of active catalytic species (**I**). Instead, a Rh-Cl species is formed which undergoes slow conversion to complex **II**. Other potential modes of catalyst inhibition, such as product inhibition, were considered but were not experimentally evaluated.

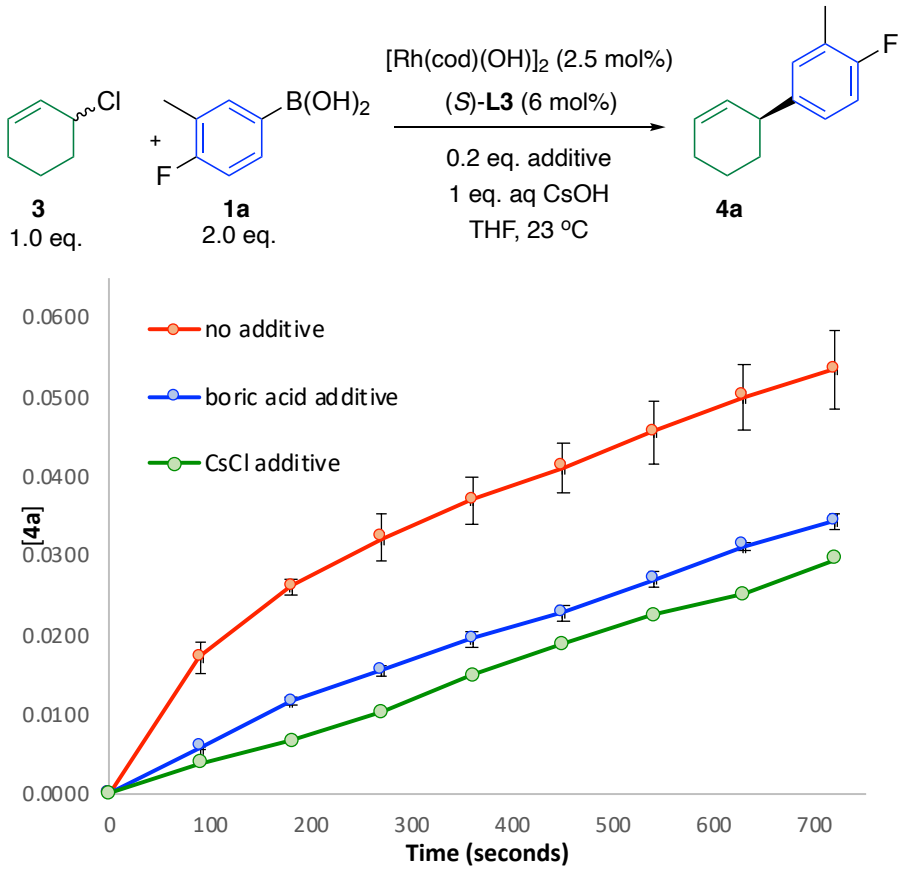


Figure 38. Examining potential modes of inhibition. [Rh] = 0.005 M, $[\mathbf{3}]_0$ = 0.100 M, $[\mathbf{1a}]_0$ = 0.200 M.

The experimental datasets obtained could be satisfactorily simulated using a kinetic model based on all of the key mechanistic features (see Fig. 39) evaluated in a pseudo steady-state rate equation (Equation 1) with five concentration terms ($[Rh]_{TOT}$, [**4a**], [**2**], [**1a**] and [**3**]) and three simplified empirical constants, *a*, *b*, and *c*. For clarity, inhibition by caesium chloride is not included in this model.

Equation 1

$$\frac{d[\mathbf{4a}]}{dt} \approx \frac{[Rh]_{TOT}}{a + \frac{b}{[\mathbf{3}]} + \frac{c\,[\mathbf{2}]}{[\mathbf{1a}]}}$$

a = 9.0±2.6 s
b = 2.3±0.5 ×10^{-1} M s
c = 4.2±0.3 ×10^{2} s

Apparent orders in cyclohexenyl chloride **3** and arylboronate **1a** evolve between limits of pseudo zero-order to first-order as the reactions proceed, with no simple relationships dominant for either component. The reaction rate is initially independent of boronic acid **1a** and allyl chloride **3** concentrations (pseudo zero-order in both components). At this early stage of the reaction, reductive elimination is the turnover rate controlling step. Our DFT

calculations (Fig. 32), indicate that reductive elimination or transmetalation would be the turnover rate controlling step(s). However according to our kinetic model, the speciation of rhodium evolves as the reactions proceed, with no resting state dominant throughout, leading to the turnover rate controlling event(s) varying between reductive elimination, and boronate transmetalation competing with boric acid (**2**) complexation (see Fig. 39). As boric acid (**2**) by-product builds up, the order in arlyboronate **1a** tends towards pseudo first-order and boronate transmetalation competing with boric acid (**2**) complexation becomes turnover rate controlling. Kinetic dependence on allyl chloride is only evident at very low concentrations, such as in the very final stages of reaction. Under these extremely limiting conditions at the very final stages of the reaction, the dominance of **V** and **VI** diminishes due to exhaustion of the cyclohexenyl chloride (**3**).

In Figure 39, we have not specified the identity of the counterion (X^-) in complex **V**. This counterion was initially assumed to be a chloride anion, but an arylboronate counterion is also plausible ($ArB(OH)_3^-$). In the latter case, catalyst turnover could occur *via* the direct formation of complex **II** after reductive elimination, with complex **I** only being relevant in the first catalyst turnover. However, in accordance with the data presently available, our kinetic model is based on and consistent with the catalytic cycle shown in Figure 39.

It is also worth noting that a kinetic model based on the scenario where oxidative addition occurs before transmetalation is also consistent with our experimental kinetic data (K_{ene} and k_{OA} occurring immediately after reductive elimination of **4a**, and before K_{inh}, K_{co} and k_{TM} will give the same steady state approximation). However, that scenario is inconsistent with our preliminary NMR studies (section 2.1) and therefore we have proposed the cycle shown in Fig. 39.

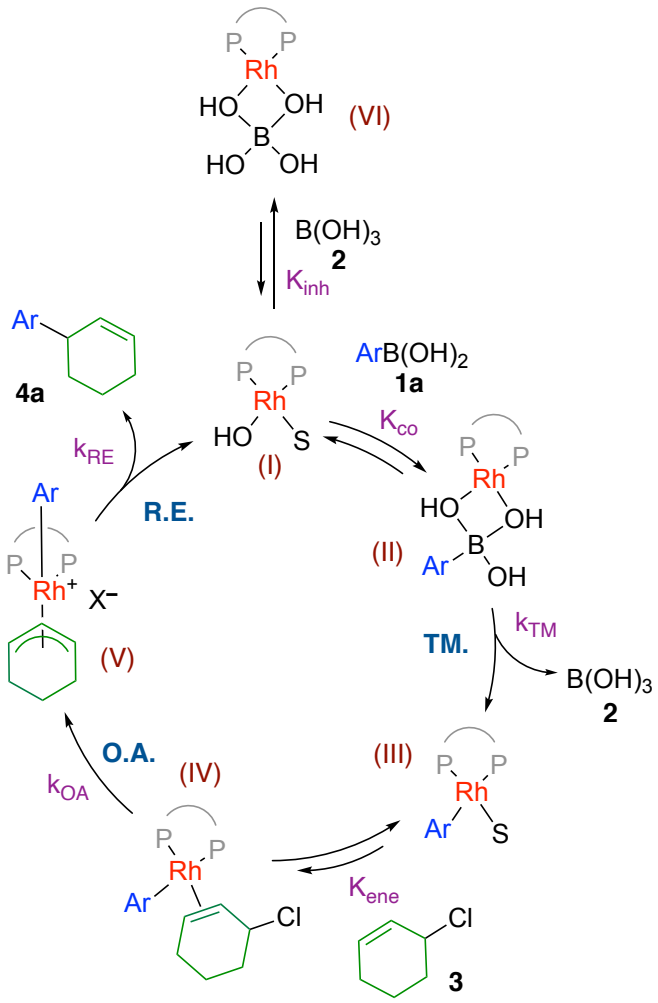


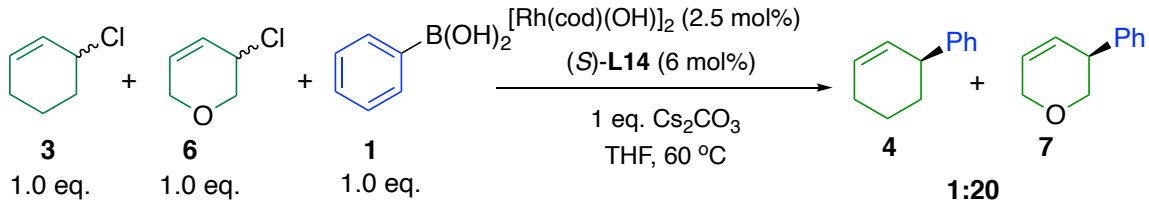
Figure 39. Scheme for Rh-catalysed reaction of arylboronic acid (**1a**, Ar = 4-fluoro-3-methylphenyl) with cyclohexenyl chloride (**3**) to generate 3-arylcyclohex-2-ene (**4a**), with inhibition by exogenous and endogenous $B(OH)_3$ (**2**), employed for the steady state model. The model proceeds *via* three key irreversible steps; transmetalation (TM), oxidative addition (O.A.) and reductive elimination (R.E.). Acid/ate speciation is not considered. S = Solvent or vacant site.

To conclude, these reaction kinetics studies support our proposed mechanism as the experimental datasets obtained can be satisfactorily simulated using a kinetic model based on the key mechanistic features of our proposed catalytic cycle (Fig. 39). Additionally, these studies revealed progressive inhibition over the course of the reaction and provided us with insight into the rate determining events.

2.7 Arylation with Heterocyclic Allyl Chlorides

Aside from cyclohexenyl chloride (**3**), this Rh-catalysed arylation reaction can also tolerate a range of other cyclic allyl halide coupling partners, including heterocyclic allyl chlorides.[54] We were interested to see what further insights into the mechanism we could uncover from examining this Rh-catalysed arylation with alternative electrophiles.

We calculated the energy profile for the pyranyl substrate **6** and found that the reaction barrier (activation energy for oxidative addition) is much lower than that of **3**. This presented an opportunity to experimentally evaluate our computational study. We performed a competition experiment between allyl chlorides **6** and **3** (Scheme 15) and observed a 20:1 product ratio in favour of pyranyl product **7**. This supports oxidative addition being faster for **6**, which qualitatively agrees with the results of our DFT calculations. This experimental result is also consistent with our hypothesis of irreversible oxidative addition.



Scheme 15. Competition experiment with allyl chlorides (±)-**3** and (±)-**6**.

Both our ^{13}C KIE experiments (section 2.3) and DFT calculations (section 2.5) indicate a difference in the rate of oxidative addition for the two enantiomers of racemic **3**. This would result in an increase in the ee of **3** as the reaction evolves. However, the ee of **3** could not be reliable measured and enantiopure **3** could not be synthesised which prevented us from directly examining the relative rate of oxidative addition of the enantiomers of **3**. Piperidinyl allyl chloride **8** is configurationally stable and could therefore be used to probe this effect.[122] We monitored the ee of **8** under the conditions previously used to probe the ^{13}C KIE and observed the ee of **8** increasing from 0 to 94% ee over 1 hour (Fig. 40a). This supports the

proposed differing rates of oxidative addition for the two enantiomers of the substrate. This is also consistent with our hypothesis that fast interconversion of substrate enantiomers is not required for this transformation.

Interestingly, under alternative conditions previously optimised for the synthesis of **9** using (S)-Cl-MeO-BIPHEP (**L15**), enantioenrichment of **8** was not observed (Fig. 40b). This observation was unchanged at a reduced temperature of 30 °C. We concluded that the resolution of starting materials is likely a ligand effect. These ligands impose different steric environments, which likely results in different $\Delta\Delta G^{\ddagger}$ values for the oxidative addition TSs of the two enantiomers of the allyl chloride. When **L15** is used (Fig. 40b), both enantiomers of **8** may react at comparable rates due to reduced steric constraints in the oxidative addition TSs.

Under all conditions examined, the ee of **9** was found to be constant as a function of time (Fig. 40). This supports the proposition that reductive elimination is the stereodetermining step.

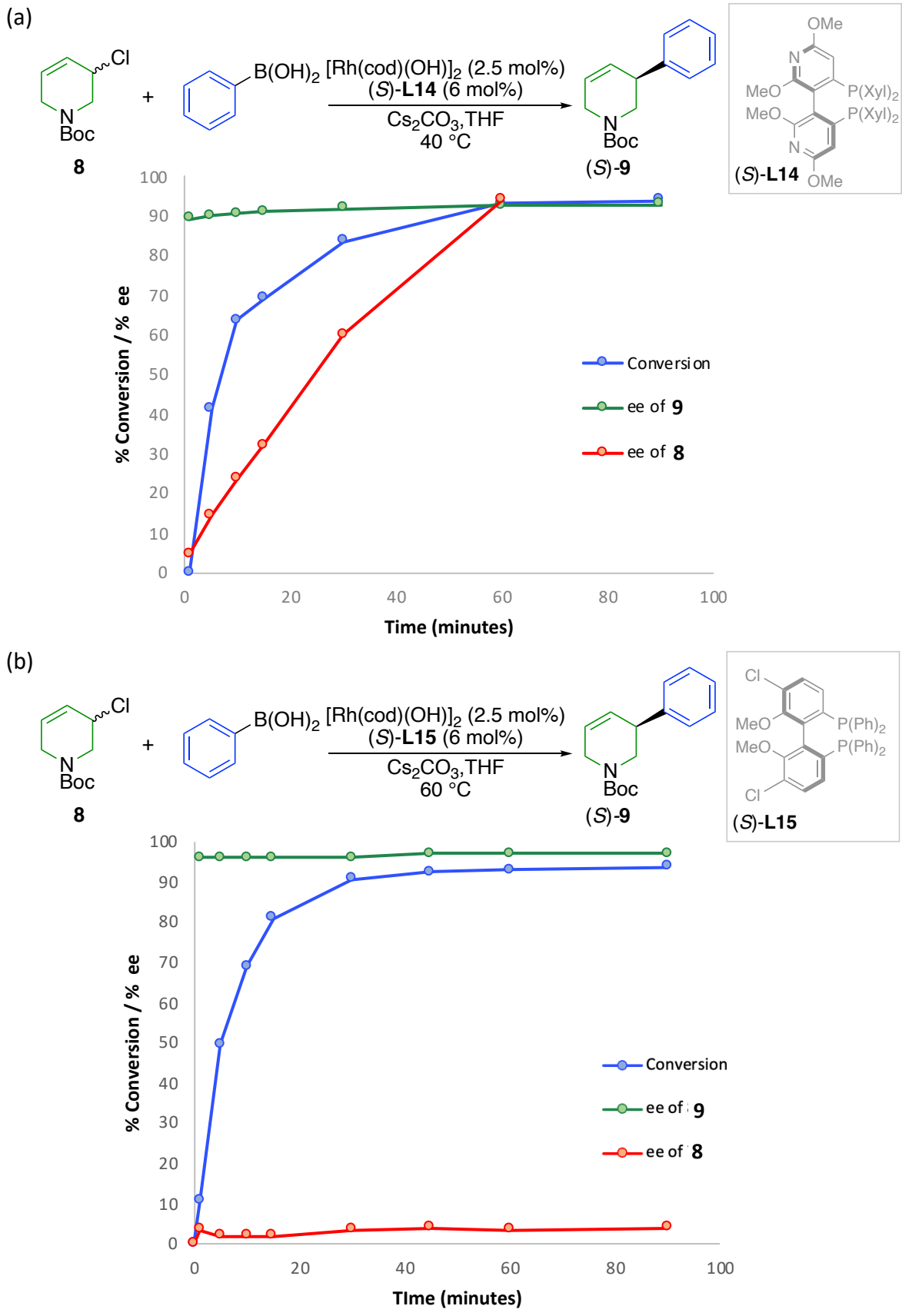


Figure 40. (a) Measuring the ee over the course of the Rh-catalysed coupling of **1** and **8** with **L14**. (b) Measuring the ee over the course of the Rh-catalysed coupling of **1** and **8** with **L15**.

Dr. S. Karabiyikoglu developed a method for the synthesis of enantioenriched tetrahydropyridine allyl chlorides *via* Cu-catalysed kinetic resolution (Fig. 41a).[122] Enantioenriched (*R*)-**8** (94 % ee) was synthesised by Dr. S. Karabiyikoglu (Fig. 41a) and subjected to reaction conditions with each of the two enantiomers of **L15** (Fig. 41b). With (*S*)-**L15**, we obtained (*S*)-**9** (95 % ee), whereas with (*R*)-**L15**, (*R*)-**9** (–95 % ee) was obtained. This demonstrates that the absolute stereochemistry of the product is set due to the stereochemistry of the ligand and not due to the stereochemistry of the electrophilic coupling partner (**8**). This is consistent with our proposed formation of a common intermediate after oxidative addition where the stereochemistry of the starting material is lost, followed by a reductive elimination where the stereochemistry of the product is set.

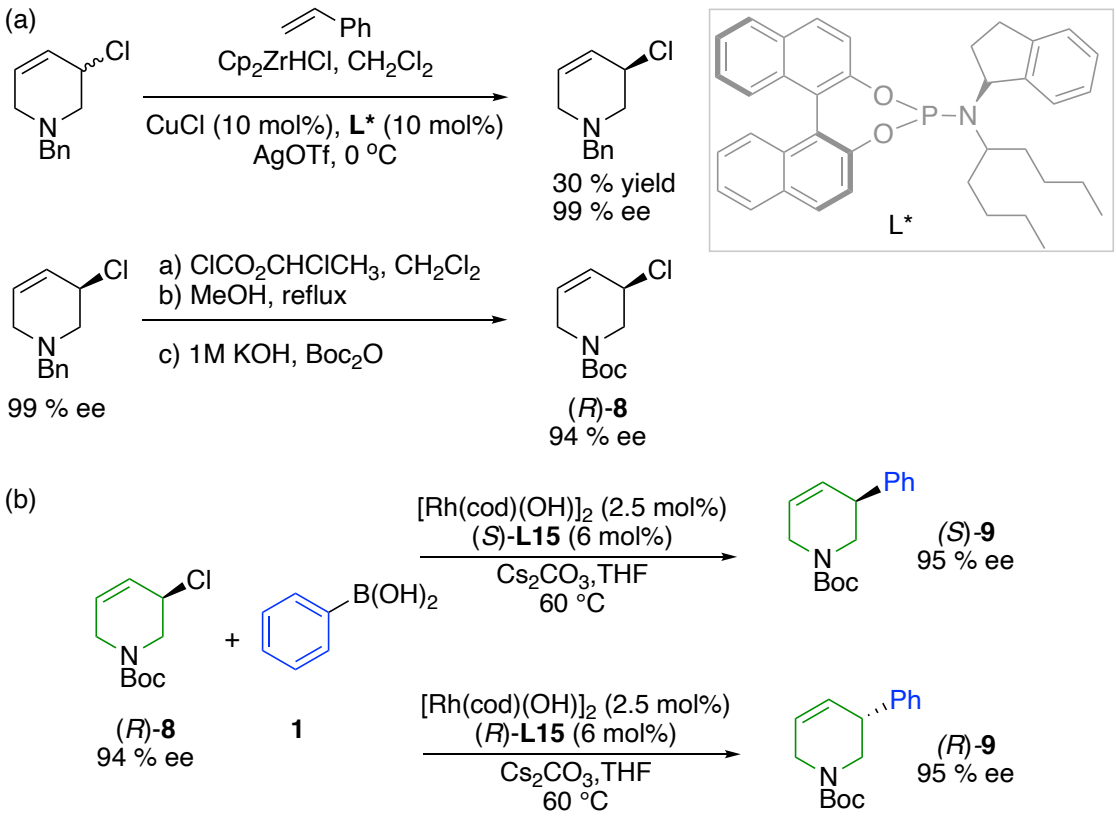


Figure 41. (a) Synthesis of enantioenriched (*R*)-**8** as described by Karabiyikoglu and co-workers.[122] (b) Arylation of enantioenriched (*R*)-**8** with both enantiomers of **L4**. *Experiments were performed by S.K.*

Deuterium-labelled substrates have previously been successfully used to assess the stereochemical outcome of the individual steps of allylic substitution reactions.[123-126]

Isotopically labelled **8**-*d* was synthesized with a deuterium atom at the vinylic (C_3) position.[122] Addition to (±)-**8**-C_3-*d* gave a 1:1 ratio of pseudo-regioisomeric products with deuterium at C_3 and C_5 (Fig. 42a). The ^{2}H-label at the vinylic position in the starting material precludes the formation of a common intermediate from both enantiomers of the starting material after oxidative addition. Therefore, we propose that two different η^3 Rh-complexes would be formed after oxidative addition of this ^{2}H-labelled racemic substrate (Fig. 42b). One η^3 Rh-intermediate, formed from one enantiomer of the starting material, results in one product pseudo-regioisomer. The other η^3 Rh-intermediate generates the alternative pseudo-regioisomeric product.

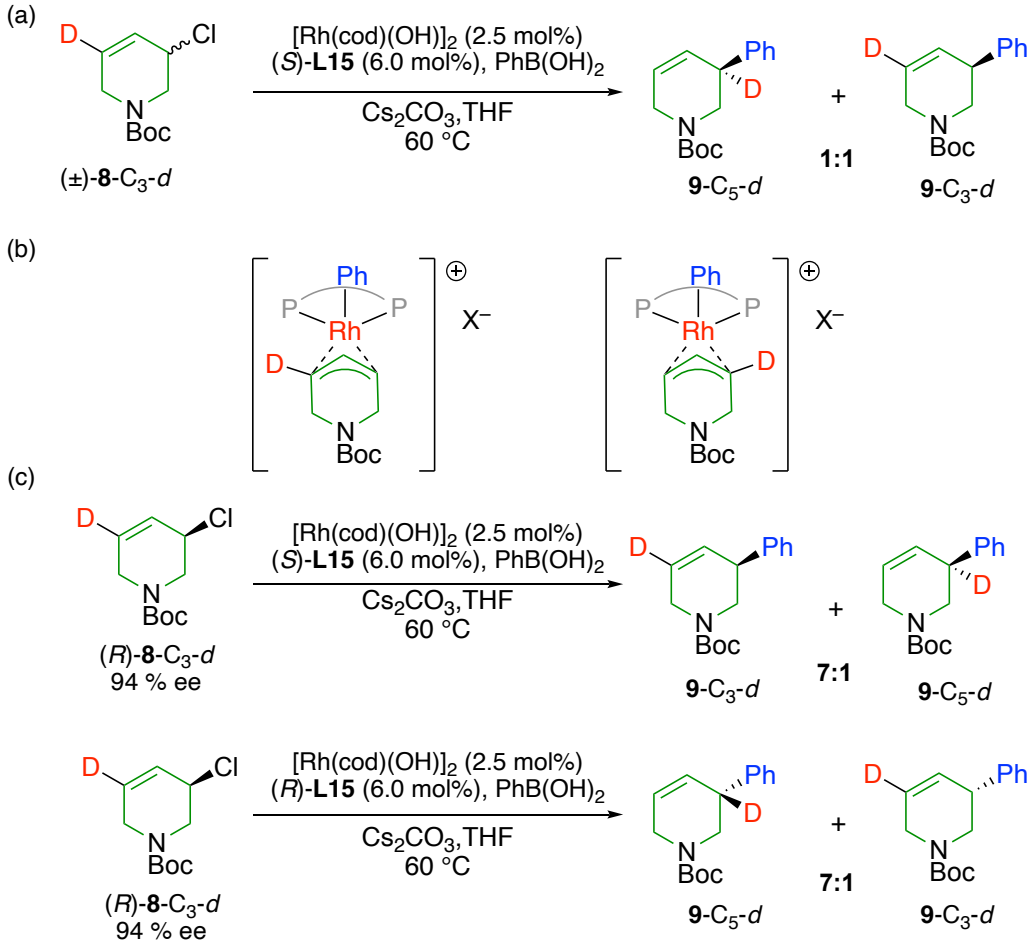


Figure 42. (a) Arylation of (±)-*d*-**8**. (b) η^3 Rh-complexes formed after oxidative additions. (c) Arylation of (*R*)-*d*-**8** with both enantiomers of **L15**. *This figure shows experiments performed by S.K., with interpretation of the results in terms of mechanistic implication conducted by L.v.D. and S.P.F.*

To test this hypothesis, enantioenriched ^{2}H-labelled **8** was synthesised. When (*R*)-**8**-C_3-*d* (94 % ee) was subjected to optimised reaction conditions with (*S*)-**L15**, the majority of deuterium remained at C_3 in product (*S*)-**9**, whereas with (*R*)-**L15**, the majority of deuterium was found at the allylic position (C_5) of (*R*)-**9** (Fig. 42c). The products generated have an excess of the deuterium label at one position (allylic or vinylic) depending on the stereochemistry of the ligand used which is consistent with our proposal.

However, with our proposed mechanism of *anti*-oxidative addition, we anticipated the arylation of (*R*)-**8**-C_3-*d* with (*S*)-**L15**, would give the majority of deuterium at C_5 in the product, and with (*R*)-**L15**, the majority of deuterium would be found at C_3 (Fig. 43a). Surprisingly, we obtained the opposite results in terms of observed pseudo-regioisomer preference (Fig. 42c). These experimental results suggest that with **8**, *syn*-oxidative addition (rather than *anti*-oxidative addition) is the major pathway (Fig. 43b). This is a significant deviation from our proposed mechanism of *anti*-oxidative addition for cyclohexenyl chloride **3** (section 2.5).

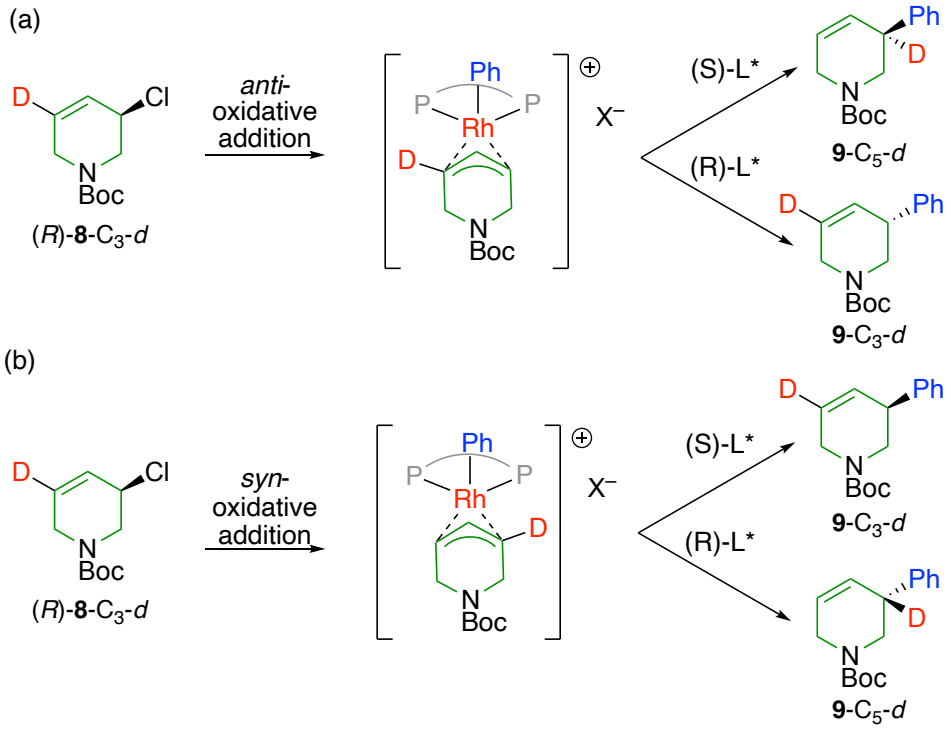
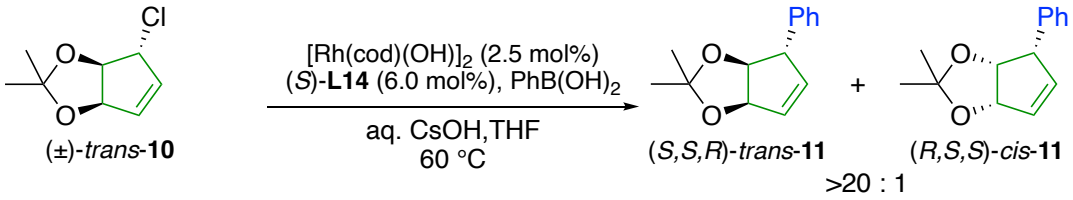


Figure 43. Simplified schematic diagram displaying (a) our expected results based on the *anti*-oxidative addition mechanism previously proposed. (b) *Syn*-oxidative addition accounts for the results obtained.

In each case, there is a small percentage of deuterium scrambling (7:1 ratio, Fig. 42c) which may be due to a 7:1 ratio of *syn*- and *anti*-oxidative addition occurring. Alternatively, this may also be a result of slow racemization of **8** over the course of the reaction, or isomerisation after oxidative addition *via* nucleophilic displacement with a Rh(I) species, analogous to mechanistic pathways observed in Pd(0)-catalysis.[127]

2.8 Arylation with Diastereomeric Allyl Chlorides

The consequence of an irreversible oxidative addition is that the diastereoselectivity is determined in this step. Our group has previously reported a Rh-catalysed enantioselective addition to fused bicyclic substrates (Scheme 16).[56] This transformation proceeds with overall retention of the relative stereochemistry. The stereochemical results observed are consistent with *syn*-oxidative addition to the racemic bicyclic starting material.



Scheme 16. Previously reported arylation of bicyclic substrate (**10**) showing experimental evidence for *syn*-oxidative addition.[56]

To understand this observation, we calculated the *syn*- and *anti*-oxidative addition transition states for **10** (see Fig. 44 for favoured *syn*-TS). Our computed structures reveal steric interaction between the ligand and the acetal bridge of **10** is key to determining the facial selectivity of oxidative addition. This selective oxidative addition step controls the diastereoselectivity observed in this system, while reductive elimination remains responsible for the absolute stereochemistry.

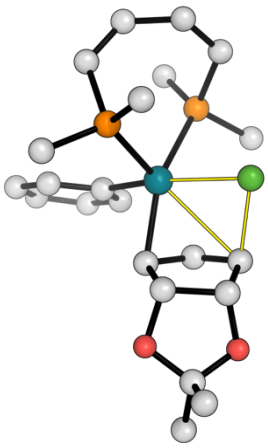
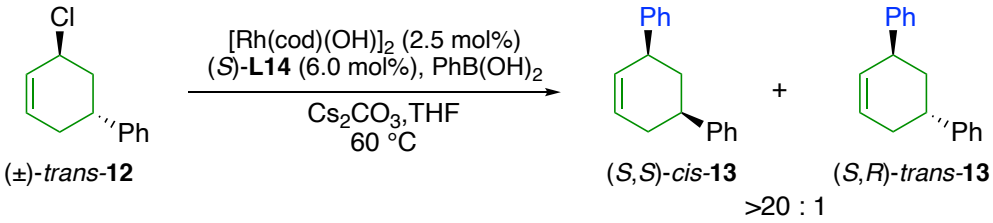


Figure 44. Favoured *syn*-oxidative addition TS for bicyclic chloride **10**. Visualised using PyMOL Molecular Graphics System and shown with cropped ligand for clarity.

Previously, we discussed the Gibbs energy profile for cyclohexenyl model substrate **3**, where our calculations predicted that *anti*-oxidative addition is favoured (section 2.5). However, this system does not allow for experimental examination of the stereochemical outcome of the oxidative addition step. Our group previously reported asymmetric addition to phenyl-substituted allyl chlorides,[53] where the *trans* stereoisomer of allyl chloride (**12**) gave overall enantioselective inversion to *cis*-**13** (Scheme 17). This experimental result is indicative of *anti*-oxidative addition.



Scheme 17. Previously reported arylation of diastereomeric 5-phenyl substituted allyl chloride (**12**) showing experimental evidence for *anti*-oxidative addition.[53]

Therefore, we have observed experimentally[53,56] and now validated computationally that the aryl-Rh species can oxidatively add to the electrophiles *via syn*- or *anti*-oxidative addition pathways, depending on the steric accessibility of the substrate. This oxidative addition step

controls diastereoselectivity and is influenced by the substrate, while the enantioselectivity is dictated by the catalyst and set in the reductive step.

3. Conclusions

Combined experimental and computational studies have been used to elucidate a proposed mechanism for the highly enantioselective Rh(I)-catalysed coupling of arylboronic acids with racemic allylic halides. The reaction proceeds *via* three key irreversible steps; transmetalation, oxidative addition and reductive elimination (Fig. 45). The active catalytic species is monomeric in Rh and ligand and irreversible transmetalation between boron and Rh is the first step in the cycle. Hammett analysis revealed an increased rate of transmetalation for electron deficient aryl species which may be attributed to increased Lewis acidity of the boron favouring formation of the boronate and/or enhanced ability of the electron poor substrates to stabilise partial negative charge during transmetalation. Experimentally observed natural abundance ^{13}C KIEs in combination with theoretical calculations were key to demonstrating that oxidative addition occurs irreversibly with both enantiomers of the racemic substrate, with addition of one enantiomer occurring at a faster rate than the other. DFT calculations revealed a common pseudo-symmetrical η^3 Rh-allyl complex is formed from the irreversible oxidative addition of Rh-aryl intermediates to both enantiomers of the racemic substrates. Subsequently, the enantiodetermining reductive elimination sets the stereochemistry of the product. Reaction kinetics studies showed that experimental datasets obtained could be satisfactorily simulated using a kinetic model based on these key mechanistic features.

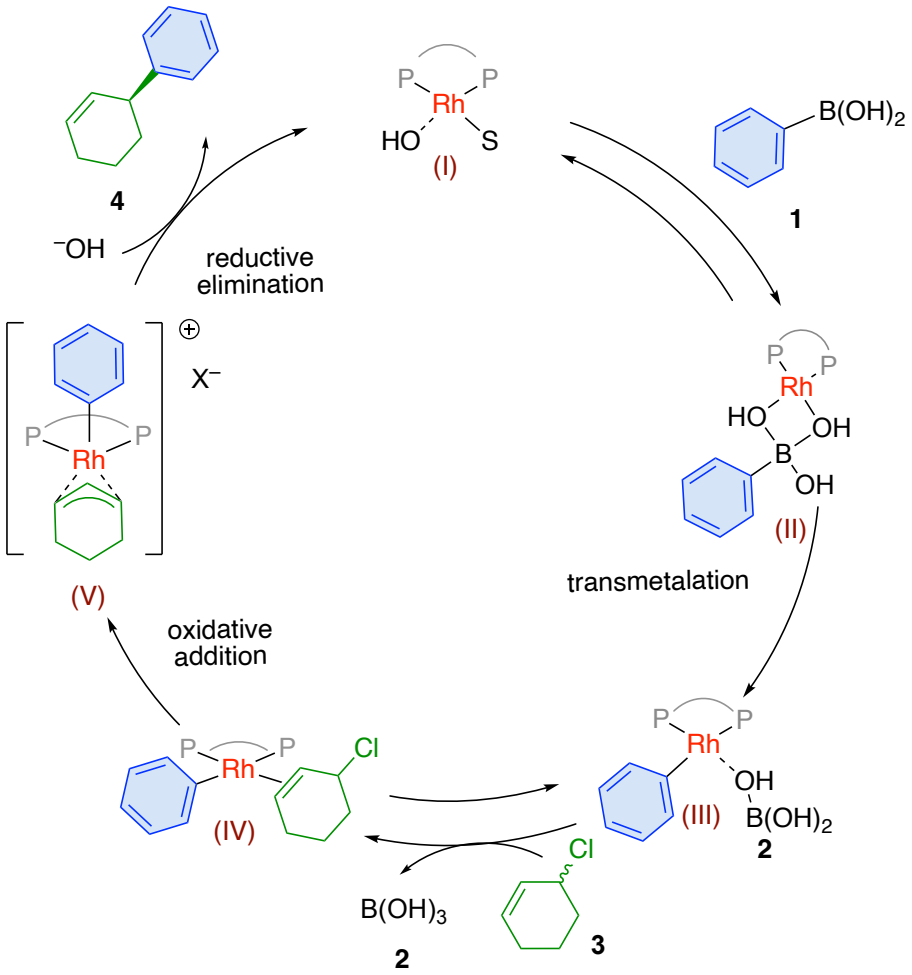


Figure 45. A simplified catalytic cycle showing the proposed mechanism in this work with key steps including transmetalation, oxidative addition and reductive elimination.

Further insights were gained by examining the reaction with alternative electrophilic coupling partners such as heterocyclic, configurationally stable, deuterium labelled and diastereomeric allyl chlorides. We found that changing the ligand or substrate used in this transformation has implications for the mechanism. Although the key steps in the catalytic cyclic are likely the same with the alternative coupling partners and ligands examined, it is interesting to note the mechanistic discrepancies observed. Oxidative addition can occur *via* a *syn*- or *anti*-pathway depending on the steric accessibility of the substrate. The diastereoselectivity is determined

in the oxidative addition step and is influenced by the substrate, while the absolute stereochemistry of the product is set in the reductive elimination step (Fig. 46).

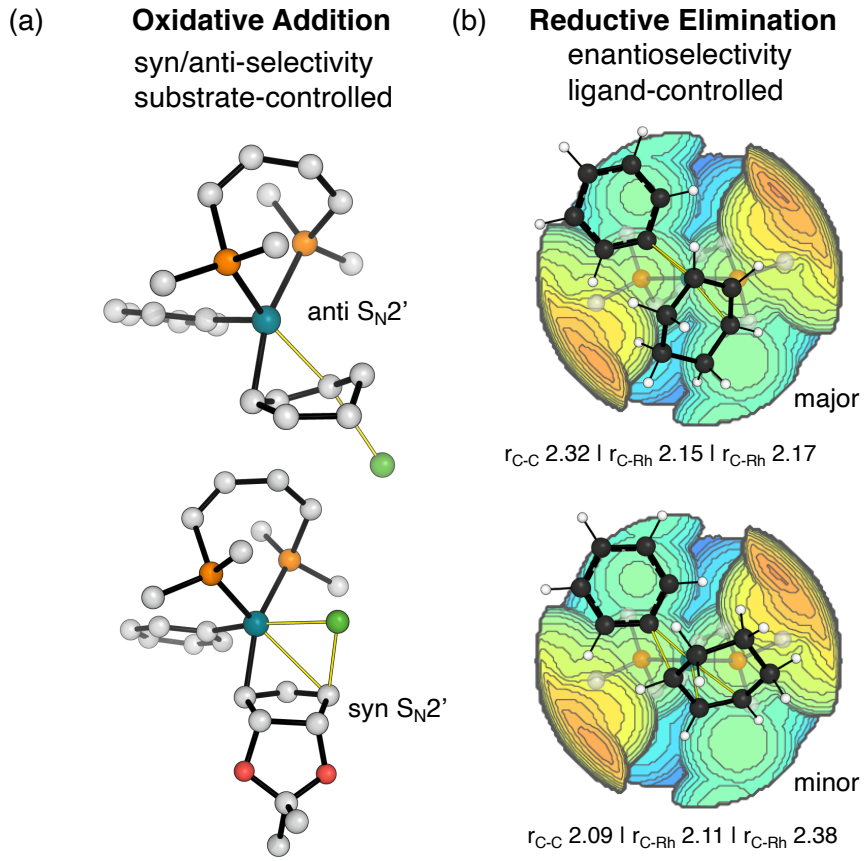


Figure 46. Simplified models showing the origins of (a) diastereoselectivity and (b) enantioselectivity in this Rh(I)-catalysed asymmetric arylation.

We anticipate that this study will contribute towards the wider understanding of Rh-catalysed asymmetric allylic addition reactions and asymmetric chemistry with racemic substrates in general.

Chapter 3: Rhodium-Catalysed Regiodivergent Suzuki-Miyaura Couplings to form Quaternary Stereocentres

1. Introduction

1.1 Quaternary Stereocentres

Quaternary stereocentres are ubiquitous motifs prevalent in natural products and biologically active compounds (Fig. 47).[128,129] Quaternary stereocentres are a useful way to introduce three-dimensionality into molecules, which can be highly desirable in drug discovery programs.[7,130] Many top selling drugs contain quaternary centres (e.g. morphine, Fig. 47), however, most are derived from natural products rather than synthesised using chemical methods.[131]

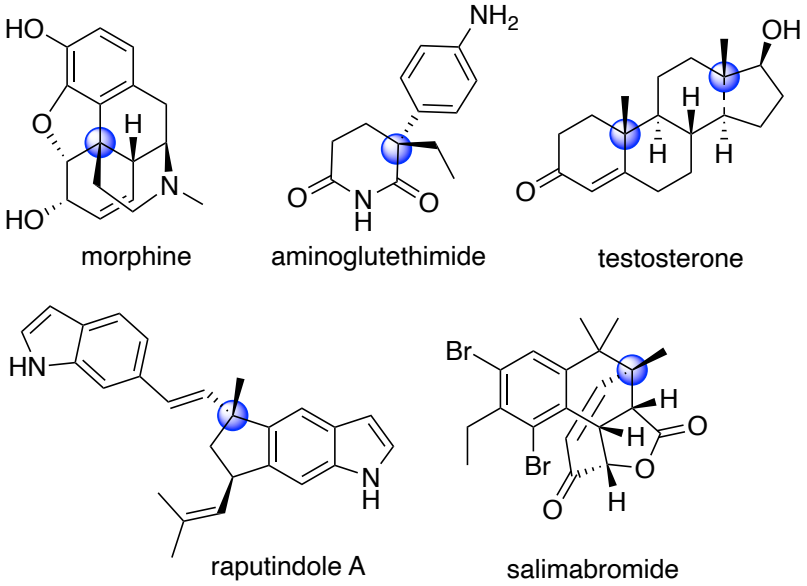


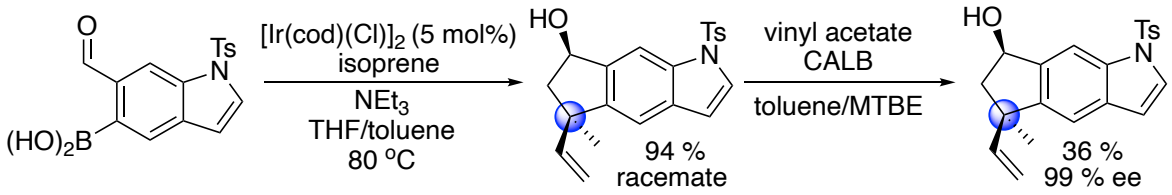
Figure 47. Examples of quaternary stereocentre containing biologically active compounds.

The enantioselective generation of quaternary stereocentres remains a major challenge for synthetic chemists today. There is a need for reliable asymmetric methods to synthesis quaternary centres to facilitate the further design, synthesis and evaluation of quaternary

stereocentre containing molecules. However due to steric demand, developing these asymmetric catalytic C-C bond forming methods is challenging.[131,132]

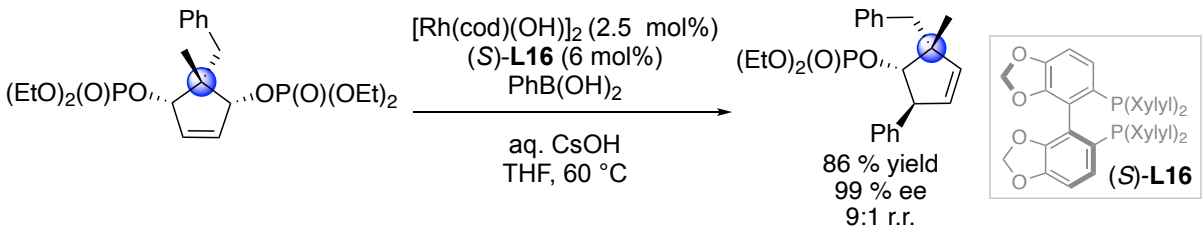
1.2 Preparation of Asymmetric Quaternary Stereocentres in Cyclic Molecules

Enantiomerically pure quaternary stereocentre containing molecules can be accessed by the resolution of racemic compounds. For example, in a recent total synthesis of raputindole A (see Fig. 47 for structure) an Ir-catalysed cyclization strategy was employed to synthesise a key racemic intermediate which was then resolved by enzymatic resolution (Scheme 18).[133] Although kinetic resolutions generally give the desired product in high enantiopurity, these transformations are limited to a maximum yield of 50%.[18]



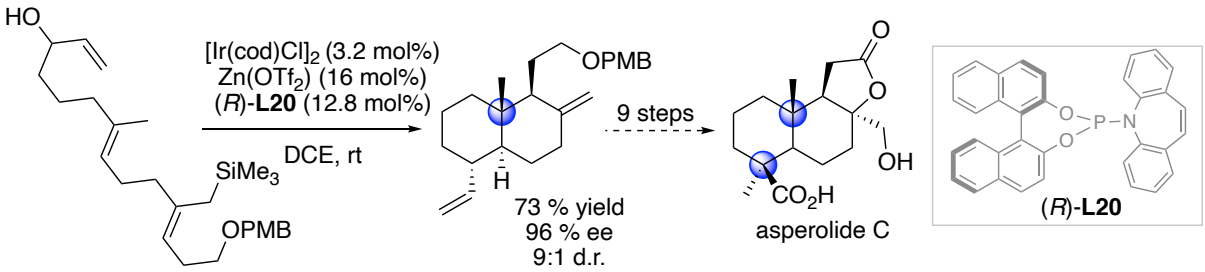
Scheme 18. Ir-catalysed cyclisation to form a racemic quaternary stereocentre, followed by enzymatic resolution used in a recent total synthesis of raputindole A.[133] CALB = *Candida antarctica* lipase B.

An alternative strategy to access asymmetric quaternary stereocentres involves the desymmetrisation of molecules containing prochiral quaternary stereocentres.[20] Our group has previously explored the desymmetrisation of cyclic meso-substrates to enantioselectively reveal quaternary stereocentres installed prior to the enantioselective catalytic reaction (Scheme 19, previously discussed in Chapter 1, section 4.2).[49,134]



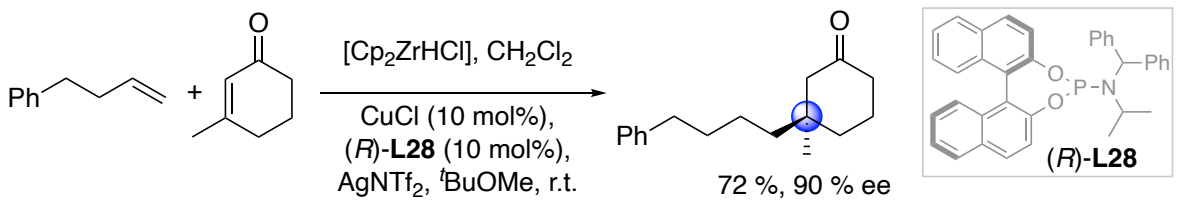
Scheme 19. Rh-catalysed desymmetrisation to access quaternary stereocentre containing compounds.[49]

Transition metal catalysed cyclisation strategies are commonly employed in asymmetric constuction of quaternary stereocentres.[128] Asymmetric Diels-Alder reactions and intramolecular Heck reactions to synthesis quaternary stereocentres have been widely reported,[129,135] and many other cyclisation processes have also been developed to enantioselectively generate quaternary stereocentres including dearomative cyclisations, cycloaddition reactions, radical processes and polyene cyclisations.[128,129] For example, Carreira and co-workers have developed an Ir-catalysed polyene cyclisation[136] which they utilised in the synthesis of quaternary stereocentre containing natural product asperolide C (Scheme 20).[137]



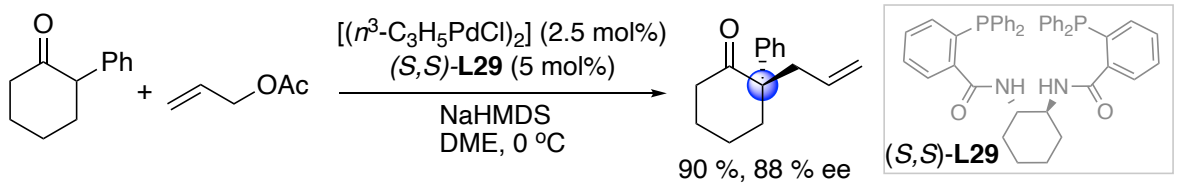
Scheme 20. Carreira and co-worker's synthesis of natural product asperolide C.[137]

Conjugate addition reactions with cyclic substrates can be employed the synthesis of quaternary stereocentres. The generation of quaternary stereocentres has been realised by our group, and others, though Cu-catalysed enantioselective addition of nucleophiles to prochiral enones (Scheme 21).[138-140] Related Rh- and Pd-catalysed conjugate additions to 3-methyl-2-cyclohexen-1-one allow for the use of boron nucleophiles to form arylated quaternary stereocentre containing products.[141,142]



Scheme 21. Our group's previously developed Cu-catalysed conjugate addition for the asymmetric construction of quaternary stereocentres.[138]

Metal catalysed asymmetric allylic addition reactions have proven to be a highly successful strategy for the synthesis of quaternary stereocentres.[143,144] Initially reported over 20 years ago, Pd-catalysed asymmetric allylic alkylation reactions to form quaternary stereocentres have been extensively developed (Scheme 22).[145,146] This transformation has been exploited in the synthesis of natural products containing quaternary stereogenic centres.[147,148]



Scheme 22. Pd-catalysed asymmetric allylic alkylation to form quaternary stereocentres.[146]

Cyclic, α-quaternary stereocentre containing products can also be formed by Pd-catalysed α-arylation reactions.[149,150] Quaternary stereocentres can be synthesised from di-substituted carbenes generated from diazo-compounds using Rh-catalysis.[151-153] Other transition-metal-catalysed arylations, vinylations and alkylations have been reported for the enantioselective synthesis of quaternary stereocentres but the scope is often relatively limited.[129,131]

A wide variety of strategies can be employed in the synthesis of quaternary stereocentres in cyclic molecules, however, the enantioselective synthesis of all-carbon quaternary centres, with high steric congestion, remains an area of active investigation. The development of reliable and modular methods for quaternary stereocentre synthesis will allow for the further design, synthesis and evaluation of compounds containing this biologically relevant moiety.

1.3 Project's Initial Aims

The objective of the project described in this chapter is to design a reliable asymmetric Csp^2-Csp^3 cross-coupling of racemic cyclic electrophiles with arylboronic acid nucleophiles to generate quaternary stereocentres. We recognised that this aim could be achieved by

significantly expanding on our group's Rh-catalysed asymmetric allylic arylation methodology (Fig 48a, previously discussed in Chapter 1, section 4.2) to allow for the use of substituted allyl halide substrates (Fig 48b).[53,54]

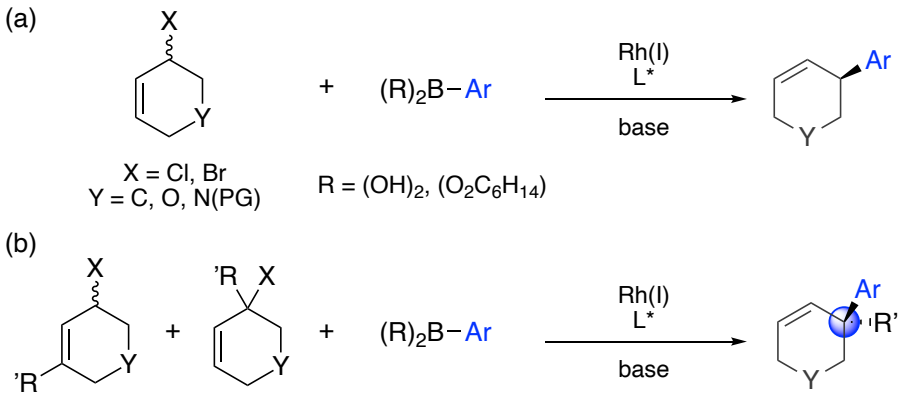
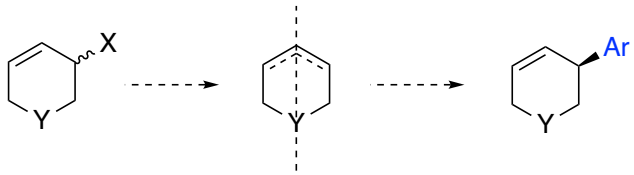


Figure 48. (a) Our group's previous work on Rh-catalysed asymmetric allylic arylation.[53,54] (b) Aim of this work; Rh-catalysed asymmetric allylic arylation of substituted racemic cyclic allyl halides with arylboronic acids.

The Rh-catalysed asymmetric allylic arylation reactions our group has developed are limited to electrophiles that, after cleavage of the carbon–halogen bond, are achiral about the allyl unit (Scheme 23).[56,154] Using unsymmetrically substituted allylic substrates leads to significant challenges in regiocontrol.[155-158]



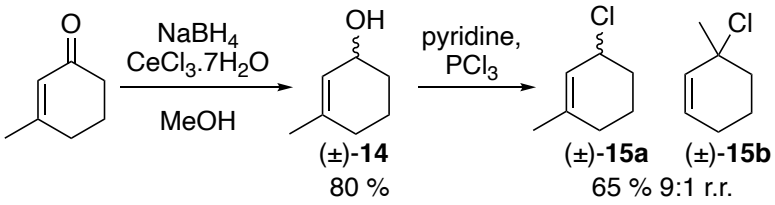
Scheme 23. Schematic diagram displaying the symmetry about the allyl unit for unsubstituted substrates.

The allylic substitution reaction we hope to develop could result in two possible regioisomeric arylated products, each of which have two possible enantiomers. The ambitious goal at the outset of this project was to design a reliable asymmetric Rh-catalysed Csp^2-Csp^3 cross-coupling to generate an enantiopure quaternary stereocentre containing product from a racemic mixture of regioisomers.

2. Results and Discussion, Part I

2.1 Preliminary Investigation of Rh-Catalysed Asymmetric Arylation to form Quaternary Stereocentres

Methyl substituted cyclic allyl chloride (±)-**15** was initially selected as a model substrate for the investigation into the Rh-catalysed asymmetric allylic arylation with arylboronic nucleophiles. When allylic alcohol (±)-**14** was synthesised and chlorinated, it was found that a mixture of (±)-**15a** and (±)-**15b** was formed with a regioisomeric ratio (r.r.) of 9:1 (Scheme 24). These regioisomers were not readily separable and therefore, we aimed to develop conditions to form a single enantiomerically pure product from this racemic mixture of regioisomers ((±)-**15a** and (±)-**15b**).



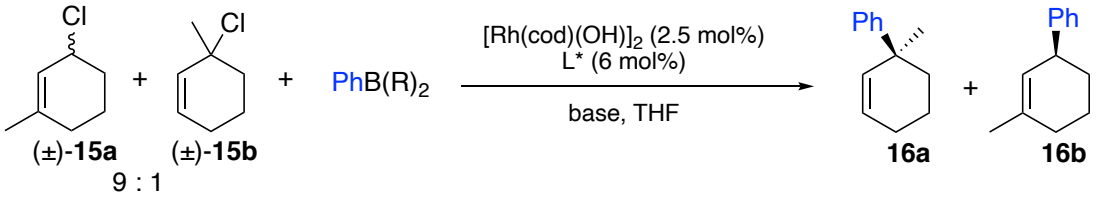
Scheme 24. Synthesis of substrates (±)-**15a** and (±)-**15b**.

High enantioselectivities for the desired quaternary stereocentre containing product (**16a**) were observed (up to 97 % ee, see Table 2). However, low yields were obtained mainly due to the competitive formation of the allylic alcohol by-products 1-methylcyclohex-2-en-1-ol and 3-methylcyclohex-2-en-1-ol. It was found that these allylic alcohols were racemic when formed as a by-product in the Rh-catalysed asymmetric allylic arylation. The instability of the starting material led to issues with reproducibility of results and contributed to the general impracticality of this system.

Along with the desired arylation product **16a**, the tertiary stereocentre containing regioisomeric arylation product **16b** was also observed with moderate enantioenrichment. The regioselectivity was poor and not improved with further screening. Changing parameters

such as ligand, temperature, base or arylboronic nucleophile seemed to have little or no effect on the regioselectivity (see Table 2).

Table 2. Selected results for the asymmetric allylic arylation with substrate (±)-**15**. Yield = isolated yield of **16a** + **16b**. pin = pinacol ester ($O_2C_6H_{14}$). L* = chiral ligand. The absolute stereochemistry of **16a** and **16b** is not known.

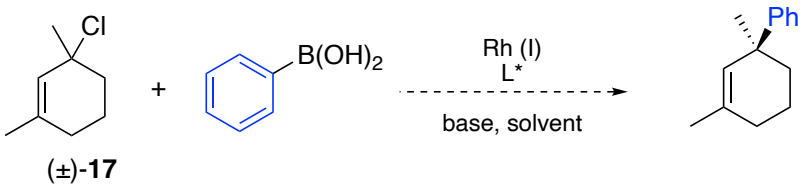


	L*	base	nucleophile	Temp (°C)	Yield (%)	**16a**:**16b**	ee **16a** (%)	ee **16b** (%)
1	(*S*)-BINAP	Cs_2CO_3	$PhB(OH)_2$	35	-	-	-	-
2	(*S*)-BINAP	Cs_2CO_3	$PhB(OH)_2$	60	25	2.5 : 1.0	94	48
3	(*S*)-SegPhos	Cs_2CO_3	$PhB(OH)_2$	60	11	2.5 : 1.0	97	66
4	(*S*)-SegPhos	Cs_2CO_3	PhB(pin)	60	<5	2.0 : 1.0	91	88
5	(*S*)-SegPhos	aq. CsOH	PhB(pin)	60	12	2.5 : 1.0	86	84
6	(*S*)-SegPhos	Cs_2CO_3	PhB(pin)	80	15	2.5 : 1.0	75	11

Although some promising results were observed in terms of enantioselectivity, this substrate is a problematic electrophile for optimisation of this asymmetric allylic arylation due to stability issues, along with the poor yields and regioselectivity observed.

2.2 Asymmetric Allylic Arylation of 'Pseudo-Symmetrical' Disubstituted Substrates

Having experienced the challenge of regioselectivity, we decided to investigate alternative disubstituted 'pseudo-symmetrical' substrates which, after cleavage of the carbon-halogen bond, would be symmetric about the allyl unit (Scheme 25). Here, quaternary stereocentres would be generated but the issue of regioselectivity is eliminated by substrate design. The dimethyl substituted substrate (±)-**17** was synthesised (Scheme 25). Unfortunately, this substrate proved unsuitable for this system due to its inherent instability.



(±)-**17**

Scheme 25. Asymmetric allylic arylation for 'pseudo-symmetrical' disubstituted substrates (±)-**17**.

2.3 Understanding the Stability of Allyl Halides

Issues encountered over substrate stability motivated us to computationally probe the thermodynamic stability of cyclic allyl halides. The difference in Gibbs energy between the geometry-optimised allyl halide and the products of autoionisation (a carbocation and free halide anion) is one such way to quantify allyl halide stability. We hypothesised that this calculated energy difference (ΔG) of heterolytic cleavage of the C-Cl bond would be a straight-forward and useful metric to correlate with empirically observed allyl halide stability.[159]

Allyl chlorides which had been previously synthesised by our group were qualitatively ranked by their relative stability based on empirical observations (e.g. can be purified by column chromatography, must be stored below 0 °C, etc.). Upon ranking these allyl chlorides of known empirical stability and calculating their energy difference of autoionisation, we found that a correlation exists between the calculated energy change for C-Cl dissociation and our empirical observations of allyl chloride stability in the laboratory (Fig. 49). This crude model demonstrates that heteroatoms in the cycle can play a stabilising role (Fig. 49, cf. (±)-**3** and (±)-**6** or (±)-**8**).

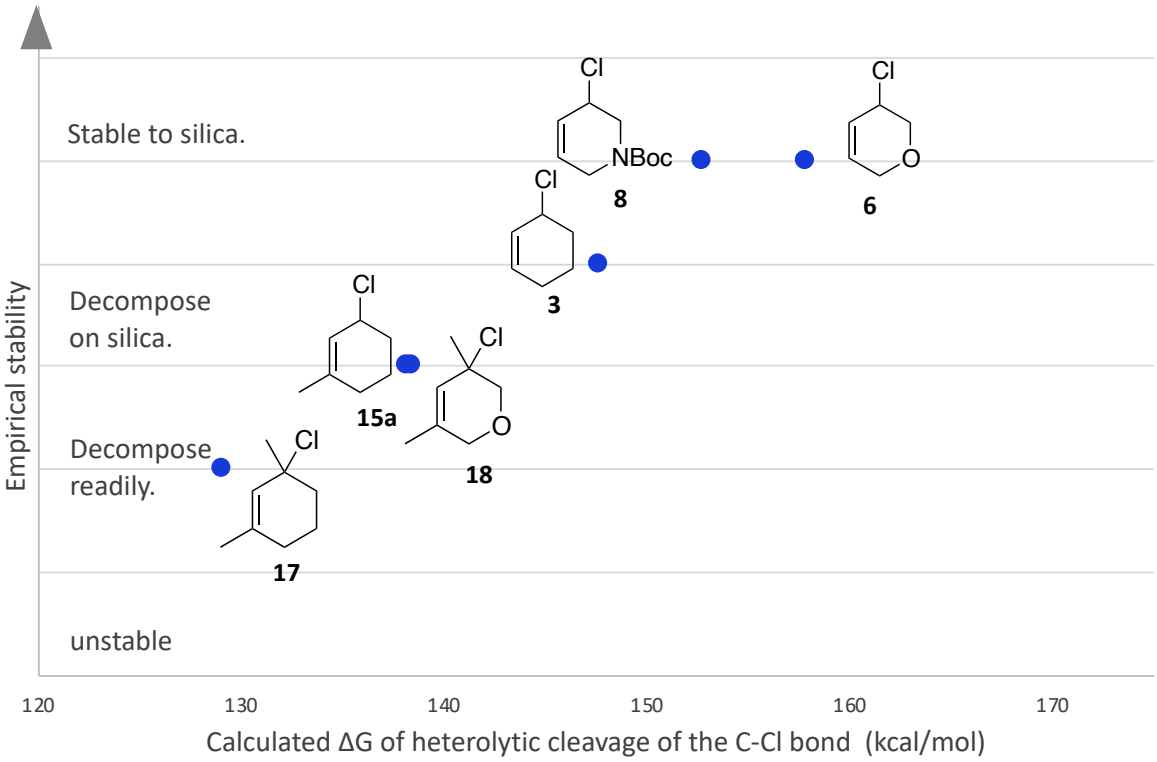


Figure 49. Graph illustrating the correlation between known qualitative empirical stability of previously synthesised allyl halides and the calculated energy difference (ΔG in kcal/mol) of autoionisation of these allyl chlorides (m062x/6-31++G(d,p)).

2.4 Selection of a Suitable Model Substrate

Using this simplistic model, we predicted the expected relative stability of some unknown allyl halides. We found that electron donating substituents on the allyl chloride stabilise the carbocation and therefore destabilise the allyl chloride. Along with heteroatoms playing a stabilising role in the cycle, electron withdrawing substituents were predicted to increase the stability of the allyl halide (Fig. 50).

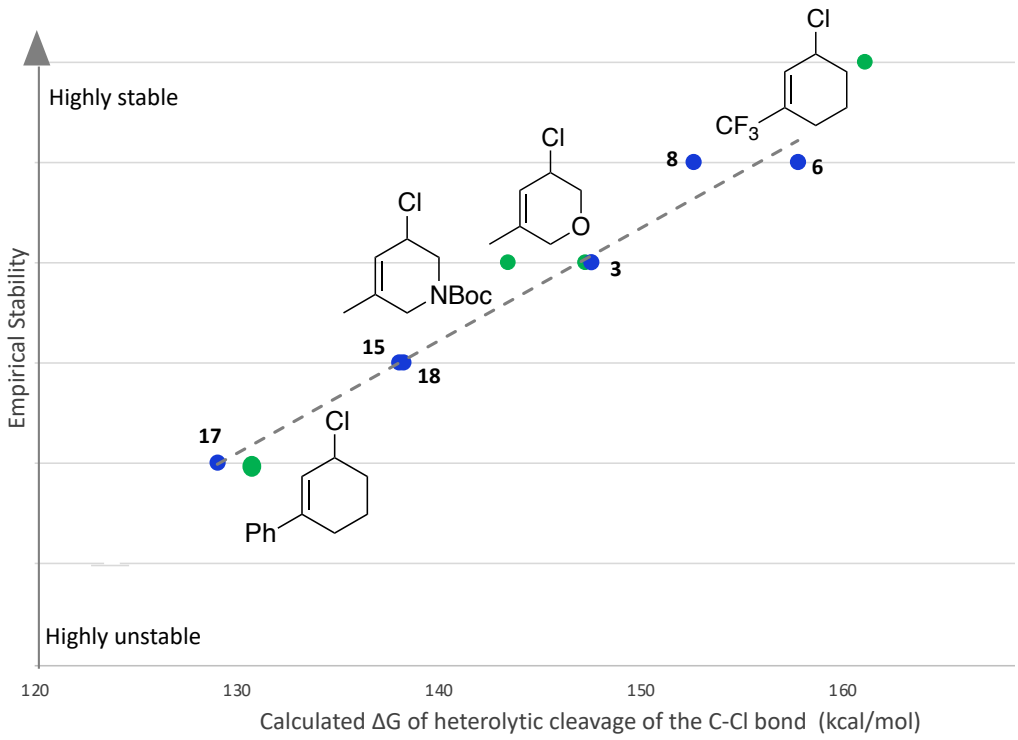


Figure 50. The relationship between known qualitative empirical stability of previously synthesised allyl halides and the calculated energy difference (ΔG in kcal/mol) of autoionisation of these allyl chlorides is shown by the dashed grey line and blue points. The change in Gibbs energy of heterolytic cleavage of the C-Cl bond of previously unknown allyl halides was calculated (m062x/6-31++G(d,p)) and their empirical stability was thus predicted using this model (green points).

Trifluoromethyl substituted allyl chlorides were computationally predicted to be highly stabilised (Fig. 50). As trifluoromethyl groups are privileged motifs in medicinal chemistry,[160] we decided to investigate these compounds as substrates for our asymmetric allylic arylation transformation.

Trifluoromethyl substituted allyl halides (±)-**20** and (±)-**21** were synthesised (Fig. 51a). We were pleased to find these allyl halides were stable as expected. However, under previously optimised reaction conditions, no conversion of starting material was observed. After several unsuccessful attempts to achieve conversion, we hypothesised that perhaps these di-substituted allyl halides are simply too sterically hindered to undergo oxidative addition.

Therefore, we decided to return to our original objective to use mono-substituted allyl halides and thus, re-introduce the challenge of regioselectivity.

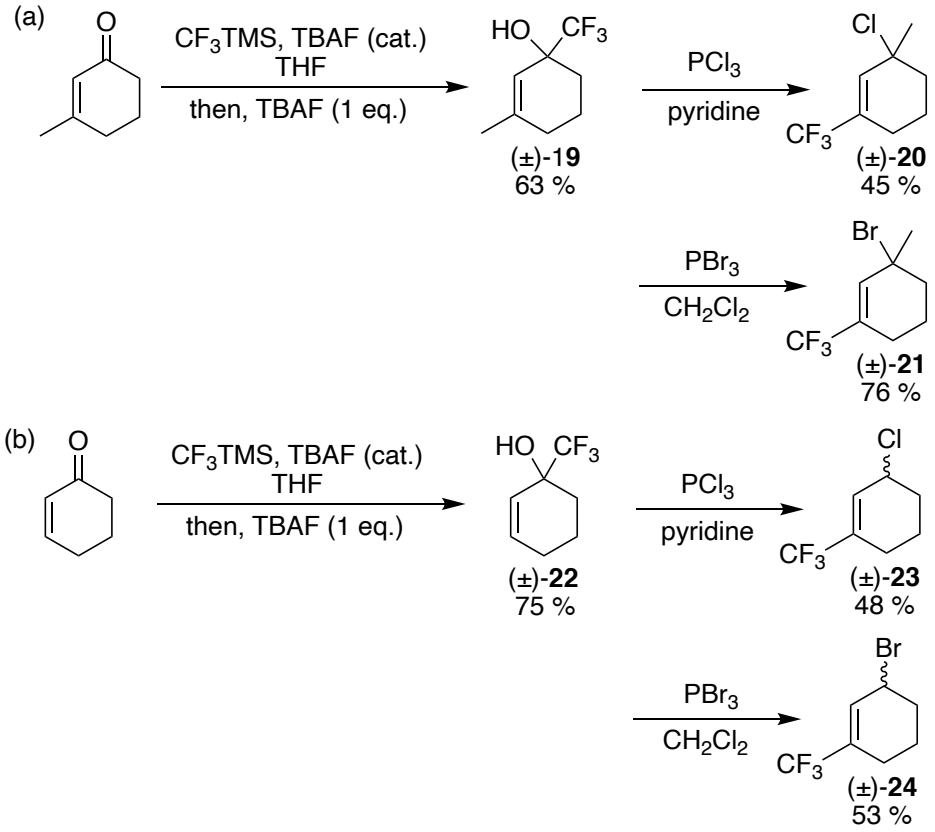


Figure 51. Synthesis of triflouromethylated substrates. (a) Synthesis of substrates (±)-**20** and (±)-**21**. (b) Synthesis of substrates (±)-**23** and (±)-**24**.

We remained motivated to investigate triflouromethyl substituted allyl halides and next synthesised (±)-**23** and (±)-**24** (Fig. 51b). Again, the model proved fruitful, and the substrates were stable as predicted. However, under the previously optimised reaction conditions low conversion of starting material was observed in all cases. Alternative rhodium sources, ligands, solvents, bases and temperatures were screened. Although conditions for higher conversion of starting material were discovered, under any conditions we examined the desired asymmetric allylic arylation products were not observed for any of these trifluoromethyl substituted cyclic allyl halide substrates.

After considering the predicted stability and investigating the synthetic routes to several allyl chlorides, the methyl substituted heterocyclic allyl chloride (±)-**21** was selected as an alternative model substrate.

Our group has previously reported the synthesis of allyl alcohol (±)-**26** (Fig. 52a),[161] with an epoxide opening followed by Grubbs-catalysed ring closing metathesis allowing access to the desired heterocyclic core. Allylic oxidation to give **27** was followed by a low yielding methyl lithium addition. The quaternary stereocentre containing racemic allyl alcohol (±)-**28** can be chlorinated resulting in an inseparable mixture of the desired racemic allyl chloride regioisomers (±)-**31a** and (±)-**31b** (4:1 r.r.). However, upon screening, the yield of the 1,2-addition was not readily improved. We therefore set out to develop a more efficient route to the model substrate (±)-**31**. In this newly developed route, we have shown that the tertiary allyl alcohol (±)-**30** can be accessed in just two steps (Fig. 52b). Grubbs 2nd generation catalyst must be employed in the ring closing metathesis step as the 1,1-disubstitued olefin (±)-**29** is a more challenging substrate than olefin (±)-**25**. Fortunately, the use of very low catalyst loading (<1 mol%) was possible. Chlorination of tertiary alcohol (±)-**30** results in an inseparable mixture of the desired racemic allyl chloride regioisomers (±)-**31a** and (±)-**31b** with the same regioisomer ratio (4:1) and yield as previously obtained using (±)-**28**.

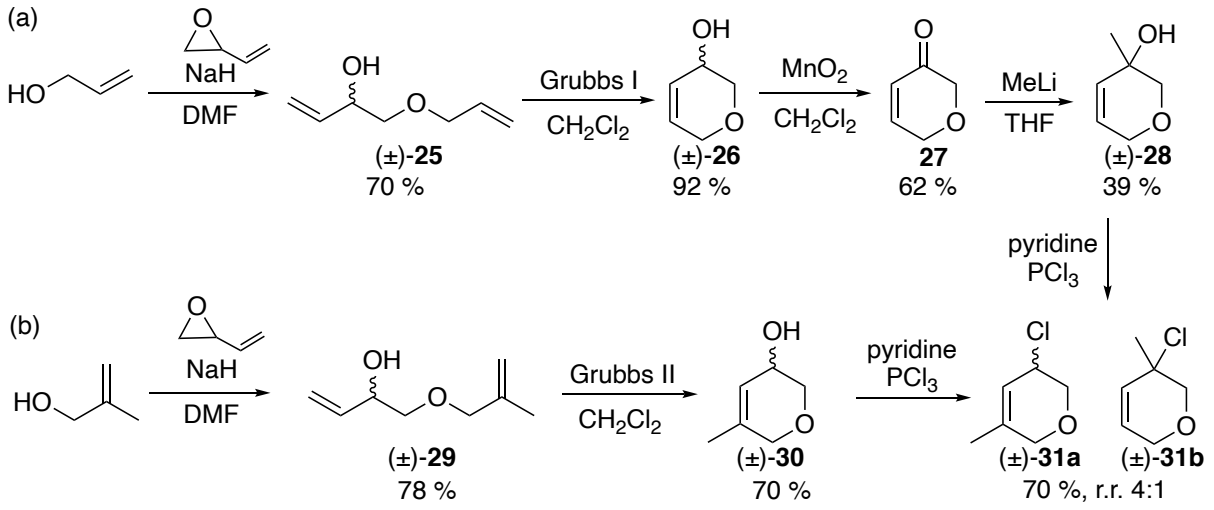
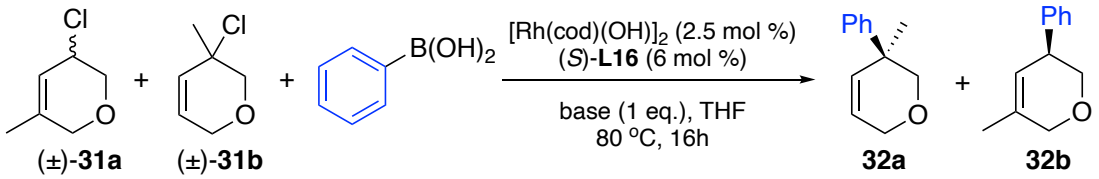


Figure 52. (a) Initial synthetic route to substrate (±)-**31**. (b) Improved synthetic route to substrate (±)-**31**.

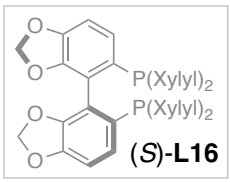
2.5 Optimisation of the Rh-Catalysed Asymmetric Arylation with a Racemic Substrate

With the substrate in hand, conditions using $[Rh(cod)(OH)]_2$ (2.5 mol%), (*S*)-Xylyl-P-Phos ligand (6 mol%), Cs_2CO_3 (1 eq.) with phenylboronic acid (2 eq.) in THF at 60 °C were selected as a starting point based on previous work.[53] However, no reactivity was observed under these conditions. Base screening at an increased temperature of 80 °C with (*S*)-Xylyl-Segphos ligand ((*S*)-**L16**) revealed that using aqueous CsOH (50 wt. % in H_2O) the desired products (**32a** and **32b**) can be accessed in moderate yield (Table 3). Previously, we obtained reduced yields due to the formation of undesired by-products (section 2.1). Here, yields were reduced due to incomplete conversion of the starting material (Table 3).

Table 3. Base screening results for the asymmetric allylic arylation optimisation for substrate (±)-**31** (r.r. 4:1). Yield = Isolated yield of **32a** + **32b**. The absolute stereochemistry of **32a** and **32b** is not known.

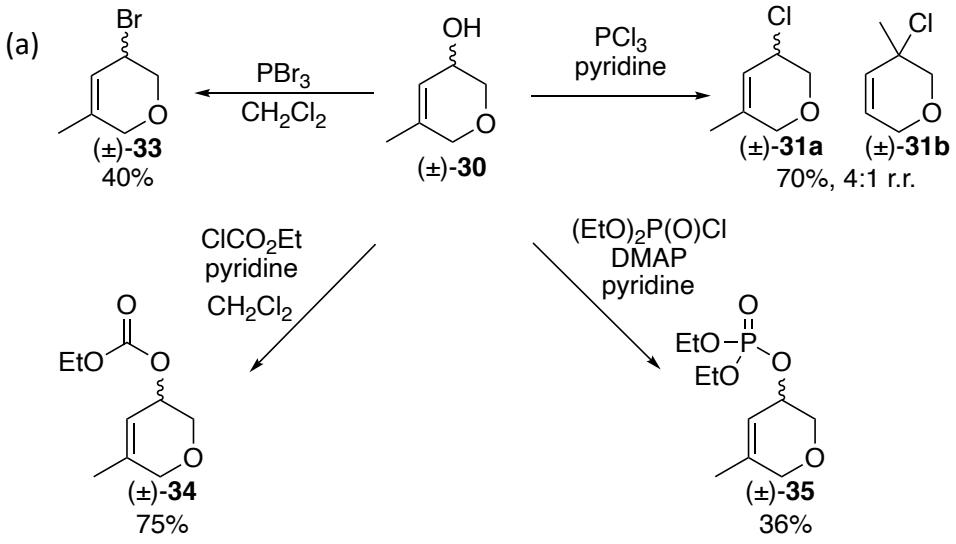


	Base	Yield (%)	Ratio **32a**:**32b**
1	KOH	29	2.0 : 1.0
2	$CsOH.H_2O$	40	2.0 : 1.0
3	K_2CO_3	41	1.5 : 1.0
4	aq. CsOH	56	2.0 : 1.0

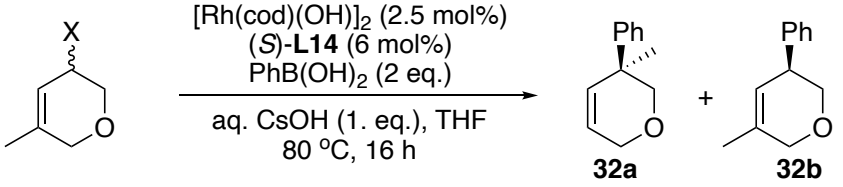


Various potential substrates can be accessed from allylic alcohol (±)-**30** (Fig. 53a). We synthesised a selection of racemic substrates with the same heterocyclic core and different leaving groups in the allylic position. Unlike the allyl chloride substrate, we found allylic phosphates, bromides and carbonates could all be accessed in regioisomerically pure form. We tested these various substrates in the Rh-catalysed asymmetric allylic arylation reaction using aqueous CsOH, with $[Rh(cod)(OH)]_2$, (*S*)-Xyl-P-Phos ligand ((*S*)-**L14**, and phenylboronic acid in THF at 80 °C. No conversion was observed with allyl carbonate substrate (±)-**34** (Fig. 53b). With the other substrates, conversion to product was observed with excellent

enantioselectivities (>90% ee) in all cases. The best results, in terms of yield and enantioselectivity, were obtained with the allyl chloride electrophile **31** (Fig. 53b).



(b)



	Leaving group (X)	Yield (%)	Ratio **32a**:**22b**	ee **32a** (%)	ee **32b** (%)
1[a]	OCO_2Et	0	-	-	-
2	Br	12	2.0 : 1.0	95	93
3[a]	$OP(O)(OEt)_2$	60	1.3 : 1.0	99	99
4	Cl	71	1.6 : 1.0	98	>99

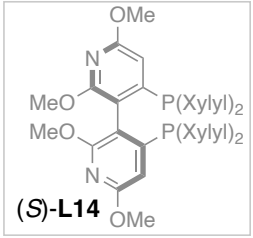
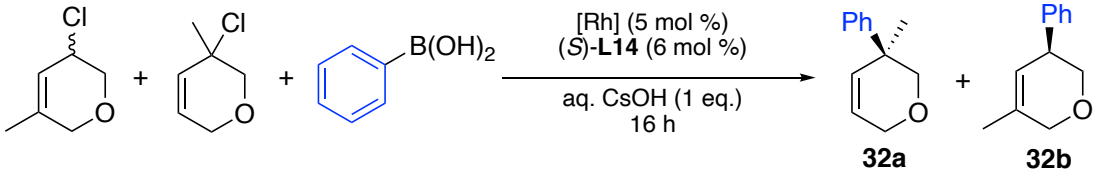


Figure 53. (a) Synthesis of various substrates from allyl alcohol **30**. (b) Leaving group screening results for the asymmetric arylation optimisation with different allylic substrates. Yield = Isolated yield of **32a** + **32b**. [a] Increased catalyst loading, $[Rh(cod)(OH)]_2$ (5 mol %), (*S*)-**L14** (12 mol %).

Continuing our optimisation using allyl chloride **31**, we attempted to increase the conversion. Full conversion of the starting material was observed with an increased reaction temperature of 100 °C with 1,4-dioxane as solvent and but reduced yield and ee of **32** were obtained (Table 4, entry 2). Alternative rhodium sources were examined (Table 4, entries 3 and 4). Although $[Rh(cod)(Cl)]_2$ gave a promising result, the yield was not improved. Doubling the catalyst loading with $[Rh(cod)(OH)]_2$ improved the conversion and yield (Table 4, entry 5).

Table 4. Selection of screening results for the asymmetric allylic arylation optimisation for substrate (±)-**21** (4:1 r.r.). Yield = Isolated yield of **32a** + **32b** [b]5 mol% $[Rh(cod)(OH)]_2$ and 12 mol% (*S*)-**L14**. The absolute stereochemistry of **32a** and **32b** is not known.

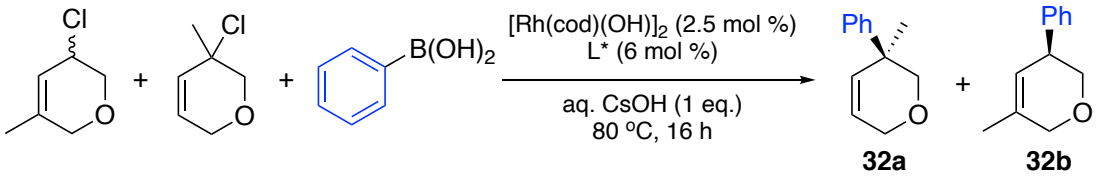


32a **32b**

	Rhodium source	Solvent	Temp (°C)	Yield (%)	Ratio 12a:12b	ee (%)	ee (%)
1	$[Rh(cod)(OH)]_2$	THF	80	71	1.6 : 1.0	98	>99
2	$[Rh(cod)(OH)]_2$	1,4-dioxane	100	19	2.2 : 1.0	79	61
3	$[Rh(cod)(Cl)]_2$	THF	80	53	3.0 : 1.0	99	98
4	$[Rh(cod)(MeCN)_2]BF_4$	THF	80	28	2.4 : 1.0	80	83
5[b]	$[Rh(cod)(OH)]_2$	THF	80	90	1.5 : 1.0	99	>99

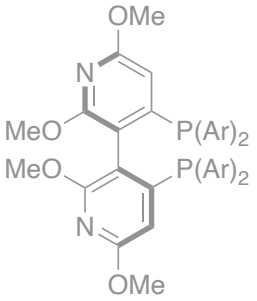
A variety of chiral ligands were screened and it was found that bisphosphine ligands with a biaryl backbone performed best in this reaction (Table 5). Other ligand classes such as monophosphine ligands and diene ligands were tested but we're found to generally perform worse than the bisphosphine ligands tested.

Table 5. A selection of ligand screening results for the asymmetric allylic arylation optimisation using substrate (±)-**31** (4:1 r.r.). L* = chiral ligand. Yield = Isolated yield of **32a** + **32b.** DTBM = 3,5-di-tert-butyl-4-methoxyphenyl. The absolute stereochemistry of **32a** and **32b** is not known.

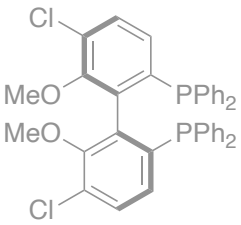


32a **32b**

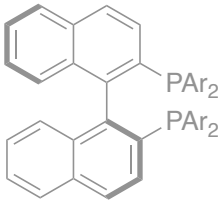
	L*	Yield (%)	Ratio **32a**:**32b**	ee (%)	ee (%)
1	(*S*)-**L14**	71	1.6 : 1.0	98	>99
2	(*S*)-**L17**	22	1.7 : 1.0	92	97
3	(*S*)-**L15**	41	1.4 : 1.0	98	>99
4	(*S*)-**L30**	21	1.8 : 1.0	92	98
5	(*S*)-**L31**	60	1.8 : 1.0	98	99
6	(*S*)-**L32**	30	1.7 : 1.0	97	93
7	(*S*)-**L16**	56	2.0 : 1.0	98	>99
8	(*S*)-**L19**	30	1.5 : 1.0	93	92
9	(*S*)-**L33**	0	-	-	-
10	(*S*)-**L34**	0	-	-	-
11	(*S*)-**L1**	0	-	-	-
12	(*S*)-**L21**	0	-	-	-



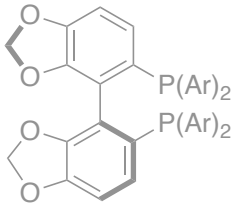
(*S*)-**L14** Ar = Xylyl
(*S*)-**L17** Ar = Ph



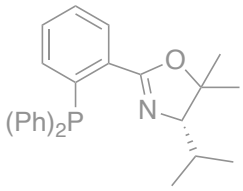
(*S*)-**L15**



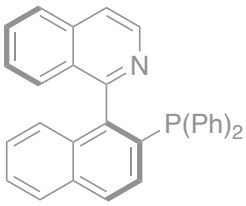
BINAP (*S*)-**L30** Ar = Ph
(*S*)-**L31** Ar = Xylyl



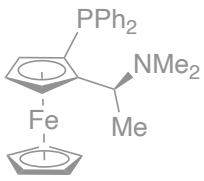
SegPhos (*S*)-**L32** Ar = Ph
(*S*)-**16** Ar = Xylyl
(*S*)-**L19** Ar = DTBM



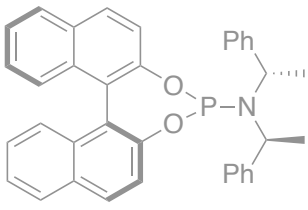
(*S*)-**L33**



(*R*)-**L34**



(*S,R*)-**L1**



(S,S,S)-**L21**

In this multi-parameter optimisation, infinite experiments could be envisaged varying the Rh source, ligand, base, solvent, temperature, arylboronic nucleophile and concentration. After several rounds of screening varying different parameters, some overall trends could be identified within the data. Ethereal solvents give higher yields than alcohol, polar aprotic or

non-polar aprotic solvents in this system. A wide variety of bases can be employed in the reaction – hard, soft, organic and inorganic bases are all tolerated. The reaction can also tolerate some water although a clear trend between the amount of water added and the results obtained was not evident.

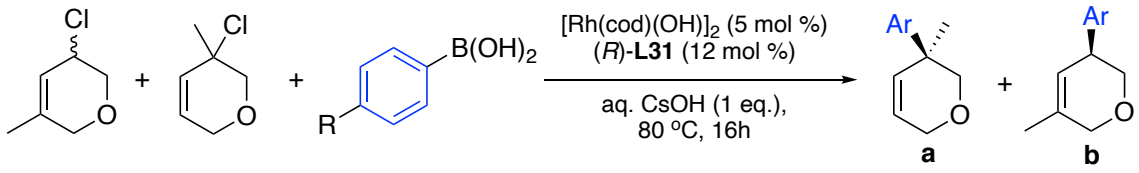
Some interesting observations uncovered during this process may give some limited mechanistic insight. The reaction was sampled over time and it was found that the regioselectivity and enantioselectivity do not change over the course of the reactions under the conditions tested. With $[Rh(cod)(OH)]_2$ and no added chiral ligand, the reaction does not proceed and no arylated product is obtained. With no base the reaction gives 0-5% yield of arylated product, depending on specific conditions used. This may indicate that the base is involved in catalyst turnover. However, the ratio of boronic acid equivalents to base equivalents is also an important factor governing yield, perhaps indicating that the base plays an additional role in boronic acid activation. Significant protodeborylation is observed under some conditions and increasing the equivalents of the boronic acid generally increases the yield.

After carrying out hundreds of reactions on this system, it was concluded that altering the regioselectivity is not an easy problem to ameliorate. Although we gained some interesting insights, our optimal results obtained after a small number of experiments were not greatly improved. Using $[Rh(cod)(OH)]_2$ (5 mol%), (*S*)-Xylyl-BINAP ligand ((*S*)-**L31**, 12 mol%), aq. CsOH (1 eq.) and phenylboronic acid (2 eq.) in THF at 80 ^{o}C the asymmetric allylic arylation products can be accessed with excellent enantioselectivities (98 %, 99 % ee) and yield (90 %) but with poor regioselectivity (1.8:1 r.r.).

2.6 Scope of the Rh-Catalysed Asymmetric Arylation with a Racemic Substrate

With conditions for the Rh-catalysed reaction to form a regioisomeric mixture of enantioenriched products to hand, some preliminary exploration of the potential scope of this regiodivergent reaction was conducted by examining a small number of arylboronic acid nucleophiles (Table 6). Good yields and excellent enantioselectivities were obtained for the *para*-substituted arylboronic acids tested (Table 6, entries 2 and 3). However, the regioselectivity remained low. From this limited investigation of the nucleophile scope, we can surmise that the reaction tolerates electron rich and electron poor arylboronic acids.

Table 6. Results with different arylboronic acids tested in the Rh-catalysed asymmetric regiodivergent arylation with allyl chloride (±)-**31** (4:1 r.r.). Yield = combined isolated yield of both regioisomeric products. The absolute stereochemistry of the arylated products formed is not known.



	R	Yield (%)	Ratio a : b	ee (%)	ee (%)
1	H	90	1.8 : 1.0	98	>99
2	OMe	74	2.1 : 1.0	>99	>99
3	CF_3	92	1.4 : 1.0	>99	>99

2.7 Considering the Mechanism of this Rh-Catalysed Asymmetric Arylation

Mechanistic studies on the unsubstituted model system (see chapter 2), indicate that this Rh-catalysed cross-coupling reaction likely proceeds *via* transmetalation, followed by oxidative addition to generate an η^3 Rh-complex. Subsequent reductive elimination liberates the enantioenriched arylated product. Oxidative addition occurs irreversibly in this transformation and can occur in a *syn*- or *anti*-manner (i.e. the Rh-aryl intermediate can add to either face of the allyl unit) depending on the steric accessibility of the substrate. Reductive elimination is the enantiodetermining step.

In chapter 2, a deuterium labelling study revealed some interesting insight into our Rh-catalysed allylic arylation with allyl chlorides that do not form a symmetric allyl unit after cleavage of the C-Cl bond (Fig. 54). Here we see that with racemic substrate **8** with a ^{2}H-label at the vinylic position, we get a 1:1 ratio of two pseudo-regioisomeric arylated products with the ^{2}H-label at the vinylic or allylic position. We hypothesised that one of these pseudo-regioisomers is formed from one enantiomer of the starting material, and the other is produced from the alternative enantiomer of the starting material. Thus, when enantioenriched ^{2}H-labelled starting material was employed, the regioselectivity observed in the product formation was improved to a 7:1 ratio of pseudo-regioisomers (Fig. 54, see chapter 2, section 2.7 for details).

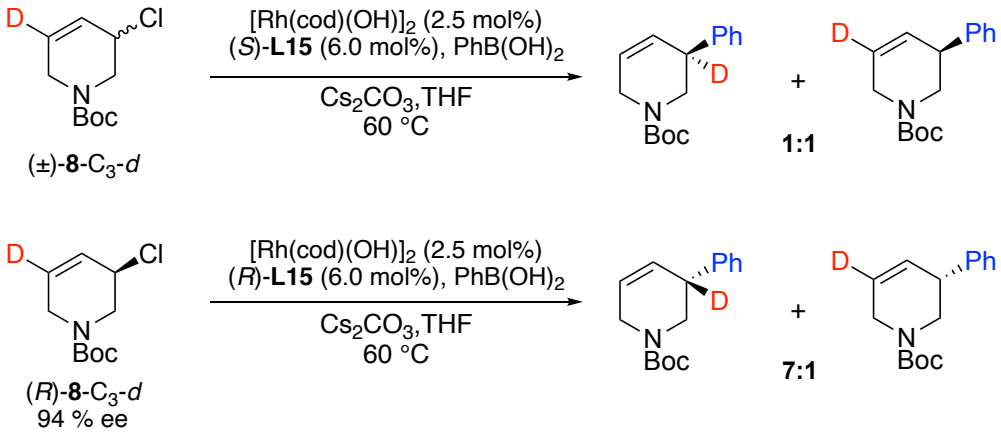


Figure 54. Selected deuterium-labelling study results from mechanistic investigation, see chapter 2 for details.

In our current study, assuming the mechanism operates in an analogous manner to that detailed in chapter 2, oxidative addition to both enantiomers of the racemic substrate could produce two different η^3 Rh-complex intermediates (Fig. 55). Starting from a racemic mixture of allyl chloride regioisomers, sixteen potential pathways can be envisioned within the mechanistic pathways known to be operative in this transformation (as discussed in chapter 2). Interconversion of starting material enantiomers and/or regioisomers may, or may not, be occurring here. Interconversion between the η^3 Rh-complexes may also be possible.

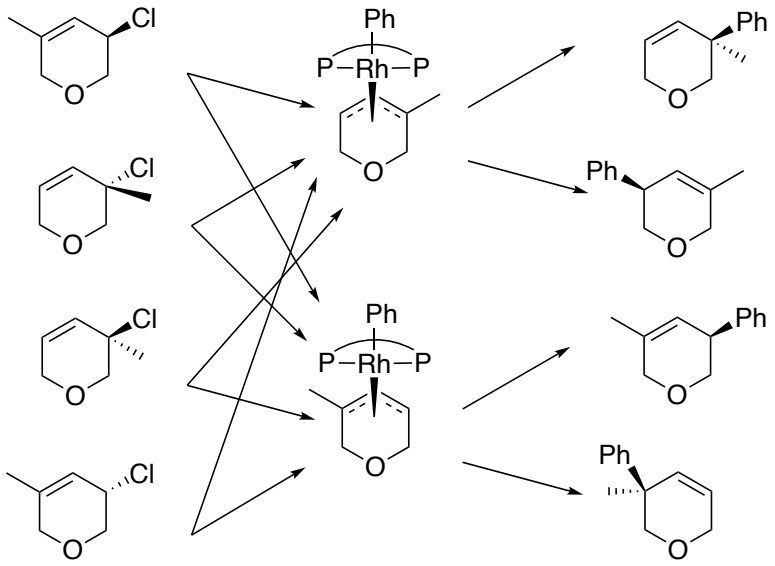


Figure 55. Simplified schematic highlighting the different potential mechanistic pathways by which this arylation reaction may occur.

3. Results and Discussion, Part II

3.1 Regiodivergent Reactions with Enantioenriched Substrates

A simplified schematic diagram for a hypothetical reaction of a racemic starting material is shown in Fig. 56a, whereby each enantiomer of the starting material reacts with the chiral catalyst to give a different product. Reactions of this type are known as divergent reactions on racemic mixtures,[162,163] and when enantioenriched starting material is used each of the two potential products can be accessed using each of the two enantiomers of the chiral catalyst (Fig. 56b).[164] In cases where 'product A' and 'product B' are regioisomers,[165] this concept can be applied to achieve regioselective reactions with enantioenriched substrates for reactions that operate *via* this general mechanistic paradigm.[158,166-169]

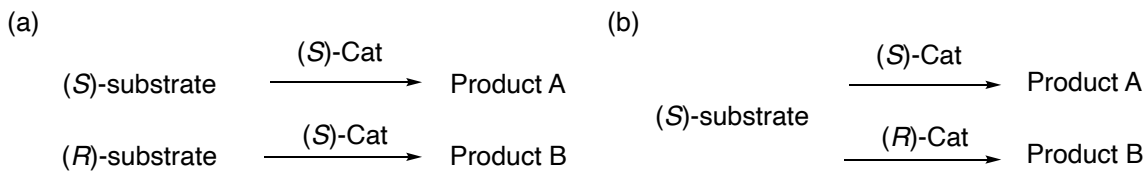


Figure 56. Simplified general schematic for (a) a divergent reaction on a racemic substrate and (b) a selective reaction on an enantioenriched substrate.

Although the mechanism of the transformation under investigation here may be more complicated than the simple concept illustrated in Fig. 56 (see Fig. 55), based on insights into the potential mechanism (see Fig. 54 and chapter 2), we hypothesised that if an enantioenriched starting material was employed, oxidative addition could potentially generate just one of the two possible unsymmetric η^3 Rh-complex intermediates. Subsequent ligand-controlled reductive elimination would give one regioisomer of the product with high enantioselectivity. The four prospective enantioenriched isomeric products could potentially be accessed using this strategy, if both enantiomers of the starting material and chiral ligand were accessible and employed (Fig. 57).

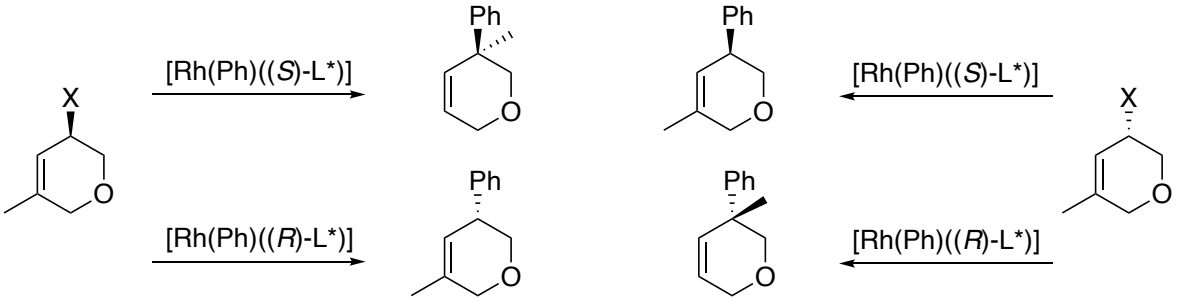
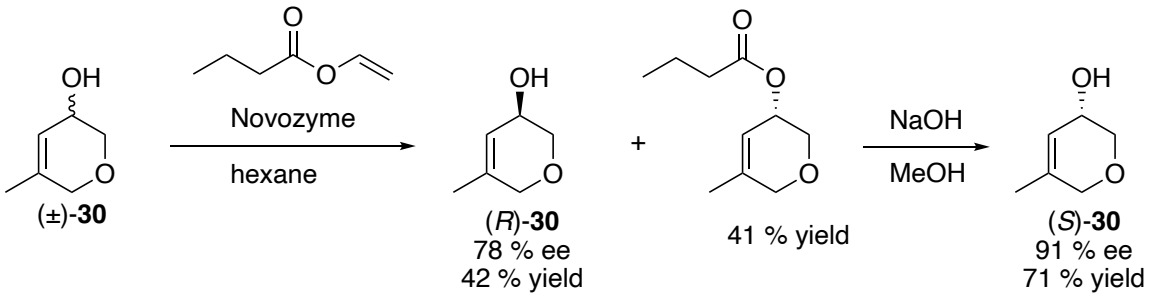


Figure 57. Hypothesis for accessing four isomers of the product through four different arylation reactions using the two enantiomers of the starting material and the two enantiomers of the chiral ligand.

3.2 Preparation of Enantioenriched Allylic Substrates

Allyl alcohols are generally readily accessible in enantiopure form *via* asymmetric reduction of carbonyls[170,171] or using enzymatic methods.[172,173] Enantioenriched allyl alcohol (*R*)-**30** (78 % ee) can be accessed by enzyme resolution (Scheme 26).[174] Hydrolysis of the ester formed allows access to the (*S*)-**30** enantiomer in 91 % ee.



Scheme 26. Enzyme resolution to access enantioenriched (*R*)- and (*S*)-**30**.

Attempts to synthesis enantioenriched allyl chloride **31** from enantioenriched allyl alcohol **30** were unsuccessful.[122] Guided by our screen of potential leaving groups for racemic substrates (section 2.5), we next attempted the synthesis of enantioenriched allyl phosphate **35**. We were pleased to find that the phosphorylation reaction proceeded with complete stereoretention.[175]

3.3 Preliminary Results for the Rh-Catalysed arylation of Enantioenriched Allylic Substrates

With the enantioenriched substrate **35** to hand, our hypothesis (shown in Fig. 57) could be tested. As anticipated, with an enantioenriched allylic substrate the regioselectivity was improved. Under the conditions shown in Figure 58, using the racemic phosphate **35** (0 % ee) no regioselectivity was observed in the product formation (Fig. 58a). Using enantioenriched starting material ((*R*)-**35**, 78 % ee) a regioisomeric ratio of almost 6:1 is obtained (Fig. 58b). Using the (*S*)-enantiomer of the chiral ligand ((*S*)-**L14**), the quaternary stereocentre containing product (**32a**) is favoured. Using (*R*)-**L14**, the tertiary stereocentre containing product (**32b**) is the major regioisomer (Fig. 58b). These results are consistent with our hypothesis.

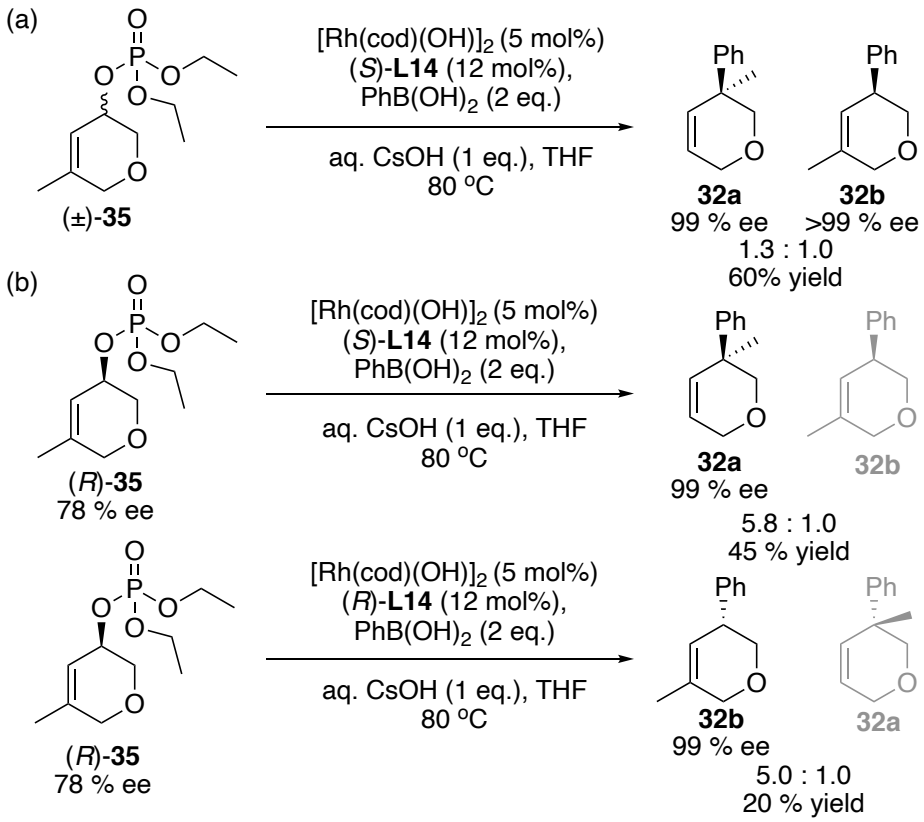


Figure 58. (a) Rh-catalysed arylation with racemic allyl phosphate substrate. (b) Preliminary results for the Rh-catalysed arylation of enantioenriched allyl phosphates with the two enantiomers of the chiral ligand.

Acquiring the enantioenriched allyl alcohol by resolution allows access to both enantiomers of **30**. Thus, the (*S*)-enantiomer of the allyl phosphate **35** could also be obtained. As anticipated, this led to opposite results in terms of regioselectivity with each enantiomer of the ligand (Fig. 59). (*S*)-**35** was synthesised with a higher enantioenrichment (90 % ee, compared to 78 % ee for (*R*)-**35**) and this led to a further increase in the regioselectivity observed (Fig. 59). These results also align with our hypothesis.

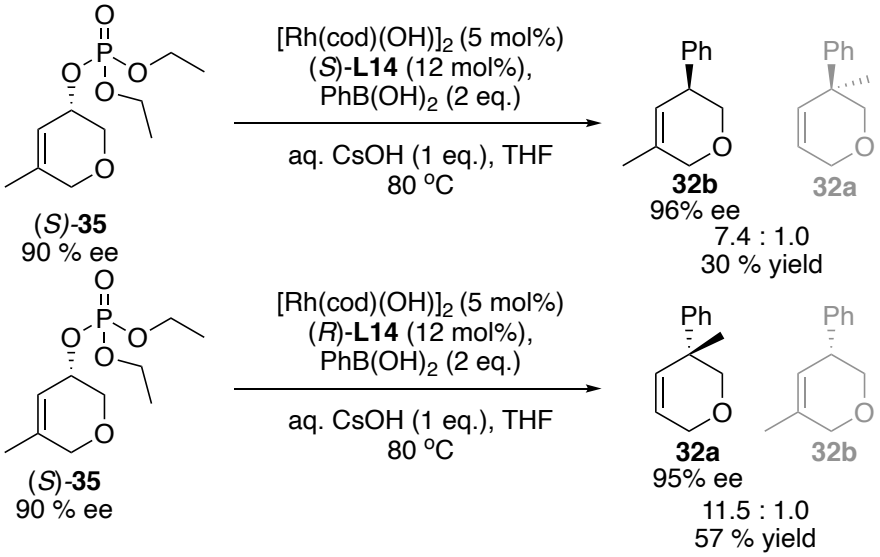
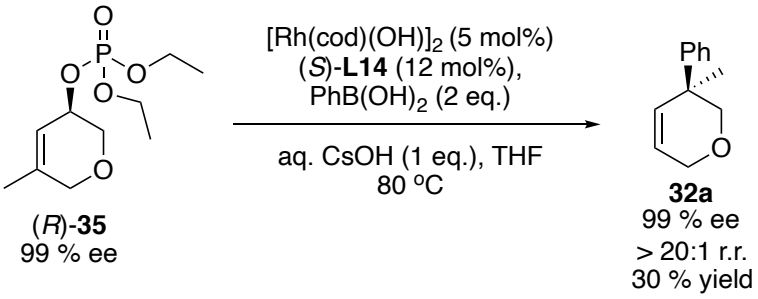


Figure 59. Preliminary results for the Rh-catalysed arylation of enantioenriched allyl phosphates with the (*S*)-enantiomer of the starting material and with the two enantiomers of the chiral ligand.

In order to achieve desired regioselectivities (>20:1), we needed to access enantiopure starting material (>99 % ee). We found that re-submitting the enantioenriched allyl alcohol (*R*)-**20** (78 % ee) to the enzyme resolution could further improve the enantioenrichment and (*R*)-**20** could be obtained with 99 % ee. With a highly enantioenriched allyl phosphate ((*R*)-**25**, 99 % ee), the quaternary stereocentre containing product (**22a**) can be obtained in excellent enantioselectivity (99 % ee) and regioselectivity (>20:1) (Scheme 27).



Scheme 27. Rh-catalysed regioselective arylation of an enantioenriched allyl phosphate.

4. Conclusions

Regioisomeric mixtures of racemic substituted cyclic allyl halides have been used in asymmetric Rh-catalysed Csp^2-Csp^3 cross-couplings with arylboronic nucleophiles in an attempt to generate single enantiomer quaternary stereocentre containing products. Some promising results have been obtained, showing the desired arylated products can be formed with excellent ee (up to 99 %) and yield (up to 90 %) but with poor regioselectivity (r.r. 1.8:1) (Fig. 60a). This work displays the potential to extend Rh-catalysed asymmetric allylic arylation methodology to the formation of quaternary streocentres. Using this regiodivergent transformation, the tertiary stereocentre containing product can also be accessed with excellent enantioselectivity (99 % ee, Fig. 60a).

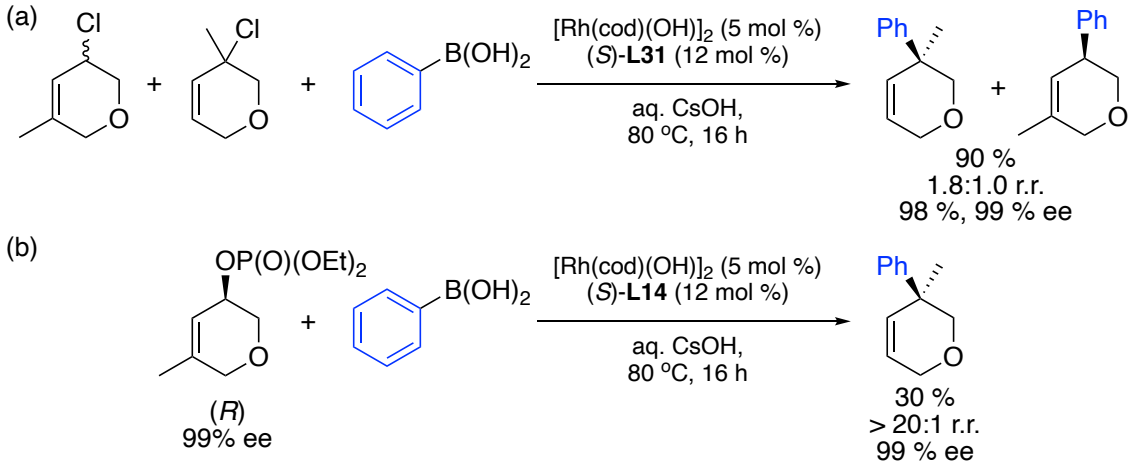


Figure 60. (a) Regiodivergent Rh-catalysed asymmetric allylic arylation of a racemic mixture. (b) Regioselective Rh-catalysed stereospecific allylic arylation.

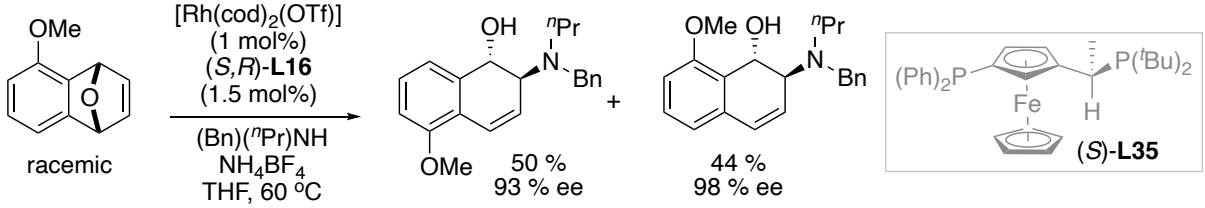
The study described in Chapter 2 gave us extraordinary insight into the mechanism of our Rh-catalysed asymmetric allylic arylation methodology. This provided us with a much deeper understanding of some of the problems encountered in this project. Armed with this information, we were able to develop a new strategy to tackle this project aim. We synthesised enantioenriched allyl phosphates and subjected them to our Rh-catalysed arylation conditions. Although poor yields were obtained in these preliminary results with

enantiopure substrates, the desired quaternary stereocentre containing product was synthesised with excellent enantio- and regioselectivity (99 % ee, >20:1 r.r.) disclosing a promising proof of concept (Fig. 60b). The tertiary stereocentre containing product can also be selectively accessed using this method by employing the alternative enantiomer of either the starting material or the ligand.

5. Future Directions

5.1 Regiodivergent Reactions on Racemic Mixtures

With racemic substrates, we have developed a regiodivergent strategy to access two highly enantioenriched products. Regioselectivity was a key focus of our project throughout this study, however, regiodivergent reactions on racemic mixtures can be a powerful tool for complex molecule synthesis.[163,165] For example, Lautens and co-workers developed a Rh-catalysed regiodivergent resolution of unsymmetrical, racemic oxabicyclic alkenes (Scheme 28).[158] They later demonstrated the utility of this method by synthesising a different biologically relevant molecule from each of the two regioisomeric products formed in the regiodivergent transformation.[176]



Scheme 28. Lauten's regiodivergent resolution which has been used in the synthesis of biologically active compounds.[176]

Other strained heterocycles, such as aziridines, are commonly employed as substrates for regiodivergent processes.[167,177] However, many other reaction types are suitable for exploitation as useful regiodivergent processes such as functionalization of polyols,[178]

hydroarylation processes,[166] and potentially our Rh-catalysed arylation of allyl halide substrates.

Although the particular examples we focused on produced regioisomeric products which were not readily separable, likely other examples within the potential substrate scope would be separable by column chromatography and therefore could be used to develop useful regiodivergent reactions on a racemic mixture. These processes where two highly enantioenriched products are accessed in one transformation can be employed in diversity orientated synthesis which has applications in drug discovery.[179]

5.2 Regiodivergent Reactions with Enantiopure Substrates

However, our primary focus in this project was to develop a regioselective arylation. For this reason, we chose to pursue the strategic employment of enantioenriched starting materials. Although, some excellent preliminary results have been obtained with this strategy, further screening is required in order to improve the yield of this transformation. We have established a strong proof of concept with these promising preliminary results and this work is will be continued within the Fletcher group. We hope that a relatively small amount of optimisation will be required to improve the yield, now that we have demonstrated that our regioselectivity problem has been solved and the products can be selectively accessed with high enantiopurity.

The synthesis of one isomer of the product in high regioselectivity and enantioselectivity is demonstrated in Scheme 27. Our preliminary results (Fig. 58 and 59) show that all four isomers, each with high regioselectivity and enantioselectivity, should be possible to access with the appropriate choice of ligand and substrate stereochemical configuration (Fig. 61). Once conditions have been found which result in higher conversion, the scope of this transformation will be explored. We have seen that electron rich and electron deficient

arylboronic acids are tolerated in the regiodivergent Rh-catalysed asymmetric allylic arylation on a racemic mixture. Likely a range of aryl and heteroaryl boronic acids will be tolerated, along with the potential for vinylboronic acids to be employed.[54]

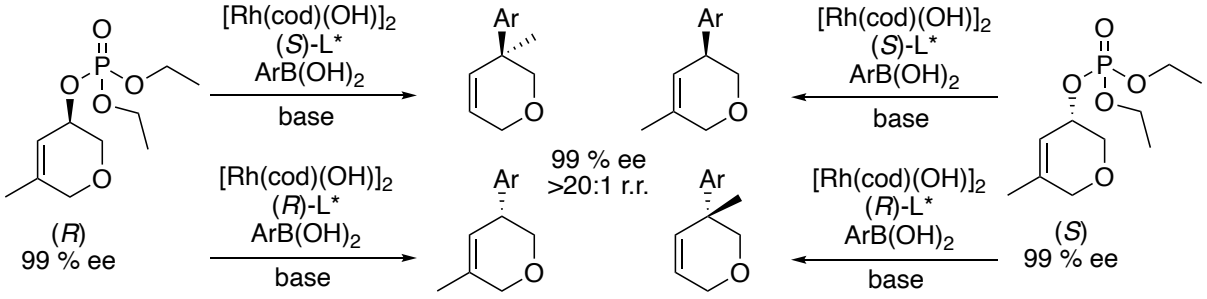
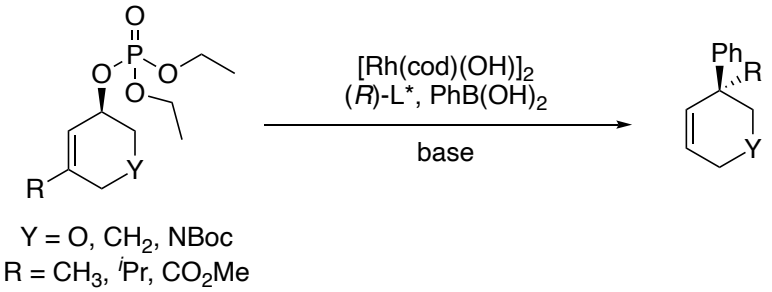


Figure 61. Future work will involve the synthesis of the four potential isomers, each with high regioselectivity and enantioselectivity (as demonstrated for one isomer in scheme 27). The scope of the optimised reaction will be explored using various boronic acid nucleophiles.

Other electrophiles could also be examined (Scheme 29). Piperidine based electrophiles would make for excellent examples to showcase the utility of this transformation as nitrogen-containing heterocycles are widely used within the pharmaceutical industry.[180] Along with methyl groups, other vinylic substituents in the starting material could be tested. Exploration of the effects of steric and electronic factors at this position may reveal further mechanistic insights.



Scheme 29. Future work may explore the electrophile scope which may also provide further mechanistic insight.

A synergistic combination of experimental and computational studies could be undertaken to further develop this method and also perhaps lead us to greater understanding of the mechanism of Rh-catalysed asymmetric allylic arylations. A feedback loop could be developed and implemented where experimentation and computational results can each inform the

other. We have already put this into practice by developing a fast and efficient way to predict the qualitative relative stability of unknown allyl halides (section 2.3). In future work, DFT calculations could be employed to examine the relationship between mechanism and substituents, and therefore direct rational design of asymmetric reactions with new substrates.

5.3 Rh-Catalysed Suzuki-Miyaura Cross-Coupling in Natural Product Synthesis

Natural product synthesis is an excellent way to demonstrate the utility of a new method while testing its limitations when applied to complex molecule synthesis. As discussed in the introduction to this chapter, many natural products and drugs contain quaternary stereocentres. This Rh-catalysed method could potentially be employed in the synthesis of quaternary stereocentre containing natural products, such salimabromide or raputindole A (Fig. 62).[181,182] The potential cross-coupling partners for the key Rh-catalysed reaction to form the quaternary stereocentre are shown in each case.

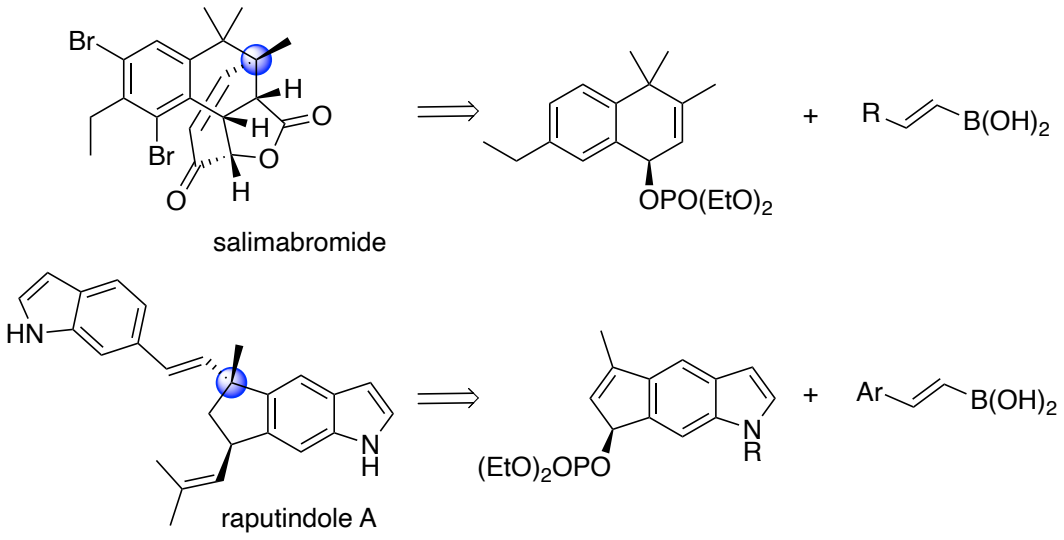


Figure 62. Quaternary stereocentre containing natural products that could potentially be synthesised using this Rh-catalysed method.

This regiodivergent Rh-catalysed method also enables the synthesis tertiary sterecentre containing molecules with high enantioselectivity. Figure 16 displays a selection of related

tertiary stereocentre containing natural products and drugs.[183] The synthesis of this series of complex molecules could be envisioned by exploiting our Rh-catalysed method (Fig. 63).

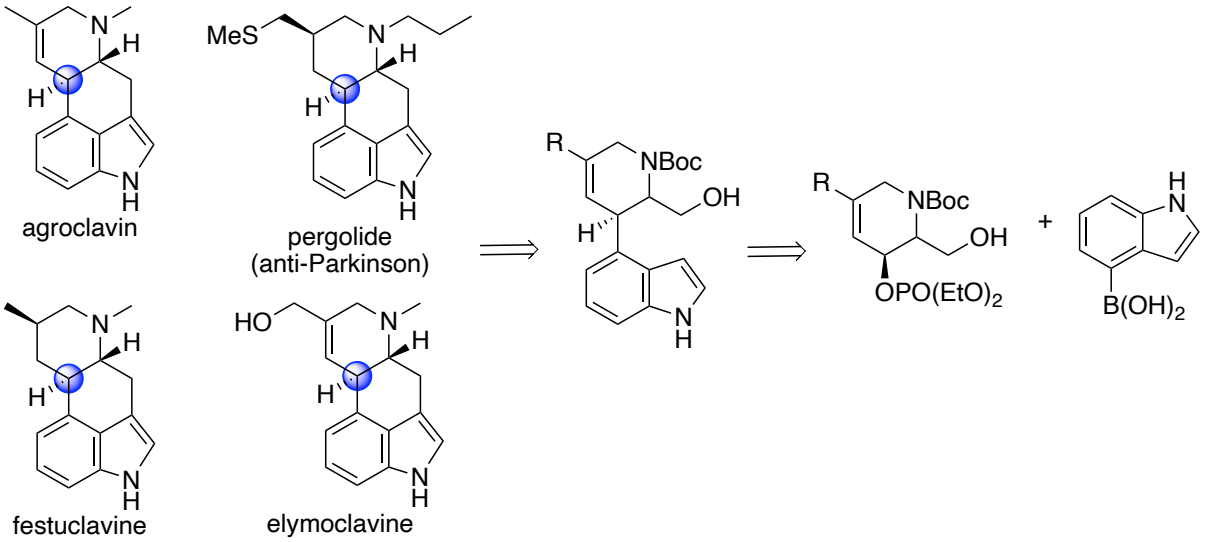
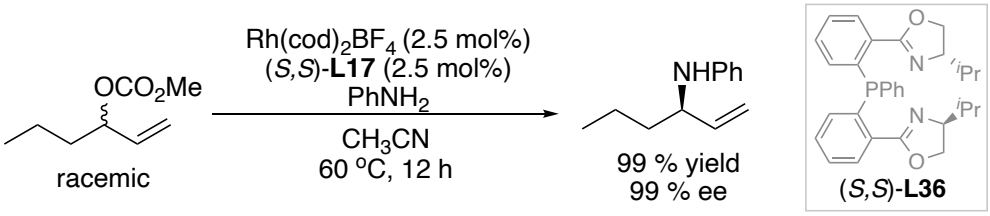


Figure 63. Tertiary stereocentre containing natural products and drugs that could potentially be synthesised using this method.

5.4 Rh-Catalysed Suzuki-Miyaura Cross-Coupling with Acyclic Substrates

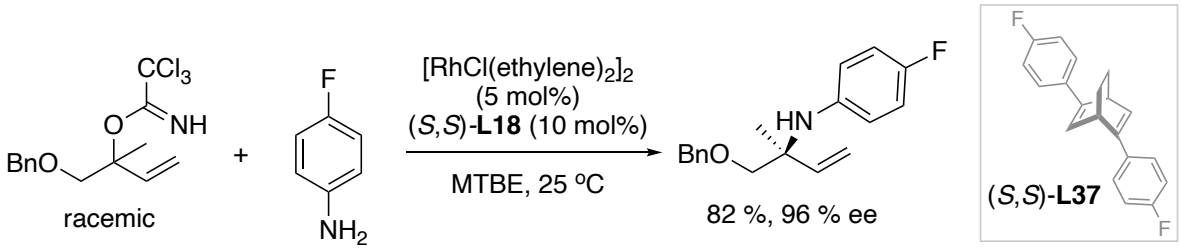
Beyond cyclic electrophilic coupling partners, the scope of this Rh-catalysed arylation could be extended to acyclic allylic substrates. With acyclic substrates, the potential challenge of *E*/*Z* selectivity is added. Evans and co-workers have reported a Rh-catalysed allylic arylation of acyclic enantioenriched allyl carbonates.[184] Aryl zinc bromide nucleophiles are employed in this enantiospecific, regioselective reaction. Lauten's and co-workers have reported a Rh-catalysed desymmetrisation of acyclic allylic biscarbonates employing arylboronic acid nucleophiles.[185] Recently, Li and co-workers reported a Rh-catalysed regio- and enantioselective allylic substitution of racemic acyclic allyl carbonates (Scheme 30),[82] which builds on earlier work by Breit and co-workers.[186] Along with branched allylic substrates (Scheme 30), linear allyl carbonates can also be tolerated with (*E*)- or (*Z*)-alkene stereochemistry. Addition of a variety of nitrogen-based nucleophiles was demonstrated along with the addition of weakly acidic carbon, oxygen, and sulphur-based nucleophiles. An

analogous transformation could potentially be realised with our Rh-catalysed system which would allow for the addition of arylboronic acid nucleophiles to acyclic allylic substrates.



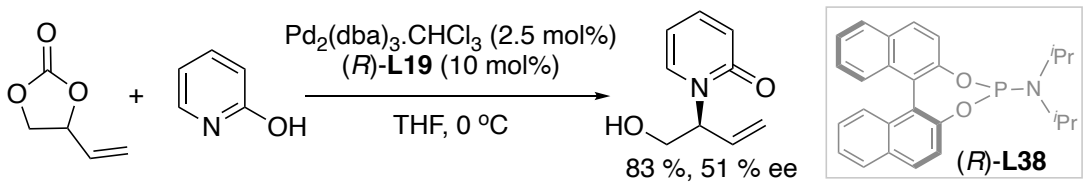
Scheme 30. Li and co-workers regio- and enantioselective allyl substitution of acyclic carbonates.[82]

Nguyen and co-workers successfully developed a Rh-catalysed regio- and enantioselective allylic amination with acyclic substrates to form quaternary stereocentre containing products (Scheme 31).[187] Further advancing our Rh-catalysed addition of boronic acids to enable the synthesis of acyclic quaternary stereocentre containing molecules would be an ambitious project where perhaps enantioenriched substrates could be again employed to solve possible selectivity issues that may arise.[188]



Scheme 31. Nguyen and co-workers regio- and enantioselective allyl substitution.[187]

Interestingly, the driving force here is the liberation of trichloroacetimidate. In this chapter we have examined some potential leaving groups for use in our Rh-catalysed arylation reactions such as halides, carbonates and phosphates. Allylic substitution reactions can operate with a wide variety of leaving groups and can also be driven by ring-opening or decarboxylation. For example, the Pd-catalysed regio- and enantioselective allylic substitution reaction shown in Scheme 32.[189] Pd-catalysed DyKATs with vinyl aziridines[190] and vinyl epoxide[191] electrophiles have been established. Electrophilic coupling partners like these may also be possible to employ in our Rh-catalysed arylation to generate acyclic products with more functionality.[192,193]



Scheme 32. Pd-Catalysed enantio- and regioselective allylic substitution.[189]

There are many exciting potential avenues to pursue within Rh-catalysed asymmetric Suzuki-Miyaura cross-couplings. We hope that the results described in this chapter, and in chapter 2, will inspire others to continue developing and utilising Rh-catalysed regio- and enantioselective arylation chemistry.

Chapter 4: Regioselective Synthesis of Cyclobutanes *via* Rhodium Catalysed Carbometallation

This chapter is based on a section of the following publication.

- F.W. Goetzke, A.M.L. Hell, L. van Dijk, & S. P. Fletcher, A General Catalytic Asymmetric Cross-Coupling Approach to the Synthesis of Cyclobutanes, *Nat. Chem.,* manuscript accepted (2021).

The results and discussion section of this chapter focuses on experiments performed by L.v.D. which will be published as part of this larger study. Experiments performed by co-authors of this publication are described in the introduction to this chapter (section 1.3).

1. Introduction

1.1 The Importance of Cyclobutanes

Cyclobutane motifs are found in many biologically active compounds.[194,195] These 4-membered carbocycles are found in natural products such as rumphellaone A and pentacycloanammoxic acid which has a pentacyclic ladderane core (Fig. 64). The cyclobutane structure is also found in many pharmaceutically relevant molecules such as drug candidate lobucavir (Fig. 64). Its prevalence in drug discovery is due to the structural rigidity of the 4-membered ring allowing for a defined spatial arrangement of its substituents, which is often favourable in drug design.[76,196]

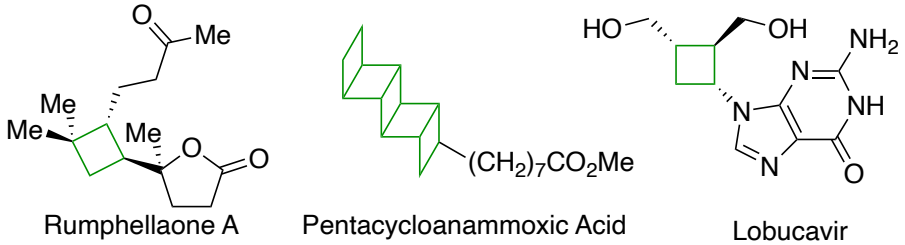


Figure 64. A selection of biologically active cyclobutanes.

The release of ring strain is commonly leveraged as a driving force in organic chemistry reactions and small carbocycles are primed for ring-expansion or ring-cleavage

transformations due to their inherent ring strain.[197] For this reason, cyclobutanes are strategically important intermediates in organic chemistry.[198]

1.2 Synthesis of Cyclobutanes

Photochemical and metal-catalysed [2+2] cycloaddition reactions are an efficient method for the synthesis of cyclobutanes from readily available starting materials.[199,200] Cyclobutanes can also be accessed *via* cyclisation of acyclic precursors, ring-expansion of cyclopropanes or *via* ring-contraction strategies.[201] For example, the cyclobutene core of natural product grandisol can be constructed *via* a photocatalysed [2+2] cycloaddition (Fig. 65a)[202] or *via* a transition metal catalysed cyclisation (Fig. 65b).[203]

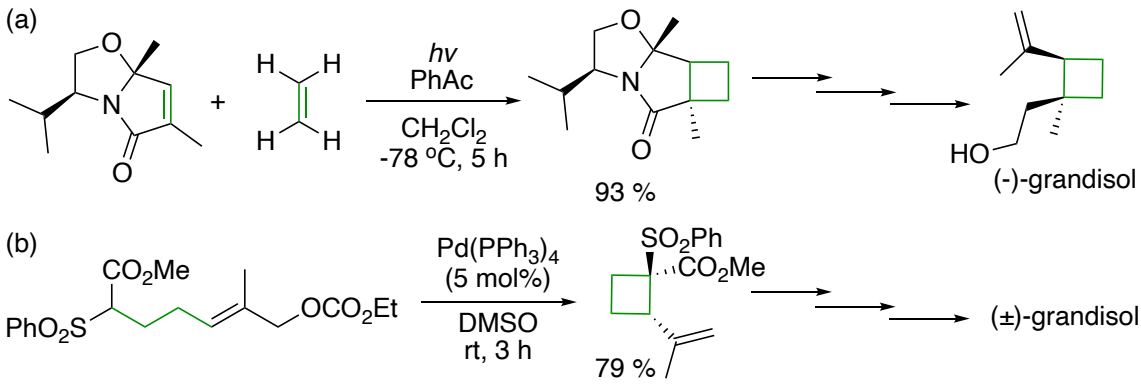
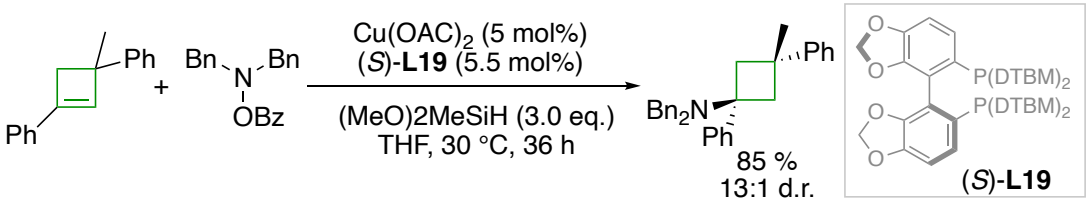


Figure 65. Two synthetic routes to the natural product grandisol showcasing the synthesis of a cylcobutane ring (a) *via* [2+2] photocyclisation[202] or (b) *via* transition metal-catalysed cyclisation.[203]

Photochemical and metal-catalysed [2+2] addition reactions,[200,204-207] and cyclisation reactions[208,209] are often employed in the enantioselective synthesis of chiral cyclobutanes, but are limited to specific substrate classes and substitution patterns. Alternatively, chiral cyclobutanes can be accessed by addition to activated cyclobutenes[210-212] or by functionalisation of 4-membered carbocycles using directing-group controlled C–H activation strategies.[213] Enantioselective copper-catalysed hydroboration and hydroamination reactions have been developed for the addition of heteroatom nucleophiles to cyclobutenes (Scheme

33),[214,215] but an analogous transformation to form new carbon-carbon bonds by asymmetric addition *via* carbometallation of cyclobutenes remains elusive.[216]



Scheme 33. Cu-catalysed hydroamination of cyclobutenes.[215] DTBM = 3,5-di-tert-butyl-4-methoxyphenyl

Despite recent advances in the area, there remains a dearth of general synthetic methods to synthesise complex, substituted cyclobutanes in a modular fashion.

1.3 Enantioselective Synthesis of Cyclobutanes *via* Rhodium Catalysed Carbometallation

Carbometallation is a commonly employed strategy in asymmetric catalysis and often exploits the release of ring strain as a driving force. This is exemplified by the reductive Heck reactions reported for unfunctionalised cyclopropenes[217] and (di-)azabicycles[218,219] triggered by the release of olefinic-strain (27.7 kcal/mol for cyclopropene and 4.8 kcal/mol for norbornene).[220] The hydroarylation of pyrrolines is also known.[221]

An analogous carbometallation process was previously unknown for unactivated cyclobutenes which possess a relatively small olefinic-strain of 1.9 kcal/mol.[220] However, we found that this is sufficient to drive carbometallation of cyclobutenes and thus developed a Rh-catalysed arylation of cyclobutenes. This reaction proceeds with a variety of aryl and heteroarylboronic acids to enantioselectively form chiral cyclobutane products with good to excellent enantioselectivity in a range of yields (Fig. 66).

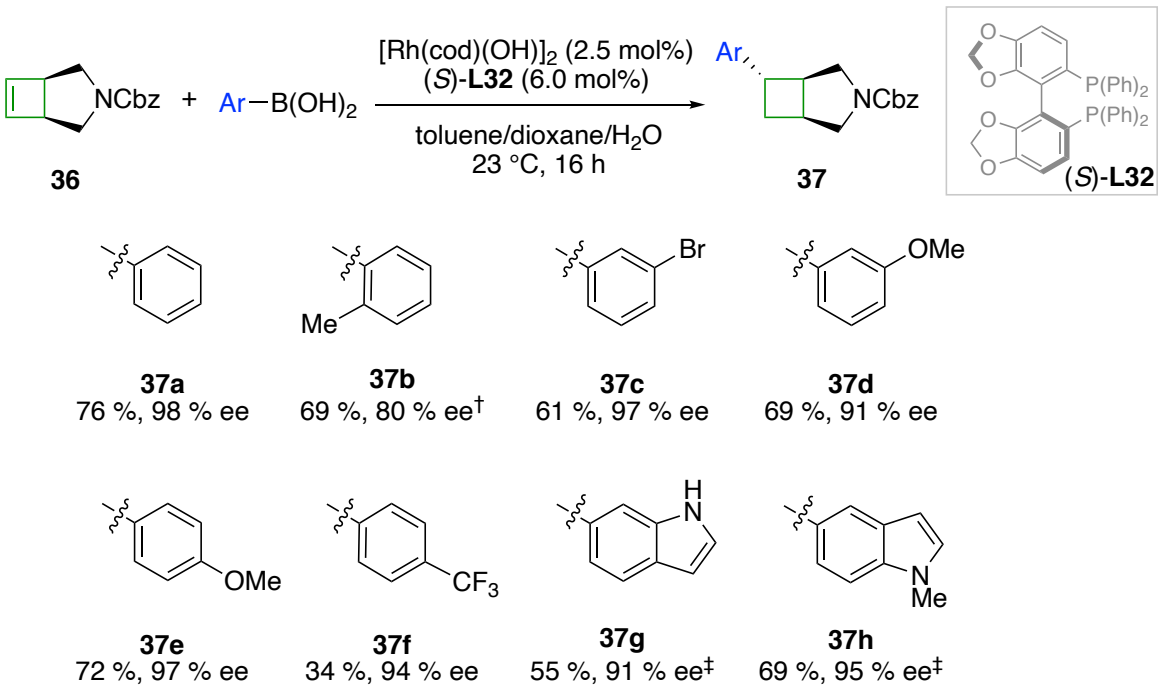


Figure 66. Rh-catalysed hydroarylation of bicyclic cyclobutenes with various (hetero-)arylboronic acids. Reaction conditions: toluene/dioxane/H_2O (25:25:1) †(*S*)-BINAP ligand used ‡at 60 °C.

We propose that this transformation occurs *via* a mechanism initiated by transmetalation to give Rh-aryl complex **II** (Fig. 67a).[77] The cyclobutene then undergoes rhodoarylation with **II** to give intermediate **III**. A chain-walking process *via* reversible β-hydride elimination and subsequent 1,2-hydride shifts leads to Rh-alkyl complex **IV**.[222] Remarkably, it appears that this chain-walking process can occur over the bridgehead of a fused bicycle (Fig. 67b). Protonation of **IV** with H_2O liberates the product **37** and regenerates catalyst **I**. A reaction performed in D_2O resulted in exclusive deuterium incorporation at the C_2 position (see Fig. 67a) which supports this proposed mechanism.

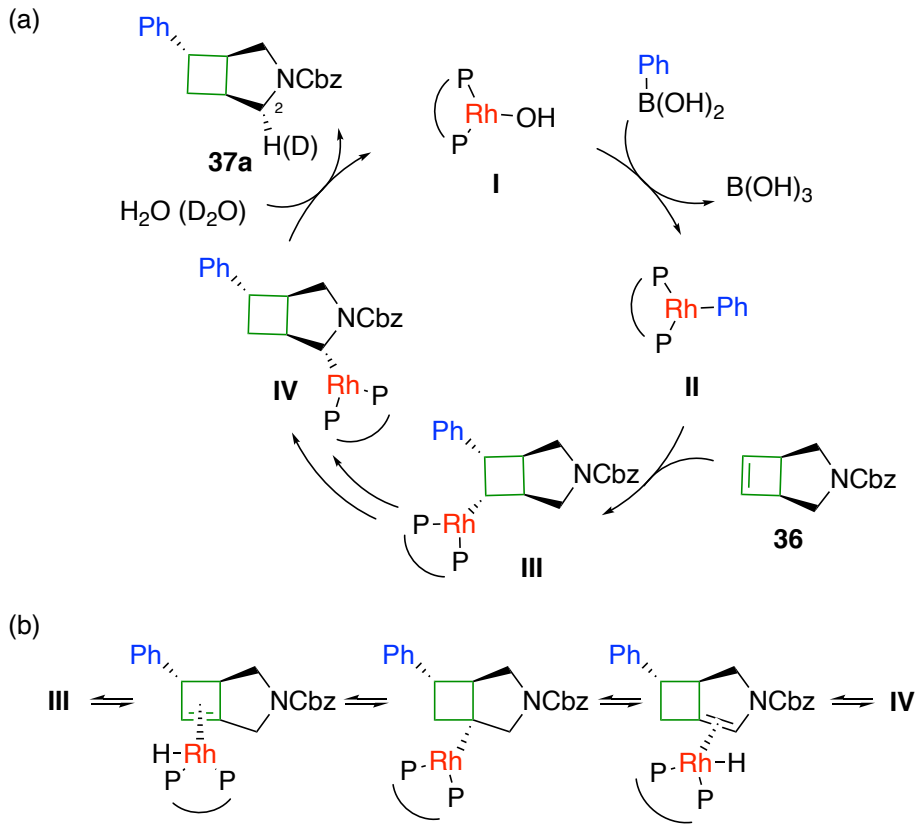


Figure 67. (a) Proposed mechanism based on deuterium-labelling. (b) Chain-walking mechanism.

To further explore the potential of the chain-walking mechanism proposed above (Fig. 67b), we investigated an asymmetric 1,5-addition to substituted cyclobutenes. The Rh-catalysed addition of 4-fluorophenylboronic acid to bicyclic cyclobutene **38** was achieved in good yield and with high enantioselectivity (Fig. 68a). This reaction can be scaled-up to gram quantities and the catalyst loading can be decreased from 2.5 to 0.5 mol% of dimeric $[Rh(cod)OH]_2$ to give 1.3 g of **39**.

The first two steps of the catalytic cycle likely occur *via* the same transmetalation and carbometallation sequence as with substrate **36** (Fig. 67a). After carbometallation, we propose that chain-walking *via* a β-hydride elimination/conjugated 1,4-hydride-addition sequence forms an oxa-π-allyl Rh-complex (Fig. 68b).[77] This is supported by a reaction with D_2O that resulted in 88% deuterium incorporation at the C_1 position (Fig. 68b).

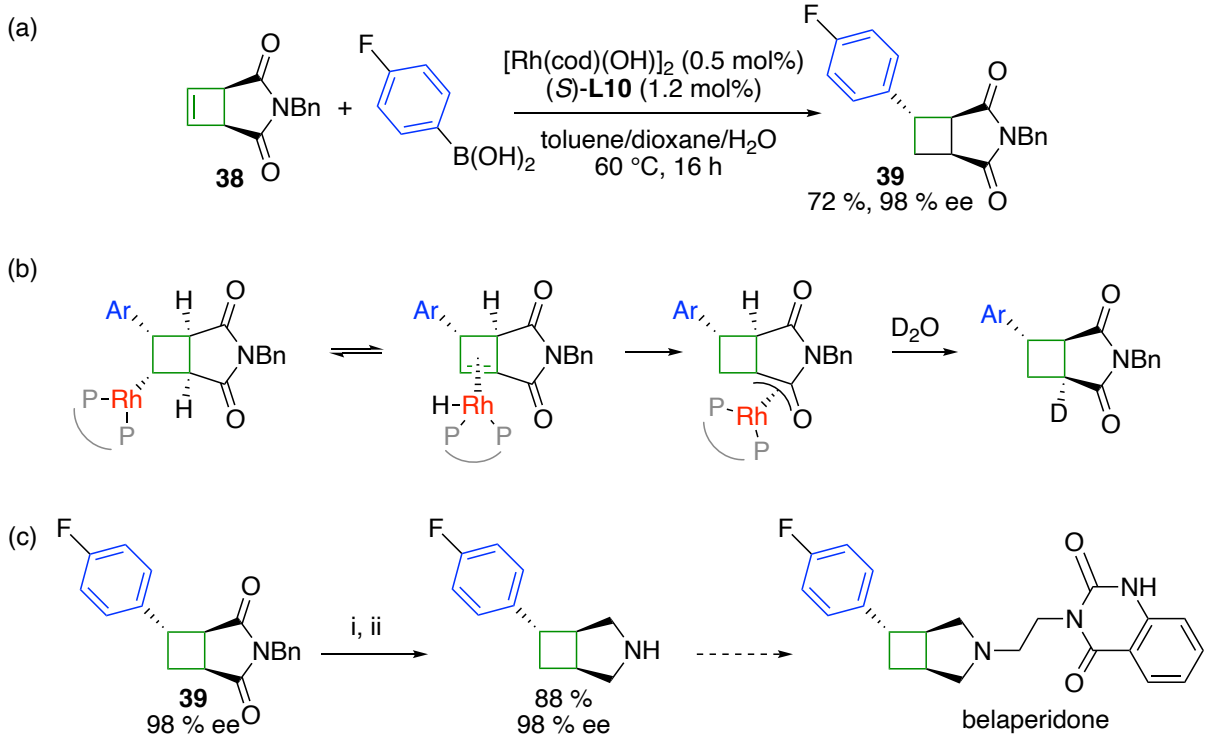


Figure 68. (a) Asymmetric 1,5-addition triggered by carbometallation. Reaction conditions: toluene/dioxane/H_2O (5:5:1). (b) Proposed mechanism of formation of a Rh oxa-π-allyl complex, supported by deuterium labelling. (c) Formal syntheses of belaperidone. Reaction conditions: (i) $LiAlH_4$, Et_2O/CH_2Cl_2, 23 °C, 16 h, 89 %. (ii) H_2, $Pd(OH)_2/C$, MeOH, 23 °C, 16 h, 99 %.

We have seen that this Rh-catalysed carbometallation of cyclobutenes enables addition reactions with arylboronic acids including the reductive Heck reaction and 1,5-addition described above (Fig. 66 and 68a). The synthetic applicability of these highly stereoselective transformations has been demonstrated in a concise synthesis of the D4/5-HT2 antagonist belaperidone (Fig. 68c).

1.4 Project Aim

The Rh-cyclobutyl intermediates formed in this catalytic carbometallation could conceivably engage in multiple pathways, including chain-walking (as seen in Fig. 67b and 68b) or C–H insertion. We wanted to further explore the potential of this promising transformation, which could be envisioned to enable the synthesis of a diverse range of substituted cyclobutanes. We were particularly interested to find if our strategy could be applied to the synthesis of other biologically active compounds.

Spirocyclic motifs are prevalent in drug discovery and agrochemistry research (Fig. 69).[196,223] We chose to investigate the application of our Rh-catalysed carbometallation method to the synthesis of cyclobutene-containing spirocyclic scaffolds. This presented the opportunity to synthesis drug-like molecules alongside the challenge of achieving high regioselectivity in the carbometallation of non-symmetrical cyclobutenes.

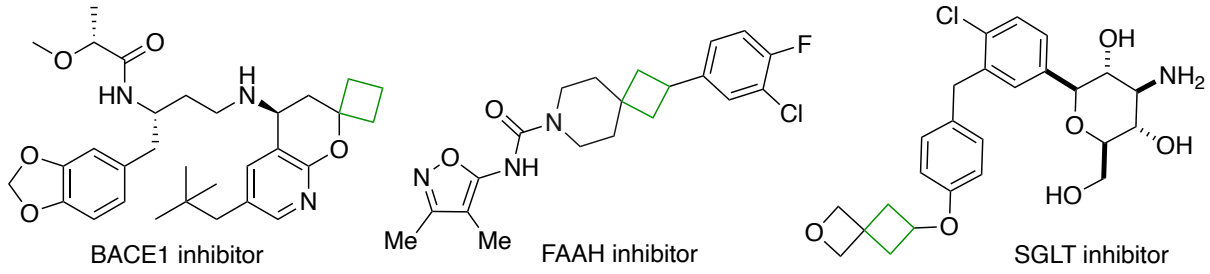
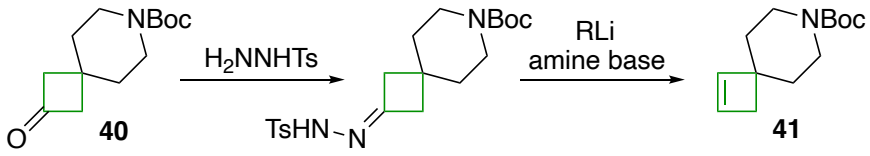


Figure 69. A selection of biologically active spirocyclic compounds containing cyclobutanes.[223] BACE1 = beta-site APP cleaving enzyme 1. FAAH = fatty acid amide hydrolase. SGLT = Sodium Glucose Linked Co-Transporter.

2. Results and Discussion

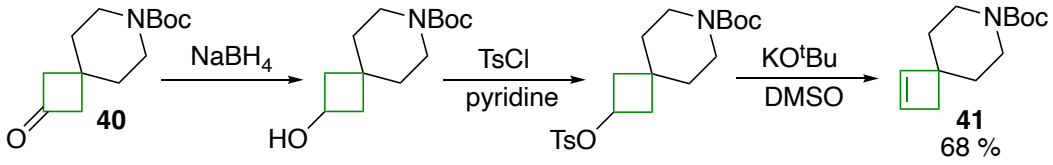
2.1 Spirocyclic Cyclobutene Synthesis

Prochiral, spirocyclic 7-azaspiro[3.5]non-1-ene **41** was chosen as a model substrate, with synthesis from readily available cyclobutanone **40** envisaged. A synthetic route employing the Shapiro reaction was initially trialled[224] but it was found that the hydrazone elimination step was capricious and often low yielding on gram-scale (Scheme 34, 20-40 % yield over two steps).



Scheme 34. Synthetic route to **41** employing the Shapiro reaction.

An alternative synthetic route was proposed with reduction of the ketone to give an alcohol which could then be transformed into a suitable leaving group and eliminated. After screening some potential organosulphonate leaving groups, tosylate was selected as its elimination proceeded in good yield. This synthetic route can be reliably used to synthesis gram quantities of **41** in 68 % yield over 3 steps (Scheme 35).

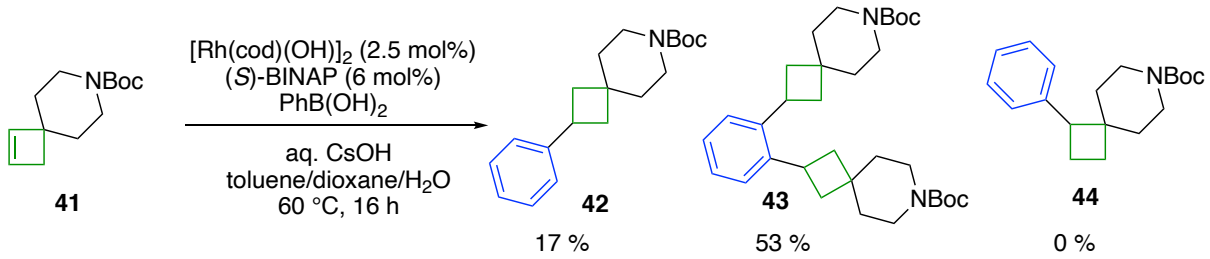


Scheme 35. Optimised synthetic route to **41**.

2.2 Optimisation of the Hydroarylation of Spirocyclic Cyclobutenes

An insightful preliminary experiment performed by F.W. Goetzke, revealed that prochiral, spirocyclic 7-azaspiro[3.5]non-1-ene **41** was a suitable substrate for hydroarylation (Scheme 36). The addition of phenylboronic acid to cyclobutene **41** showed complete regioselectivity for achiral cyclobutane **42** and the regioisomeric chiral 1,2-substituted cyclobutene **44** was not

observed. However, the yield of **42** was low (17 % yield) with dimer **43** being the major product observed (53 % yield).

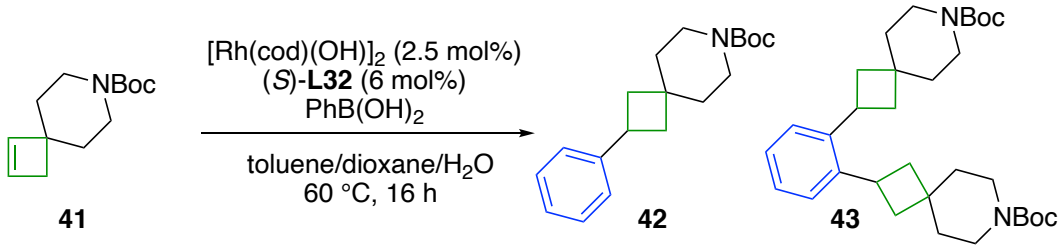


Scheme 36. Initial experiment performed by F.W. Goetzke which provided an excellent starting point for the optimisation of this Rh-catalysed carbometallation reaction.

A variety of conditions for the Rh-catalysed arylation were screened with the aim of increasing the yield of **42** by improving the selectivity for the monomeric product. Alternative conditions were selected based on those previously optimised for the enantioselective reductive Heck reaction shown in Fig. 66 using a Rh/(*S*)-Segphos ((*S*)-**L32**) chiral catalyst. Under these conditions (Table 4, entry 1), the addition of phenylboronic acid to cyclobutene **41** again showed complete regioselectivity for achiral cyclobutane **42** and the regioisomeric chiral cyclobutene **44** was not observed. The yield was improved and **42** was generated as the major product. However, the yield obtained was still low due to the competitive formation of dimeric product **43**, along with incomplete conversion of starting material.

With this result to hand, various conditions were screened with the aim of optimising the synthesis of **42** by increasing the conversion of starting material and improving the selectivity for the monomeric product. The conversion was improved by doubling the number of equivalents of phenylboronic acid (Table 4, entry 2). Adding one equivalent of base improved the monomer/dimer selectivity but reduced the conversion (Table 4, entry 3). This was rectified by increasing the percentage of H_2O in the solvent system which improved both conversion and selectivity (Table 4, entry 4 and 5).

Table 4 Optimisation of the regioselective Rh-catalysed reductive Heck reaction to form achiral product **42** with formation of undesired dimeric side-product **43**. Conversion and monomer:dimer ratio determined by ^{1}H NMR.

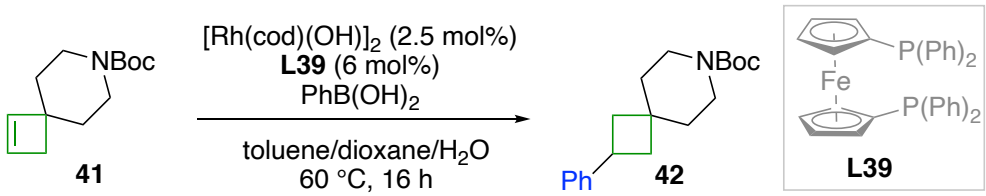


41 **42** **43**

	Ligand	Eq. $PhB(OH)_2$	toluene/dioxane/H_2O ratio	Base	Conv. (%)	**42** : **43**
1	(*S*)-**L32**	2.0	1.0 : 1.0 : 0.04	-	60	2.0 : 1.0
2	(*S*)-**L32**	4.0	1.0 : 1.0 : 0.04	-	80	3.0 : 1.0
3	(*S*)-**L32**	4.0	1.0 : 1.0 : 0.04	Cs_2CO_3	75	4.0 : 1.0
4	(*S*)-**L32**	4.0	1.0 : 1.0 : 0.22	Cs_2CO_3	70	5.5 : 1.0
5	(*S*)-**L32**	4.0	1.0 : 1.0 : 0.22	CsOH	80	5.0 : 1.0

As this transformation is not asymmetric, a chiral ligand is not required and thus an achiral ligand would be much preferable. After screening a variety of chiral and achiral phosphine ligands, achiral 1,1'-Bis(diphenylphosphino)ferrocene (dppf, **L39**) was selected as it enabled high conversion of starting material and increased selectivity for the monomeric product **42** (Table 5). With achiral Rh/dppf catalyst, the conversion and selectivity were improved in the presence of aqueous CsOH base (Table 5, entry 1 vs. 2). Optimal results were achieved with three equivalents of phenylboronic acid at 60 °C for 16 hours (Table 5, entries 3-5). Under these optimised conditions (Table 5, entry 3), the regioselective Rh/dppf catalysed addition of phenylboronic acid to spirocyclic cyclobutene **41** resulted in an 84 % isolated yield of achiral cyclobutane **42**.

Table 5. Optimisation of the regioselective Rh-catalysed reductive Heck reaction to form achiral product **7**. Conversion and monomer:dimer (**42**:**43**) ratio determined by ^{1}H NMR.



	Eq. $PhB(OH)_2$	toluene/dioxane/H_2O ratio	Base	Time (h)	Conv. (%)	**42** : **43**
1	4.0	1.0 : 1.0 : 0.2	CsOH	16	100	8 : 1
2	4.0	1.0 : 1.0 : 0.2	-	16	98	7 : 1
3	2.0	1.0 : 1.0 : 0.2	CsOH	16	90	8 : 1
4	3.0	1.0 : 1.0 : 0.2	CsOH	16	100	8 : 1
5	3.0	1.0 : 1.0 : 0.2	CsOH	1.5	70	8 : 1

2.3 Scope of the Hydroarylation of Spirocyclic Cyclobutenes

With optimised conditions for the regioselective Rh-catalysed reductive Heck reaction to form achiral product **42** to hand, the scope of the reaction was explored by examining a range of arylboronic acid nucleophiles (Fig. 70). Good to moderate yields for a range of functionalised *meta*- and *para*-substituted arylboronic acids were achieved (Fig. 70). Several functional groups including halides that can serve as handles for subsequent complementary cross-coupling reactions were tolerated (**46**-**49**, **54**). Lower yields were obtained with boronic acids with electron-donating groups in the *para*-position (**50** and **51**). With *ortho*-substituted arylboronic acids, which often suffer from low yields in transition metal catalysed reactions,[225] we also obtained a reduced yield (**45**). The heterocyclic coupling partner benzofuran-2-ylboronic acid gave a good yield (**55**).

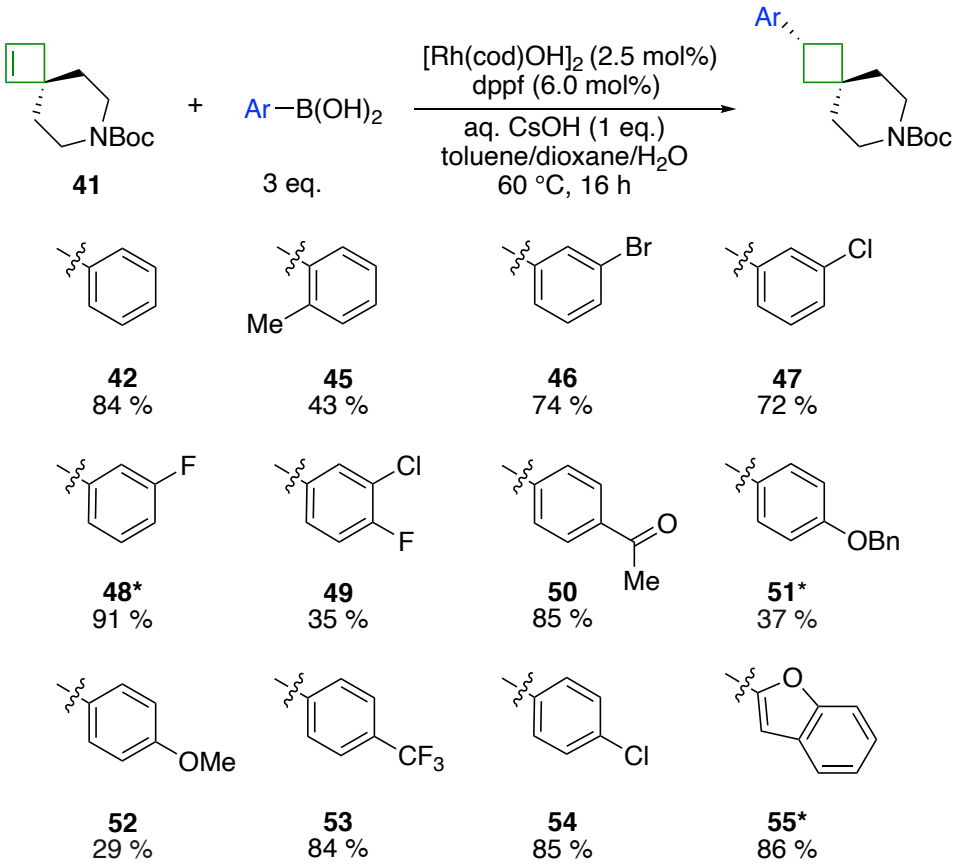
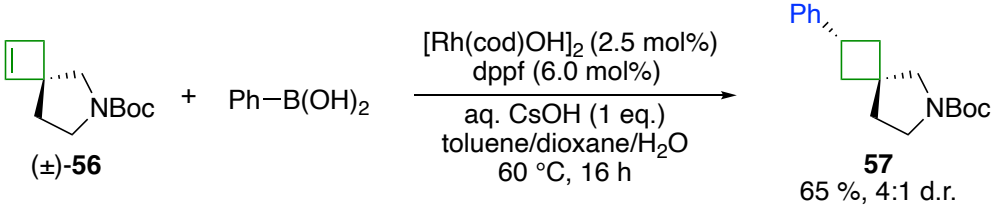


Figure 70. Rh-catalysed regioselective reductive Heck of various arylboronic acids with prochiral, spirocyclic cyclobutene **6**. **Examples with an asterisk were synthesised by F.W.G.*

In order to investigate the potential for diastereoselectivity in this regioselective cross-coupling reaction, racemic spirocyclic 6-azaspiro[3.4]oct-1-ene (**56**) was synthesised from the corresponding, readily available cyclobutanone *via* an analogous synthetic route to that detailed in scheme 35 (39 % yield over 3 steps). Under the reaction conditions optimised for the Rh-catalysed arylation of **41**, addition of phenylboronic acid to cyclobutene (±)-**56** gave achiral **57** with a diastereomeric ratio of 4:1 (Scheme 37).



Scheme 37. Diastereo- and regioselective reductive Heck with a racemic cyclobutene. Major diastereomer of product shown. The relative stereochemistry was assigned using 2D NOESY NMR.

2.4 Application to the Target Synthesis of a Biologically Active Cyclobutane

We chose to investigate these spirocyclic cyclobutene scaffolds as this moiety is common in a number of promising drug candidates. This is exemplified by the spirocyclic cyclobutene-containing core of orally efficacious fatty acid amide hydrolase (FAAH) inhibitor PF-04862853 (Fig. 71a).[226]

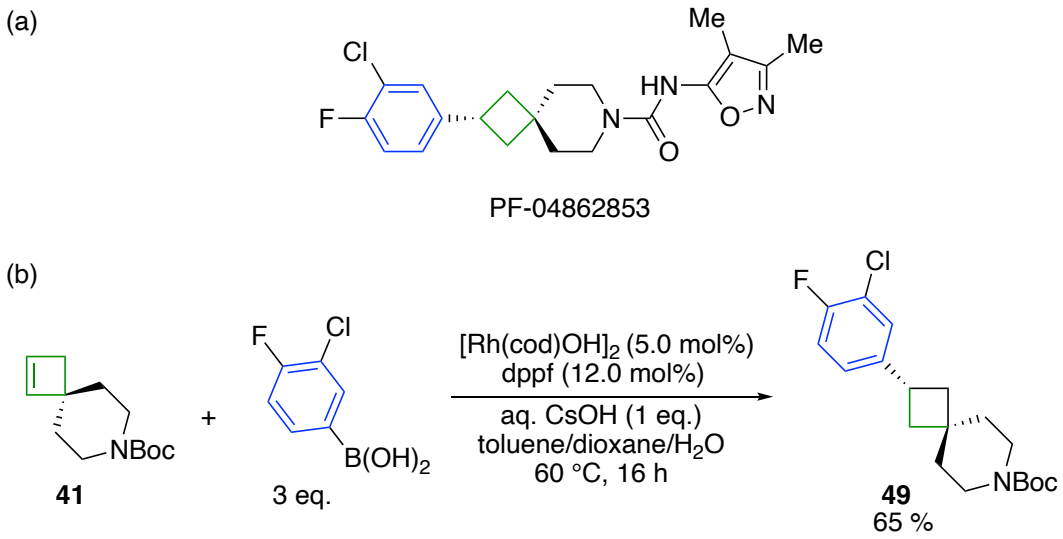


Figure 71. (a) Drug candidate PF-04862853 (b) Regioselective Rh-catalysed arylation with with (3-chloro-4-fluorophenyl)boronic acid.

Under previously optimised conditions, the Rh-catalysed coupling of **41** with (3-chloro-4-fluorophenyl)boronic acid gave a low yield (35 %, Fig. 70, **49**). However, doubling the Rh/dppf catalyst loading to 10 % (5 mol% of the dimer) increased the yield to an acceptable 65 % (Fig. 71b). It has been reported that **49** can be converted into PF-04862853 in two steps; removal of the Boc protecting group under acidic conditions followed by construction of the urea moiety.[226] Thus, this regioselective Rh-catalysed arylation reaction enables a concise and modular formal synthesis of this pharmaceutically relevant FAAH inhibitor.[226,227]

2.5 Mechanism of the Hydroarylation of Spirocyclic Cylobutenes

We were interested in gaining some insight into the mechanism of this reaction. As shown previously (section 1.3), transmetalation from boron to Rh is the first step in our proposed catalytic cycle (Fig. 72a). This is followed by a regioselective carbometallation step to give **IIIa**. It is quite remarkable that we see excellent selectivity for this achiral product **42**, and don't observe the chiral 1,2 substituted cyclobutene (**44**, Fig. 72b), as the Rh adds to the more hindered position than the aryl group in the carbometallation step.

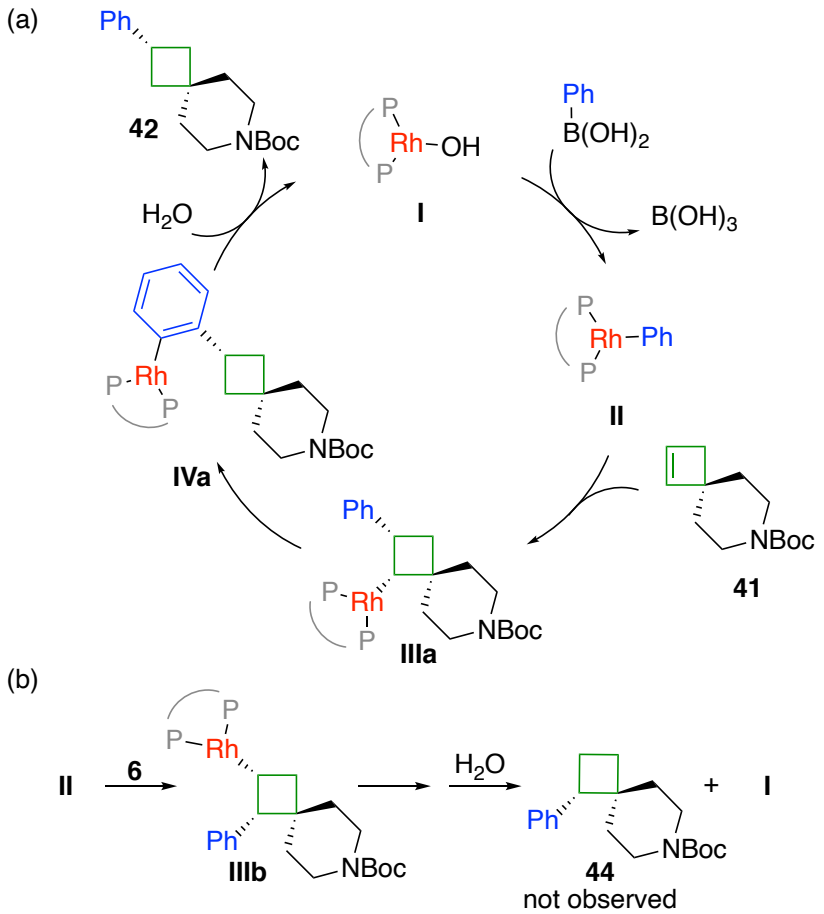
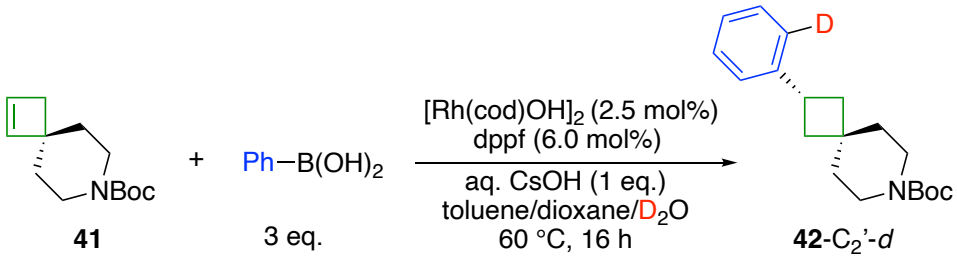


Figure 72. (a) Proposed catalytic cycle for the Rh-catalysed addition of phenylboronic acid to prochiral cyclobutene **41** *via* regioselective carbometallation. (b) Potential pathway for the formation of chiral 1,2 disubstituted cyclobutane **44** which is not observed.

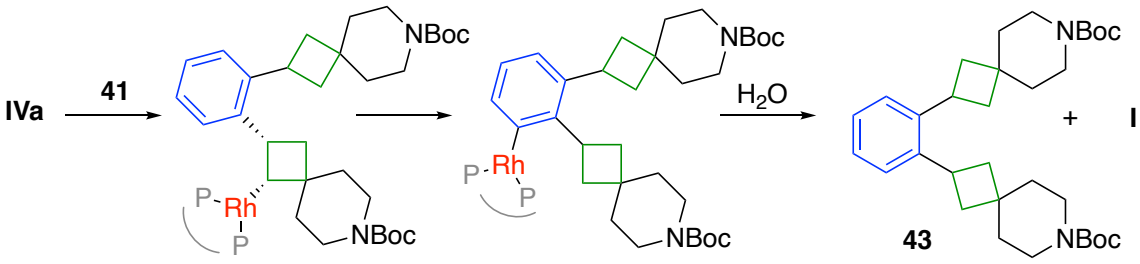
A deuterium labelling experiment using D_2O in place of H_2O resulted in 80 % deuterium incorporation at the C_2' position (Scheme 38). In contrast to the systems described in the introduction to this chapter, here there is no β-hydride available in complex **IIIa** to allow the

chain-walking process to occur (section 1.3, chain-walking proposed to occur *via* reversible β-hydride elimination and subsequent 1,2-hydride shifts). The deuterium labelling experiment shown in scheme 38, confirms that here protonation occurs *via* a C-H insertion pathway. Rhodium inserts in the ortho-aryl C–H bond in complex **IIIa** resulting in Rh-aryl complex **IVa** (Fig. 72a).



Scheme 38. Experiment with D_2O resulting in 80% deuterium incorporation at the C_2' position.

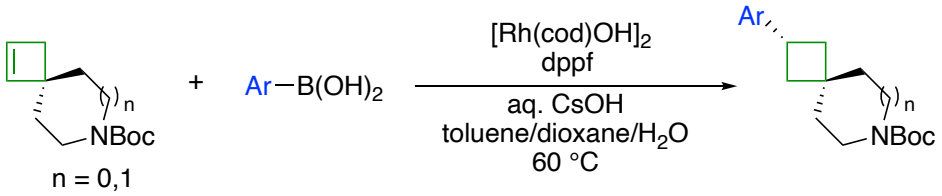
The dimeric side-product can be accounted for by Rh complex **IVa** undergoing a second carbometallation step with another molecule of **41** leading to the formation of dimer **43** (Scheme 39).[228] Alternatively, Rh complex **IVa** is directly protonated to release the arylated achiral product **42**.



Scheme 39. Proposed mechanism for the competing side-reaction to form dimer **43**.

3. Conclusions

We have developed a Rh-catalysed regioselective carbometallation reaction to synthesis achiral spirocyclic cyclobutanes (Scheme 40). A range of electron rich and electron poor arylboronic acids are tolerated in this regioselective reductive Heck reaction and we have also shown the potential for heteroarylboronic acid to be employed. A catalytic cycle is proposed involving transmetalation, followed by a regioselective carbometallation. A deuterium labelling experiment revealed that the protonation proceeds *via* a C-H insertion pathway to give the arylated cyclobutane product.



Scheme 40. Rh-catalysed regioselective cross-coupling of spirocyclic cyclobutenes and arylboronic acids.

The utility of this chemistry is demonstrated by the concise modular formal total synthesis of drug candidate PF-04862853 which is a FAAH inhibitor that possesses a spirocyclic core. We anticipate the use of this cross-coupling procedure in biomedical and agrochemical research and the fine chemicals industry.

4. Future Directions

This transformation could almost certainly be applied to additional arylboronic and heteroarylboronic acid coupling partners, and also potentially to vinylboronic acids with some optimisation likely to be required (Fig. 73a).[54]

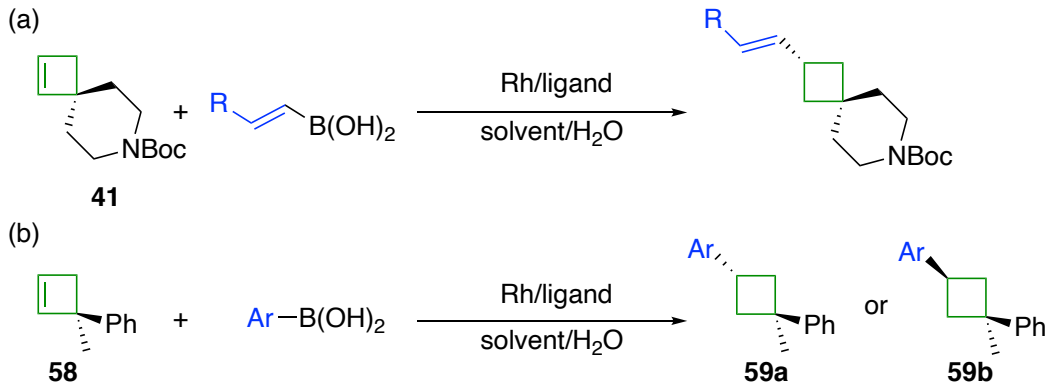


Figure 73. Proposed future work (a) Extension of the nucleophile scope to include vinyl boronic acids. (b) Extension of the electrophile scope to include non-spirocyclic cyclobutenes and potentially other diastereoselective transformations such as the example shown here.

The diastereoselectivity observed when a racemic cyclobutene was employed (section 2.3) displays the potential to develop other regio- and diastereoselective transformations. Likely, non-spirocyclic prochiral cyclobutene substrates could also be employed and racemic cyclobutenes (such as (±)-**58**) could be used to further investigate the potential to achieve diastereoselective transformations (Fig. 73b).

This Rh-catalysed transformation could also be envisioned to be employed in the synthesis of 4-membered heterocycles such as azetidines which can be found in biologically active compounds (Fig. 74a).[229,230] As they are attractive moieties in drug discovery programs, the development of new generally applicable methods to synthesis azetidines in a modular fashion is highly desirable.[231,232] Azetidine **60** is readily available and an analogous synthetic route to that used for the spirocyclic substrates described in this chapter can be applied to the synthesise of 1,2-dihydroazete **61** (Fig. 74b).[233] This substrate could then be exploited in a Rh-catalysed cross coupling with arylboronic acid nucleophiles to form arylated azetidine products (Fig. 74c).[234]

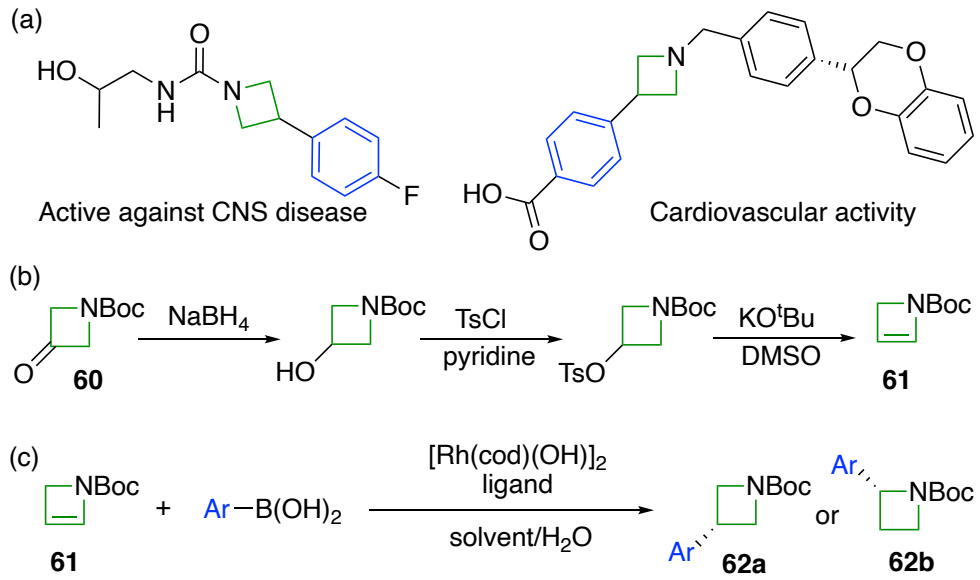


Figure 74. Proposed future work (a) Biologically active arylated azetidines.[229] (b) Synthetic route developed can likely also be applied to the synthesis of **61**. (c) Rh-catalysed arylation to synthesis arylated azetidines.

4-membered heterocycles are important motifs in drug discovery.[196] This transformation would not necessarily be limited to azetidines, arylation of other small molecule 4-membered heterocycles could also be envisioned such as oxetanes[235,236], thietanes,[196] diazetidines[237] or oxazetidines.[238]

This newly developed Rh-catalysed arylation of cyclobutenes opens up many potential exciting pathways and opportunities to be explored. Aside from Rh-catalysed cyclobutene carbometallation, other transition metal catalysed cyclobutene carbometallation processes with alternative nucleophiles are likely to be possible, and we anticipate their investigation will uncover additional new and useful reactivity patterns.

Supplementary Information

1. Instrumentation, Methods and Materials

Procedures using oxygen and/or moisture-sensitive materials were performed with anhydrous solvents with rigorous exclusion of air under an inert atmosphere of argon in flame-dried glassware with magnetic stirring, using standard Schlenk techniques. Heating was performed using Drysyn® heating blocks and the heating plate of the stirrer and cooling was performed using a Julabo FT902 immersion cooler. Argon-flushed plastic syringes were used to transfer air and moisture sensitive reagents. Anhydrous solvents were obtained from the mBraun SPS-800 solvent purification system equipped with anhydrous alumina columns. The evaporation of solvent under reduced pressure with heating on a rotary evaporator has been referred to as *in vacuo*. THF-d_8 was purchased from Fluorochem. Other deuterated solvents were purchased from Sigma-Aldrich. $[Rh(cod)(OH)]_2$ was purchased from Sigma Aldrich and (*S*)-Xylyl-P-Phos ligand was purchased from Alfa Aesar. Other commercially available reagents were purchased from Sigma-Aldrich, Fisher Scientific, Apollo Scientific, Acros Organics, Strem Chemicals, Alfa Aesar or TCI UK and were used without purification, unless otherwise stated.

Analytical thin-layer chromatography was performed on pre-coated glass-backed plates (Silica Gel 60 F254; Merck) and visualised using a combination of UV light (λ_{max} = 254 nm) and aqueous ceric ammonium molybdate, aqueous basic potassium permanganate stains or *p*-anisaldehyde solution, sometimes followed by heating. Flash column chromatography was carried out using Apollo Scientific silica gel 60 (0.040 – 0.063 nm), Merck 60 Å silica gel, VWR (40-63 μm) silica gel and Sigma Aldrich silica gel. Pressure was applied at the column head *via* a flow of nitrogen. For the reactions described in Chapter 4, medium-pressure chromatography was performed on a CombiFlash Next Gen 100 system.

^{1}H, ^{2}H, ^{13}C, ^{31}P, ^{19}F NMR and 2D NMR experiments were carried out using Bruker AVIII HD 400 (400/100 MHz), AVIII HD 500 (500/125 MHz) or AVII 500 (500/125 MHz) spectrometers. Unless stated otherwise, solution NMR spectra were recorded at room temperature. All ^{13}C spectra were ^{1}H decoupled. Chemical shifts (δ) have been quoted in parts per million (ppm) downfield of tetramethylsilane (TMS) and referenced to residual solvent peak. Assignments were made with the assistance of two-dimensional NMR techniques including 1H-gCOSY, HSQC and NOESY. NMR data has been represented as follows: chemical shift (δ ppm), multiplicity (s = singlet, d = doublet, t = triplet, q = quartet, dd = doublet of doublets, dt = doublet of triplets, m = multiplet), coupling constant (*J*) in Hertz (Hz), integration.

Chiral HPLC separations were achieved using an Agilent 1230 Infinity series normal phase HPLC unit and HP Chemstation software. Chiralpak® columns (250 × 4.6 mm), fitted with matching Chiralpak® Guard Cartridges (10 × 4 mm), were used as specified in the text. Solvents used were of HPLC grade (Fisher Scientific, Sigma Alrich or Rathburn); all eluent systems were isocratic. Chiral supercritical fluid chromatography (SFC) separations were conducted on a Waters Acquity UPC^2 (Ultra Performance Convergence Chromatography) system equipped with a fluid delivery module (a liquid CO_2 pump and a modifier pump), a sampler manager (FL autosampler), a heated column manager 30s fitting eight installed columns and a photodiode array detector. Daicel Chiralpak® IA-3, IB-3, IC-3, ID-3, IE-3, IF-3 or IG-3 columns were used as indicated. Gas chromatography (GC) was also used in some cases to determine enantiomeric excess. This was performed on an Agilent Technologies GC system with a non-racemic β-DEX column.

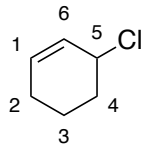
Low resolution mass spectrometry (electrospray ionisation (ESI-TOF)) (LRMS) was completed on a Fisons Platform II mass spectrometer. Low resolution (LRMS) and high resolution (HRMS) mass spectral analyses were acquired by electrospray ionisation (ESI), electron impact (EI) and/or field ionisation (FI). Low resolution ESI were recorded using an Agilent 6120 quadrupole LC/MS. High resolution accurate ESI were recorded using a Thermo Exactive 1.1 SP5 Benchtop orbitrap MS and EI/FI on a Waters GTC Temperature programmed solid probe inlet performed by the internal service within the department of chemistry, University of Oxford. Infrared measurements were carried out using a Bruker Tensor 27 FT-IR with internal calibration in the range 600-4000 cm^{-1} equipped with a PIKE Miracle Attenuated Total Reflectance sampling accessory.

2. Supplementary Information for Chapter 2

2.1 Preliminary NMR Spectroscopic Experiments

NMR experiments were carried out on AVIIIHD 500 and AVII 500 spectrometers equipped with conventional or cryo-probes. Processing was performed using MNova 12.0. All solvents were dried over 3Å molecular sieves and degassed under a flow of argon for a minimum of 30 min. The solvents were stored at 0 °C, in a Schlenk flask on molecular sieves, protected from light.

3-chlorocyclohex-1-ene (**3**)



Phosphorus trichloride (0.92 mL, 11.0 mmol, 0.37 eq.) was added dropwise at 0 °C to a solution of cyclohex-2-en-1-ol (2.8 mL, 28.5 mmol, 1.0 eq.) and pyridine (0.23 mL, 2.9 mmol, 0.1 eq.). After vigorously stirring at 0 °C for 15 min, the solution was allowed to warm up to room temperature and stirred overnight. With a pipette the supernatant oil was transferred to a new flask and then purified by Külgelrohr distillation (60 mbar, 110 °C) to afford the title product (**3**, 3.5 g, 30 mmol, 79 %) as a colourless oil.

^{1}H NMR (500 MHz, $CDCl_3$): δ 5.94-5.85 (m, 1H; C(1)-H), 5.85-5.79 (m, 1H; C(6)-H), 4.62 (br dd, *J*=11.5, 4.3 Hz, 1H; C(5)-H), 2.18 - 2.08 (m, 1H), 2.08-2.01 (m, 3H), 1.96-1.83 (m, 1H), 1.71-1.61 (m, 1H).

^{13}C NMR (125 MHz, $CDCl_3$) δ 131.3 (C(6)), 128.1 (C(1)), 55.5 (C(5)), 32.4 (C(4)), 24.7, 18.4.

^{1}H NMR (500 MHz, THF-d_8) δ 5.82 (dt, *J* = 10.1, 3.6 Hz, 1H; C(1)-H), 5.79 – 5.73 (m, 1H; C(6)-H), 4.60 (dt, *J* = 4.7, 4.6 Hz, 1H; C(5)-H), 2.14 – 1.93 (m, 4H), 1.93 – 1.80 (m, 1H), 1.67 – 1.57 (m, 1H).

^{13}C NMR (126 MHz, THF-d_8) δ 131.6 (C(6)), 129.4 (C(1)), 56.1 (C(5)), 33.6, 25.6, 19.5.

HRMS (EI/FI) *m/z* calcd for C_6H_9Cl [M]+: 116.0393; found: 116.0390.

Physical data identical to that which was previously reported by our group.[53] Spectra were previously reported in $CDCl_3$, here spectra are also reported in THF-d_8.

Pre-catalyst formation with (*S*)-Xylyl-P-Phos ((*S*)-L14)

Formation of complex [Rh(**L14**)(OH)]$_2$ observed by ^{31}P NMR

This experiment was performed by M.S. In a flame-dried NMR tube (*S*)-Xylyl-P-PHOS ((*S*)-**L14**, 16.6 mg, 0.02 mmol, 1.0 eq.) was dissolved in 0.4 mL of THF-d_8 under argon and ^{31}P NMR data was acquired. In a flame-dried 5 mL round-bottomed flask, [Rh(cod)(OH)]$_2$ (5.0 mg, 0.01 mmol, 0.5 eq.) and Cs_2CO_3 (7.2 mg, 0.02 mmol, 1.0 eq.) were dissolved in THF-d_8 (0.2 mL) under argon. The suspension was transferred *via* syringe to the NMR tube containing the ligand. Immediately the tube was inserted in the AVH III 500 spectrometer and the formation of the complex was monitored by a multiscan sequence at different temperatures (295 to 333 K) (Fig. S1).

^{31}P NMR of **L14** (202 MHz, THF-d_8) δ –13.19.

^{31}P NMR of [Rh$_2$(cod)(**L14**)(OH)$_2$] (202 MHz, THF-d_8) δ 53.19 ($J_{Rh\text{-}P}$ = 192.8 Hz).

^{31}P NMR of [Rh(**L14**)(OH)]$_2$ (202 MHz, THF-d_8) δ 51.99 ($J_{Rh\text{-}P}$ = 182.2 Hz).

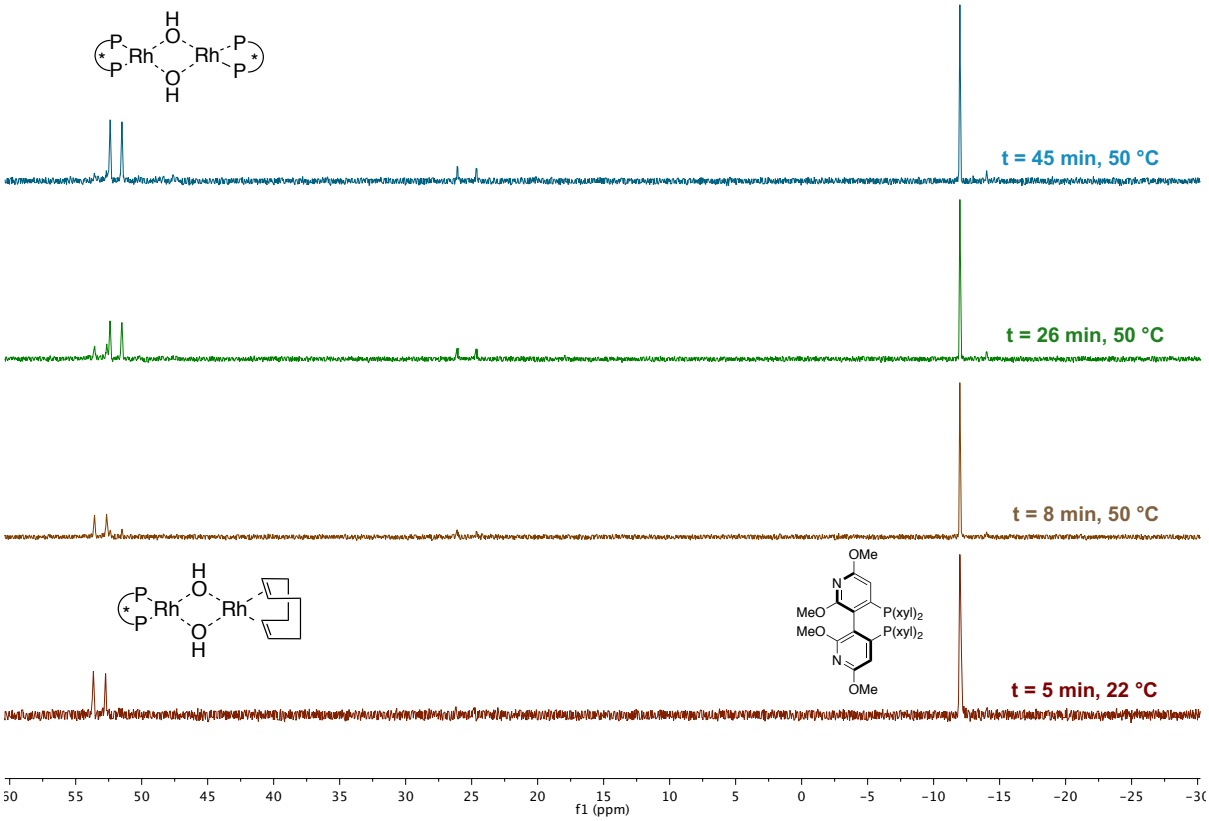


Figure S1 ^{31}P NMR spectra showing the formation of [Rh(**L14**)(OH)]$_2$.

Transmetalation with PhB(OH)$_2$

This experiment was performed by M.S. In a 5 mL flame-dried round bottomed flask, (*S*)-Xylyl-P-PHOS (**L14**, 16.6 mg, 0.02 mmol, 1.00 eq.) and [Rh(cod)(OH)]$_2$ were dissolved in 0.4 mL of anhydrous THF (in this case non-deuterated solvent was used) under argon. The reaction was stirred for 30 min at 60 °C and then transferred to a flame-dried NMR tube under argon. An initial ^{31}P NMR without locking was acquired before adding PhB(OH)$_2$ (**1**, 2.4 mg, 0.02 mmol, 1.00 eq.) in THF (0.3 mL). The doublet corresponding to the [Rh(**L14**)(OH)]$_2$ dimer immediately broadens and two sets of peaks appeared at 29.60 (dd, *J* = 104.6, 37.2 Hz) and 25.16 (dd, *J* = 145.6, 37.1 Hz) which belong to the same compound according to ^{31}P COSY NMR. We assigned the two sets of dd to belong to a phenyl-rhodium intermediate. However, attempts to unravel expected correlations between the ^{31}P and the aromatic protons of the phenyl group were unsuccessful due to the high complexity of the aromatic region in the ^{1}H NMR.

EXSY Experiment

In a 10 mL round bottomed flask $[Rh(cod)(OH)]_2$ (2.3 mg, 0.015 mmol, 0.025 eq.), (*S*)-Xylyl-P-PHOS (**L14**, 4.0 mg, 0.012 mmol, 0.06 eq.) and Cs_2CO_3 (65.2 mg, 0.20 mmol, 1.0 eq.) were stirred in THF-d_8 (0.5 mL) at 60 °C for 30 min. A solution of phenylboronic acid (**1**, 24.4 mg, 0.1 mmol, 0.5 eq.) and 3-chlorocyclohex-1-ene (**3**, 22.5 µL, 0.20 mmol, 1.0 eq.) in THF-d_8 (1.0 mL) was added and the flask rinsed with THF-d_8 (0.5 mL). The mixture was stirred at 60 °C for 1 hr before being transferred to a flame-dried NMR tube under argon. The 1D EXSY spectrum acquired showed no evidence for exchange of vinylic and allylic protons in **3** at 323.2 K.

2.2 Preliminary Mechanistic Experiments

Non-Linear effects

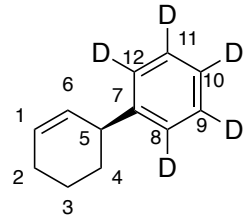
This set of experiments was performed by M.S. In a 10 mL round bottomed flask flame-dried and purged with argon, $[Rh(cod)(OH)]_2$ (4.6 mg, 0.01 mmol, 0.025 eq.), a mixture of (*R*) and (*S*)-Xylyl-P-PHOS (18.2 mg in total, 0.024 mmol, 0.06 eq., the enantiomeric ratio of chiral ligand **L14** was varied by varying the ratio of (*S*) and (*R*) ligand used) and Cs_2CO_3 (130.3 mg, 0.40 mmol, 1.00 eq.) were stirred in THF (2.0 mL) at 60 °C for 30 min. A solution of phenylboronic acid (**1**, 97.5 mg, 0.80 mmol, 2.00 eq.) and 3-chlorocyclohex-1-ene (**3**, 45 µL, 0.40 mmol, 1.00 eq.) in THF (1.5 mL) was then added *via* syringe and the flask rinsed with THF (0.5 mL). The resulting mixture was then stirred for 1 h at 60 °C. The solvent was then carefully evaporated and the crude reaction mixture directly analysed by HPLC.

Enantiomeric excess was determined by HPLC [Chiralpak® ID; flow: 0.6 mL/min; hexane/i-PrOH: 99.9: 0.1; λ = 210 nm; major enantiomer R_t = 8.3 min; minor enantiomer R_t = 8.9 min]. The relationship between the ee of ligand **L14** and product **4** is shown in Figure 27.

Experiment with Diene Electrophile (5)

In a 10 mL round-bottomed flask flame-dried and purged with argon, $[Rh(cod)(OH)]_2$ (4.6 mg, 0.01 mmol, 0.025 eq.), (*S*)-Xylyl-P-PHOS ((*S*)-**L14**, 18.2 mg, 0.06 mmol, 0.06 eq.) and Cs_2CO_3 (130.3 mg, 0.4 mmol, 1.0 eq.) were dissolved in 2.0 mL of dry THF and stirred at 60 °C for 30 min. Then a mixture of phenylboronic acid (**1**, 97.5 mg, 0.80 mmol, 1.0 eq.) and cyclohexa-1,3-diene (**5**, 32.0 mg, 0.40 mmol, 1.0 eq.) in THF (2.0 mL) were added using a syringe. The resulting mixture was stirred at 60 °C for 1 h and then the crude reaction mixture was analysed by ^1H NMR revealing no formation of the arylated product (**4**).

Experiment with Deuterated $PhB(OH)_2$



In a 10 mL round-bottomed flask flame-dried and purged with argon, $[Rh(cod)(OH)]_2$ (4.6 mg, 0.01 mmol, 0.025 eq.), (*S*)-Xylyl-P-PHOS ((*S*)-**L14**, 18.2 mg, 0.06 mmol, 0.06 eq.) and Cs_2CO_3 (130.3 mg, 0.4 mmol, 1.0 eq.) were dissolved in 2.0 mL of dry THF and stirred at 60 °C for 30 min. Then a mixture of d_5-phenylboronic acid (101.6 mg, 0.80 mmol, 2.0 eq.) and 3-chlorocyclohex-1-ene (**3**, 45 µL, 0.40 mmol, 1.0 eq.) in THF (2.0 mL) were added using a syringe. The resulting mixture was stirred at 60 °C for 1 h, then SiO_2 (50 mg) was added and the volatiles carefully evaporated. The crude was purified by flash column chromatography eluting with pentane and the d_5-phenyl-substiuted product was obtained in quantitative yield (63.7 mg, 0.39 mmol).

^{1}H NMR (400 MHz, $CDCl_3$) δ 5.97 – 5.86 (m, 1H; C(1)-H), 5.78 – 5.71 (m, 1H; C(6)-H), 3.47 – 3.38 (m, 1H; C(5)-H), 2.15 – 2.08 (m, 2H), 2.04 (dt, J = 12.6; 5.8 Hz, 1H), 1.82 – 1.73 (m, 1H), 1.70 – 1.52 (m, 2H).

^{13}C NMR (101 MHz, $CDCl_3$) δ 146.6 (C(7)), 130.3 (C(6)), 128.5 (C(1)), 127.6 (apparent m, C(8), C(9), C(11), C(12)), 125.6 (t, *J* = 24.0, C(10)) 41.9 (C(5)), 32.8 (C(2)), 25.2, 21.4.

2.3 Transmetalation Competition Experiments

General procedure for the competition experiments between phenyl-boronic acid (**1**) and other substituted boronic acids:

In a 10 mL round-bottomed flask flame-dried and purged with argon, [Rh(cod)(OH)]2 (2.3 mg, 0.005 mmol, 0.025 eq.), (*S*)-Xylyl-P-PHOS (**L14**, 9.1 mg, 0.012 mmol, 0.06 eq.) and Cs_2CO_3 (65.2 mg, 0.2 mmol, 1.0 eq.) were dissolved in 1.0 mL of dry THF and stirred at 60 °C for 30 min. Then a mixture of phenylboronic acid (**1**, 48.8 mg, 0.40 mmol, 2.0 eq.), substituted boronic acid (0.40 mmol, 2.0 eq.) and 3-chlorocyclohex-1-ene (**3**, 23 μL, 0.20 mmol, 1.0 eq.) in 1.0 mL THF was added using a syringe. The resulting mixture was stirred at 60 °C for 1 h and then cooled. THF was removed and CH_2Br_2 added as an internal standard for reference. The crude reaction mixture was analysed by ^{1}H NMR to obtain the ratio of products. Although in some cases overlapping peaks made the ratio difficult to precisely quantify, our best approximations were made, and the overall trend is clear. The results are summarised in table S1.

^{1}H NMR of 4 (400 MHz, $CDCl_3$) δ 7.31 (m, 3H), 7.27 – 7.17 (m, 2H), 5.90 (dq, *J* = 9.8, 3.4 Hz, 1H), 5.73 (dq, *J* =10.0, 2.4 Hz, 1H), 3.42 (m, 1H), 2.15 – 1.95 (m, 3H), 1.85 – 1.70 (m,1H), 1.70 – 1.51 (m, 2H).

^{1}H NMR of 3-(4-MeO-phenyl)cyclohexene (400 MHz, $CDCl_3$) δ 7.15 (dd, *J* = 7.8, 1.4 Hz, 2H), 6.93 – 6.76 (m, 2H), 5.88 (dt, *J* = 10.2, 3.2 Hz, 1H), 5.78 – 5.61 (m, 1H), 3.80 (s, 3H), 3.37 (m, 1H), 2.14 – 2.05 (m, 2H), 2.05 – 1.95 (m, 1H), 1.74 (m, 1H), 1.69 – 1.45 (m, 2H)

^{1}H NMR of 3-(4-F-phenyl)cyclohexene (400 MHz, $CDCl_3$) δ 7.17 (dd, *J* = 8.3, 5.5 Hz, 2H), 6.98 (t, *J* = 8.5 Hz, 2H), 5.89 (dq, *J* = 9.9, 3.4 Hz, 1H), 5.68 (dd, *J* = 10.1, 2.5 Hz, 1H), 3.39 (m, 1H), 2.08 (m, 2H), 2.00 (m, 1H), 1.79 – 1.44 (m, 3H).

^{1}H NMR of 3-(4-Cl-phenyl)cyclohexene (400 MHz, $CDCl_3$) δ 7.23 – 7.14 (m, 2H), 7.14 –7.04 (m, 2H), 5.83 (dq, *J* = 9.9, 2.3 Hz, 1H), 5.59 (dq, *J* = 10.0, 2.3 Hz, 1H), 3.30 (m, 1H), 2.01 (m, *J* = 3.5, 1.7 Hz, 2H), 1.97 – 1.87 (m, 1H), 1.64 (m, 1H), 1.59 – 1.50 (m, 1H), 1.43 (m, 1H).

^{1}H NMR of 3-(3-Cl-phenyl)cyclohexene (400 MHz, $CDCl_3$) δ 7.25 – 7.14 (m, 3H), 7.10 (dt, *J* = 7.2, 1.6 Hz, 1H), 5.92 (dq, *J* = 9.8, 2.3 Hz, 1H), 5.76 – 5.54 (m, 1H), 3.38 (m, 1H), 2.18 – 1.94 (m, 3H), 1.73 (m, 1H), 1.68 – 1.45 (m, 2H).

^{1}H NMR of 3-(3-Br-phenyl)cyclohexene (400 MHz, $CDCl_3$) δ 7.25 – 7.15 (m, 3H), 7.10 (dt, *J* = 7.2, 1.6 Hz, 1H), 5.92 (dq, *J* = 9.8, 2.3 Hz, 1H), 5.76 – 5.59 (m, 1H), 3.38 (m, 1H), 2.20 – 1.94 (m, 3H), 1.73 (m, 1H), 1.69 – 1.45 (m, 2H).

^{1}H NMR of 3-(4-CF_3-phenyl)cyclohexene (400 MHz, $CDCl_3$) δ 7.55 (d, *J* = 8.0 Hz, 2H), 7.33 (d, *J* = 8.0 Hz, 2H), 5.94 (dq, *J* = 9.9, 2.3 Hz, 1H), 5.68 (dq, *J* = 9.9, 2.3 Hz, 1H), 3.47 (m, 1H), 2.16 – 1.91 (m, 3H), 1.81 – 1.66 (m, 1H), 1.67 – 1.59 (m, 1H), 1.59 – 1.41 (m, 1H).

Physical data for all compounds prepared has been previously reported by our group.[53]

Table S1 Results of competition experiments

	σ value	**Ratio of Products**
*p*MeO	–0.27	0.6 : 1.0
H	0	1.0 : 1.0
p F	0.15	2.3 : 1.0
p Cl	0.23	3.3 : 1.0
m Cl	0.37	3.8 : 1.0
m Br	0.39	4.4 : 1.0
p CF_3	0.54	4.7 : 1.0

Table S2 Data for Hammett Plot. A = substituted boronic acid, B = phenyl boronic acid, A_0 = 0.2 M and B_0 = 0.2 M. Assume in each case a total 0.2 mmol of product is formed (0.1 M) and s.m. goes to product only.

	Conc. of substituted boronic acid (A)	**Conc. of Ph boronic acid (B)**	**A_0/A**	**B_0/B**	**$\ln(A_0/A)$**	**$\ln(B_0/B)$**	**$k_{rel} = \ln(A_0/A)/\ln(B_0/B)$**	**Log (k_{rel})**
*p*MeO	0.1625	0.1375	1.231	1.455	0.208	0.375	0.56	-0.25
H	0.1500	0.1500	1.333	1.333	0.287	0.287	1.00	0.00
p F	0.1303	0.1697	1.535	1.179	0.429	0.165	2.60	0.42
p Cl	0.1233	0.1783	1.622	1.122	0.484	0.115	4.21	0.62
m Cl	0.1209	0.1792	1.654	1.116	0.503	0.110	4.57	0.66
m Br	0.1185	0.1815	1.688	1.102	0.523	0.097	5.39	0.73
p CF_3	0.1175	0.1825	1.701	1.096	0.531	0.092	5.77	0.76

2.4 ^{13}C Kinetic Isotope Effect

Reference reaction

In a 10 mL round-bottomed flask flame-dried and purged with argon, $[Rh(cod)(OH)]_2$ (4.6 mg, 0.01 mmol, 0.025 eq.), Cs_2CO_3 (130.3 mg, 0.40 mmol, 1.00 eq.) and (*S*)-Xylyl-P-PHOS ((*S*)-**L14**, 18.2 mg, 0.024 mmol, 0.06 eq.) were suspended in THF (2.0 mL) and stirred at 60 °C for 30 min. In another flame-dried flask, $PhB(OH)_2$ (**1**, 97.5 mg, 0.80 mmol, 2.00 eq) and 3-chlorocyclohex-1-ene (**3**, 45 µL, 0.40 mmol, 1.00 eq.) were dissolved in THF (1.5 mL) and transferred to the first flask using a syringe and the flask rinsed with THF (0.5 mL). The mixture was stirred at 60 °C for 1 h before adding SiO_2, and carefully evaporating the solvent. The resulting solid was loaded onto a chromatographic column and eluted with pentane affording 61.0 mg of pure product (**4**, 0.39 mmol, 97 % yield). 39.0 mg of product was used for quantitative ^{13}C NMR. Physical data for **4** has been previously reported by our group.[53]

Low conversion reaction procedure

These experiments were performed by M.S. In a 100 mL round-bottomed flask flame-dried and purged with argon, $[Rh(cod)(OH)]_2$ (79.8 mg, 0.18 mmol, 0.025 eq.), Cs_2CO_3 (2.28 mg, 7.00 mmol, 1.00 eq.) and (*S*)-Xylyl-P-PHOS ((*S*)-**L14**, 317.9 mg, 0.42 mmol, 0.06 eq.) were suspended in THF (50 mL) and stirred at 60 °C for 30 min. After this time the flask was allowed to cool to 40 °C. In another flame-dried flask $PhB(OH)_2$ (**1**, 1.71 g, 14.00 mmol, 2.00 eq.) was dissolved in THF (10 mL) and transferred to the first flask using a syringe and the flask rinsed with THF (10 mL). 3-chlorocyclohex-1-ene (**3**, 0.8 mL, 7.00 mmol, 1.00 eq.) was then added and the timer started. After 20 seconds the flask was opened and SiO_2 (2 g) immediately introduced to stop the reaction. The solvent was carefully evaporated, and a crude NMR was acquired to check the conversion. Then the product **4** was purified by flash column chromatography eluting with pentane. The experiment was repeated three times obtaining the following conversions by NMR: 10 %, 11 % and 17 % with 20 mg, 21 mg and 40 mg of product used for quantitative ^{13}C NMR respectively.

Quantitative ^{13}C NMR acquisition parameters

Quantitative ^{13}C NMR spectra were recorded at 298K on a Bruker AVII500 spectrometer equipped with a dual $^{13}C\{^1H\}$ helium cryoprobe using the zgig30 pulse programme (inverse-gated Waltz-16 ^1H decoupling with a 30^o ^{13}C excitation pulse). Acquisition parameters were as follows: spectral width 200 ppm; data size 256k points; acquisition time 5.2 s; recovery delay d1 75s; number of transients 32 or 64 according to sample concentration. Data were processed as 512k points (0.05 Hz/pt digital resolution) using 1 Hz exponential multiplication (lb = 1 Hz), and spectra were subject to a 3^{rd}-order polynomial baseline correction. Peak intensities were assessed by direct integration and by peak deconvolution using the Bruker "dcon" line-fitting routine.

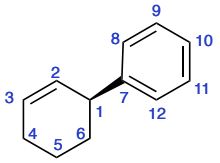
Results

Carbon-13 KIEs (K_P) were determined from analysis of the product spectra *via* quantitative measurements of ^{13}C peak intensities obtained from peak deconvolution and were calculated using the formula shown in supplementary equation 1.[239]

$$(1) \quad K_P = \frac{\ln(1-F)}{\ln\left(1 - F\left(\frac{R_P}{R_0}\right)\right)}$$

Where F represents the fractional conversion of starting material to product and R the carbon peak intensity ratios of the target carbon versus the reference carbon peak (C_5 in all cases). R_P is the peak ratio for the product at low conversion and R_0 is the peak ratio for the fully converted product.

Table S3 ^{13}C Kinetic Isotope Effect results.



		Sample 1. 10 % conversion		**Sample 2.** 11 % conversion		**Sample 3.** 17 % conversion	
	C no.	**ratio ref/reacted**	**ratio reacted/ref (R_P/R_0)**	**ratio ref/reacted**	**ratio reacted/ref (R_P/R_0)**	**ratio ref/reacted**	**ratio reacted/ref (R_P/R_0)**
1	7	1.0318	0.969	1.0140	0.9862	1.0298	0.9711
2	2	0.9973	1.003	0.9924	1.0077	0.9964	1.0036
3	3	1.0225	0.978	1.0190	0.9813	1.02604	0.9746
4	9, 11	0.9984	1.002	1.0015	0.9985	1.0021	0.9979
5	8, 12	1.0027	0.997	0.9945	1.0056	1.0077	0.9923
6	10	1.0041	0.996	0.9958	1.0043	1.0134	0.9867
7	1	1.0174	0.983	1.0055	0.9945	1.0042	0.9958
8	6	0.9893	1.011	1.0031	0.9969	1.0027	0.9973
9	4	1.0140	0.986	1.0010	0.9990	1.0084	0.9917
10	5	1.000	1.000	1.000	1.000	1.000	1.000

Table S4 ^{13}C Kinetic Isotope Effects Average of 3 samples.

Integral	Carbon no.	KIE 1	KIE 2	KIE 3	Average	Standard error
1	7	1.03368	1.01478	1.03356	1.02734	0.00628
2	2	0.99713	0.99194	0.99641	0.99516	0.00162
3	3	1.02386	1.02015	1.02933	1.02445	0.00267
4	9 & 11	0.99830	1.00159	1.00242	1.00077	0.00126
5	8 & 12	1.00286	0.99414	1.00871	1.00191	0.00424
6	10	1.00436	0.99551	1.01515	1.00501	0.00568
7	1	1.01840	1.00585	1.00473	1.00966	0.00438
8	6	0.98865	1.00326	1.00304	0.99832	0.00483
9	4	1.01478	1.00108	1.00945	1.00844	0.00399
10	5	1.00000	1.00000	1.00000	1.00000	0.00000

2.5 Reaction Kinetics

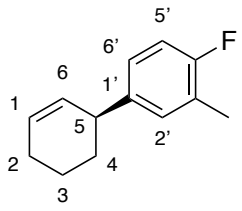
General Procedure 1: Procedure used for Kinetic Experiments.

Stock solution preparation for triplicate experiments:

Catalyst stock solution: In a 25 mL round-bottomed flask flame-dried and purged with argon, $[Rh(cod)(OH)]_2$, (*S*)-Xylyl-P-PHOS (**L14**) and 4,4'-difluorobiphenyl (66.5 mg, 0.18 mmol) were dissolved in 7.0 mL of dry THF and stirred at 60 °C for 30 min. This catalyst stock solution was then allowed to cool to 23 °C.

Arylboronic acid stock solution: In a 25 mL round-bottomed flask flame-dried and purged with argon, (4-fluoro-3-methylphenyl)boronic acid (**1a**) was dissolved in 7.0 mL THF at 23 °C.

Reaction procedure:



A 10 mL round-bottom flask was flame-dried and purged with argon, 2 mL of the catalyst stock solution was added to the flask followed by aqueous CsOH solution (50 %, 70 µL, 0.4 mmol). The resulting mixture was stirred at 23 °C under argon for 2 minutes and then 2 mL of the

arylboronic acid stock solution was added. 3-Chlorocyclohex-1-ene (**3**) was added using a microlitre syringe and the stopwatch was started. The reaction was stirred at 23 °C under argon and samples were taken every 90 seconds. The samples were quenched by injecting into a vial of pentane in air and then passing the mixture through a silica plug with pentane. The samples were then analysed by quantitative ^{19}F NMR in C_6D_6.

^{1}H NMR (400 MHz, $CDCl_3$) δ 7.08 – 6.85 (m, 3H; C(2')-H, C(6')-H, C(5')-H), 5.88 (dtd, *J* = 9.8, 3.6, 2.3 Hz, 1H), 5.75 – 5.59 (m, 1H), 3.34 (ddp, *J* = 8.3, 5.6, 2.8 Hz, 1H; C(5)-H), 2.25 (d, J = 2.0 Hz, 3H, C-H_3), 2.08 (tdd, *J* = 5.5, 4.0, 2.4 Hz, 2H), 2.03 – 1.93 (m, 1H), 1.78 – 1.69 (m, 1H), 1.67 – 1.56 (m, 1H), 1.56 – 1.46 (m, 1H).

^{13}C NMR (100 MHz, $CDCl_3$) δ 159.9 (d, *J* = 241.0 Hz; C(4')), 142.1 (d, *J* = 3.3 Hz; C(1')), 130.7 (d, *J* = 4.4 Hz; C(2')), 130.3 (C(6)), 128.6 (C(1)), 126.5 (d, *J* = 7.9 Hz; C(6')), 124.5 (d, *J* = 17.3 Hz; C(3')), 114.7 (d, *J* = 23.0 Hz; C(5')), 41.3 (C(5)), 32.9 (C(2)), 25.1, 21.3, 14.8 (C(H_3)).

^{19}F NMR (377 MHz, $CDCl_3$) δ -122.0.

^{19}F NMR (377 MHz, C_6D_6) δ -121.9.

^{19}F NMR of 4,4'-difluorobiphenyl biphenyl (internal standard) (C_6D_6) δ -115.8.

HRMS (EI/FI) m/z calcd for $C_{13}H_{15}F$ [M]+ : 190.1158, found: 190.1160.

IR ($CDCl_3$ film): 2929 (broad), 2837 (w), 1498 (s) 1382 (w), 1227, 1296, 1118, 821 cm^{-1}.

SFC conditions for analysis of **4a**; Chiralpak® ID; 1500 psi, 30°C; flow: 0.5 mL/min; 100 % CO_2, λ = 211.5 nm; R_t = 2.96 min and 3.29 min).

Reaction Kinetics Experimental Results

The general procedure 1 above was followed using $[Rh(cod)(OH)]_2$ (16 mg, 0.035 mmol) and (*S*)-Xylyl-P-PHOS ((*S*)-**L14**, 64 mg, 0.084 mmol) in the catalyst stock solution with 3-chlorocyclohex-1-ene (**3**, 45 µL, 0.4 mmol) and (4-fluoro-3-methylphenyl)boronic acid (**1a**, 123 mg, 0.8 mmol) used in each reaction. The entire procedure was repeated twice (two sets of triplicate experiments). The results are summarised in supplementary table S5.

Table S5 Reaction kinetics, conditions (i) Stock solutions prepared and reaction performed in triplicate twice as described by the general procedure for kinetic experiments with $[3\text{-chlorocyclohex-1-ene}]_0 = 0.100$ M, $[(4\text{-fluoro-3-methylphenyl})\text{boronic acid}]_0 = 0.200$ M and $[Rh]_{Tot} = 0.005$ M.

time (sec)	Repeat 1 [**4a**]	Repeat 2 [**4a**]	Repeat 3 [**4a**]	Repeat 4 [**4a**]	Repeat 5 [**4a**]	Repeat 6 [**4a**]	Average [**4a**]
0	0.0000	0.0000	0.0000	0.0000	0.0000	0.0000	0.0000
90	0.0175	0.0197	0.0181	0.0150	0.0167	0.0160	0.0172
180	0.0261	0.0279	0.0262	0.0245	0.0252	0.0268	0.0261
270	0.0321	0.0363	0.0313	0.0277	0.0329	0.0327	0.0322
360	0.0385	0.0410	0.0380	0.0323	0.0344	0.0375	0.0370
450	0.0438	0.0458	0.0401	0.0349	0.0403	0.0419	0.0411
540	0.0472	0.0514	0.0434	0.0385	0.0467	0.0465	0.0456
630	0.0516	0.0540	0.0465	0.0431	0.0508	0.0542	0.0500
720	0.0550	0.0599	0.0507	0.0443	0.0541	0.0568	0.0535

The general procedure 1 above was followed using $[Rh(cod)(OH)]_2$ (16 mg, 0.035 mmol) and (*S*)-Xylyl-P-PHOS ((*S*)-**L14**, 64 mg, 0.084 mmol) in the catalyst stock solution with 3-chlorocyclohex-1-ene (**3**, 23 µL, 0.2 mmol) and (4-fluoro-3-methylphenyl)boronic acid (**1a**, 123 mg, 0.8 mmol) used in each reaction. The results are summarised in supplementary table S6.

Table S6 Reaction kinetics, conditions (ii): Stock solutions prepared and reaction performed in duplicate as described by the general procedure for kinetic experiments with [3-chlorocyclohex-1-ene]$_0$ = 0.050 M, [(4-fluoro-3-methylphenyl)boronic acid]$_0$ = 0.200 M and [Rh]$_{Tot}$ = 0.005 M.

time (sec)	Repeat 1 [**4a**]	Repeat 2 [**4a**]	average
0	0.0000	0.0000	0.0000
90	0.0142	0.0147	0.0145
180	0.0247	0.0225	0.0236
270	0.0283	0.0280	0.0281
360	0.0337	0.0321	0.0329
450	0.0363	0.0337	0.0350
540	0.0421	0.0384	0.0403
630	0.0443	0.0407	0.0425
720	0.0464	0.0437	0.0451

The general procedure 1 above was followed using [Rh(cod)(OH)]$_2$ (16 mg, 0.035 mmol) and (*S*)-Xylyl-P-PHOS ((*S*)-**L14**, 64 mg, 0.084 mmol) in the catalyst stock solution with 3-chlorocyclohex-1-ene (**3**, 12 µL, 0.1 mmol) and (4-fluoro-3-methylphenyl)boronic acid (**1a**, 123 mg, 0.8 mmol) used in each reaction. The results are summarised in supplementary table S7.

Table S7 Reaction kinetics, conditions (iii): Stock solutions prepared and reaction performed in triplicate as described by the general procedure for kinetic experiments with [3-chlorocyclohex-1-ene]$_0$ = 0.025 M, [(4-fluoro-3-methylphenyl)boronic acid]$_0$ = 0.200 M and [Rh]$_{Tot}$ = 0.005 M.

time (sec)	Repeat 1 [**4a**]	Repeat 2 [**4a**]	Repeat 3 [**4a**]	average
0	0.0000	0.0000	0.0000	0.0000
90	0.0138	0.0139	0.0131	0.0136
180	0.0214	0.0194	0.0196	0.0201
270	0.0223	0.0243	0.0210	0.0225
360	0.0224	0.0251		0.0238
450	0.0229	0.0253		0.0241
540	0.0238	0.0249		0.0243
630	0.0238	0.0250		0.0244
720	0.0238	0.0250		0.0244

The general procedure 1 above was followed using [Rh(cod)(OH)]$_2$ (16 mg, 0.035 mmol) and (*S*)-Xylyl-P-PHOS ((*S*)-**L14**, 64 mg, 0.084 mmol) in the catalyst stock solution with 3-chlorocyclohex-1-ene (**3**, 45 µL, 0.4 mmol) and (4-fluoro-3-methylphenyl)boronic acid (**1a**, 185 mg, 1.2 mmol) used in each reaction. The results are summarised in supplementary table S8.

Table S8 Reaction kinetics, conditions (iv): Stock solutions prepared and reaction performed in triplicate as described by the general procedure for kinetic experiments with [3-chlorocyclohex-1-ene]$_0$ = 0.100 M, [(4-fluoro-3-methylphenyl)boronic acid]$_0$ = 0.300 M and [Rh]$_{Tot}$ = 0.005 M.

time (sec)	Repeat 1 [**4a**]	Repeat 2 [**4a**]	Repeat 3 [**4a**]	average
0	0.0000	0.0000	0.0000	0.0000
90	0.0162	0.0185	0.0158	0.0168
180	0.0276	0.0297	0.0252	0.0275
270	0.0351	0.0368	0.0341	0.0353
360	0.0430	0.0483	0.0425	0.0446
450	0.0477	0.0547	0.0477	0.0500
540	0.0560		0.0555	0.0558
630	0.0597	0.0583	0.0581	0.0587
720	0.0603	0.0635	0.0609	0.0615

The general procedure 1 above was followed using [Rh(cod)(OH)]$_2$ (16 mg, 0.035 mmol) and (*S*)-Xylyl-P-PHOS ((*S*)-**L14**, 64 mg, 0.084 mmol) in the catalyst stock solution with 3-chlorocyclohex-1-ene (**3**, 45 µL, 0.4 mmol) and (4-fluoro-3-methylphenyl)boronic acid (**1a**, 247 mg, 1.6 mmol) used in each reaction. The results are summarised in supplementary table S9.

Table S9 Reaction kinetics, conditions (v): Stock solutions prepared and reaction performed in triplicate as described by the general procedure for kinetic experiments with [3-chlorocyclohex-1-ene]$_0$ = 0.100 M, [(4-fluoro-3-methylphenyl)boronic acid]$_0$ = 0.400 M and [Rh]$_{Tot}$ = 0.005 M.

time (sec)	Repeat 1 [**4a**]	Repeat 2 [**4a**]	Repeat 3 [**4a**]	average
0	0.0000	0.0000	0.0000	0.0000
90	0.0155	0.0178	0.0128	0.0154
180	0.0302	0.0303	0.0221	0.0275
270	0.0421	0.0422	0.0318	0.0387
360	0.0516	0.0514	0.0381	0.0471
450	0.0567	0.0580	0.0451	0.0533
540	0.0608	0.0621	0.0522	0.0583
630		0.0640	0.0565	0.0603
720	0.0660	0.0687	0.0602	0.0650

The general procedure 1 above was followed using [Rh(cod)(OH)]$_2$ (16 mg, 0.035 mmol) and (*S*)-Xylyl-P-PHOS ((*S*)-**L14**, 64 mg, 0.084 mmol) in the catalyst stock solution with 3-chlorocyclohex-1-ene (**3**, 45 µL, 0.4 mmol) and (4-fluoro-3-methylphenyl)boronic acid (**1a**, 123 mg, 0.8 mmol) used in each reaction. Additionally, B(OH)$_3$ (**2**, 5 mg, 0.08 mmol per reaction)

was added to the boronic acid stock solution. The results are summarised in supplementary table S10.

Table S10 Reaction kinetics, conditions (vi): Stock solutions prepared and reaction performed in triplicate as described by the general procedure for kinetic experiments with $[3\text{-chlorocyclohex-1-ene}]_0 = 0.100$ M, $[(4\text{-fluoro-3-methylphenyl})\text{boronic acid}]_0 = 0.200$ M and $[Rh]_{Tot} = 0.005$ M with $[B(OH)_3]_0 = 0.020$ M.

time (sec)	Repeat 1 [**4a**]	Repeat 2 [**4a**]	Repeat 3 [**4a**]	average
0	0.0000	0.0000	0.0000	0.0000
90	0.0057	0.0059	0.0058	0.0058
180	0.0113	0.0117	0.0119	0.0116
270	0.0151	0.0155	0.0157	0.0155
360	0.0193	0.0204	0.0190	0.0196
450	0.0232	0.0233	0.0218	0.0228
540	0.0272	0.0275	0.0264	0.0270
630	0.0313	0.0314	0.0309	0.0312
720	0.0338	0.0348	0.0347	0.0344

The general procedure 1 above was followed using $[Rh(cod)(OH)]_2$ (8 mg, 0.018 mmol) and (*S*)-Xyl-P-PHOS ((*S*)-**L14**, 32 mg, 0.042 mmol) in the catalyst stock solution with 3-chlorocyclohex-1-ene (**3**, 45 µL, 0.4 mmol) and (4-fluoro-3-methylphenyl)boronic acid (**1a**, 123 mg, 0.8 mmol) used in each reaction. The results are summarised in supplementary table S11.

Table S11 Reaction kinetics, conditions (vii): Stock solutions prepared and reaction performed in triplicate as described by the general procedure for kinetic experiments with $[3\text{-chlorocyclohex-1-ene}]_0 = 0.100$ M, $[(4\text{-fluoro-3-methylphenyl})\text{boronic acid}]_0 = 0.200$ M and $[Rh]_{Tot} = 0.003$ M.

time (sec)	Repeat 1 [**4a**]	Repeat 2 [**4a**]	Repeat 3 [**4a**]	average
0	0.0000	0.0000	0.0000	0.0000
90	0.0110	0.0105	0.0124	0.0113
180	0.0191	0.0171	0.0209	0.0190
270	0.0256	0.0216	0.0247	0.0240
360	0.0291	0.0247	0.0282	0.0273
450	0.0324	0.0285	0.0293	0.0301
540	0.0344	0.0287	0.0321	0.0317
630	0.0375	0.0304	0.0348	0.0343
720	0.0379	0.0329	0.0356	0.0355

The general procedure 1 above was followed using $[Rh(cod)(OH)]_2$ (24mg, 0.053 mmol) and (*S*)-Xylyl-P-PHOS ((*S*)-**L14**, 96 mg, 0.126 mmol) in the catalyst stock solution with 3-

chlorocyclohex-1-ene (**3**, 45 µL, 0.4 mmol) and (4-fluoro-3-methylphenyl)boronic acid (**1a**, 123 mg, 0.8 mmol) used in each reaction. The results are summarised in supplementary table S12.

Table S12 Reaction kinetics, conditions (viii): Stock solutions prepared and reaction performed in duplicate as described by the general procedure for kinetic experiments with [3-chlorocyclohex-1-ene]$_0$ = 0.100 M, [(4-fluoro-3-methylphenyl)boronic acid]$_0$ = 0.200 M and [Rh]$_{Tot}$ = 0.008 M.

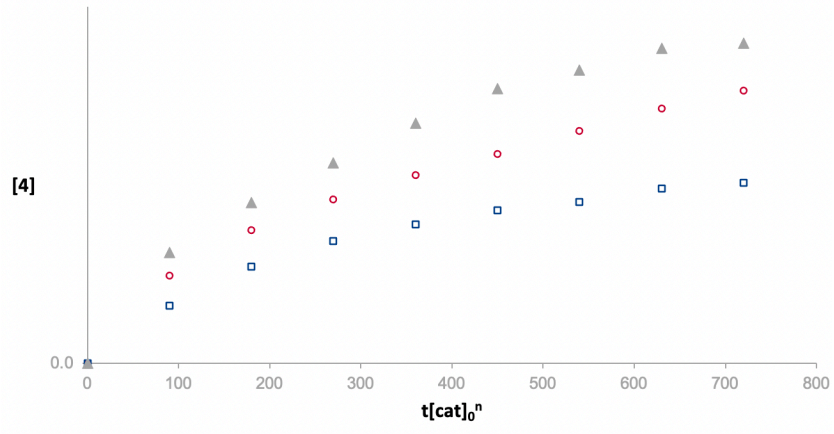
time (sec)	Repeat 1 [**4a**]	Repeat 2[**4a**]	average
0	0.0000	0.0000	0.0000
90	0.0236	0.0199	0.0218
180	0.0348	0.0283	0.0315
270	0.0417	0.0368	0.0393
360	0.0510	0.0432	0.0471
450	0.0583	0.0495	0.0539
540	0.0595	0.0556	0.0576
630	0.0653	0.0583	0.0618
720	0.0663	0.0593	0.0628

Visual Kinetic Analysis to Find the Order in Catalyst

In order to use this graphical kinetic analysis method,[121] the concentration of the product was plotted against a normalized time scale, t[cat]$_0^n$ (where t = time, [cat]$_0$ = the initial concentration of catalyst and n is an arbitrary variable) for reactions with different catalyst concentrations (Table S5 (reaction kinetics, conditions (i)), Table S11 (reaction kinetics, conditions (vii)) and Table S12 (reaction kinetics, conditions (viii)). These graphs were then visually compared with different values for n tested. The n value that results in curves which overlay gives the order in catalyst.

Testing n = 0.

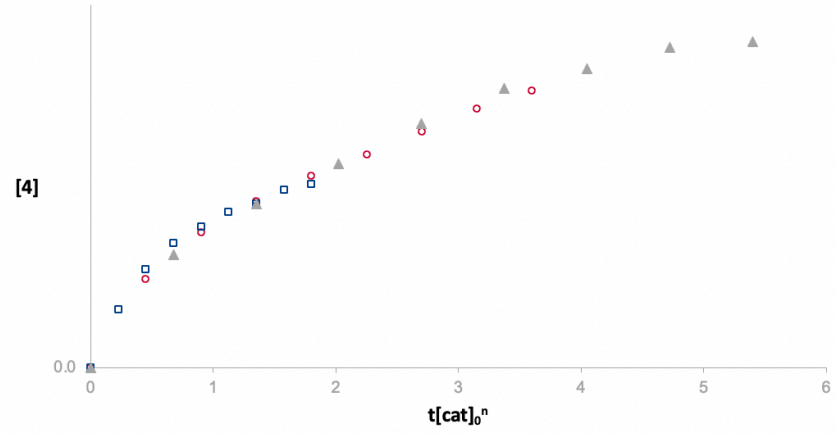
Reaction kinetics, conditions (i)				Reaction kinetics, conditions (vii)				Reaction kinetics, conditions (viii)			
t (sec)	t[cat]0^n	[Rh]	[4]	t (sec)	t[cat]0^n	[Rh]	[4]	t (sec)	t[cat]0^n	[Rh]	[4]
0.00	0.00	0.005	0.000	0.00	0.00	0.0025	0.000	0.00	0.00	0.0075	0.000
90.00	90.00	0.005	0.017	90.00	90.00	0.0025	0.011	90.00	90.00	0.0075	0.022
180.00	180.00	0.005	0.026	180.00	180.00	0.0025	0.019	180.00	180.00	0.0075	0.032
270.00	270.00	0.005	0.032	270.00	270.00	0.0025	0.024	270.00	270.00	0.0075	0.039
360.00	360.00	0.005	0.037	360.00	360.00	0.0025	0.027	360.00	360.00	0.0075	0.047
450.00	450.00	0.005	0.041	450.00	450.00	0.0025	0.030	450.00	450.00	0.0075	0.054
540.00	540.00	0.005	0.046	540.00	540.00	0.0025	0.032	540.00	540.00	0.0075	0.058
630.00	630.00	0.005	0.050	630.00	630.00	0.0025	0.034	630.00	630.00	0.0075	0.062
720.00	720.00	0.005	0.054	720.00	720.00	0.0025	0.036	720.00	720.00	0.0075	0.063



When n = 0, these graphs of the concentration of **4** against $t[cat]_0^n$ at different initial catalyst concentrations do not overlay. Therefore, the reaction does not proceed with zeroth order dependence on $[Rh]_{TOT}$.

Testing n = 1.

Reaction kinetics, conditions (i)				Reaction kinetics, conditions (vii)				Reaction kinetics, conditions (viii)			
t (sec)	t[cat]0^n	[Rh]	[4]	t (sec)	t[cat]0^n	[Rh]	[4]	t (sec)	t[cat]0^n	[Rh]	[4]
0.00	0.00	0.005	0.000	0.00	0.00	0.0025	0.000	0.00	0.00	0.0075	0.000
90.00	0.45	0.005	0.017	90.00	0.23	0.0025	0.011	90.00	0.68	0.0075	0.022
180.00	0.90	0.005	0.026	180.00	0.45	0.0025	0.019	180.00	1.35	0.0075	0.032
270.00	1.35	0.005	0.032	270.00	0.68	0.0025	0.024	270.00	2.03	0.0075	0.039
360.00	1.80	0.005	0.037	360.00	0.90	0.0025	0.027	360.00	2.70	0.0075	0.047
450.00	2.25	0.005	0.041	450.00	1.13	0.0025	0.030	450.00	3.38	0.0075	0.054
540.00	2.70	0.005	0.046	540.00	1.35	0.0025	0.032	540.00	4.05	0.0075	0.058
630.00	3.15	0.005	0.050	630.00	1.58	0.0025	0.034	630.00	4.73	0.0075	0.062
720.00	3.60	0.005	0.054	720.00	1.80	0.0025	0.036	720.00	5.40	0.0075	0.063



When n = 1, visual interrogation of these graphs of the concentration of **4** against $t[cat]_0^n$ at different initial catalyst concentrations shows that the plots overlay well. Therefore, the reaction proceeds with first order dependence on $[Rh]_{TOT}$.

Derivation and fitting of a steady-state rate equation for the Rh-catalysed coupling.

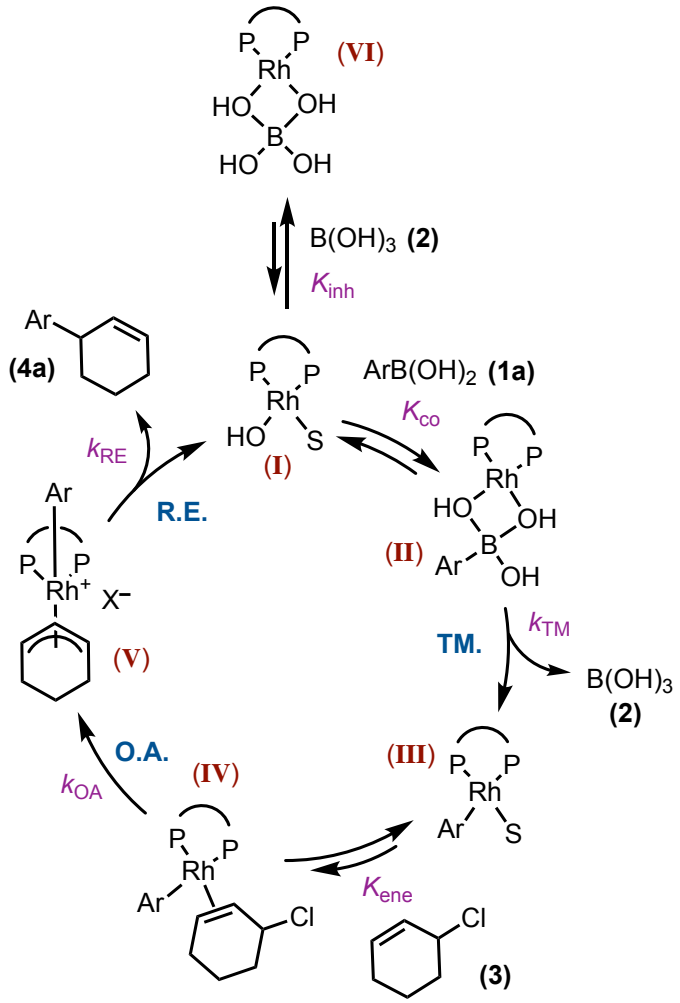


Figure S2 Scheme for Rh-catalysed reaction of arylboronate (**1a**; Ar = 4-fluoro-3-methylphenyl) with 3-chlorocyclohex-2-ene (**3**) to generate 3-arylcyclohex-2-ene (**4a**), with inhibition by exogenous and endogenous $B(OH)_3$ (**2**), employed for the steady state model given in equations S2-S18. The model proceeds via three key irreversible steps: transmetalation (TM), oxidative addition (O.A.) and reductive elimination (R.E.). Acid/ate speciation is not considered. An alternative arrangement where K_{ene} and k_{OA} occur immediately after reductive elimination of **4a**, and before K_{inh}, K_{co} and k_{TM} will give the same steady state approximation, equation S8. S = Solvent or vacant site.

The pseudo steady-state rate equation was derived by G.C.L-J. Equation 2 describes the rate of turnover by a pseudo steady-state catalytic system, figure S2, comprising five on-cycle active rhodium intermediates (**I**-**V**), and off-cycle inhibition species (**VI**). The pre-reductive elimination complex, **V**, present in total Rh mol-fraction x_V (equations 3 and 4) irreversibly

liberates (k_{RE}) product (**4a**). Boronic/ate speciation is not considered. Under all conditions, complexes **I**-**V** (or **I**-**VI** with exogenous $B(OH)_3$) are assumed to be present from the start. King-Altman extraction of terms for [**I**] to [**VI**] gives the steady state rate equation 5, which can be reformulated as equation 6, and then by collecting terms, equation 7. By assuming that K_{inh} is large enough for (1 + K_{inh}[**2**]) to reduce to K_{inh}[**2**] very early in the reaction evolution, equation 7 can be simplified to equation 8, with five concentration terms ($[Rh]_{TOT}$; **1a** (boronic acid); **2** (boric acid); **3** (cyclohexenyl chloride) and **4a** (arylation product)), and three collections of constants: *a*, *b*, and *c*.

$$\frac{d[\mathbf{4a}]}{dt} = k_{RE}\, x_{\mathbf{V}}\, [Rh]_{TOT} \tag{2}$$

$$x_{\mathbf{V}} = [\mathbf{V}] / [Rh]_{TOT} \tag{3}$$

$$[\mathbf{I}] + [\mathbf{II}] + [\mathbf{III}] + [\mathbf{IV}] + [\mathbf{V}] + [\mathbf{VI}] = [Rh]_{TOT} \tag{4}$$

$$\frac{d[\mathbf{4a}]}{dt} = \frac{k_{-inh}k_{co}k_{TM}k_{ene}k_{OA}k_{RE}[\mathbf{1a}][\mathbf{3}][Rh]_{TOT}}{\left[\begin{array}{lll} k_{-inh}k_{co}k_{TM}k_{ene}k_{OA}[\mathbf{1a}][\mathbf{3}] & + & k_{-inh}k_{co}k_{TM}k_{ene}k_{RE}[\mathbf{1a}][\mathbf{3}] \\ + & k_{-inh}k_{co}k_{TM}k_{-ene}k_{RE}[\mathbf{1a}] & \\ k_{-inh}k_{co}k_{TM}k_{OA}k_{RE}[\mathbf{1a}] & + & k_{-inh}k_{co}k_{ene}k_{OA}k_{RE}[\mathbf{1a}][\mathbf{3}] \\ + & k_{-inh}k_{TM}k_{ene}k_{OA}k_{RE}[\mathbf{3}] & \\ k_{-inh}k_{ene}k_{OA}k_{RE}k_{-co}[\mathbf{3}] & + & k_{TM}k_{ene}k_{OA}k_{RE}k_{inh}[\mathbf{3}][\mathbf{2}] \\ + & k_{-co}k_{ene}k_{OA}k_{RE}k_{inh}[\mathbf{3}][\mathbf{2}] & \end{array}\right]} \tag{5}$$

$$\frac{d[\mathbf{4a}]}{dt} = \frac{[Rh]_{TOT}}{\frac{1}{k_{RE}} + \frac{1}{k_{OA}} + \frac{1}{K_{ene}k_{OA}[\mathbf{3}]} + \frac{1}{k_{ene}[\mathbf{3}]} + \frac{1}{k_{TM}} + \frac{1}{k_{co}[\mathbf{1a}]} + \frac{1}{K_{co}k_{TM}[\mathbf{1a}]} + \frac{K_{inh}[\mathbf{2}]}{k_{co}[\mathbf{1a}]} + \frac{K_{inh}[\mathbf{2}]}{K_{co}k_{TM}[\mathbf{1}]}} \tag{6}$$

$$\frac{d[\mathbf{4a}]}{dt} = \frac{[Rh]_{TOT}}{\left[\frac{1}{k_{RE}} + \frac{1}{k_{OA}} + \frac{1}{k_{TM}}\right] + \frac{1}{[\mathbf{3}]}\left[\frac{1}{K_{ene}k_{OA}} + \frac{1}{k_{ene}}\right] + \frac{1}{[\mathbf{1a}]}\left[\frac{1}{k_{co}} + \frac{1}{K_{co}k_{TM}}\left(1 + K_{inh}[\mathbf{2}]\right)\right]} \tag{7}$$

$$\left[\frac{1}{k_{RE}} + \frac{1}{k_{OA}} + \frac{1}{k_{TM}}\right] = a \qquad \left[\frac{1}{K_{ene}k_{OA}} + \frac{1}{k_{ene}}\right] = b \qquad \left[\frac{K_{inh}}{k_{co}} + \frac{K_{inh}}{K_{co}k_{TM}}\right] = c$$

$$\frac{d[\mathbf{4a}]}{dt} \approx \frac{[Rh]_{TOT}}{a + \frac{b}{[\mathbf{3}]} + \frac{c\,[\mathbf{2}]}{[\mathbf{1a}]}} \tag{8}$$

Equation 9 describes the mol-fraction x_V of pre-reductive elimination complex, **V**, based on equations 2 and 8. Based on the observed kinetics, where during the early phases of reaction the rate of product generation d[**4a**]/dt, is near-independent of [**1a**] and [**3**], the empirical fitting value a can be approximated to represent the inverse reductive elimination rate, $1/k_{RE}$. Substituting this into equation 9, gives equation 10, which is used in an analysis of estimated speciation as function of conversion (see later, supplementary Fig. S4).

$$x_{\mathbf{V}} = \frac{\mathrm{d}[\mathbf{4a}]}{\mathrm{d}t\,[\mathrm{Rh}]_{TOT}\,k_{RE}} \approx \frac{\frac{1}{k_{RE}}}{a + \frac{b}{[\mathbf{3}]} + \frac{c\,[\mathbf{2}]}{[\mathbf{1a}]}} \qquad (9)$$

$k_{OA}, k_{TM} >> k_{RE}$

$$\left[\frac{1}{k_{RE}} + \frac{1}{k_{OA}} + \frac{1}{k_{TM}}\right] = a \approx \left[\frac{1}{k_{RE}}\right]$$

$$x_{\mathbf{V}} \approx \frac{1}{1 + \frac{b}{a\,[\mathbf{3}]} + \frac{c\,[\mathbf{2}]}{a\,[\mathbf{1a}]}} \qquad (10)$$

Supplementary equation 11 describes the mol-fraction x_{VI} of off-cycle inhibited complex, **VI**, and is constructed by King-Altman extraction of terms for [**I**] to [**VI**]. This can be reformulated as supplementary equation 12, and then divided through by the second half of the numerator to give supplementary equation 13, which is then divided through by $-k_{inh}k_{CO}k_{TM}$ to give supplementary equation 14, and then supplementary equation 15 by substituting in c in the numerator. After collecting terms (supplementary equation 16), substitution of a and b in the denominator (supplementary equation 17), and assuming that K_{inh}[**2**] is large, gives supplementary equation 18, which is used for estimation of speciation as a function of conversion (Fig. S4).

$$x_{VI} = \frac{k_{TM}k_{ene}k_{OA}k_{RE}k_{inh}[\mathbf{3}][\mathbf{2}] \quad + \quad k_{-co}k_{ene}k_{OA}k_{RE}k_{inh}[\mathbf{3}][\mathbf{2}]}{\left[\begin{array}{lll} k_{-inh}k_{co}k_{TM}k_{ene}k_{OA}[\mathbf{1a}][\mathbf{3}] & + \; k_{-inh}k_{co}k_{TM}k_{ene}k_{RE}[\mathbf{1a}][\mathbf{3}] & + \; k_{-inh}k_{co}k_{TM}k_{-ene}k_{RE}[\mathbf{1a}] \\ k_{-inh}k_{co}k_{TM}k_{OA}k_{RE}[\mathbf{1a}] & + \; k_{-inh}k_{co}k_{ene}k_{OA}k_{RE}[\mathbf{1a}][\mathbf{3}] & + \; k_{-inh}k_{TM}k_{ene}k_{OA}k_{RE}[\mathbf{3}] \\ k_{-inh}k_{ene}k_{OA}k_{RE}k_{-co}[\mathbf{3}] & + \; k_{TM}k_{ene}k_{OA}k_{RE}k_{inh}[\mathbf{3}][\mathbf{2}] & + \; k_{-co}k_{ene}k_{OA}k_{RE}k_{inh}[\mathbf{3}][\mathbf{2}] \end{array}\right]} \tag{11}$$

$$x_{VI} = \frac{\left[k_{inh}k_{TM} + k_{inh}k_{-co}\right] k_{ene}k_{OA}k_{RE}[\mathbf{3}][\mathbf{2}]}{\left[\begin{array}{lll} k_{-inh}k_{co}k_{TM}k_{ene}k_{OA}[\mathbf{1a}][\mathbf{3}] & + \; k_{-inh}k_{co}k_{TM}k_{ene}k_{RE}[\mathbf{1a}][\mathbf{3}] & + \; k_{-inh}k_{co}k_{TM}k_{-ene}k_{RE}[\mathbf{1a}] \\ k_{-inh}k_{co}k_{TM}k_{OA}k_{RE}[\mathbf{1a}] & + \; k_{-inh}k_{co}k_{ene}k_{OA}k_{RE}[\mathbf{1a}][\mathbf{3}] & + \; k_{-inh}k_{TM}k_{ene}k_{OA}k_{RE}[\mathbf{3}] \\ \multicolumn{3}{c}{k_{-inh}k_{ene}k_{OA}k_{RE}k_{-co}[\mathbf{3}] \quad + \quad \left[k_{inh}k_{TM} + k_{inh}k_{-co}\right] k_{ene}k_{OA}k_{RE}[\mathbf{3}][\mathbf{2}]} \end{array}\right]} \tag{12}$$

$$x_{VI} = \frac{\left[k_{inh}k_{TM} + k_{inh}k_{-co}\right]}{\left[\begin{array}{l} \dfrac{k_{-inh}k_{co}k_{TM}[\mathbf{1a}]}{k_{RE}[\mathbf{2}]} + \dfrac{k_{-inh}k_{co}k_{TM}[\mathbf{1a}]}{k_{OA}[\mathbf{2}]} + \dfrac{k_{-inh}k_{co}k_{TM}[\mathbf{1a}]}{K_{ene}k_{OA}[\mathbf{3}][\mathbf{2}]} + \dfrac{k_{-inh}k_{co}k_{TM}[\mathbf{1a}]}{k_{ene}[\mathbf{3}][\mathbf{2}]} \\ + \dfrac{k_{-inh}k_{co}[\mathbf{1a}]}{[\mathbf{2}]}\dfrac{k_{-inh}k_{-co}}{[\mathbf{2}]} + \dfrac{k_{-inh}k_{TM}}{[\mathbf{2}]} + \left[k_{inh}k_{TM} + k_{inh}k_{-co}\right] \end{array}\right]} \tag{13}$$

$$\frac{\left\{\dfrac{\left[k_{inh}k_{TM} + k_{inh}k_{-co}\right]}{k_{-inh}k_{co}k_{TM}}\right\}}{\left\{\dfrac{\left[\begin{array}{l} \dfrac{k_{-inh}k_{co}k_{TM}[\mathbf{1a}]}{k_{RE}[\mathbf{2}]} + \dfrac{k_{-inh}k_{co}k_{TM}[\mathbf{1a}]}{k_{OA}[\mathbf{2}]} + \dfrac{k_{-inh}k_{co}k_{TM}[\mathbf{1a}]}{K_{ene}k_{OA}[\mathbf{3}][\mathbf{2}]} + \dfrac{k_{-inh}k_{co}k_{TM}[\mathbf{1a}]}{k_{ene}[\mathbf{3}][\mathbf{2}]} \\ + \dfrac{k_{-inh}k_{co}[\mathbf{1a}]}{[\mathbf{2}]} + \dfrac{k_{-inh}k_{-co}}{[\mathbf{2}]} + \dfrac{k_{-inh}k_{TM}}{[\mathbf{2}]} + \left[k_{inh}k_{TM} + k_{inh}k_{-co}\right] \end{array}\right]}{k_{-inh}k_{co}k_{TM}}\right\}} \tag{14}$$

$$x_{\mathbf{VI}} = \frac{c}{\left[\frac{[\mathbf{1a}]}{k_{RE}[\mathbf{2}]} + \frac{[\mathbf{1a}]}{k_{OA}[\mathbf{2}]} + \frac{[\mathbf{1a}]}{K_{ene}k_{OA}[\mathbf{3}][\mathbf{2}]} + \frac{[\mathbf{1a}]}{k_{ene}[\mathbf{3}][\mathbf{2}]} + \frac{[\mathbf{1}]}{k_{TM}[\mathbf{2}]} + \frac{1}{k_{TM}K_{co}[\mathbf{2}]} + \frac{1}{k_{co}[\mathbf{2}]} + c\right]} \quad (15)$$

$$x_{\mathbf{VI}} = \frac{c}{\left[\frac{[\mathbf{1a}]}{[\mathbf{2}]}\left[\frac{1}{k_{RE}} + \frac{1}{k_{OA}} + \frac{1}{k_{TM}}\right] + \frac{[\mathbf{1a}]}{[\mathbf{3}][\mathbf{2}]}\left[\frac{1}{K_{ene}k_{OA}} + \frac{1}{k_{ene}}\right] + \frac{1}{[\mathbf{2}]}\left[\frac{1}{k_{co}} + \frac{1}{k_{TM}K_{co}}\right] + c\right]} \quad (16)$$

$$\left[\frac{K_{inh}}{k_{co}} + \frac{K_{inh}}{K_{co}k_{TM}}\right] = c$$

$$\left[\frac{1}{k_{co}} + \frac{1}{k_{TM}K_{co}}\right] = \frac{c}{K_{inh}}$$

$$\left[\frac{1}{K_{ene}k_{OA}} + \frac{1}{k_{ene}}\right] = b$$

$$\left[\frac{1}{k_{RE}} + \frac{1}{k_{OA}} + \frac{1}{k_{TM}}\right] = a$$

$$x_{\mathbf{VI}} = \frac{1}{\frac{a[\mathbf{1a}]}{c[\mathbf{2}]} + \frac{b[\mathbf{1a}]}{c[\mathbf{3}][\mathbf{2}]} + \frac{c}{K_{inh}[\mathbf{2}]} + 1} \quad (17)$$

$$x_{\mathbf{VI}} \approx \frac{1}{\frac{a[\mathbf{1a}]}{c[\mathbf{2}]} + \frac{b[\mathbf{1a}]}{c[\mathbf{3}][\mathbf{2}]} + 1} \quad (18)$$

Using Excel, and the appropriate initial values for concentrations of aryl boronic acid (**1a**), cyclohexenyl chloride (**3**), $B(OH)_3$ (**2**), and $[Rh]_{TOT}$ equation 8 was evolved in 2000 steps of 0.34 second intervals, to generate a temporal concentration profile for [**4a**] over 720 seconds, for each of the conditions explored. Values for the constants, *a*, *b*, and *c*, were estimated by using the solver function to minimize the sum square errors (SSE) between predicted and observed concentrations of arylation product **4a**, at 90, 180, 270, 360, 450, 540, 630, and 720 seconds across all eight datasets (56 datapoints in total, Fig, 3b). Plots of the individual datasets, (i), (ii), (iii), (iv), (v), (vi), (vii), and (viii), together with model (blue lines) are provided in Fig. S3c. Standard errors (SE) for fitting parameters *a*, *b* and *c* were determined from the standard deviations of minimised SSE solver fits (in the 56 step sequence of n-1; i.e. jackknife re-sampling), and are given by $SE = s(n-1)/(n)^{0.5}$. The maximum errors in *a*, *b* and *c* were propagated to estimate the fitting in Fig. S3b.

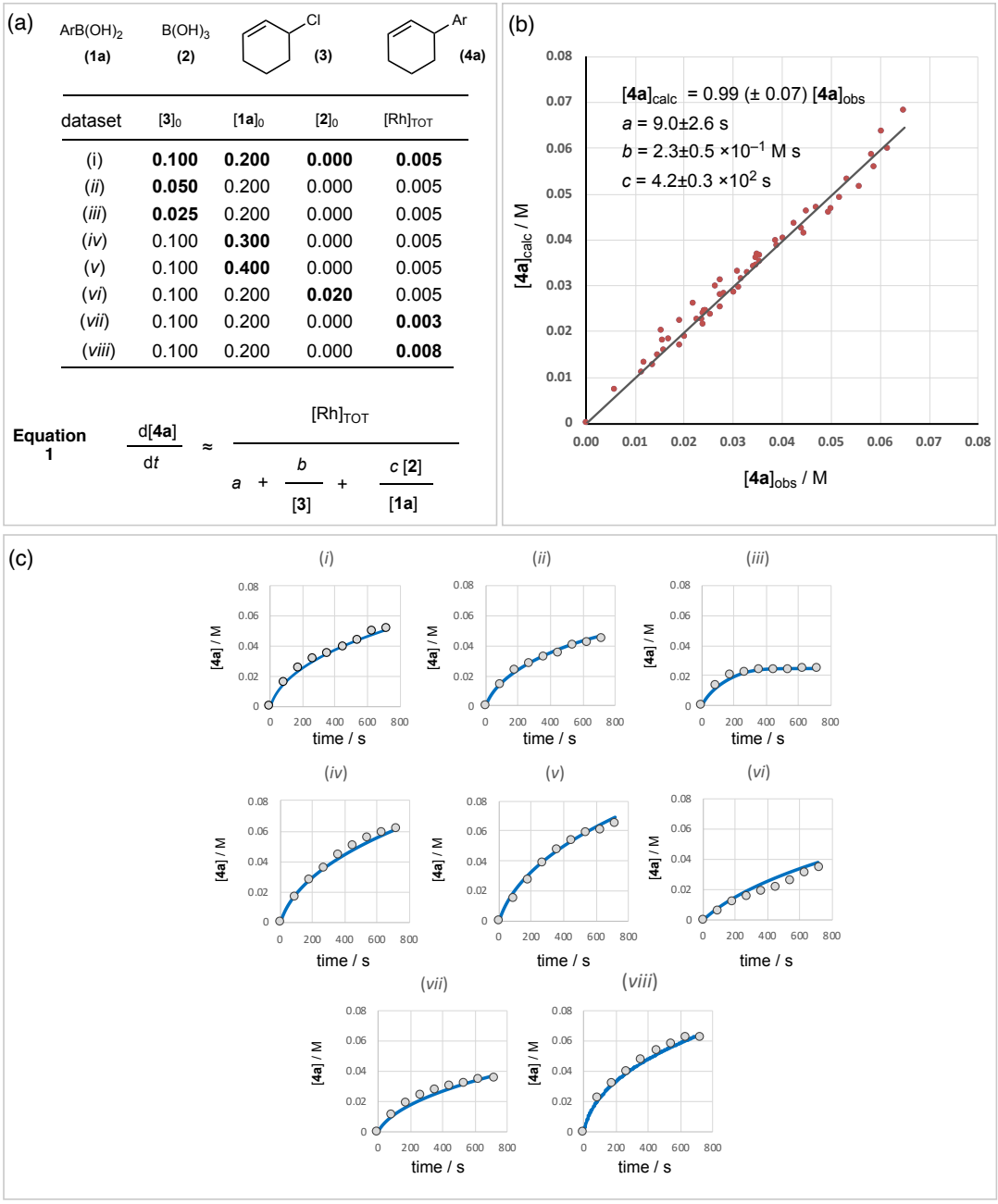
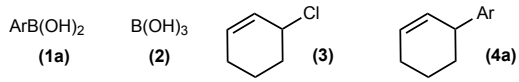


Figure S3. (a) Details the concentrations at time = 0 in each data set. All eight of these datasets could be satisfactorily simulated using a kinetic model based on all of the key mechanistic features evaluated in a pseudo steady-state rate equation (Equation 1) (b) Correlation between temporal concentration calculated in Excel using equation 1 in 0.34 sec interval step-evolution, $[\mathbf{4a}]_{calc.}$ *y*-axis, and the experimentally-determined concentrations, *x*-axis, by ^{19}F NMR spectroscopy (each an average of triplicate runs) starting from the initial conditions indicated in the table. (c) Graphs (i) to (viii) showing experimental data (open circles, average of triplicate runs) for growth of [**4a**] versus time at 23 °C under initial conditions indicated in the table. Solid lines are the model obtained by linear regression of the SSE against the total 56 datapoints.

The relative magnitudes of the fitted parameters *a*, *b* and *c* indicate that (in the absence of exogenous boric acid (**2**)), the reaction rate is initially independent on boronic acid (**1a**) and cyclohexenyl chloride (**3**) concentrations (Fig. S3c graphs i, ii, iv, v). As boric acid (**2**) develops, the rate becomes governed by boronic acid (**1a**) / boric acid (**2**) ratio (Fig. S3c, graphs i, iv, v). Kinetic dependence on cyclohexenyl chloride (**3**) is only evident at very low concentrations (Fig. S3c, graph iii). The speciation of rhodium (mol fraction, *x*) for the two major catalyst components (**V** and **VI**) as estimated by supplementary equations 11 and 18 have been analysed as a function of conversion of the limiting reagent, the cyclohexenyl chloride (**3**), for each of the 8 datasets (i)-(viii). These plots are shown in Fig. S4, where the speciation evolves as the reactions proceed, with no resting state dominant throughout, leading to the turnover rate controlling step(s) varying between reductive elimination and boronic acid transmetalation competing with boric acid complexation. In the very final stages of reaction, the dominance of **V** and **VI** diminishes due to exhaustion of the cyclohexenyl chloride (**3**).

(a)



dataset	$[3]_0$	$[1a]_0$	$[2]_0$	$[Rh]_{TOT}$
(i)	**0.100**	**0.200**	**0.000**	**0.005**
(*ii*)	**0.050**	0.200	0.000	0.005
(*iii*)	**0.025**	0.200	0.000	0.005
(*iv*)	0.100	**0.300**	0.000	0.005
(*v*)	0.100	**0.400**	0.000	0.005
(*vi*)	0.100	0.200	**0.020**	0.005
(*vii*)	0.100	0.200	0.000	**0.003**
(*viii*)	0.100	0.200	0.000	**0.008**

$$x_V \approx \frac{1}{\frac{b}{a\,[3]} + 1 + \frac{c\,[2]}{a\,[1a]}}$$

$$x_{VI} \approx \frac{1}{\frac{b\,[1a]}{c\,[3]\,[2]} + \frac{a\,[1a]}{c\,[2]} + 1}$$

(b)

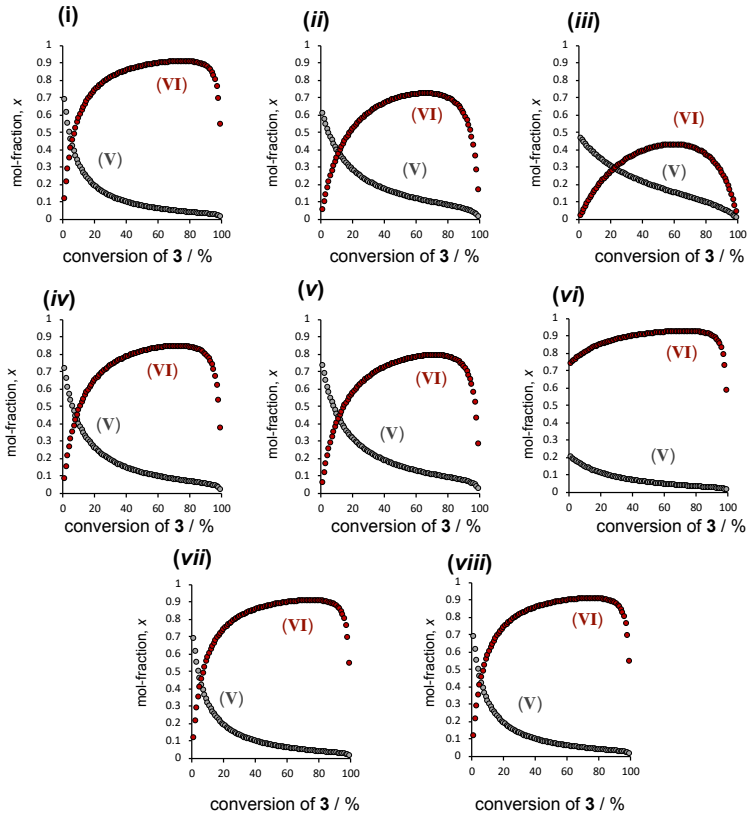


Figure S4. The speciation of rhodium for the major catalyst components as a function of conversion of the limiting reagent. The speciation of rhodium for the two major catalyst components (**V** and **VI**) as estimated by supplementary equations 10 and 18 have been analysed as a function of conversion of the limiting reagent, the cyclohexenyl chloride (**3**), for each of the 8 datasets (I)-(viii). (a) Details the concentrations at time = 0 in each data set. (b) Graphs (i)-(viii): major Rh-speciation (mol fraction, *x*, of $[Rh]_{TOT}$) as a function of conversion (of cyclohexenyl chloride **3**, %) predicted by approximate steady-state speciation equations 10 and 18.

Reaction with CsCl additive

In a 10 mL round-bottomed flask flame-dried and purged with argon, $[Rh(cod)(OH)]_2$ (4.6 mg, 0.01 mmol), (*S*)-Xylyl-P-PHOS (**L14**, 18.2 mg, 0.06 mmol), 4,4'-difluorobiphenyl (19.0 mg, 0.05 mmol) and CsCl (13.5 mg, 0.08 mmol) were dissolved in 2.0 mL of dry THF and stirred at 60 °C for 30 min. This solution was then allowed to cool to 23 °C. In a 10 mL round-bottomed flask flame-dried and purged with argon, (4-fluoro-3-methylphenyl)boronic acid (**1a**, 154 mg, 1.0 mmol) was dissolved in 2.5 mL THF at 23 °C. Aqueous CsOH solution (50 %, 70 µL, 0.4 mmol) was added to the flask containing the catalyst solution. The resulting mixture was stirred at 23 °C under argon for 2 minutes and then 2 mL of the arylboronic acid stock solution was added. 3-Chlorocyclohex-1-ene (**3**, 45 µL, 0.4 mmol) was added using a microlitre syringe and the stopwatch was started. The reaction was stirred at 23 °C under argon and samples were taken every 90 seconds. The samples were quenched by injecting into a vial of pentane and then passing the mixture through a silica plug with pentane. The samples were then analysed by quantitative ^{19}F NMR in C_6D_6.

Table S13 Reaction kinetics with exogenous CsCl.

time (sec)	[**4a**]
0	0.0000
90	0.0039
180	0.0067
270	0.0103
360	0.0148
450	0.0188
540	0.0225
630	0.0252
720	0.0296

2.6 Arylation with Heterocyclic Allyl Chlorides

Competition Experiments between Different Allyl Chloride Starting Materials

Allyl chloride **6** was prepared as previously described.[161]

In a 10 mL round-bottomed flask flame-dried and purged with argon, $[Rh(cod)(OH)]_2$ (4.6 mg, 0.01 mmol, 0.025 eq.), (*S*)-Xylyl-P-PHOS (**L14**, 18.2 mg, 0.06 mmol, 0.06 eq.) and Cs_2CO_3 (130.3 mg, 0.4 mmol, 1.0 eq.) were dissolved in 2.0 mL of dry THF and stirred at 60 °C for 30 min. Then a mixture of phenylboronic acid (**1**, 48.8 mg, 0.40 mmol, 1.0 eq.), 3-chlorocyclohex-1-ene (**3**, 45 µL, 0.40 mmol, 1.0 eq.) and 3-chloro-3,6-dihydro-2H-pyran (**6**, 45 µL, 0.40 mmol, 1.0 eq.) in THF (2.0 mL) were added using a syringe. The resulting mixture was stirred at 60 °C for 1 h and then cooled. THF was removed and CH_2Br_2 added as an internal standard. The crude reaction mixture was then analysed by ^{1}H NMR in $CDCl_3$ to obtain the ratio of products.

^{1}H NMR of 4 (400 MHz, $CDCl_3$) δ 7.31 (m, 3H), 7.27 – 7.17 (m, 2H), 5.90 (dq, *J* = 9.8, 3.4 Hz, 1H), 5.73 (dq, *J* =10.0, 2.4 Hz, 1H), 3.42 (m, 1H), 2.15 – 1.95 (m, 3H), 1.85 – 1.70 (m, 1H), 1.70 – 1.51 (m, 2H).

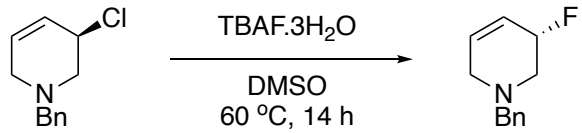
^{1}H NMR of 7 (400 MHz, $CDCl_3$) δ 7.38 – 7.28 (m, 2H), 7.27 – 7.20 (m, 3H), 5.94 (s, 2H), 4.23 (d, J = 2.1 Hz, 2H), 4.10 – 3.99 (m, 1H), 3.62 – 3.50 (m, 2H).

Physical data for all compounds prepared has been previously reported by our group.[53]

Synthesis of tetrahydropyridine allyl chlorides

tert-Butyl 5-chloro-5,6-dihydropyridine-1(2*H*)-carboxylate (**8**) was prepared as previously described.[54] Enantiomerically enriched and deuterium labelled **8** were prepared according to the reported literature procedure[122] and patent (GB1815018.5) application.

Determination of Absolute Stereochemistry of enantiomerically enriched tetrahydropyridine allyl chlorides

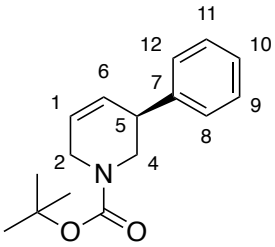


The absolute stereochemistry of the enantiomerically enriched allyl chloride substrates was determined as described in the reported literature procedure.[122] In this literature report,[122] the stereochemistry is assigned by conversion of the allyl chloride to an allyl fluoride (substitution reaction shown above) and the absolute stereochemistry of the allyl fluoride product was determined by comparison to the previous assignment by Doyle and co-workers which was determined by x-ray crystallographic analysis.[240] Mechanistic studies with racemic deuterium labelled tetrahydropyridine allyl chloride show that the substitution reaction occurs *via* an S_N2 pathway and therefore proceeds with inversion of the configuration at the stereocentre.[122] Using this method of assigning configuration, we assume that changing the protecting group on the nitrogen does not affect the stereochemical configuration.

General Procedure 2: for monitoring the ee of starting material and products in the Rh-catalysed coupling of tetrahydropyridine allyl chloride 8 with $PhB(OH)_2$.

In a 10 mL round-bottomed flask flame-dried and purged with argon, $[Rh(cod)(OH)]_2$ (4.6 mg, 0.01 mmol, 0.025 eq.), Cs_2CO_3 (130.3 mg, 0.40 mmol, 1.00 eq.) and (*S*)-Cl-MeO-BIPHEP ((*S*)-**L15**, 15.6 mg, 0.024 mmol, 0.06 eq.) were suspended in THF (2.0 mL) and stirred at 60 °C for 30 min. This mixture was then cooled to the required temperature, or continued to be stirred at 60 °C. In a flame-dried 5 mL flask $PhB(OH)_2$ (**1**, 97.5 mg, 0.80 mmol, 2.00 eq.) was dissolved in THF (1.0 mL). In another flame-dried 5 mL flask, tert-butyl 5-chloro-5,6-dihydropyridine-1(2H)-carboxylate (**8**, 87 mg, 0.40 mmol, 1.00 eq.) was dissolved in THF (1.0 mL). These two solutions were added to the first flask simultaneously and the timer was started immediately

after the additions were completed. Aliquots were taken at the indicated times. The aliquots were quenched with pentane and then passed through a small plug of silica. The volatiles were removed using a rotary evaporator and the sample was then dissolved in hexane. The ee of the starting material and product was measured by SFC using chiral non-racemic stationary phase (Chiralpak® IF; 1500 psi, 30°C; flow: 1.5 mL/min; from 1 % to 30 % MeOH in 5 min; λ = 214.5 nm; starting material (**8**) R_t = 1.59 min and 1.63 min, product (**9**) R_t = 2.09 min and 2.17 min). The product (**9**) ee can also be determined by HPLC using a chiral non-racemic stationary phase (Chiralpak® IA; flow: 1.0 mL/min; hexane/i-PrOH: 99.4: 0.6; λ = 210 nm; major enantiomer R_t = 7.5 min; minor enantiomer R_t = 8.1 min). The conversion was approximated from the SFC traces after calibration with known amounts of starting material and product.

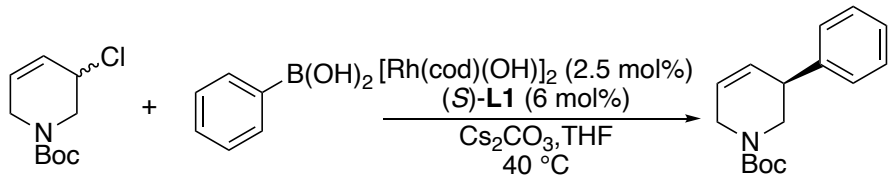


^{1}H NMR of 9 (400 MHz, $CDCl_3$) δ 7.31 (m, 2H), 7.19 – 7.27 (m, 3H), 5.89 (br s, 2H; C(1), C(6)), 3.82 and 4.07 (rot. m, 2H), 3.46 – 3.62 (m, 1H), 3.70 – 3.79 and 4.07 (rot. m, 2H), 3.01, 3.33 – 3.46, 1.19 – 1.63 (m, 9H; 3 x C(C)-H_3).

^{13}C NMR of 9 (101 MHz, $CDCl_3$) δ 154.7 (C=O), 142.2 (C(7)), 128.5 (2 x C_{Ar}), 128.2, 127.9 (2 x C_{Ar}), 126.7, 125.9, 79.5 ($C(CH_3)$), 47.3 and 48.5 (rot.; 1 x $C(H_2)$), 42.9 and 43.6 (rot.; 1 x $C(H_2)$), 41.5, 28.3 (3 x $C(H_3)$).

Physical data identical to that which was previously reported by our group.[54]

Monitoring the ee of starting material and products in time



The general procedure 2 described above was followed using (*S*)-Xylyl-P-PHOS ((*S*)-**L14**, 18.2 mg, 0.024 mmol, 0.06 eq.) in place of **L15**. The catalyst mixture was then cooled to 40 °C and the reaction monitored at 40 °C. The resulting traces from the SFC can be seen in Fig. S5 and the results are summarised in Supplementary Table S14.

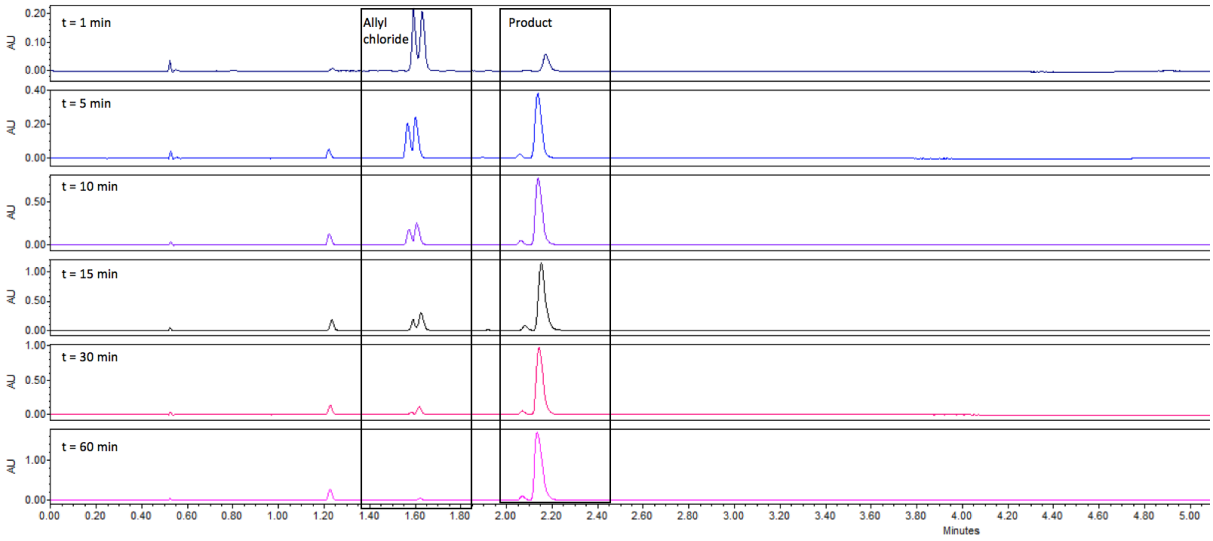
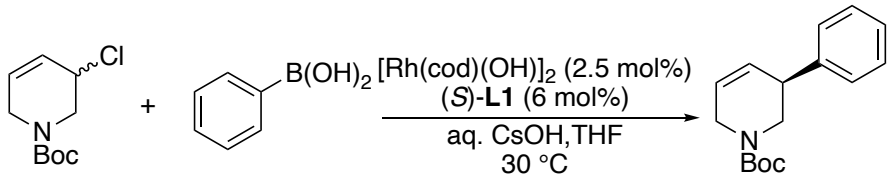


Figure S5 SFC traces showing the results of monitoring the ee of starting material and products in time.

Table S14 Monitoring the ee of starting material and products in time.

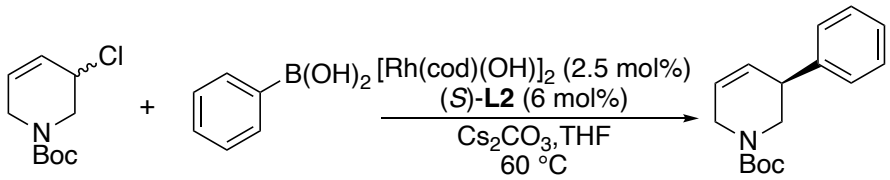
Time (minutes)	ee of **8** (%)	ee of **9** (%)	Approx. Conversion (%)
1	5	89	<5
5	15	90	41
10	24	91	64
15	32	91	69
30	60	92	84
60	94	93	93
90	Peaks too small to accurately integrate	93	94
120	No s.m. remaining	93	100



The general procedure 2 above was followed using (*S*)-Xylyl-P-PHOS ((*S*)-**L14**, 18.2 mg, 0.024 mmol, 0.06 eq.) in place of **L15** and aqueous CsOH (70 µL, 0.40 mmol, 1.00 eq.) in place of Cs_2CO_3. The catalyst mixture was cooled to 30 °C and the reaction monitored at 30 °C. The results are summarised in supplementary table S15.

Table S15 Monitoring the ee of starting material and products in time.

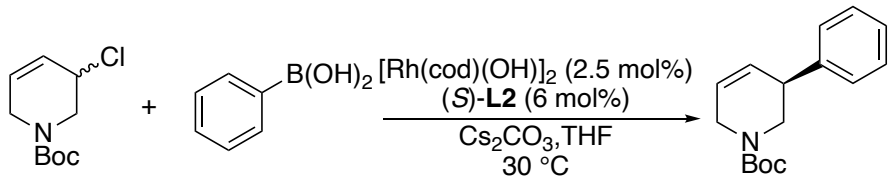
Time (minutes)	ee of **8** (%)	ee of **9** (%)	Approx. Conversion (%)
1	4	88	<5
5	8	88	9
11	18	88	49
20	29	87	65
30	37	86	74
90	74	86	88
120	78	86	90
180	83	86	93
220	~ 91	86	94



The general procedure 2 described above was followed and the results are summarised in supplementary table S16.

Table S16 Monitoring the ee of starting material and products in time.

Time (minutes)	ee of **8** (%)	ee of **9** (%)	Approx. Conversion (%)
1	3	96	10
5	2	96	50
10	2	96	69
15	2	96	81
30	4	96	91
45	4	97	92
60	~ 4	97	93
90	~ 4	97	94
120	No s.m. remaining	97	100

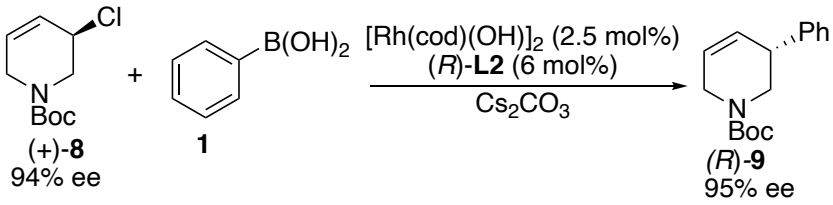


The general procedure 2 described above was followed with the catalyst mixture was cooled to 30 °C and the reaction monitored at 30 °C. After monitoring the reaction for 45 minutes, >90 % conversion to product was observed with no significant increase in the ee of the starting material. The results are summarised in the supplementary table S17.

Table S17 Monitoring the ee of starting material and products in time.

Time (minutes)	ee of **8** (%)	ee of **9**(%)
5	2	96
10	3	96
15	3	96
30	4	96
45	4	96

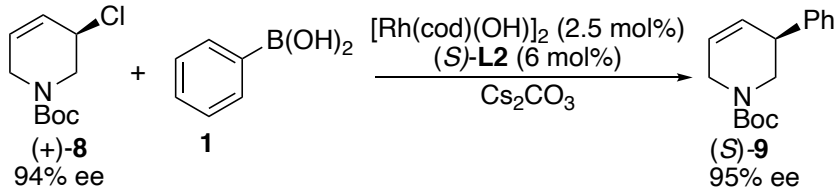
Enantiomerically Enriched Starting Materials



This experiment was performed by M.S. The general procedure 2 described above was followed using enantiomerically enriched (*R*)-**8** (94 % ee) with (*R*)-Cl-MeO-BIPHEP ((*R*)-**L15**, 15.6 mg, 0.024 mmol, 0.06 eq.) in place of (*S*)-Cl-MeO-BIPHEP. The results are summarised in supplementary table S18.

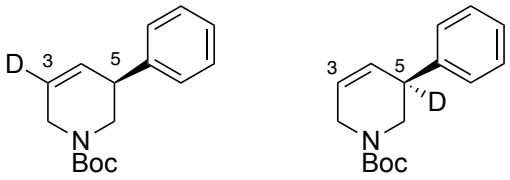
Table S18 Monitoring the ee of starting material and products in time with enantiomerically enriched allyl chloride.

Time (minutes)	ee of **8** (%)	ee of **9** (%)	Approximate Conversion (%)
15	94	>99	59
30	93	97	73
60	87	97	78
75	86	97	81
90	85	96	81
105	84	96	82
255	82	95	86
355	~ 82	95	86



This experiment was performed by M.S. The general procedure 2 described above was followed using enantiomerically enriched (*R*)-**8** (94 % ee). The (*S*) enantiomer of the product was formed with 95 % ee and >80 % conversion to product had occurred in the first 15 minutes.

General procedure 3: for experiments with deuterated *tert*-butyl 5-chloro-5,6-dihydropyridine-1(2*H*)-carboxylate.



In a 10 mL round-bottomed flask flame-dried and purged with argon, $[Rh(cod)(OH)]_2$ (3 mg, 0.006 mmol, 0.025 eq.), Cs_2CO_3 (84 mg, 0.256 mmol, 1.00 eq.) and (*S*)-Cl-MeO-BIPHEP ((*S*)-**L15**, 10 mg, 0.015 mmol, 0.06 eq.) were suspended in THF (1.3 mL) and stirred at 60 °C for 30 min. In a flame-dried 5 mL flask $PhB(OH)_2$ (**1**, 63 mg, 0.512 mmol, 2.00 eq.) was dissolved in THF (0.65 mL). In another flame-dried 5 mL flask d_1-tert-butyl 5-chloro-5,6-dihydropyridine-

1(2H)-carboxylate (56 mg, 0.256 mmol, 1.00 eq.) was dissolved in THF (0.65 mL). These two solutions were added to the first flask simultaneously. The mixture was stirred at 60 °C for 16 h then SiO_2 (50 mg) was added and the volatiles carefully evaporated. The crude was purified by flash column chromatography. The ee of the product was measured by SFC using a non-racemic chiral column (Chiralpak® IF; 1500 psi, 30°C; flow: 1.5 mL/min; from 1 % to 30 % MeOH in 5 min; λ = 214.5 nm; product R_t = 2.09 min and 2.17 min). The deuterium saturation at each position was determined by examining the integrals of the allylic and vinylic protons in the product in ^1H spectra and confirmed by ^2H NMR.

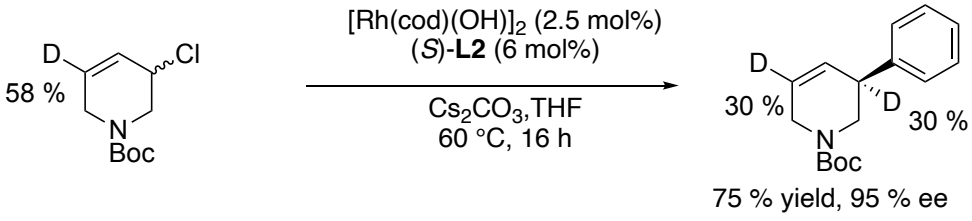
^{1}H NMR of 9 (400 MHz, $CDCl_3$) δ 7.31 (m, 2H), 7.19 – 7.27 (m, 3H), 5.89 (br s, 2H; C(1), C(6)), 3.82 and 4.07 (rot. m, 2H), 3.46 – 3.62 (m, 1H), 3.70 – 3.79 and 4.07 (rot. m, 2H), 3.01, 3.33 – 3.46, 1.19 – 1.63 (m, 9H, 3 x C(C)-H_3).

^{13}C NMR of 9 (101 MHz, $CDCl_3$) δ 154.7 (C=O), 142.2 (C(7)), 128.5 (2 x C_{Ar}), 128.2, 127.9 (2 x C_{Ar}), 126.7, 125.9, 79.5 ($C(CH_3)$), 47.3 and 48.5 (rot.; 1 x $C(H_2)$), 42.9 and 43.6 (rot.; 1 x $C(H_2)$), 41.5, 28.3 (3 x $C(H_3)$).

Physical data identical to that which was previously reported by our group.[54]

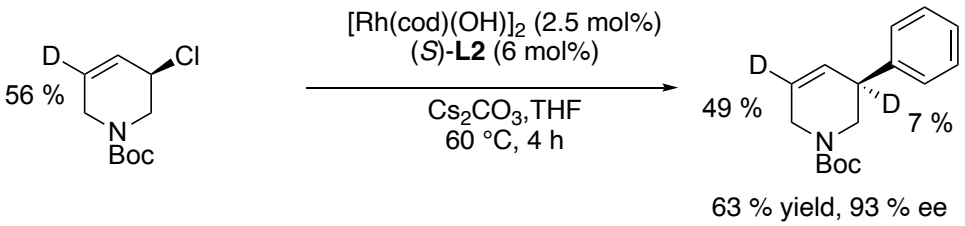
^{2}H NMR of 9-C_3-*d* (C_6D_6) δ 5.46 (br s, 1D).

^{2}H NMR of 9-C_5-*d* (C_6D_6) δ 3.23 (br s, 1D).



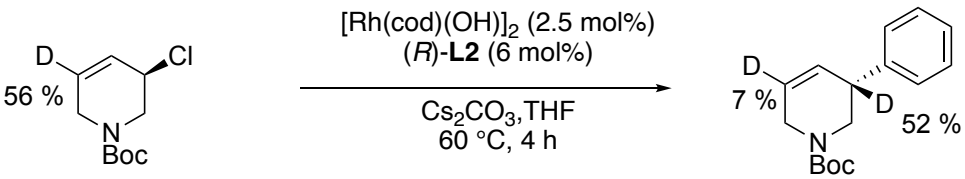
This experiment was performed by S.K. The general procedure 3 described above was followed using racemic d_1-tert-butyl-5-chloro-5,6-dihydropyridine-1(2H)-carboxylate and the

deuterated product was obtained in 75 % yield with 95 % ee. ^{1}H and ^{2}H NMR showed a 1:1 ratio of products with deuterium at C_3 and C_5.



63 % yield, 93 % ee

This experiment was performed by S.K. The general procedure 3 described above was followed using enantioenriched (*R*)-d_1-tert-butyl 5-chloro-5,6-dihydropyridine-1(2H)-carboxylate (94 % ee) and the deuterated product was obtained in 63 % yield with 93 % ee. ^{1}H and ^{2}H NMR showed a 7:1 ratio of products with deuterium at C_3 and C_5.



67 % yield, 92 % ee

This experiment was performed by S.K. The general procedure 3 described above was followed using enantioenriched (*R*)-d_1-tert-butyl 5-chloro-5,6-dihydropyridine-1(2H)-carboxylate (94 % ee) and the deuterated product was obtained in 67 % yield with 92 % ee. ^{1}H and ^{2}H NMR showed a 1:7 ratio of products with deuterium at C_3 and C_5.

2.7 General Information on Computational Methods

All DFT calculations were performed with the *Gaussian 09* program using the ωB97X-D functional.[241] The split-valence 6-31G(d) basis set was used for C, N, O, H, P and Cl atoms, and LANL2DZ(f)[242] (orbital exponent of 1.35) effective core potential/valence double zeta basis set with f polarisation function for Rh in all geometry optimizations. Single point energy corrections were obtained at the ωB97X-D /6-311+G(d,p) level of theory for C, N, O, H, P and Cl atoms, and ωB97X-D/LANL2TZ(f)[243] effective core potential/valence triple zeta basis set with f polarisation function for Rh with an implicit description of the reaction medium (THF) by SMD solvent model as implemented in Gaussian09.

Gibbs free energies were evaluated at 333 K (the reaction temperature), for which the vibrational entropy contributions were computed using a free-rotor approximation for low frequency modes. A cut off frequency of 100 cm^{-1} was used as we switch between the rigid-rotor harmonic oscillator approximation for vibrations above this value and the free-rotor approximation below. For all mechanistic studies, a conventional standard state of 1 mol/L in solution for all species was employed. Harmonic vibrational frequencies were computed for all stationary points to confirm them as either minima or transition structures (TSs), possessing zero or a single imaginary frequency, respectively.

2.8 Computed Kinetic Isotope Effects

These calculations were performed by R.A. The KIE values were calculated according to transition state theory applying the Bigeleisen–Mayer equation using scaled vibrational frequencies using Kinisot Python script (available at https://github.com/bobbypaton). The details of the KIE values with and without tunnelling (Bell infinite-parabola model) corrections are tabulated below (KIEs values with tunnelling corrections were shown in Fig. 29). The calculated $^{13}C/^{12}C$ kinetic isotope effect (KIE) for carbon atoms at 313.15 K for each elementary

step is summarized in Fig. 29 (oxidative addition and reductive elimination steps), the breakdown of these KIEs is tabulated in Table S19 and Table S20. KIE values for *syn*-oxidative addition and oxidative insertion were not calculated as, due to the high calculated energy barriers of these mechanisms, they are unlikely to significantly contribute to the reaction.

Table S19 Calculated KIE for *anti*-oxidative addition step involving complexes of (*R*)-**3**.

(*R*)-OA: C atom from complexes with *(R)*-**3**	KIE ÷ KIE(*ref*)	quantum tunneling corrected KIE ÷ KIE(*ref*)
Ipso (Ph)	0.997	0.997
o-RHS (Ph)	0.998	0.998
m-RHS (Ph)	0.999	0.999
Para (Ph)	0.999	0.999
m-LHS (Ph)	1.000	**1.000**
o-LHS (Ph)	0.999	0.999
Mid (allyl)	0.998	0.999
CCl (allyl)	1.028	**1.029**
CH_2_Cl (allyl)	1.006	1.006
Ref (allyl)	1.000	1.000
CH_2_H (allyl)	1.002	1.002
CH (allyl)	1.000	1.000

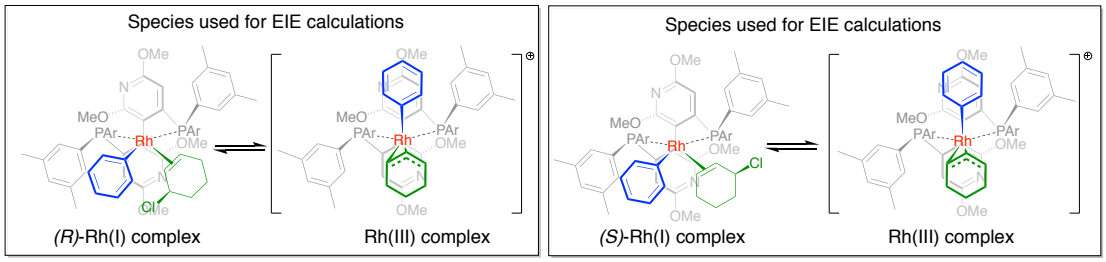
Table S20 Calculated KIE for *anti*-oxidative addition step involving complexes of (*S*)-**3**.

(*S*)-OA: C atom from complexes with *(S)*-**3**	KIE ÷ KIE(*ref*)	quantum tunneling corrected KIE ÷ KIE(*ref*)
Ipso (Ph)	0.999	0.999
o-RHS (Ph)	0.998	0.998
m-RHS (Ph)	1.000	0.999
Para (Ph)	0.999	0.999
m-LHS (Ph)	1.000	1.000
o-LHS (Ph)	1.000	1.000
Mid (allyl)	0.994	0.994
CH (allyl)	0.998	0.998
CH_2_H (allyl)	1.003	1.003
Ref (allyl)	1.000	1.000
CH_2_Cl (allyl)	1.006	1.006
CCl (allyl)	1.033	**1.035**

In an alternative scenario where the oxidative addition step is reversible, we calculated the equilibrium isotope effect (EIE or fractionation factor) between the complexes before

oxidative addition step and reductive elimination step (from the KIE of reverse oxidative addition). These are shown in Table S21.

Table S21 Calculated natural abundance kinetic isotope effect for reverse oxidative addition step.



C atoms	EIE involving complexes with (*R*)-**3**		EIE involving complexes with (*S*)-**3**	
	EIE ÷ EIE(*ref*)	quantum tunneling corrected EIE ÷ EIE(*ref*)	EIE ÷ EIE(*ref*)	quantum tunneling corrected EIE ÷ EIE(*ref*)
Ipso (Ph)	0.997	0.997	0.998	0.998
o-RHS (Ph)	0.998	0.998	0.997	0.997
m-RHS (Ph)	0.999	0.999	0.999	0.999
Para (Ph)	0.999	0.999	0.998	0.998
m-LHS (Ph)	0.999	0.999	0.999	0.999
o-LHS (Ph)	0.999	0.999	0.999	0.999
Mid (allyl)	0.995	0.995	0.992	0.992
C-LHS (allyl)	1.001	1.001	0.998	0.998
CH_2-LHS (allyl)	1.006	1.006	1.001	1.001
Ref (allyl)	1.000	1.000	1.000	1.000
CH_2-RHS (allyl)	1.001	1.001	1.005	1.005
C-RHS (allyl)	1.003	1.003	1.004	1.004

2.9 Energies of Optimised Structures

All Python scripts used for data analysis have been made available - https://github.com/bobbypaton - under a creative commons CC-BY license. Energies are given in terms of zero point energy (ZPE)-corrected total energy (E_{el}+ZPE), enthalpy (E_{el}+H) and Gibbs free-energy (E_{el}+G) as extracted from Gaussian output of each structure (E_{el} = total electronic energy). Only the lowest energy conformations of each species are tabulated.

Table S22. Absolute energies of optimised structures shown in Fig. 32 in gas phase (ωB97XD/6-31G(d)/LANL2DZ(f)) and single point energy (SMD(THF)-ωB97XD/6-31+G(d,p) LANL2TZ(f)). Generated at 333K and concentration = 1 mol/L. E_{el} = Total electronic energy. ZPE = Zero point energy correction. H = Enthalpy correction at 298.15 K. G = Gibbs free energy correction at 298.15 K. Gcorr = Gibbs free energy evaluated at 333 K, with quasi-harmonic approximation. SPE = Total electronic energy with large basis set (SMD(THF)-ωB97XD/6-31+G(d,p) LANL2TZ(f)). R.E. = reductive elimination. O.A. = oxidative addition.

	ωB97X-D/6-31G(d), LANL2DZ(f)					**THF**
	E_{el} (au)	**ZPE (au)**	**H (au)**	**G (au)**	**G_{corr} (au)**	**SPE (au)**
3 (pseudo axial)	-694.160144	0.139852	-694.011425	-694.052144	-694.052030	-694.257108
transmetalation TS	-3468.949015	1.013068	-3467.853707	-3468.055513	-3468.039105	-3469.749858
post-transmetalation	-3468.983789	1.013998	-3467.886357	-3468.093853	-3468.074729	-3469.782029
(*R*)-reactant complex	-3910.736886	1.104755	-3909.546037	-3909.757016	-3909.739001	-3911.541681
(*S*)-reactant complex	-3910.739063	1.105354	-3909.548057	-3909.757054	-3909.739562	-3911.545192
(*S*)-TS O.A.	-3910.702421	1.104971	-3909.511920	-3909.720989	-3909.703735	-3911.541746
(*R*)-TS O.A.	-3910.712464	1.105016	-3909.522466	-3909.728248	-3909.712305	-3911.540045
Intermediate (**V**)	-3450.372624	1.105792	-3449.183538	-3449.385377	-3449.369941	-3451.176092
(*S*)-TS R.E.	-3450.357861	1.104811	-3449.170166	-3449.372352	-3449.356344	-3451.155695
(*R*)-TS R.E.	-3450.349051	1.104797	-3449.161620	-3449.361275	-3449.346409	-3451.146438
(*S*)-product complex	-3450.419228	1.106593	-3449.229383	-3449.432829	-3449.416054	-3451.216129
Chloride	-460.232420	0.000000	-460.229784	-460.246002	-460.246002	-460.376417
$B(OH)_3$ (**2**)	-252.388470	0.048954	-252.332993	-252.366452	-252.366456	-252.503478

Table S23. *These calculations were performed by R.A.* Absolute energies of optimised structures in gas phase (ωB97XD/6-31G(d)/LANL2DZ(f)) and single point energy (SMD(THF)-ωB97XD/6-31+G(d,p) LANL2TZ(f)) for **6** energy profile. E_{el} = Total electronic energy. ZPE = Zero point energy correction. H = Enthalpy correction at 298.15 K. G = Gibbs free energy correction at 298.15 K. Gcorr = Gibbs free energy evaluated at 333 K, with quasi-harmonic approximation. SPE = Total electronic energy with large basis set (SMD(THF)-ωB97XD/6-31+G(d,p) LANL2TZ(f)). R.E. = reductive elimination.

	ωB97X-D/6-31G(d), LANL2DZ(f)					**THF**
	E_{el} (au)	**ZPE (au)**	**H (au)**	**G (au)**	**G_{corr} (au)**	**SPE (au)**
6 (Pseudo equatorial)	-730.032621	0.115341	-729.91014	-729.947984	-729.952385	-730.1325653
(*S*)-TS O.A.	-3946.5732	1.079781	-3945.4235	-3945.5996	-3945.6035	-3947.4202
(*R*)-TS O.A.	-3946.5791	1.080434	-3945.4295	-3945.6003	-3945.6063	-3947.4268
Intermediate	-3486.240816	1.08088	-3485.09177	-3485.261387	-3485.26658	-3487.062315
(*S*)-TS R.E.	-3486.228595	1.080378	-3485.08058	-3485.24866	-3485.254357	-3487.041358
(*R*)-TS R.E.	-3486.213487	1.080379	-3485.06551	-3485.23472	-3485.239342	-3487.025773
(*S*)- product complex **7**	-3486.289862	1.082118	-3485.13969	-3485.310606	-3485.314483	-3487.103501

Table S24. Absolute energies of optimised structures in gas phase (ωB97XD/6-31G(d)/LANL2DZ(f)) and single point energy (SMD(THF)) for the O.A. transition state structures for **10**. E_{el} = Total electronic energy. ZPE = Zero point energy correction. H = Enthalpy correction at 298.15 K. G = Gibbs free energy correction at 298.15 K. Gcorr = Gibbs free energy evaluated at 333 K, with quasi-harmonic approximation. SPE = Total electronic energy with large basis set (SMD(THF)-ωB97XD/6-31+G(d,p) LANL2TZ(f)). O.A. = oxidative addition.

		ωB97X-D/6-31G(d), LANL2DZ(f)					**THF**
		E/au	**ZPE/au**	**H/au**	**T.qh-S/au**	**qh-G(T)/au**	**E/au**
O. A.	anti TS	-4482.05794	0.862789	-4481.138152	0.136055	-4481.274207	-4482.85665
	syn TS	-4482.08955	0.86207	-4481.170716	0.135236	-4481.305952	-4482.85899

3. Supplementary Information for Chapter 3

3.1 Synthesis of Allylic Alcohols

General Procedure 3: Manganese dioxide oxidation

Activated MnO_2 (20.5 eq.) was added to a solution of the alcohol substrate (1.0 eq.) in CH_2Cl_2 (0.25 M) and stirred at 25 ^oC for 6-16 h. The resulting mixture was filtered through a pad of celite and the filtrate was concentrated *in vacuo*. The product was purified by column chromatography (pentane:Et_2O).

General Procedure 4: Methyl lithium 1,2 addition

MeLi in Et_2O (1.6 M, 1.1 eq.) was added slowly to a solution of the appropriate enone (1.0 eq.) in Et_2O or THF at -78 ^oC. After 1-3 h, water was added and the reaction mixture was warmed to room temperature. A saturated solution of NH_4Cl was added and the mixture was then extracted with Et_2O (x3). The combined organic layers were washed with saturated NaCl solution, dried over $MgSO_4$, then filtered and concentrated *in vacuo.* The product was purified by Kugelrohr distillation or column chromatography.

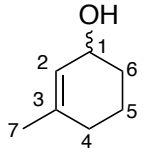
General Procedure 5: Triflouromethyl 1,2 addition

Trifluoromethyltrimethylsilane (6.2 mL, 42 mmol, 2.1 eq.) was added to a solution of enone substrate (20 mmol, 1.0 eq.) in THF (40 mL). Tetra-*n*-butylammonium fluoride (1M in THF, ~0.05 eq.) was added dropwise until the reaction became exothermic and dark brown in colour. The reaction was stirred at room temperature for 16 h. The silyl ether cleavage was then carried out at room temperature by adding tetra-*n*-butylammonium fluoride (1 M in THF, 1.0 eq.). After stirring for 1 h, water was added. The layers were separated, and the aqueous layer was extracted with Et_2O (x3), dried over $MgSO_4$, filtered and concentrated *in vacuo.* The product was purified by column chromatography.

General Procedure 6: Coupling of allyl alcohol and epoxide

Allyl alcohol (99 mmol, 2.0 eq.) was added to a solution of 2-vinyloxirane (4.0 mL, 50 mmol, 1.0 eq.) in DMF (100 mL) and the solution was cooled to 0 °C. NaH (3.97 g, 60 % w/w in mineral oil, 99.3 mmol, 2.0 eq.) was added slowly in small portions (0.5 g portions). After 30 min, the reaction was warmed to 50 °C. After 16 h stirring at 50 °C, the reaction was cooled to 0 °C, then quenched with aq. HCl (100 mL) at 0 °C and stirred for 1 h. The aqueous phase was then extracted with Et_2O (x3). The combined organic layers were washed with LiCl solution (10 % w/w), followed by saturated NaCl solution, then dried over $MgSO_4$, filtered and concentrated *in vacuo*. The crude products were sufficiently pure to be carried forward without additional purification.

3-methylcyclohex-2-enol ((±)-14)



3-methylcyclohex-2-enone (5.0 mL, 44 mmol, 1.0 eq.) and $CeCl_3.7H_2O$ (2.0 g, 52.8 mmol, 1.2 eq.) were dissolved in MeOH (250 mL) and cooled to 0 °C. $NaBH_4$ (19.7 g, 52.8 mmol, 1.2 eq.) was added in portions (2.0 g portions). The reaction vessel was allowed to warm to room temperature and stirred for 2 h at 23 °C. The reaction was quenched by adding to ice (250 mL) and stirring. Saturated NH_4Cl (80 mL) was then added before extraction using CH_2Cl_2 (x3). The organic layer was washed with water, dried over $MgSO_4$, filtered and concentrated *in vacuo*. The crude product (3.93 g, 80 % yield) was sufficiently pure to be carried forward without additional purification.

UPC^2 conditions to separate the two enantiomers were found using Chiralpak® ID; 1500 psi, 30°C; flow: 1.5 mL/min; from 1 % to 30 % MeOH in 5 min.

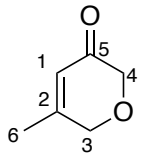
^{1}H NMR (400 MHz, $CDCl_3$) δ 5.50 – 5.44 (m, 1H; C(2)-H), 4.17 – 4.12 (m, 1H; C(1)-H), 2.40 – 2.24 (m, 1H; OH), 1.95 – 1.65 (m, 4H), 1.64 (s, 3H; C(7)-H_3), 1.57 – 1.40 (m, 2H).

^{13}C NMR (101 MHz, $CDCl_3$) δ 138.3 (C(3)), 124.4 (C(2)), 65.7 (C(1)), 31.6, 30.0, 23.6 (C(7)), 19.1.

LRMS (ESI-TOF) calcd for $C_7H_{13}O$ [M + H^+] 113.1, found 113.1.

Physical data identical to that which was previously reported.[244]

5-methyl-2*H*-pyran-3(6*H*)-one



Synthesised *via* general procedure 3 using 5-methyl-3,6-dihydro-2H-pyran-3-ol ((±)-**14**, 1.90 g, 16.7 mmol) substrate and stirring for 16 h to give the product as a yellow oil (60 % yield, 1.12 g) after column chromatography.

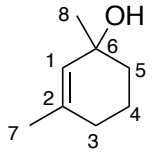
^{1}H NMR (400 MHz, $CDCl_3$) δ 6.02 (s, 1H; C(1)-H), 4.25 (s, 2H), 4.09 (s, 2H), 1.95 (s, 3H; C(6)-H_3).

^{13}C NMR (101 MHz, $CDCl_3$) δ 194.5 (C(5)), 160.6 (C(2)), 124.1 (C(1)), 71.4, 68.4, 19.7 (C(6)).

HRMS (ESI) m/z calcd for $C_6H_9O_2$ $[M+H]^+$: 113.0597, found 113.0597.

IR (ATR) ν_{max} = 3044, 2958, 1677 (s), 827, 803 cm^{-1}.

1,3-dimethylcyclohex-2-enol



Synthesised *via* general procedure 4 using 3-methylcyclohex-2-enone (2.00 g, 18.2 mmol), Et_2O solvent (25.0 mL) and quenching after 1 h. The product (colourless oil, 61 % yield, 1.39 g), was purified by Kugelrohr distillation (high vacuum, 90 ^oC).

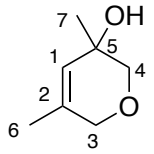
^{1}H NMR (400 MHz, $CDCl_3$) δ 5.37 (q, *J* = 1.5 Hz, 1H; C(1)-H), 1.94 – 1.80 (m, 2H; C(3)-H_2), 1.77 – 1.59 (m, 6H; C(7)-H_3, C(4)-H_2, C(5)-H), 1.59 – 1.50 (m, 1H; C(5)-H), 1.26 (s, 3H; C(8)-H_3).

^{13}C NMR (101 MHz, $CDCl_3$) δ 137.2 (C(2)), 128.5 (C(1)), 68.6 (C(6)), 37.7 (C(5)), 30.2 (C(3)), 29.8 (C(8)), 23.7 (C(7)), 19.9 (C(4)).

HRMS (GCMS EI, ionisation energy of 20 eV) m/z calcd for $C_8H_{14}O$ $[M]^+$: 126.1039, found: 126.1042.

IR (ATR) ν_{max} = 3284 (broad), 3022, 2924, 1440 cm^{-1}.

3,5-dimethyl-3,6-dihydro-2*H*-pyran-3-ol



Synthesised *via* general procedure 4 using 5-methyl-2*H*-pyran-3(6*H*)-one (1.40 g, 12.5 mmol), Et_2O solvent (18.5 mL) and quenching after 3 h. The product (colourless oil, 40 % yield, 0.64 g), was purified by column chromatography (pentane:Et_2O, 4:1).

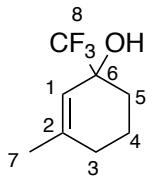
^{1}H NMR (400 MHz, $CDCl_3$) δ 5.61 – 5.46 (m, 1H; C(1)-H), 4.04 – 3.87 (m, 2H; C(3)-H_2), 3.73 (dd, *J* = 11.2, 1.3 Hz, 1H; C(4)-H), 3.39 (d, *J* = 11.2 Hz, 1H; C(4)-H), 1.62 (s, 3H; C(6)-H_3), 1.19 (s, 3H; C(7)-H_3).

^{13}C NMR (101 MHz, $CDCl_3$) δ 135.4 (C(2)), 126.7 (C(1)), 75.5 (C(4)), 68.9 (C(3)), 66.0 (C(5)), 23.9 (C(7)), 18.5 (C(6)).

HRMS (GCMS EI, ionisation energy of 35 eV) m/z cacld for $C_7H_{12}O_2$ $[M]^+$: 128.0832, found: 128.0834.

IR (ATR) ν_{max} = 3628 (broad), 2955, 1462, 1377, 1261, 1092 cm^{-1}.

3-methyl-1-(trifluoromethyl)cyclohex-2-enol ((±)-19)



Synthesised *via* general procedure 5 using 3-methylcyclohex-2-enone. The product (colourless oil, 63 % yield, 2.27 g) was purified by column chromatography (pentane:Et_2O).

^{1}H NMR (400 MHz, $CDCl_3$) δ 5.48 (s, 1H; C(1)-H), 2.03 – 1.94 (m, 2H; C(3)-H_2), 1.88 – 1.69 (m, 7H; C(7)-H_3, C(5)-H_2, C(4)-H_2).

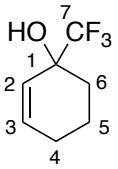
^{13}C NMR (101 MHz, $CDCl_3$) δ 145.2 (C(2)), 126.3 (q, *J* = 281.6 Hz; C(8)), 117.6 (C(1)), 71.5 (q, *J* = 28.1 Hz, C(6)), 30.1 (C(3)), 28.8 (C(5)), 24.1 (C(7)), 17.9 (C(4)).

^{19}F NMR (377 MHz, $CDCl_3$) δ -82.83.

HRMS (GCMS EI, ionisation energy of 20 eV) m/z calcd for $[M]^+$ 180.0757, found: 180.0757.

IR (ATR) ν_{max} = 3393 (broad), 2981, 1672, 1260, 1159, 1097 cm^{-1}.

1-(trifluoromethyl)cyclohex-2-enol ((±)-22)



Synthesised *via* general procedure 5 using cyclohex-2-enone as previously described by G.K.S. Prakash *et. al.*[245] The product (colourless oil, 75 % yield, 2.49 g) was purified by column chromatography (pentane:Et_2O).

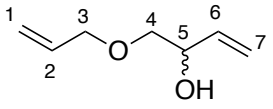
^{1}H NMR (400 MHz, $CDCl_3$) δ 6.18 (m, 1H; C(3)-H), 5.79 – 5.70 (m, 1H; C(2)-H), 2.25 – 2.01 (m, 2H), 1.96 – 1.82 (m, 2H), 1.82 – 1.72 (m, 2H).

^{13}C NMR (101 MHz, $CDCl_3$) δ 136.6 (C(2)), 126.1 (apparent d, *J* = 282.8 Hz; C(7)), 123.0 (C(3)), 70.6 (apparent d, *J* = 28.7 Hz, C(1)), 29.1, 25.0, 17.4.

^{19}F NMR (377 MHz, $CDCl_3$) δ -82.84.

Physical data identical to that which was previously reported.[245]

1-(allyloxy)but-3-en-2-ol ((±)-25)



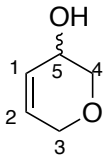
Synthesised *via* general procedure 6 using prop-2-en-1-ol to give the product as a yellow oil (70 % yield, 4.45 g) as previously described by our group.[161]

^{1}H NMR (400 MHz, $CDCl_3$) δ 5.98 – 5.77 (m, 2H; C(2)-H, C(6)-H), 5.41 – 5.09 (m, 4H; C(1)-H_2, C(7)-H_2), 4.36 – 4.29 (m, 1H; C(5)-H), 4.07 – 4.01 (m, 2H; C(3)-H_2), 3.53 – 3.42 (m, 1H; C(4)-H), 3.36 – 3.30 (m, 1H; C(4)-H), 2.49 (broad s, 1H; OH).

^{13}C NMR (101 MHz, $CDCl_3$) δ 136.7 (C(6)), 134.5 (C(2)), 117.5 (C(1)), 116.6 (C(7)), 74.1 (C(4)), 72.4 (C(3)), 71.6 (C(5)).

Physical data identical to that which was previously reported.[161]

3,6-dihydro-2*H*-pyran-3-ol ((±)-26)



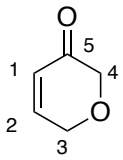
1-(allyloxy)but-3-en-2-ol ((±)-**25**, 4.98 g, 38.9 mmol, 1.00 eq.) was dissolved in CH_2Cl_2 (400 mL, 0.1 M). Grubb's 1st generation catalyst (0.64 g, 0.78 mmol, 0.02 eq.) was added and the mixture stirred at room temperature for 16 h. The solvent was removed *in vacuo* and the crude product (92 % yield, 3.58 g) was sufficiently pure to be carried forward as a brown oil without additional purification.

^{1}H NMR (400 MHz, $CDCl_3$) δ 6.11 – 5.84 (m, 2H; C(1)-H, C(2)-H), 4.21 – 4.01 (m, 2H; C(3)-CH_2), 4.01 – 3.92 (m, 1H; C(5)-H), 3.84 (dd, *J* = 11.8, 2.9 Hz, 1H; C(4)-H), 3.74 (dd, *J* = 11.8, 2.9 Hz, 1H; C(4)-H).

^{13}C NMR (101 MHz, $CDCl_3$) δ 129.9 (C(1)), 126.7 (C(2)), 70.8 (C(4)), 65.3 (C(3)), 62.7 (C(5)).

Physical data identical to that which was previously reported.[161]

2*H*-pyran-3(6*H*)-one (27)



Synthesised *via* general procedure 3 using 3,6-dihydro-2*H*-pyran-3-ol substrate ((±)-**26**, 3.37 g, 33.7 mmol) substrate and stirring for 6 h to give the product (62 % yield, 2.03 g) as a colourless oil after column chromatography.

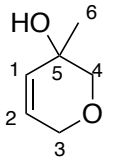
^{1}H NMR (400 MHz, $CDCl_3$) δ 7.11 (dt, *J* = 10.5, 3.1 Hz, 1H; C(2)-H), 6.19 (dt, *J* = 10.5, 2.1 Hz, 1H; C(1)-H), 4.38 – 4.37 (m, 2H; C(3)-H_2), 4.18 (s, 2H; C(4)-H_2).

^{13}C NMR (101 MHz, $CDCl_3$) δ 194.6 (C(5)), 148.4 (C(2)), 127.1 (C(1)), 72.4 (C(4)), 64.7 (C(3)).

LRMS (ESI-TOF) calcd for $C_5H_6O_2$ $[M+Na]^+$ 121.0, found 121.0.

Physical data identical to that which was previously reported.[246]

3-methyl-3,6-dihydro-2*H*-pyran-3-ol ((±)-28)



Synthesised *via* general procedure 4 using 2*H*-pyran-3(6*H*)-one substrate (**27**, 2.00 g, 20.4 mmol), THF solvent (7.0 mL) and quenching after 3 h. The product (pale yellow oil, 39 % yield 0.91 g), was purified by column chromatography (Et_2O:pentane, 2:1).

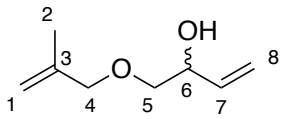
^{1}H NMR (400 MHz, $CDCl_3$) δ 5.88 – 5.69 (m, 2H; C(1)-H, C(2)-H), 4.23 – 3.95 (m, 2H; C(3)-H_2), 3.72 (d, *J* = 11.4 Hz, 1H; C(4)-H), 3.53 – 3.37 (m, 1H; C(4)-H), 2.41 (broad s, 1H; OH), 1.21 (s, 3H; C(6)-H_3).

^{13}C NMR (101 MHz, $CDCl_3$) δ 131.8 (C(1)), 127.4 (C(2)), 75.6 (C(4)), 65.5 (C(5)), 65.4 (C(3)), 23.8 (C(6)).

HRMS (GCMS EI, ionisation energy of 35 eV) m/z cacld for $C_6H_{10}O_2$ $[M]^+$: 114.0675, found: 114.0672.

IR (ATR) ν_{max} = 3422 (broad), 2925, 2855, 1456, 1094 cm^{-1}.

1-((2-methylallyl)oxy)but-3-en-2-ol ((±)-29)



Synthesised *via* general procedure 6 using 2-methylprop-2-en-1-ol. Excess 2-methylprop-2-en-1-ol was removed *in vacuo* at 50 °C to give the product as a yellow oil (78 % yield, 5.51 g).

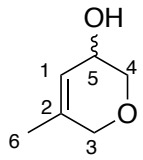
^{1}H NMR (400 MHz, $CDCl_3$) δ 5.91 – 5.78 (m, 1H; C(7)-H), 5.45 – 5.33 (m, 1H; C(8)-H), 5.24 – 5.18 (m, 1H; C(8)-H), 5.04 – 4.88 (m, 2H; C(1)-H_2), 4.37 – 4.30 (m, 1H; C(6)-H), 3.95 (s, 2H; C(4)-H_2), 3.48 (dd, *J* = 9.5, 3.5 Hz, 1H; C(5)-H), 3.35 – 3.27 (m, 1H; C(5)-H'), 2.41 (broad s, 1H; OH), 1.75 (s, 3H; C(2)-CH_3).

^{13}C NMR (101 MHz, $CDCl_3$) δ 141.8 (C(3)), 136.6 (C(7)), 116.5 (C(8)), 112.6 (C(1)), 75.2 (C(4)), 73.7 (C(5)), 71.5 (C(6)), 19.4 (C(2)).

HRMS (APCI) m/z calcd for $C_8H_{15}O_2$ $[M+H]^+$: 143.1067, found: 143.1068.

IR (ATR) ν_{max} = 3450 (broad), 2955, 2924, 1377, 1103 cm^{-1}.

5-methyl-3,6-dihydro-2*H*-pyran-3-ol ((±)-30)



1-((2-methylallyl)oxy)but-3-en-2-ol ((±)-**29**, 10.0 g, 70.3 mmol, 1.00 eq.) was dissolved in CH_2Cl_2 (700 mL, 0.1 M). Grubb's 2nd generation catalyst (0.33 g, 0.39 mmol, 0.0055 eq.) was added and the mixture refluxed for 16 h. The solvent was removed *in vacuo* and the crude product was purified by column chromatography (Et_2O:pentane gradient, 4:1 to 100 % Et_2O) to give the product as a brown oil (70 % yield, 5.90 g).

Enantiomeric excess of both enantiomers was determined by UPC^2 with a non-racemic chiral column (Chiralpak® IG; 1500 psi, 30°C; flow: 1.5 mL/min; from 1 % to 30 % MeOH in 5 min; λ = 210 nm; (*S*)-**30** R_t = 3.00 min; (*R*)-**30** R_t = 3.27 min) (Fig. S6). The enantiomers can also be separated by UPC^2 under the same conditions using non-racemic chiral column Chiralpak® IA (R_t = 1.83 min; R_t = 1.98 min) or column Chiralpak® IF (R_t = 2.66 min; R_t = 2.82 min).

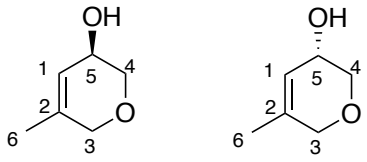
^{1}H NMR (400 MHz, $CDCl_3$) δ 5.76 – 5.64 (m, 1H; C(1)-H), 4.04 – 3.88 (m, 3H; C(5)-H, C(3)-H_2), 3.83 (dd, *J* = 11.7, 2.6, 1H; C(4)-H), 3.64 (dd, *J* = 11.7, 2.6 Hz, 1H; C(4)-H), 1.65 (s, 3H; C(6)-CH_3).

^{13}C NMR (101 MHz, $CDCl_3$) δ 138.0 (C(2)), 121.5 (C(1)), 70.8 (C(4)), 68.9 (C(3)), 63.1 (C(5)), 18.8 (C(6)).

HRMS (GCMS EI, ionisation energy of 35 eV) m/z cacld for $C_6H_{10}O_2$ $[M]^+$: 114.0675, found: 114.0673.

IR (ATR) ν_{max} = 3384 (broad), 2918, 1677, 1124, 1043 cm^{-1}.

5-methyl-3,6-dihydro-2*H*-pyran-3-ol (30) resolution



As previously described,[174] 5-methyl-3,6-dihydro-2H-pyran-3-ol ((±)-**30**, 0.5 g, 4.4 mmol, 1.0 eq.) was dissolved in hexane (3.4 mL). Vinyl butyrate (0.56 mL, 4.4 mmol, 1.0 eq.) was added along with Novozyme 435 (11 mg). The mixture was stirred at 23 °C for 5 h, then filtered through a plug of celite with Et_2O and the solvent removed *in vacuo.* The products were purified and separated by column chromatography (EtOAc:Hexane gradient, 20 to 100 % EtOAc) to give the enantioenriched allyl alcohol (*R*)-**30** as a colourless oil (42 % yield, 78% ee) and the enantioenriched ester as a colourless oil (41 % yield). The ester was then dissolved in MeOH and aq. NaOH solution (4M) was added. After stirring at 23 °C for 1 h, approximately half of the solvent was removed *in vacuo.* The organic product was then extracted using EtOAc (15 mL x2), The organic layer was washed with saturated NaCl solution (15 mL), dried over Na_2SO_4, filtered and the solvent removed *in vacuo* to give the enantioenriched alcohol (*S*)-**30** (91 % ee) as a colourless oil.

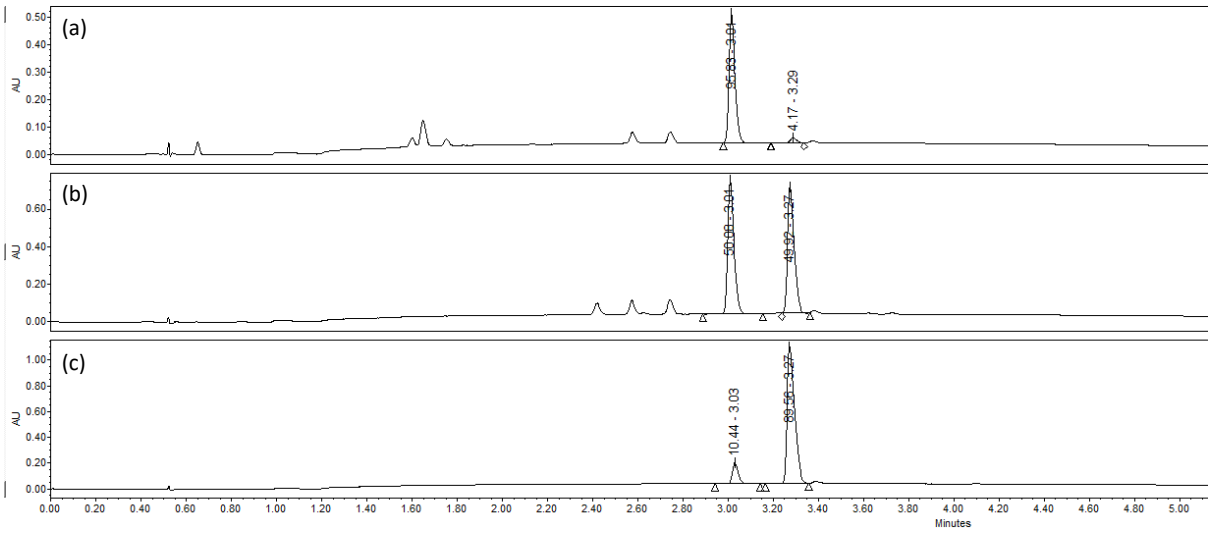


Figure S6. SFC traces for the resolution of (±)-**30** showing (a) (*S*)-**30** (b) (±)-**30** and (c) (*R*)-**30**.

The enantioenrichment of (*R*)-**30** (78 % ee, 0.2 g) was further increased by dissolving in hexane (1.4 mL), adding vinyl butyrate (0.2 mL) along with Novozyme 435 (4 mg) and stirring at 23 °C for 5 h. The mixture was then filtered through a plug of celite and the solvent removed *in vacuo.* The product was purified by column chromatography (EtOAc:Hexane gradient, 20 to 100 % EtOAc) to give the enantioenriched allyl alcohol (*R*)-**30** as a colourless oil (0.15 g, 99 % ee).

3.2 Synthesis of Allylic Substrates

General Procedure 7: Chlorination using phosphorous trichloride

A solution of the corresponding allyl alcohol (1.0 eq.) and pyridine (0.1 eq.) was added dropwise to PCl_3 (distilled before use, 0.37 eq.) at 0 °C. The mixture was stirred at 0 °C and allowed to warm to room temperature for 2-16 h. The upper layer was removed from the reaction flask and purified by filtration through a plug of silica or by Kugelrohr distillation. The resulting allyl chloride products were stored under argon in the dark below 0 °C.

General Procedure 8: Chlorination using thionyl chloride

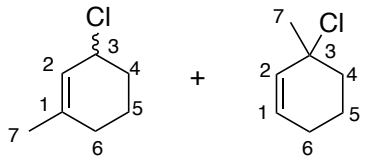
A solution of the corresponding allyl alcohol (1.0 eq., 2.4 mmol) in ether (6.3 mL) was added to a solution of thionyl chloride (1.0 eq., 2.4 mmol) in ether (2.7 mL) at 0 °C. The mixture was stirred at 0 °C for 2 h. The solvent was removed *in vacuo*.

General Procedure 9: Bromination using phosphorous tribromide

PBr_3 (1.5 eq.) was added dropwise to a solution of the corresponding allyl alcohol (1.0 eq.) in CH_2Cl_2 (1 M) at -10 °C. The mixture was stirred and allowed to warm to room temperature. After 16 h, saturated $NaHCO_3$ solution was added slowly at 0 °C. The mixture was warmed to room temperature and water was added. The layers were separated and the aqueous layer

extracted with CH_2Cl_2. The organic layer was then washed with saturated NaCl solution, dried over $MgSO_4$ and filtered. The resulting product was purified by column chromatography.

3-chloro-1-methylcyclohex-1-ene ((±)-15a) and 3-chloro-3-methylcyclohex-1-ene ((±)-15b)



Synthesised *via* general procedure 7 using 3-methylcyclohex-2-enol ((±)-**14**)and stirring for 2 h to give the product, after purification by Kugelrohr distillation (20 mbar, 100 °C), as a colourless oil (65 % yield, 9:1 r.r., 2.69 g). The resulting product decomposes over time.

^{1}H NMR (400 MHz, $CDCl_3$, 9:1 mixture (±)-**15a**:(±)-**15b**)

Major Regioisomer ((±)-**15a**): δ 5.57-5.55 (m, 1H; C(2)-H), 4.68 – 4.64 (m, 1H; C(3)-H), 2.02 – 1.89 (m, 6H; C(4)-H_2, C(5)-H_2, C(6)-H_2), 1.71 (s, 3H; C(7)-H_3).

Minor Regioisomer ((±)-**15b**): δ 5.80 – 5.70 (m, 2H; C(1)-H, C(2)-H), 1.77 (s, 3H; C(7)-H_3), 1.69 – 1.60 (m, 3H).

Overlapping peaks: (±)-**15b** 3H peaks overlapping with (±)-**15a** peaks in region δ 2.02 – 1.89 (m).

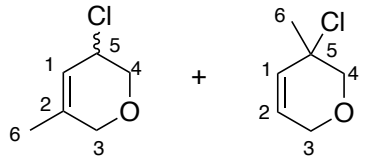
^{13}C NMR (101 MHz, $CDCl_3$)

Major Regioisomer ((±)-**15a**): 139.8 (C(1)), 122.7 (C(2)), 57.1 (C(3)), 32.1, 29.8, 23.7 (C(7)), 18.5.

Minor Regioisomer ((±)-**15b**): 133.2 (C(2)), 128.6 (C(1)), 39.8, 33.2 (C(7)), 24.6, 18.6. Quaternary centre (C(3)) of minor regioisomer not visible in spectrum.

Physical data identical to that which was previously reported.[247]

3-chloro-5-methyl-3,6-dihydro-2*H*-pyran ((±)-31a) and 3-chloro-3-methyl-3,6-dihydro-2*H*-pyran ((±)-31b)



Synthesised *via* general procedure 7 using either 3-methyl-3,6,-dihydro-2*H*-pyran-3-ol ((±)-**30**) or 5-methyl-3,6-dihydro-2H-pyran-3-ol ((±)-**28**) and stirring for 2 h to give the product after purification by filtration through a plug of silica, as a colourless oil (70 % yield, 4:1 r.r., 0.91 g).

^{1}H NMR (400 MHz, $CDCl_3$, 4:1 mixture (±)-**31a**: (±)-**31b**)

Major Regioisomer ((±)-**31a**): δ 5.71 – 5.64 (m, 1H; C(1)-H), 4.53 – 4.44 (m, 1H; C(5)-H), 4.12 – 3.93 (m, 3H; C(3)-CH_2, C(4)-H), 3.86 (dd, *J* = 12.1, 4.3 Hz, 1H; C(4)-H), 1.67 (s, 3H; C(6)-H_3).

Minor Regioisomer ((±)-**31b**): δ 5.95 – 5.74 (m, 2H; C(1)-H, C(2)-H), 4.28 – 4.19 (m, 1H; C(3)-H), 3.73 (d, *J* = 11.7 Hz, 1H; C(4)-H) 1.63 (s, 3H; C(6)-H_3). Signal C(3)-H and C(4)-H overlapping with peaks from major regioisomer in 4.14 – 3.82 ppm region.

^{13}C NMR (101 MHz, $CDCl_3$)

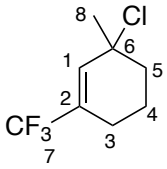
Major Regioisomer ((±)-**31a**): δ 126.9 (C(2)),120.7 (C(1)), 70.1 (C(4)), 68.6 (C(3)), 52.3 (C(5)), 18.7 (C(6)).

Minor Regioisomer ((±)-**31b**): δ 138.3 (C(1)), 131.3 (C(2)), 75.7 (C(4)), 65.2 (C(3)), 28.7 (C(6)). Quaternary centre (C(5)) of minor regioisomer not visible in spectrum.

HRMS (Methane CI) m/z cacld for C_6H_8ClO $[M-H]^+$: 131.0258, found: 131.0263.

IR (ATR) ν_{max} = 2927, 2861, 1445, 1376, 612 cm^{-1}.

3-chloro-3-methyl-1-(trifluoromethyl)cyclohex-1-ene ((±)-20)



Synthesised *via* general procedure 7 using 3-methyl-1-(trifluoromethyl)cyclohex-2-enol ((±)-**19**) and stirring for 16 h to give the product as a single regioisomer (pale yellow oil, 45 % yield, 1.08 g) after purification by column chromatography.

^{1}H NMR (400 MHz, $CDCl_3$) δ 6.36 – 6.26 (m, 1H; C(1)-H), 2.32 – 1.91 (m, 4H), 1.89 – 1.74 (m, 2H), 1.72 (s, 3H; C(8)-H_3).

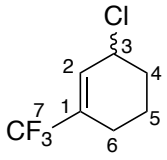
^{13}C NMR (126 MHz, $CDCl_3$) δ 134.3 (q, *J* = 6.1 Hz; C(1)), 129.1 (q, *J* = 30.7 Hz, C(2)), 123.6 (q, *J* = 273.3 Hz, C(7)), 65.0 (C(6)), 38.9, 32.5 (C(8)), 22.0, 18.7.

^{19}F NMR (377 MHz, $CDCl_3$) δ -69.94.

HRMS not found.

IR (ATR) ν_{max} = 3033, 1653, 1300, 1110, 1018, 620 cm^{-1}.

3-chloro-1-(trifluoromethyl)cyclohex-1-ene ((±)-23)



Synthesised *via* general procedure 7 using 1-(trifluoromethyl)cyclohex-2-enol ((±)-**22**) and stirring for 16 h to give the product as a single regioisomer (colourless oil, 48 % yield, 0.56 g) after purification by column chromatography.

^{1}H NMR (400 MHz, $CDCl_3$) δ 6.41 – 6.35 (m, 1H; C(2)-H), 4.67 – 4.59 (m, 1H; C(3)-H), 2.33 – 2.10 (m, 2H), 2.09 – 2.02 (m, 2H), 2.02 – 1.89 (m, 1H), 1.82 – 1.71 (m, 1H).

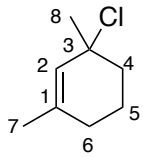
^{13}C NMR (126 MHz, $CDCl_3$) δ 131.5 (q, *J* = 31.2 Hz; C(1)), 129.8 (q, *J* = 6.1 Hz, (C(2)), 123.4 (q, *J* = 273.4 Hz, C(7)), 52.6 (C(3)), 31.4, 21.9, 17.9.

^{19}F NMR (377 MHz, $CDCl_3$) δ -70.12

HRMS (GCMS EI, ionisation energy of 20 eV) m/z calcd for $C_7H_8ClF_3$ $[M]^+$: 184.0261, found: 184.0261.

IR (ATR) ν_{max} = 2918, 2850, 2341, 1175, 669 cm^{-1}.

3-chloro-1,3-dimethylcyclohex-1-ene ((±)-17)



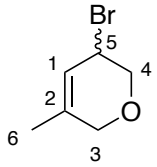
Synthesised *via* general procedure 8 using 1,3-dimethylcyclohex-2-enol to give the crude product as a colourless oil (49 % yield, 0.17g). The product was air and light sensitive and highly unstable. Purification was not possible.

^{1}H NMR (400 MHz, $CDCl_3$) δ 5.53 (s, 1H; C(2)-H), 2.23 – 214 (m, 1H), 2.05 – 1.89 (m, 4H), 1.79-1.70 (m, 1H), 1.68 (s, 3H; C(7)-H_3), 1.67 (s, 3H; C(8)-H_3).

^{13}C NMR (101 MHz, $CDCl_3$), δ 137.4 (C(1)), 128.2 (C(2)), 39.7 (C(4)), 33.8 (C(8)), 29.9 (C(6)), 23.7 (C(7)), 19.8 (C(5)). Quaternary centre C(3) not visible in ^{13}C NMR (101 MHz, $CDCl_3$).

As this compound proved highly unstable, we were unable to obtain full characterisation.

3-bromo-5-methyl-3,6-dihydro-2*H*-pyran ((±)-33)



Synthesised *via* general procedure 9 using 5-methyl-3,6-dihydro-2H-pyran-3-ol ((±)-**30**) and purified by column chromatography (pentane:Et_2O, 7:3) to give the product as single regioisomer (colourless oil, 40 % yield, 0.54 g).

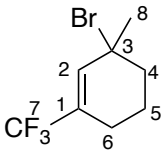
^{1}H NMR (400 MHz, $CDCl_3$) δ 5.81 – 5.75 (m, 1H; C(1)-H), 4.72 – 4.62 (m, 1H; C(5)-H), 4.15 (d, *J* = 16.6 Hz, 1H), 4.09 – 4.03 (m, 1H), 4.00 – 3.96 (m, 2H), 1.67 (s, 3H, C(6)-H_3).

^{13}C NMR (101 MHz, $CDCl_3$) δ 138.2 (C(2)), 121.7 (C(1)), 70.4, 68.6, 44.7 (C(5)), 18.8 (C(6)).

HRMS not found.

IR (ATR) ν_{max} = 2917, 1684, 1458, 740 cm^{-1}.

3-bromo-3-methyl-1-(trifluoromethyl)cyclohex-1-ene ((±)-21)



Synthesised *via* general procedure 9 using 3-methyl-1-(trifluoromethyl)cyclohex-2-enol ((±)-**19**) to give the product as single regioisomer (colourless oil, 76 % yield, 0.98 g).

^{1}H NMR (400 MHz, $CDCl_3$) δ 6.44-6.38 (m, 1H; C(2)-H), 2.43 – 2.29 (m, 2H), 2.28 – 2.13 (m, 1H), 2.10 – 1.97 (m, 1H), 1.91 (s, 3H; C(8)-H_3), 1.90 – 1.85 (m, 1H), 1.77 – 1.65 (m, 1H).

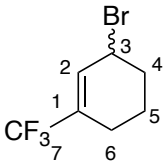
^{13}C NMR (126 MHz, CDCl3) δ 134.3 (q, *J* = 6.0 Hz, C(2)), 127.9 (apparent d, *J* = 31.6 Hz; C(1)), 123.6 (apparent d, *J* = 274.5 Hz, C(7)), 61.1 (C(3)), 40.0, 34.0 (C(8)), 21.8, 19.3.

^{19}F NMR (377 MHz, $CDCl_3$) δ -69.94.

HRMS not found.

IR (ATR) ν_{max} = 2981, 1663, 1263, 1222, 1178, 736 cm^{-1}.

3-bromo-1-(trifluoromethyl)cyclohex-1-ene ((±)-24)



Synthesised *via* general procedure 9 using 1-(trifluoromethyl)cyclohex-2-enol ((±)-**22**) to give the product as single regioisomer (colourless oil, 53 % yield, 0.34 g).

^{1}H NMR (400 MHz, $CDCl_3$) δ 6.51 – 6.43 (m, 1H; C(2)-H), 4.86 – 4.76 (m, 1H; C(3)-H), 2.42 – 2.24 (m, 2H), 2.24 – 2.14 (m, 1H), 2.11 – 2.01 (m, 1H), 2.01 – 1.92 (m, 1H), 1.86 – 1.76 (m, 1H).

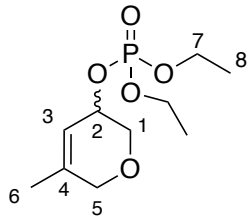
^{13}C NMR (126 MHz, $CDCl_3$) δ 130.8 (q, *J* = 31.1 Hz; C(1)), 130.4 (q, *J* = 5.9 Hz, C(2)), 123.4 (q, *J* = 123.4 Hz, C(7)), 44.3 (C(3)), 31.8, 21.9, 18.0.

^{19}F NMR (377 MHz, $CDCl_3$) δ -70.10.

HRMS not found.

IR (ATR) ν_{max} = 2960, 1674, 1230, 1216, 1177, 731 cm^{-1}.

Diethyl (5-methyl-3,6-dihydro-2H-pyran-3-yl) phosphate ((±)-35)



4-Dimethylaminopyridine (0.028 g, 0.2 mmol, 0.1 eq.) was added to a solution of allyl alcohol (±)-**30** (0.25 g, 2.2 mmol, 1.0 eq.) in pyridine (1.3 mL) at 23 °C, followed by addition of diethyl chlorophosphate (0.38 mL, 2.6 mmol, 1.2 eq.). The mixture was stirred at 23 °C for 1 h. EtOAc was added (7.5 mL) along with H_2O (3.5 mL). The layers were separated, and the aqueous layer was extract with EtOAc (2x 10 mL). The combined organic layers were washed with saturated $CuSO_4$ solution (20 mL), saturated NaCl solution (20 mL), dried over $MgSO_4$, filtered and the solvent removed *in vacuo* to give the crude product as an oil. Purification by column chromatography (Et_2O:NEt_3, 99:1) gave the product as an oil (0.2g, 36 % yield).

^{1}H NMR (400 MHz, $CDCl_3$) δ 5.78 – 5.64 (m, 1H; C(3)-H), 4.78 – 4.65 (m, 1H; C(2)-H), 4.18 – 4.07 (m, 4H; 2x C(7)-H_2), 4.07 – 3.87 (m, 3H), 3.78 – 3.70 (m, 1H), 1.69 (s, 3H, C(6)-H_3), 1.34 (tt, J = 7.1, 0.9 Hz, 6H; 2x C(8)-H_3).

^{13}C NMR (126 MHz, $CDCl_3$) δ 118.1 (d, *J* = 4.8 Hz; C(3)), 111.6 (C(4), 69.0 (d, *J* = 4.9 Hz; C(2)), 68.5 (C(5)), 68.4 (d, *J* = 5.2 Hz; C(1)), 63.9 (d, *J* = 6.1 Hz; 2x C(7)), 18.8 (C(6)), 16.3 (d, *J* = 7.0 Hz; 2x C(8)).

^{31}P NMR (162 MHz, $CDCl_3$) δ -1.23.

HRMS (ESI) m/z calcd for $C_{10}H_{19}O_5PNa^+$ $[M+Na]^+$: 273.0862, found: 273.0862.

IR ($CDCl_3$ film): 2981, 1446, 1261 (broad), 1134, 1027 (s), 983 (s), 846 cm^{-1}.

The enantiomers of this racemate can be separated for analysis of enantiomeric excess by UPC^2 with a non-racemic chiral column (Chiralpak® IF; 1500 psi, 30°C; flow: 1.5 mL/min; from 1 % to 30 % MeOH in 5 min; λ = 210 nm; (*R*)-**35** R_t = 2.50 min; (*S*)-**35** R_t = 2.68 min).

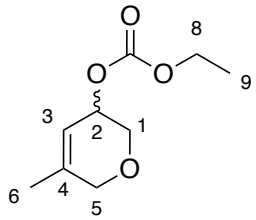
(*R*)-Diethyl (5-methyl-3,6-dihydro-2H-pyran-3-yl) phosphate ((*R*)-35)

(*R*)-**35** was sythesised as above but with (*R*)-**30** in place of (±)-**30**. The enantioenrichment of the allyl alcohol is conserved in the phosphorylated product.

(*S*)-Diethyl (5-methyl-3,6-dihydro-2H-pyran-3-yl) phosphate ((*R*)-35)

(*S*)-**35** was sythesised as above but with (*S*)-**30** in place of (±)-**30**. The enantioenrichment of the allyl alcohol is conserved in the phosphorylated product.

Ethyl (5-methyl-3,6-dihydro-2H-pyran-3-yl) carbonate ((±)-34)



A solution of allyl alcohol (±)-**30** (0.3 g, 2.6 mmol, 1.0 eq.) in CH_2Cl_2 (2.5 mL) and pyridine (0.32 mL, 3.9 mmol, 1.5 eq.) was cooled to 0 °C. Ethyl chloroformate (0.38 mL, 3.9 mmol, 1.5 eq.) was added dropwise. The mixture was allowed to warm to room temperature and stirred at 23 °C for 16 h. H_2O was added (5 mL) along with CH_2Cl_2 (3 mL). The layers were separated, and the aqueous layer extracted with CH_2Cl_2 (5 mL). The combined organic layers were washed with a saturated $CuSO_4$ solution (2x 5 mL), a saturated NaCl solution (5 mL), dried over $MgSO_4$, filtered and the solvent removed *in vacuo* to give the crude product as a yellow oil (0.36 g, 75 % yield).

^{1}H NMR (400 MHz, $CDCl_3$) δ 5.75 – 5.56 (m, 1H; C(3)-H), 5.00 – 4.79 (m, 1H; C(2)-H), 4.15 (q, *J* = 7.1 Hz, 2H; C(8)-H_2), 4.07 – 3.85 (m, 3H; C(5)-H_2, C(1)-H), 3.68 (m, 1H; C(1)-H), 1.69 – 1.60 (m, 3H; C(6)-H_3), 1.26 (t, *J* = 7.1 Hz, 3H; C(9)-H_3).

^{13}C NMR (126 MHz, $CDCl_3$) δ 141.1 (C=O), 116.7 (C(3)), 111.9 (C(4)), 68.8, 68.5 (C(2)), 67.3, 64.1 (C(8)), 18.9 (C(6)), 14.4 (C(9)).

HRMS (ESI) m/z calcd for $C_9H_{14}O_4Na^+$ $[M+Na]^+$: 209.0784, found: 209.0785.

IR ($CDCl_3$ film): 3417, 2982, 2859, 1736 (s), 1447, 1372, 1250 (s), 1176, 1134, 1031, 991 cm^{-1}.

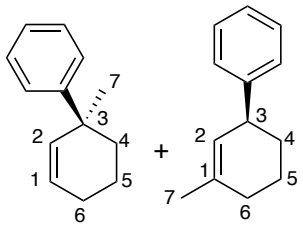
3.3 Rhodium-Catalysed Allylic Arylation with Arylboronic Acids

General Procedure 10

In a flame-dried 5 mL flask under an argon atmosphere, $[Rh(cod)(OH)]_2$, chiral bisphosphine ligand and base were dissolved in anhydrous THF (1.0 mL). This catalyst mixture was stirred at 60 °C for 30 min resulting in an orange-red solution.

In a second flame-dried 5 mL flask, arylboronic acid (0.4 mmol, 2.00 eq.) and the allylic electrophile (0.2 mmol, 1.00 eq.) were dissolved in anhydrous THF (0.7 mL). This solution was then added to the catalyst solution *via* syringe, and the flask rinsed with THF (0.3 mL). The resulting mixture was then stirred for 16 hours, at the specified temperature. The mixture was diluted with hexane (1 mL) and concentrated *in vacuo*. The crude mixture was directly loaded on a silica gel flash column and eluted with the indicated solvent mixture to afford the desired product.

3-phenyl-3-methylcyclohex-1-ene (16a) and 3-phenyl-1-methylcyclohex-1-ene (16b)



Synthesised *via* general procedure 10 using $[Rh(cod)(OH)]_2$ (0.003 g, 0.005 mmol, 2.5 mol %), (*S*)-BINAP (0.008 g, 0.012 mmol, 6.0 mol %) and Cs_2CO_3 base (0.065 g, 0.20 mmol, 1.00 eq) in the catalyst solution. Phenylboronic acid (0.049 g, 0.40 mmol, 2.00 eq) and allyl chloride (±)-**15a** and (±)-**15b** (29 μL, 0.2 mmol, 1.0 eq). were added and the resulting mixture was stirred at 60 °C. Purification by dry loaded flash column chromatography (100 % pentane) gave a mixture of **16a** and **16b** as an oil (25 % yield, 2.5:1 r.r., 94 and 48 % ee).

Reactions screening ligands, bases and other variables were all carried out using this same procedure and varying the appropriate parameter.

^{1}H NMR (400 MHz, $CDCl_3$, 3:1 mixture **16a**:**16b**)

Major Regioisomer (**16a**): δ 5.89 – 5.81 (m, 1H; C(2)-H), 5.74 – 5.68 (m, 1H; C(1)-H), 1.39 (s, 3H; C(7)-H_3).

Minor Regioisomer (**16b**): 5.45 - 5.42 (m, 1H; C(2)-H), 3.41 – 3.32 (m, 1H; C(3)-H), 1.54 (s, 3H; C(7)-H_3).

Not readily assignable overlapping peaks: 7.41 – 7.34 (aromatic, m, 2H), 7.33 – 7.27 (aromatic, m, 3H), 7.24 – 7.14 (aromatic, m, 2H), 1.93 – 1.85 (aliphatic, m, 2H), 1.76 – 1.73 (aliphatic, m, 2H), 1.69 – 1.55 (aliphatic, m, 4H).

Physical data identical to that which was previously reported.[247]

Enantiomeric excess of both regioisomers was identified by GC with a non-racemic chiral column (β - DEX, flow 10.3 mL/min, 109 kPa, 80 °C for 60 min, increase 1 °C/min for 15 min, increase 10 °C/min up to 160 °C, 160 °C for 10 min). The absolute stereochemistry is not known.

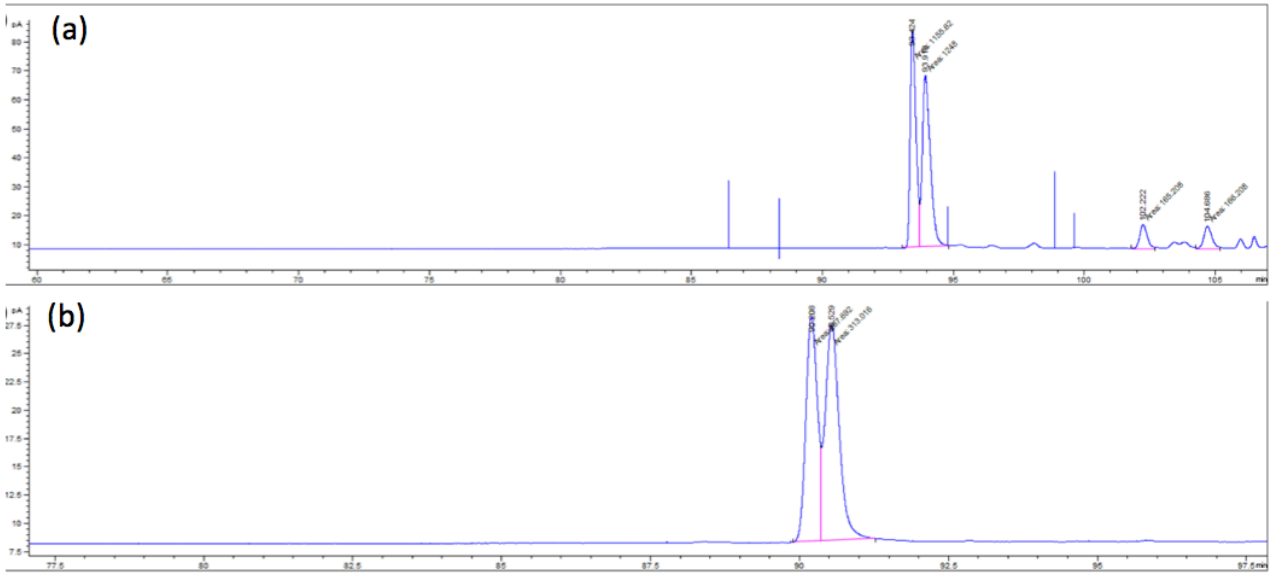


Figure S7. GC traces. (a) Racemic sample of **16a** and **16b** synthesised using (±)-BINAP ligand. (b) Racemic sample of **2a** only (under same conditions, retention times shifted slightly).

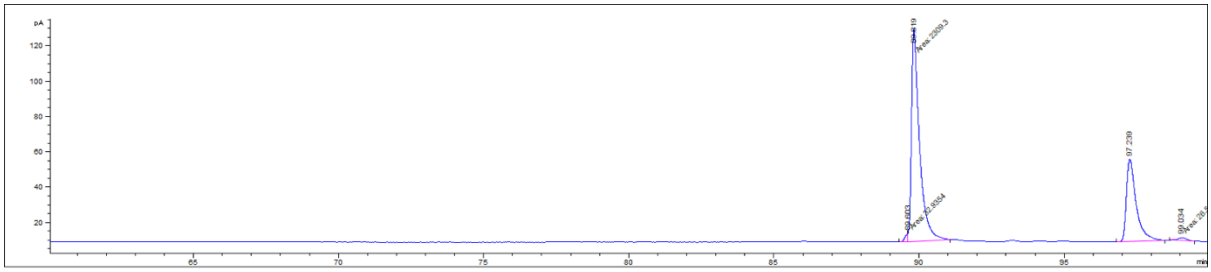
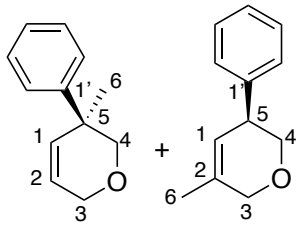


Figure S8. GC trace (conditions as above) from enantioenriched sample of **16a** and **16b**.

3-methyl-3-phenyl-3,6-dihydro-2H-pyran (32a) and 5-methyl-3-phenyl-3,6-dihydro-2H-pyran (32b)



Synthesised *via* general procedure 10 using $[Rh(cod)(OH)]_2$ (0.005 g, 0.01 mmol, 5.0 mol %), (*S*)-Xylyl-BINAP (0.018 g, 0.024 mmol, 12.0 mol %) and aq. CsOH (35 μL, 50 % w/w, 0.2 mmol, 1.00 eq.) in the catalyst solution. Phenylboronic acid (0.049 g, 0.40 mmol, 2.00 eq) and allyl chloride (±)-**31a** and (±)-**31b** (25 μL, 0.2 mmol, 1.00 eq.) were added and the resulting mixture was stirred at 80 °C. Purification by dry loaded flash column chromatography (pentane:Et_2O, 95:5) gave a mixture of **32a** and **32b** as an oil (90 % yield, 1.8:1 r.r., 98 and 99 % ee).

Reactions screening ligands, bases and other variables were all carried out using this procedure and varying the appropriate parameter.

Rh-catalysed reactions with racemic phosphate ((±)-**35**), bromide ((±)-**33**), carbonate ((±)-**34**), and enantiopure phosphates ((*S*)-**35** and (*R*)-**35**) to form **32a** and **32b** were all carried out using this same procedure and replacing allyl chloride (±)-**31a** and (±)-**31b** with the desired electrophile.

^{1}H NMR (400 MHz, $CDCl_3$, 2:1 mixture **32a**: **32b**)

Major Regioisomer (**32a**): δ 5.96 – 5.81 (m, 2H; C(1)-H, C(2)-H), 4.20 (apparent t, *J* = 2.0 Hz, 2H; C(3)-H_2), 3.76 (d, *J* = 11.0 Hz, 1H; C(4)-H), 3.64 (dd, *J* = 11.0, 0.6 Hz, 1H; C(4)-H), 1.44 (s, 3H; C(6)-H_3).

Minor Regioisomer (**32b**): δ 5.64-5.60 (m, 1H; C(1)-H), 4.16 – 3.95 (m, 3H; C(3)-H_2, C(4)-H), 3.54-3.45 (m, 2H; C(5)-H, C(4)-H'), 1.71 (s, 3H; C(6)-H_3).

Aromatic peaks (overlapping): δ 7.44 – 7.29 (m, 5H), 7.30 – 7.18 (m, 3H).

^{13}C NMR (101 MHz, $CDCl_3$)

Major Regioisomer (**32a**): 133.4 (C(1)), 124.9 (C(2)), 76.5 (C(4)), 65.5 (C(3)), 39.4 (C(5)), 24.3 (C(6)).

Minor Regioisomer (**32b**): 133.8 (C(2)), 122.4 (C(1)), 71.0 (C(4)), 68.8 (C(3)), 41.4 (C(5)), 18.9 (C(6)).

Aromatic peaks (not readily assignable): 145.8(C(1')), 142.4(C(1')), 128.5, 128.3, 128.1, 126.6, 126.6, 126.3.

HRMS (APCI) m/z calcd for $C_{12}H_{15}O$ $[M+H]^+$: 175.1117, found: 175.1118.

IR (ATR) ν_{max} = 2980, 2928, 1458, 1432, 1381 cm^{-1}.

Enantiomeric excess of both regioisomers was determined by UPC^2 with a non-racemic chiral column (Chiralpak® IF; 1500 psi, 30°C; flow: 1.5 mL/min; from 1 % to 30 % MeOH in 5 min; λ = 214.5 nm; enantiomer **32a** R_t = 1.65 min; enantiomer **32a** R_t = 1.77 min; enantiomer **32b** R_t = 1.88 min; enantiomer **32b** R_t = 2.09 min, see Fig. S9). The absolute stereochemistry is not known.

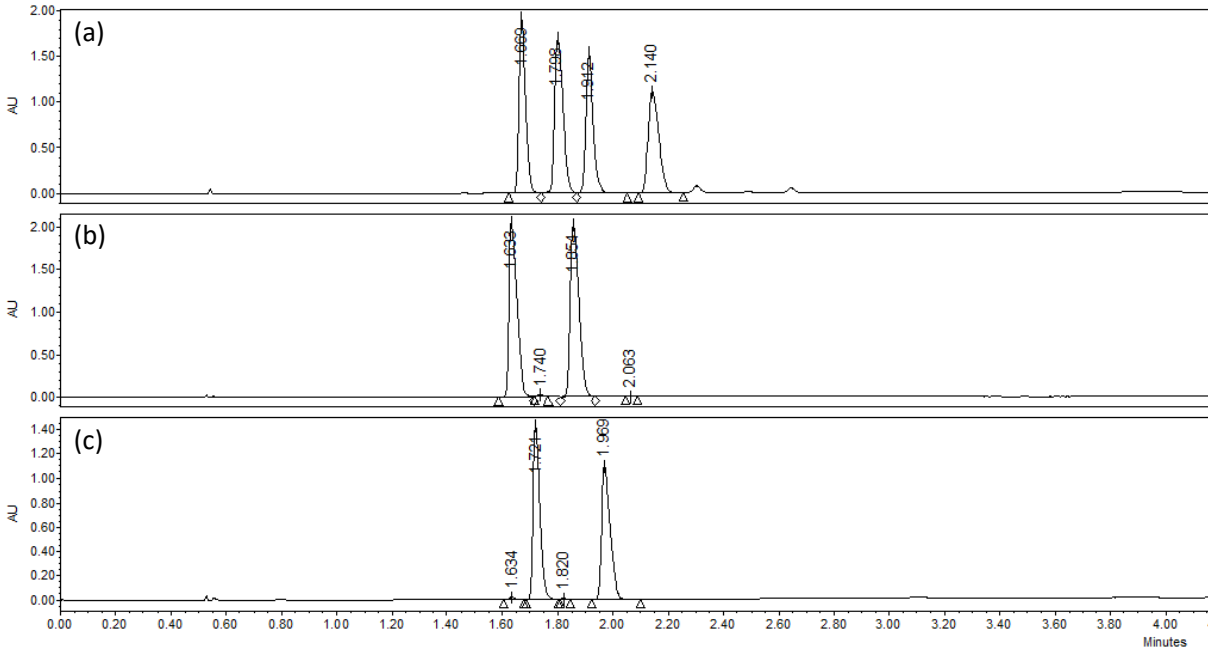
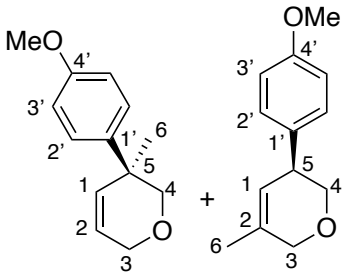


Figure S9. SFC Traces. (a) Racemic sample of (±)-**32a** and (±)-**32b** synthesised using (±)-BINAP ligand. (b) Enantioenriched sample of **32a** and **32b** synthesised using (*S*)-Xylyl-BINAP. (c) Enantioenriched sample of **32a** and **32b** synthesised using (*R*)-Xylyl-BINAP.

3-(4-methoxyphenyl)-3-methyl-3,6-dihydro-2H-pyran and 3-(4-methoxyphenyl)-5-methyl-3,6-dihydro-2H-pyran



Synthesised *via* general procedure 10 using $[Rh(cod)(OH)]_2$ (0.005 g, 0.01 mmol, 5.0 mol %), (*R*)-Xylyl-BINAP (0.018 g, 0.024 mmol, 12.0 mol %) and aq. CsOH (35 µL, 50 % w/w, 0.2 mmol, 1.00 eq.) in the catalyst solution. (4-Methoxyphenyl)boronic acid (0.061 g, 0.40 mmol, 2.00 eq) and allyl chloride (±)-**31a** and (±)-**31b** (25 µL, 0.2 mmol, 1.00 eq.) were added and the resulting mixture was stirred at 80 °C. Purification by dry loaded flash column chromatography (pentane:Et_2O, 9:1) gave a mixture of 3-(4-methoxyphenyl)-3-methyl-3,6-dihydro-2H-pyran

and 3-(4-methoxyphenyl)-5-methyl-3,6-dihydro-2H-pyran as an oil (74 % yield, 2.1:1 r.r., >99 % ee for both regioisomers, see Fig. S10).

^{1}H NMR (400 MHz, $CDCl_3$)

Major Regioisomer (quaternary stereocentre containing product): δ 7.36 – 7.28 (m, 2H; 2x C(2')-H), 5.91 – 5.79 (m, 2H; C(1)-H, C(2)-H), 4.19 (t, *J* = 1.8 Hz, 2H; C(3)-H_2), 3.80 (s, 3H; OCH_3), 3.71 (d, *J* = 10.9 Hz, 1H; C(4)-H), 3.61 (d, *J* = 10.9 Hz, 1H; C(4)-H), 1.42 (s, 3H; C(6)-H_3).

Minor Regioisomer (tertiary stereocentre containing product): δ 7.20 – 7.11 (m, 2H; 2x C(2')-H), 5.63 – 5.56 (m, 1H; C(1)-H), 4.16 – 3.91 (m, 3H; C(3)-H_2, 1x C(4)-H), 3.79 (s, 3H; OCH_3), 3.51 – 3.40 (m, 2H; 1x C(5)-H, 1x C(4)-H), 1.70 (s, 3H; C(6)-H_3).

Overlapping: δ 6.92 – 6.81 (m, major regioisomer (2H), minor regioisomer (2H)).

^{13}C NMR (101 MHz, $CDCl_3$)

Major Regioisomer: δ 133.8 (C(1)), 127.8 (C(2x 2'), 124.9 (C(2)), 76.8 (C(4)), 65.6 (C(3)), 38.9 (C(5)), 24.5 (C(6)).

Minor Regioisomer: δ 129.1 (C(2x 2'), 122.9 (C(1)), 114.0 (C(2)), 71.3 (C(4)), 68.9 (C(3)), 40.7 (C(5)), 19.0 (C(6)).

Overlapping or not readily assignable to regioisomers: δ 158.5 (C(4')), 158.2 (C(4')), 138.0 (C(1')), 134.7 (C(1')), 113.8 (4x C(3')) 55.4 (apparent d; 2x O(C)-H_3).

HRMS (APCI) m/z calcd for $C_{13}H_{17}O_2^+$ $[M+H]^+$: 205.1223, found: 205.1222.

IR (ATR) ν_{max} = 2958, 2931, 2835, 1512 (s), 1251, 1182, 1094, 1036, 986, 828 cm^{-1}.

Enantiomeric excess of both regioisomers was determined by UPC^2 with a non-racemic chiral column (Chiralpak® IF; 1500 psi, 30°C; flow: 1.5 mL/min; from 1 % to 30 % MeOH in 5 min; λ = 214.5 nm; minor enantiomer a R_t = 2.35 min; minor enantiomer b R_t = 2.46 min; major

enantiomer a R_t = 2.66 min; major enantiomer b R_t = 3.22 min). The absolute stereochemistry is not known.

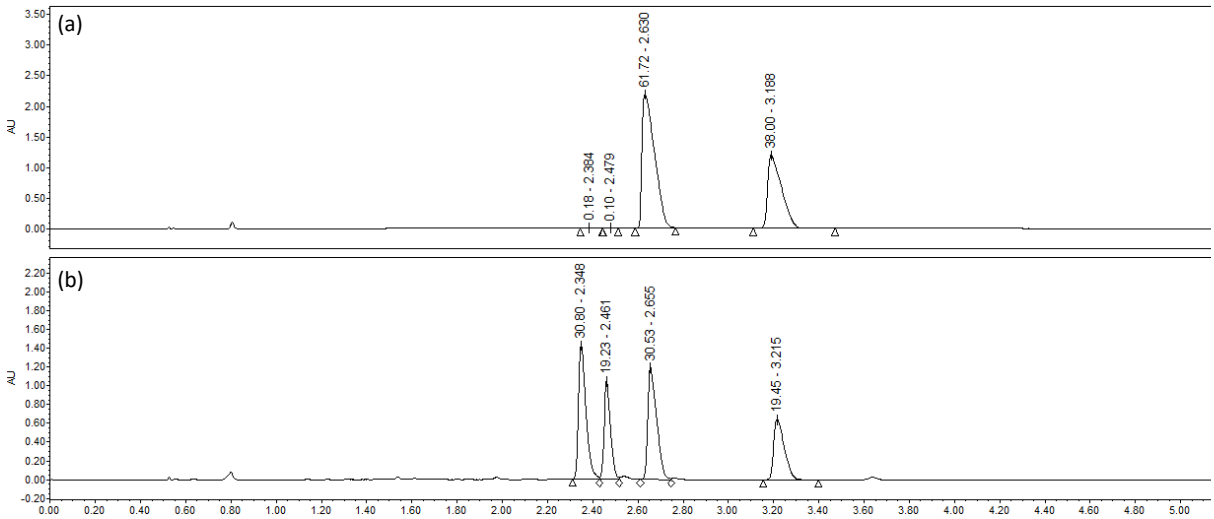
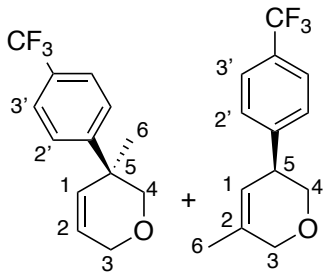


Figure S10. SFC Traces. (a) Enantioenriched sample of 3-(4-methoxyphenyl)-3-methyl-3,6-dihydro-2H-pyran and 3-(4-methoxyphenyl)-5-methyl-3,6-dihydro-2H-pyran synthesised with (*R*)-Xylyl-BINAP ligand as described above. (b) Racemic sample synthesised as described above but using (±)-BINAP ligand in place of (*R*)-Xylyl-BINAP.

3-methyl-3-(4-(trifluoromethyl)phenyl)-3,6-dihydro-2H-pyran and 5-methyl-3-(4-(trifluoromethyl)phenyl)-3,6-dihydro-2H-pyran



Synthesised *via* general procedure 10 using $[Rh(cod)(OH)]_2$ (0.005 g, 0.01 mmol, 5.0 mol %), (*S*)-Xylyl-BINAP (0.018 g, 0.024 mmol, 12.0 mol %) and aq. CsOH (35 μL, 50 % w/w, 0.2 mmol, 1.00 eq.) in the catalyst solution. (4-(Trifluoromethyl)phenyl)boronic acid (0.076 g, 0.40 mmol, 2.00 eq) and allyl chloride (±)-**31a** and (±)-**31b** (25 μL, 0.2 mmol, 1.00 eq.) were added and the resulting mixture was stirred at 80 °C. Purification by dry loaded flash column chromatography (pentane:Et_2O, 95:5) gave a mixture of 3-methyl-3-(4-(trifluoromethyl)phenyl)-3,6-dihydro-

2H-pyran and 5-methyl-3-(4-(trifluoromethyl)phenyl)-3,6-dihydro-2H-pyran as an oil (92 % yield, 1.4:1 r. r., >99 % ee for both regioisomers).

^{1}H NMR (400 MHz, $CDCl_3$)

Major Regioisomer (quaternary stereocentre containing product): δ 5.94 – 5.84 (m, 2H; (C1)-H, C(2)-H), 4.20 (t, *J* = 2.1 Hz, 2H; C(3)-H_2), 3.79 (dd, *J* = 11.1, 0.8 Hz, 1H; C(4)-H), 3.63 (d, *J* = 11.0 Hz, 1H; C(4)-H), 1.43 (s, 3H; C(6)-H_3).

Minor Regioisomer (tertiary stereocentre containing product): δ 5.61 – 5.57 (m, 1H; C(1)-H), 4.14 – 4.04 (m, 2H), 4.02 – 3.92 (m, 1H), 3.58 – 3.45 (m, 2H), 1.72 (s, 3H; C(6)-H_3).

Overlapping and not readily assignable to regioisomers peaks: δ 7.63 – 7.46 (m, 6H; 4x C(3')-H, 2x C(2')-H), 7.40 – 7.32 (m, 2H; 2x C(2')-H).

^{13}C NMR (101 MHz, $CDCl_3$)

Major Regioisomer: δ 132.7 (C(1)), 125.9 (C(2)), 76.3 (C(4)), 65.6 (C(3)), 39.7 (C(5)), 24.3 (C(6)).

Minor Regioisomer: δ 121.5 (C(1)), 100.1 (C(2)), 70.6 (C(4)), 68.9 (C(3)), 41.4 (C(5)), 19.0 (C(6)).

Not readily assignable to regioisomers: δ 150.1 (C(1')), 134.5 (apparent d, *J* = 32; (C(4')), 128.6 (C(2')), 127.2 (C(2')), 125.5 (q, *J* = 4.2 Hz; C(3')), 125.3 (q, *J* = 4.2 Hz; C(3')), 121.7 (apparent d, *J* = 280.0 Hz; CF_3).

^{19}F NMR (376 MHz, $CDCl_3$) δ -62.41, -62.46.

HRMS (APCI) m/z calcd for $C_{13}H_{14}F_3O^+$ $[M+H]^+$: 243.0991, found: 243.0992.

IR (ATR) ν_{max} = 3658, 2981 (s), 1382, 1253, 1162, 1081, 965, 954, 828 cm^{-1}.

Enantiomeric excess of both regioisomers was determined by UPC^2 with a non-racemic chiral column (Chiralpak® IG; 1500 psi, 30°C; flow: 1.5 mL/min; from 1 % to 30 % MeOH in 5 min; λ = 214.5 nm; minor enantiomer a R_t = 1.44 min; minor enantiomer b R_t = 1.52 min; major

enantiomer b R_t = 1.80 min; major enantiomer a R_t = 2.06 min). The absolute stereochemistry is not known.

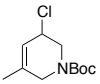
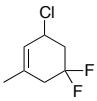
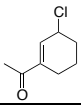
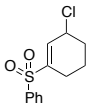
3.4 Computational Details

Density functional theory (DFT) calculations were performed with Gaussian 09 rev. D.01. Geometry optimisations used the M06-2X functional with the Gaussian basis set 6-31++G(d,p). Minima on the potential energy surface were confirmed as such by harmonic frequency analysis at the same level of theory. Gibbs energies were evaluated at 298.15 K, using a quasi-RRHO treatment of vibrational entropies introduced by Grimme.[248] Vibrational entropies of frequencies below 100 cm^{-1} were obtained according to a free rotor description, using a smooth damping function to interpolate between the two limiting descriptions. This was implemented in Python (GoodVibes script available on GitHub).

Table S25. Absolute energy contributions to the Gibbs energy (Hartree) for substrates of known empirical stability.

Compound no.		M06-2X/6-31++G(d,p)				
		E/au	**ZPE/au**	**H/au**	**T.qh-S/au**	**qh-G(T)/au**
	Chloride	-460.235139	-	-	-	-
	Allyl chloride	-694.114933	0.138453	-693.969038	0.038269	-694.007307
	Carbocation	-233.644537	0.134519	-233.503512	0.035139	-233.538651
	Allyl chloride	-772.71654	0.193923	-772.512172	0.044464	-772.556636
	Carbocation	-312.275767	0.190608	-312.075567	0.042337	-312.117903
	Allyl chloride **a**	-733.416561	0.166206	-733.241290	0.041866	-733.283156
	Allyl chloride **b**	-733.414977	0.166085	-733.240058	0.040970	-733.281028
	Carbocation	-272.961358	0.162430	-272.790869	0.038810	-272.829678
	Allyl chloride	-808.602484	0.170143	-808.422132	0.044119	-808.466252
	Carbocation	-348.146956	0.166106	-347.971477	0.041955	-348.013433
	Allyl chloride	-654.810335	0.108593	-654.695925	0.034770	-654.730694
	Carbocation	-194.344554	0.104638	-194.234403	0.032671	-194.267074
	Allyl chloride	-1055.855803	0.254841	-1055.585284	0.056438	-1055.641723
	Carbocation	-595.377354	0.250228	-595.112428	0.053665	-595.166093
	Allyl chloride	-729.998963	0.114576	-729.877224	0.037800	-729.915024
	Carbocation	-269.512371	0.110345	-269.395870	0.034482	-269.430352

Table S26. Absolute energy contributions to the Gibbs energy (Hartree) for substrates of unknown empirical stability.

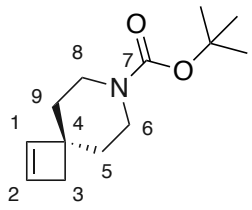
Compound no.		M06-2X/6-31++G(d,p)				
		E/au	**ZPE/au**	**H/au**	**T.qh-S/au**	**qh-G(T)/au**
	Allyl chloride	-1070.373396	0.171794	-1070.18931	0.049161	-1070.238471
	Carbocation	-609.900062	0.167785	-609.720899	0.046973	-609.767873
	Allyl chloride	-1031.073107	0.144100	-1030.918157	0.046527	-1030.964684
	Carbocation	-570.581177	0.139788	-570.431473	0.043896	-570.475369
	Allyl chloride **a**	-769.300979	0.142381	-769.149762	0.041540	-769.191302
	Allyl chloride **b**	-769.300553	0.142206	-769.149764	0.040584	-769.190347
	Carbocation	-308.831107	0.138161	-308.685218	0.038173	-308.723391
	Allyl chloride	-1156.052234	0.301445	-1155.734234	0.058285	-1155.792519
	Carbocation	-695.635612	0.299647	-695.320558	0.055949	-695.376507
	Allyl chloride	-1191.9386	0.277735	-1191.644513	0.058040	-1191.702553
	Carbocation	-731.510223	0.275539	-731.219436	0.055929	-731.275365
	Allyl chloride	-851.310597	0.250199	-851.047294	0.049691	-851.096985
	Carbocation	-390.874615	0.246250	-390.615989	0.047994	-390.663983
	Allyl chloride	-925.087906	0.220265	-924.855634	0.048875	-924.904509
	Carbocation	-464.646268	0.217507	-464.417913	0.045757	-464.46367
	Allyl chloride	-960.971971	0.196512	-960.763711	0.048497	-960.812208
	Carbocation	-500.518806	0.193297	-500.314880	0.045444	-500.360323
	Allyl chloride	-1095.157727	0.282535	-1094.85779	0.060074	-1094.917865
	Carbocation	-634.694042	0.278069	-634.399586	0.057258	-634.456844
	Allyl chloride	-847.892292	0.199552	-847.681302	0.047207	-847.728508
	Carbocation	-387.428246	0.195562	-387.222289	0.044051	-387.266341
	Allyl chloride	-1031.073107	0.144100	-1030.918157	0.046527	-1030.964684
	Carbocation	-570.581177	0.139788	-570.431473	0.043896	-570.475369
	Allyl chloride	-931.857159	0.150429	-931.696243	0.045318	-931.741561
	Carbocation	-471.384073	0.146302	-471.228334	0.042372	-471.270706
	Allyl chloride	-846.709285	0.176285	-846.522011	0.046453	-846.568464
	Carbocation	-386.228469	0.171661	-386.046676	0.043948	-386.090624
	Allyl chloride	-1473.574379	0.230817	-1473.328223	0.056402	-1473.384625
	Carbocation	-1013.09043	0.226841	-1012.849236	0.053805	-1012.903041
	Allyl chloride	-1106.256391	0.147679	-1106.096638	0.048875	-1106.145513
	Carbocation	-645.767376	0.143195	-645.612954	0.046821	-645.659775
	Allyl chloride	-878.535075	0.135414	-878.388676	0.046475	-878.435151
	Carbocation	-418.035004	0.131685	-417.893314	0.044076	-417.93739
	Allyl chloride	-1368.023854	0.148909	-1367.860697	0.053603	-1367.9143
	Carbocation	-907.516497	0.145116	-907.358052	0.051751	-907.409804

	Allyl chloride	-1066.954425	0.119987	-1066.823785	0.046305	-1066.87009
	Carbocation	-606.446528	0.115566	-606.321377	0.043311	-606.364688
	Allyl chloride	-1403.903538	0.124733	-1403.764664	0.053650	-1403.818314
	Carbocation	-943.379502	0.120749	-943.245653	0.051437	-943.297089

4. Supplementary Information for Chapter 4

4.1 Cyclobutene Starting Materials Synthesis

Synthesis of **41**



$NaBH_4$ (0.57 g, 15.0 mmol) was added in small portions to a solution of *tert*-butyl 2-oxo-7-azaspiro[3.5]nonane-7-carboxylate (3.00 g, 12.5 mmol) in MeOH (30 mL) at 0 °C open to air. The reaction mixture was allowed to reach room temperature (23 °C) and stirred at that temperature for 2.5 h. The solvent was removed under reduced pressure to an approximate volume of ~5 mL. EtOAc (30 mL) and aq. NH_4Cl solution (10 mL) were added. The layers were separated, and the aqueous layer extracted with EtOAc (2x 20 mL). The combined organic layers were washed with brine (50 mL) and dried over $MgSO_4$. The solvent was removed under reduced pressure and a crude white solid was obtained which was used in the next step without further purification.

This crude solid product was dissolved in pyridine (18 mL) and *p*-toluenesulfonyl chloride (2.62 g, 13.8 mmol) was added at 0 °C under an argon atmosphere. The reaction mixture was allowed to reach room temperature (23 °C) and stirred at this temperature. After 20 h, EtOAc (20 mL) followed by aq. 1 M HCl (20 mL) were added to reaction mixture at 0 °C. The layers were separated, and the organic layer was again washed with aq. 1 M HCl (20 mL), followed by brine (20 mL) and then dried over $MgSO_4$. The solvents were removed under reduced pressure. The crude oil was then dissolved in toluene (5 mL) and the solvents were again removed under reduced pressure. A crude solid was obtained which was used in the next step

without further purification.

DMSO (90 mL) was added to a mixture of potassium *tert*-butoxide (1.95 g, 17.4 mmol) and the crude product from the previous step at 0 °C under an argon atmosphere. The reaction was allowed to reach room temperature (23 °C) and stirring was continued for 16 h. EtOAc (180 mL) was added followed by brine (120 mL) at 0 °C. The layers were separated, and the aqueous layer extracted with EtOAc (2x 120 mL). The combined organic layers were washed with brine (200 mL) and dried over $MgSO_4$. Purification by automated medium-pressure liquid chromatography (hexane:EtOAc = 100/0 to 80/20) afforded **41** (1.90 g, 68 % over 3 steps) as a colourless oil.

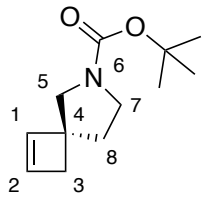
^{1}H NMR (400 MHz, $CDCl_3$) δ 6.22 (d, *J* = 2.9 Hz, 1H; C(1)-H), 6.12 (dd, *J* = 2.6, 1.3 Hz, 1H; C(2)-H), 3.62 – 3.48 (m, 2H; 1x C(6)-H, 1x C(8)–H), 3.30 – 3.16 (m, 2H; 1x C(6)-H, 1x C(8)-H), 2.26 (d, *J* = 0.9 Hz, 2H; C(3)-H_2), 1.64 – 1.52 (m, 4H; C(9)-H_2 , C(5)-H_2), 1.43 (s, 9H; $C(CH_3)_3$).

^{13}C NMR (101 MHz, $CDCl_3$) δ 155.1 (C=O), 143.4 (C(1)), 134.3 (C(2)), 79.3 ($C(CH_3)_3$), 47.6 (C(4)), 42.4 (C(6), C(8)), 41.6 (C(3)), 35.4 (C(5), C(9)), 28.5 ($C(CH_3)_3$).

IR ($CHCl_3$ film): 3046 (w), 2976 (w), 2915 (w), 2842 (w), 1694 (s), 1457, 1417 (s), 1365, 1275, 1244, 1173, 1131 (s), 1012 (w), 973 (w), 864 (w), 711 (w) cm^{-1}.

HRMS (ESI): m/z calcd for $C_{13}H_{21}NO_2Na^+$ $[M + Na]^+$ 246.1465 found 246.1465.

Synthesis of **56**



$NaBH_4$ (0.15 g, 4.00 mmol) was added in small portions to a solution of *tert*-butyl 2-oxo-6 azaspiro[3.4]octane-6-carboxylate (0.75 g, 3.33 mmol) in MeOH (8 mL) at 0 °C open to air. The reaction mixture was allowed to reach room temperature (23 °C) and stirred at that temperature for 2.5 h. The solvent was removed under reduced pressure to an approximate volume of ~1 mL. EtOAc (8 mL) and aq. NH_4Cl solution (2.5 mL) were added. The layers were separated, and the aqueous layer extracted with EtOAc (2x 5 mL). The combined organic layers were washed with brine (5mL) and dried over $MgSO_4$. The solvent was removed under reduced pressure and a crude white solid was obtained which was used in the next step without further purification.

This crude solid product was dissolved in pyridine (4.8 mL) and *p*-toluenesulfonyl chloride (0.69 g, 3.6 mmol) was added at 0 °C under an argon atmosphere. The reaction mixture was allowed to reach room temperature (23 °C) and stirred at this temperature. After 20 h, EtOAc (5 mL) followed by aq. 1 M HCl (5 mL) were added to reaction mixture at 0 °C. The layers were separated, and the organic layer was again washed with aq. 1 M HCl (5 mL), followed by brine (5 mL) and then dried over $MgSO_4$. The solvents were removed under reduced pressure. The crude oil was then dissolved in toluene (1 mL) and the solvents were again removed under reduced pressure. A crude white solid was obtained which was used in the next step without further purification.

DMSO (25 mL) was added to a mixture of potassium *tert*-butoxide (0.56 g, 4.95 mmol) and the

crude product from the previous step at 0 °C under an argon atmosphere. The reaction was allowed to reach room temperature (23 °C) and stirring was continued for 16 h. EtOAc (50 mL) was added followed by brine (30 mL) at 0 °C. The layers were separated, and the aqueous layer extracted with EtOAc (2x 30 mL). The combined organic layers were washed with brine (50 mL) and dried over $MgSO_4$. Purification by automated medium-pressure liquid chromatography (hexane:EtOAc = 100/0 to 80/20) afforded **56** (0.27 g, 39 % over 3 steps) as a colourless oil.

^{1}H NMR (400 MHz, $CDCl_3$) δ 6.13 (dt, *J* = 2.8, 1.0 Hz, 1H; C(2)-H), 6.04 (d, *J* = 2.8 Hz, 1H; C(1)-H), 3.52 – 3.29 (m, 4H; C(5)–H_2 , C(7)-H_2), 2.50 (dt, *J* = 13.1, 0.9 Hz, 1H; C(3)-H), 2.41 (dt, *J* = 13.2, 0.9 Hz, 1H; C(3)-H), 2.03 – 1.83 (m, 2H; C(8)-H_2), 1.46 (s, 9H; $C(CH_3)_3$).

^{13}C NMR (101 MHz, $CDCl_3$) δ 154.8 (C=O), 139.4 (C(1)), 135.7 (C(2)), 79.2 ($C(CH_3)_3$), 53.7 (C(5)), 53.3 (C(4)), 45.1 (C(7)), 43.4 (C(3)), 34.9 (C(8)), 28.7 ($C(CH_3)_3$).

IR ($CHCl_3$ film): 3050 (w), 2973 (w), 2921 (w), 2866 (w), 1696 (s), 1476 (w), 1400 (s), 1365, 1255 (w), 1164, 1101, 974 (w), 934 (w), 879 (w), 772 (w), 715 (w) cm^{-1}.

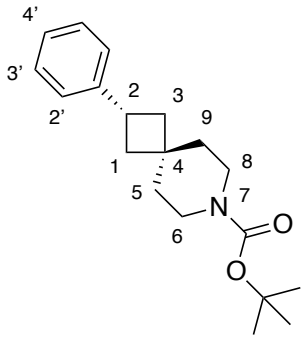
HRMS: m/z calcd for $C_{12}H_{19}NO_2Na^+$ $[M + Na]^+$ 232.1309 found 232.1308.

General Procedure 11

A solution of the rhodium hydroxy phosphine complex was prepared by stirring a solution of $[Rh(cod)OH]_2$ (5.1 mg, 0.011 mmol) and dppf (19.8 mg, 0.027 mmol) in dry dioxane (2.0 mL) under an argon atmosphere at 60 °C for 30 min.

A portion of the resulting orange-red solution (1.8 mL; 0.05 equiv. [Rh]) was added to a 10 mL round-bottom flask containing a mixture of boronic acid (1.2 mmol, 3.0 equiv.) and cyclobutene (0.40 mmol, 1.0 equiv.) in toluene (1.8 mL) and H_2O (0.4 mL) *via* syringe. The resulting mixture was then stirred at 60 °C for 16 hours. The mixture was diluted with hexane (1 mL) and concentrated *in vacuo*. The crude mixture was directly loaded on a silica gel flash column and eluted with the indicated solvent mixture to afford the desired product.

Synthesis of **42**



The corresponding compound was prepared following general procedure 11 using cyclobutene **41** and phenylboronic acid. Purification by automated medium-pressure flash chromatography (hexane/EtOAc = 100/0 to 80/20) afforded the product **42** as a white solid (102 mg, 84 %).

^{1}H NMR (400 MHz, $CDCl_3$) δ 7.36 – 7.26 (m, 2H; 2x C(3')-H), 7.24 – 7.14 (m, 3H; 2x C(2')-H), C(4')–H), 3.52 (p, *J* = 9.1 Hz, 1H; C(2)-H), 3.45 – 3.38 (m, 2H; 2x C(6)-H/C(8)-H), 3.34 – 3.25 (m,

2H; 2x C(6)-H/C(8)-H), 2.35 – 2.24 (m, 2H; 1x C(1)-H, 1x C(3)-H), 1.95 – 1.85 (m, 2H; 1x C(1)-H, 1x C(3)-H), 1.74 – 1.68 (m, 2H; 2x C(5)-H/C(9)-H), 1.54 – 1.48 (m, 2H; 2x C(5)-H/C(9)-H), 1.47 (s, 9H; $C(CH_3)_3$).

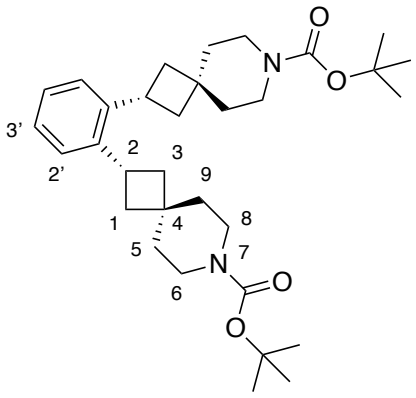
^{13}C NMR (101 MHz, $CDCl_3$) δ 155.1 (C=O), 146.2 (C(1')), 128.4 (2x C(3')), 126.5 (2x C(2')), 125.9 (C(4')), 79.4 ($C(CH_3)_3$), 41.1 (C(6)/C(8)), 40.8 (C(6)/C(8)), 39.3 (C(5)/C(9)), 39.2 (C(1), C(3)), 36.0 (C(5)/C(9)), 34.0 (C(4)), 33.6 (C(2)), 28.6 ($C(CH_3)_3$).

IR ($CHCl_3$ film): 2970 (w), 2921 (w), 2860 (w), 1677 (s), 1477, 1425 (s), 1366, 1271, 1242 (s), 1177, 1149 (s), 1110, 1076, 975, 868 (w), 747 (w), 702 (w) cm^{-1}.

HRMS (ESI): m/z calcd for $C_{14}H_{20}N^+$ $[M + H - CO_2 - CH_2{=}C(CH_3)_2]^+$ 202.1590 found 202.1592.

m.p.: 91 – 92 °C.

Synthesis of **44**



The following compound was isolated as a side-product in the synthesis of **42**. Purification by automated medium-pressure chromatography (hexane/EtOAc = 100/0 to 70/30) afforded the product **44** as a white solid (24 mg, 11 %).

^{1}H NMR (400 MHz, $CDCl_3$) δ 7.30 – 7.23 (m, 2H; 2x C(2')-H), 7.23 – 7.17 (m, 2H; 2x C(3')-H,), 3.57 (p, *J* = 9.1 Hz, 2H; 2x C(2)-H)), 3.49 – 3.38 (m, 4H; 4x C(6)-H/C(8)-H)), 3.36 – 3.24 (m, 4H; 4x C(6)-H/C(8)-H)), 2.31 – 2.19 (m, 4H; 2x C(1)-H, 2x C(3)-H), 1.90 (td, *J* = 9.5, 2.4 Hz, 4H; 2x C(1)-H, 2x C(3)-H), 1.77 – 1.66 (m, 4H; 4x C(5)-H/C(9)-H), 1.52 – 1.47 (m, 4H; 4x C(5)-H/C(9)-H), 1.46 (s, 18H; $C(CH_3)_3$).

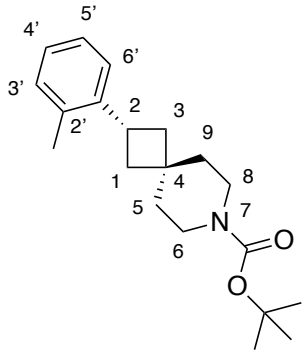
^{13}C NMR (101 MHz, $CDCl_3$) δ 155.1 (2x C=O), 143.1 (2x C(1')), 126.1 (2x C(3')), 125.8 (2x C(2')), 79.4 (2x *C*$(CH_3)_3$), 41.1 (2x C(6)/C(8)), 40.8 (2x C(6)/C(8)), 39.4 (2x C(5)/C(9)), 38.8 (2x C(1), C(3)), 36.1 (2x C(5)/C(9)), 33.8 (2x C(4)), 31.0 (2x C(2)), 28.6 (6x CH_3).

IR ($CHCl_3$ film): 2974 (w), 2921 (w), 2850 (w), 1690 (s), 1477, 1421, 1364 (s), 1270, 1243 (s), 1175, 1147 (s). 1113, 975 (w), 864 (w), 753 (w), 732 (w) cm^{-1}.

HRMS (ESI): m/z calcd for $C_{32}H_{48}N_2NaO_4^+$ $[M + Na]^+$ 547.3506 found 547.3505.

m.p.: 120 – 122 °C.

Synthesis of **45**



The corresponding compound was prepared following general procedure 11 using cyclobutene **41** and 2-methylphenylboronic acid. Purification by automated medium-pressure flash chromatography (hexane/EtOAc = 100/0 to 80/20) afforded the product **45** as a white solid (55 mg, 43 %).

^{1}H NMR (400 MHz, $CDCl_3$) δ 7.24 (d, *J* = 7.8 Hz, 1H; C(6')-H), 7.21 – 7.16 (m, 1H; C(3')-H), 7.14 – 7.07 (m, 2H; C(4')-H, C(5')-H), 3.62 (p, *J* = 9.1 Hz, 1H; C(2)-H), 3.51 – 3.42 (m, 2H; 2x C(6)-H/C(8)-H), 3.36 – 3.14 (m, 2H; 2x C(6)-H/C(8)-H), 2.39 – 2.26 (m, 2H; 1x C(1)-H, 1x C(3)-H), 2.24 (s, 3H; CH_3), 1.92 (td, *J* = 9.5, 2.5 Hz, 2H; 1x C(1)-H, 1x C(3)-H), 1.77 – 1.70 (m, 2H; 2x C(5)-H/C(9)-H), 1.52 – 1.48 (m, 2H; 2x C(5)-H/C(9)-H), 1.47 (s, 9H; $C(CH_3)_3$)

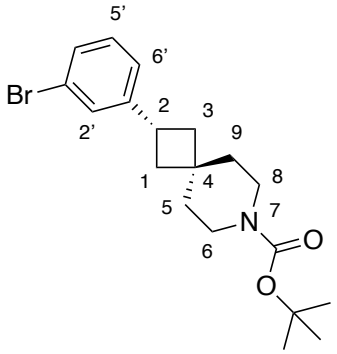
^{13}C NMR (101 MHz, $CDCl_3$) δ 155.1 (C=O), 143.5 (C(1')), 136.1 (C(2')), 130.2 (C(3')), 126.0 (C(4'), C(5')), 125.3 (C(6')), 79.4 ($C(CH_3)_3$), 41.0 (rot.; C(6), C(8)), 39.5 (C(5)/C(9)), 38.0 (C(1), C(3)), 36.1 (C(5)/C(9)), 33.9 (C(4)), 31.6 (C(2)), 28.6 ($C(CH_3)_3$), 19.8 (CH_3).

IR ($CHCl_3$ film): 2972 (w), 2920 (w), 1691 (s), 1461, 1420, 1365, 1270, 1242 (s), 1175, 1147 (s), 1111, 973 (w), 865 (w), 750 (w), 721 (w) cm^{-1}.

HRMS (ESI): m/z calcd for $C_{15}H_{22}N^+$ $[M + H - CO_2 - CH_2{=}C(CH_3)_2]^+$ 216.1747 found 216.1748.

m.p.: 86 – 87 °C.

Synthesis of **46**



The corresponding compound was prepared following general procedure 11 using cyclobutene **41** and 3-bromophenylboronic acid. Purification by automated medium-pressure flash chromatography (hexane/EtOAc = 100/0 to 80/20) afforded the product **46** as a colourless oil (112 mg, 74 %).

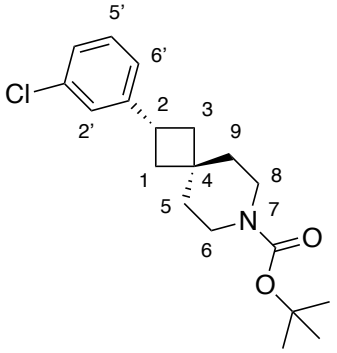
^{1}H NMR (400 MHz, $CDCl_3$) δ 7.27 – 7.25 (m, 1H; C(2')-H), 7.24 – 7.21 (m, 1H; C(4')-H), 7.08 (t, *J* = 7.6 Hz, 1H; C(5)-H), 7.03 (dtd, *J* = 7.7, 1.5, 0.7 Hz, 1H; C(6')-H), 3.47 (p, *J* = 9.2 Hz, 1H; C(2)-H), 3.43 – 3.37 (m, 2H; 2x C(6)-H/C(8)-H), 3.32 – 3.19 (m, 2H; 2x C(6)-H/C(8)-H), 2.38 – 2.17 (m, 2H; 1x C(1)-H, 1x C(3)-H), 1.87 (td, *J* = 9.5, 2.5 Hz, 2H; 1x C(1)-H, 1x C(3)-H), 1.71 – 1.66 (m, 2H; 2x C(5)-H/C(9)-H), 1.52 – 1.47 (m, 2H; 2x C(5)-H/C(9)-H), 1.46 (s, 9H; $C(CH_3)_3$).

^{13}C NMR (101 MHz, $CDCl_3$) δ 155.1 (C=O), 148.5 (C(1')), 130.0 (C(5')), 129.7 (C(2')), 129.0 (C(4')), 125.2 (C(6')), 122.6 (C(3')), 79.4 ($C(CH_3)_3$), 41.0 (C(6)/C(8)), 40.7 (C(6)/C(8)), 39.3 (C(5)/C(9)), 39.1 (C(1), C(3)), 35.9 (C(5)/C(9)), 34.1 (C(4)), 33.3 (C(2)), 28.6 ($C(CH_3)_3$).

IR ($CHCl_3$ film): 2973 (w), 2924 (w), 2848 (w), 1692 (s), 1595 (w), 1476 (w), 1422, 1365 (w), 1270 (w), 1243, 1148 (w), 1110, 997 (w), 954 (w), 865 (w), 778 (w), 691 (w) cm^{-1}.

HRMS (ESI): m/z calcd for $C_{19}H_{26}O_2{}^{79}BrNNa^+$ $[M + Na]^+$ 402.1039 found 402.1039.

Synthesis of **47**



The corresponding compound was prepared following general procedure 11 using cyclobutene **41** and 3-chlorophenylboronic acid. Purification by automated medium-pressure flash chromatography (hexane/EtOAc = 100/0 to 80/20) afforded the product **47** as a white solid (97 mg, 72 %).

^{1}H NMR (400 MHz, $CDCl_3$) δ 7.21 (apparent t, *J* = 7.7 Hz, 1H; C(5')-H), 7.17 – 7.09 (m, 2H; C(2')-H, C(4')-H), 7.06 (ddt, *J* = 7.6, 1.9, 0.9 Hz, 1H, 1H; C(6')-H), 3.48 (p, *J* = 9.1 Hz, 1H; C(2)-H), 3.45 – 3.37 (m, 2H; 2x C(6)-H/C(8)-H), 3.33 – 3.25 (m, 2H; 2x C(6)-H/C(8)-H), 2.36 – 2.21 (m, 2H; 1x C(1)-H, 1x C(3)-H), 1.97 – 1.79 (m, 2H; 1x C(1)-H, 1x C(3)-H), 1.73 – 1.65 (m, 2H; 2x C(5)-H/C(9)-H), 1.53 – 1.46 (m, 2H; 2x C(5)-H/C(9)-H), 1.46 (s, 9H; $C(CH_3)_3$).

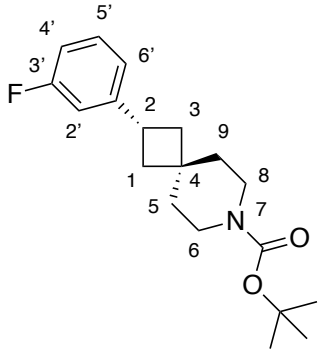
^{13}C NMR (101 MHz, $CDCl_3$) δ 155.0 (C=O), 148.2 (C(1')), 134.2 (C(3')), 129.6 (C(5')), 126.7 (C(2')), 126.0 (C(4')), 124.7 (C(6')), 79.4 ($C(CH_3)_3$), 41.0 (C(6)/C(8)), 40.7 (C(6)/C(8)), 39.3 (C(5)/C(9)), 39.0 (C(1)), C(3)), 35.9 (C(5)/C(9)), 34.0 (C(4)), 33.2 (C(2)), 28.6 ($C(CH_3)_3$).

IR ($CHCl_3$ film): 2923 (w), 2848 (w), 1677 (s), 1478, 1420, 1365 (s), 1270, 1242 (s), 1175, 1146 (s), 1079, 955 (w), 866 (w), 780, 702 (w), 692 cm^{-1}.

HRMS (ESI): m/z calcd for $C_{14}H_{19}{}^{35}ClN^+$ $[M + H - CO_2 - CH_2{=}C(CH_3)_2]^+$ 236.1201 found 236.1202.

m.p.: 71 – 72 °C.

Synthesis of **48**



This experiment was performed by F.W.G. The corresponding compound was prepared following general procedure 11 using cyclobutene **41** and 3-fluorophenylboronic acid. Purification by automated medium-pressure flash chromatography (hexane/EtOAc = 100/0 to 80/20) afforded the product **48** as a white solid (119 mg, 91 %).

^{1}H NMR (400 MHz, $CDCl_3$) δ 7.24 (td, *J* = 7.9, 6.0 Hz, 1H; C(5')-H), 6.96 (d, *J* = 7.6 Hz, 1H; C(6')-H), 6.93 – 6.79 (m, 2H; C(2')-H, C(4')-H), 3.50 (p, *J* = 9.2 Hz, 1H; C(2)-H), 3.44 – 3.38 (m, 2H; 2x C(6)-H/C(8)-H), 3.34 – 3.22 (m, 2H; 2x C(6)-H/C(8)-H), 2.29 (td, *J* = 8.9, 2.6 Hz, 2H; 2x C(5)-H/C(9)-H), 1.87 (td, *J* = 9.5, 2.4 Hz, 2H; 2x C(5)-H/C(9)-H), 1.77 – 1.64 (m, 2H; 1x C(1)-H, 1x C(3)-H), 1.50 (dd, *J* = 6.8, 4.6 Hz, 2H; 1x C(1)-H, 1x C(3)-H), 1.46 (s, 9H; $C(CH_3)_3$).

^{13}C NMR (101 MHz, $CDCl_3$) δ 163.1 (d, *J* = 245.6 Hz; C(3'')), 155.1 (C=O), 148.9 (d, *J* = 6.8 Hz; C(1'')), 129.8 (d, *J* = 8.3 Hz; C(5')), 122.1 (d, *J* = 2.8 Hz; C(6')), 113.3 (d, *J* = 21.1 Hz; C(2')), 112.7 (d, *J* = 21.1 Hz; C(4')), 79.4 ($C(CH_3)_3$), 40.9 (rot.; C(6), C(8)), 39.3 (C(5)/C(9)), 39.1 (C(1), C(3)), 35.9 (C(5)/C(9)), 34.0 (C(4)), 33.3 (d, *J* = 2.0 Hz; C(2)), 28.6 ($C(CH_3)_3$).

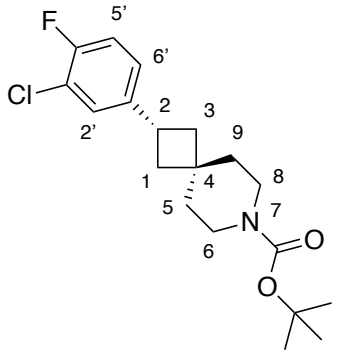
^{19}F NMR ($CDCl_3$, 377 MHz): δ (ppm) -113.65 (td, *J* = 9.5, 9.0, 6.0 Hz; C–F).

IR ($CHCl_3$ film): 2980 (w), 2926 (w), 1690 (s), 1588 (w), 1421, 1365, 1270, 1243, 1175, 1145 (s), 1108, 962(w), 862 (w), 780 (w), 691 (w) cm^{-1}.

HRMS (ESI): m/z calcd for $C_{14}H_{19}NF^+$ $[M + H - CO_2 - CH_2{=}C(CH_3)_2]^+$ 220.1496 found 220.1498.

m.p.: 89 – 90 °C

Synthesis of **49**



The corresponding compound was prepared following general procedure 11 using cyclobutene **41** and (3-chloro-4-fluorophenyl)boronic acid. Purification by automated medium-pressure flash chromatography (hexane/EtOAc = 100/0 to 80/20) afforded the product **49** as a white solid (49 mg, 35 %).

*For the target synthesis, **49** was prepared by the following amended procedure.*

A solution of the rhodium hydroxy phosphine complex was prepared by stirring a solution of $[Rh(cod)OH]_2$ (10.2mg, 0.022 mmol) and dppf (39.6mg, 0.054 mmol) in dry dioxane (2.0 mL) under an argon atmosphere at 60 °C for 30 min.

A portion of the resulting orange-red solution (1.8 mL; 0.1 equiv. [Rh]) was added to a 10 mL round-bottom flask containing a mixture of (3-chloro-4-fluorophenyl)boronic acid (1.2 mmol, 3.0 equiv.) and cyclobutene (0.40 mmol, 1.0 equiv.) in toluene (1.8 mL) and H_2O (0.4 mL) *via* syringe. The resulting mixture was then stirred at 60 °C for 16 hours. The mixture was diluted with hexane (1 mL) and concentrated *in vacuo*. The crude mixture was directly loaded on a silica gel flash column and purification by automated medium-pressure flash chromatography (hexane/EtOAc = 100/0 to 80/20) afforded the product **49** as a white solid (92 mg, 65 %).

^{1}H NMR (400 MHz, $CDCl_3$) δ 7.20 (ddt, *J* = 7.1, 1.8, 0.8 Hz, 1H; C(2')-H), 7.10 – 6.94 (m, 2H; C(5')-H, C(6')-H), 3.47 (p, *J* = 9.1 Hz, 1H; C(2)–H), 3.44 – 3.37 (m, 2H; 2x C(6)-H/C(8)-H), 3.32 – 3.14 (m, 2H; 2x C(6)-H/C(8)-H), 2.45 – 2.11 (m, 2H; 1x C(1)-H, 1x C(3)-H), 1.84 (td, *J* = 9.4, 2.5 Hz, 2H; 1x C(1)-H, 1x C(3)-H), 1.75 – 1.66 (m, 2H; 2x C(5)-H/C(9)-H), 1.55 – 1.48 (m, 2H; 2x C(5)-H/C(9)-H), 1.46 (s, 9H; $C(CH_3)_3$)

^{13}C NMR (101 MHz, $CDCl_3$) δ 156.5 (d, *J* = 246.4 Hz; C(4')), 155.1 (C=O), 143.2 (d, *J* = 3.8 Hz; C(1')), 128.6 (C(2')), 126.1 (d, *J* = 6.9 Hz; C(6')), 120.7 (d, *J* = 17.6 Hz; C(3')), 116.3 (d, *J* = 20.7 Hz; C(5')), 79.5 ($C(CH_3)_3$), 40.8 (rot.; C(6), C(8)), 39.34 (C(5)/C(9)), 39.26 (C(1), C(3)), 35.9 (C(5)/C(9)), 34.0 (C(4)), 32.8 (C(2)), 28.6 ($C(CH_3)_3$).

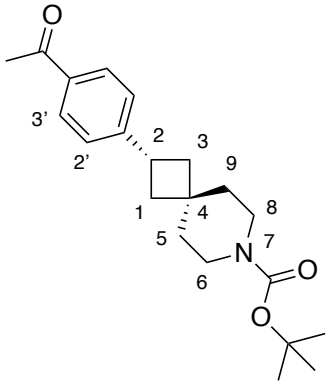
^{19}F NMR (377 MHz, $CDCl_3$) δ -119.73 – -120.59 (m; C–F).

IR ($CHCl_3$ film): 2977 (w), 2924 (w), 2852 (w), 1689 (s), 1501 (s), 1478, 1422, 1365, 1244 (s), 1175, 1148 (s), 1121 (w), 983 (w), 864 (w), 801 (w), 769 (w), 731 cm^{-1}.

HRMS (ESI): m/z calcd for $C_{14}H_{17}ClFN^+$ $[M + H - CO_2 - CH_2{=}C(CH_3)_2]^+$ 254.1106 found 254.1107.

m.p.: 71 – 72 °C.

Synthesis of **50**



The corresponding compound was prepared following general procedure 11 using cyclobutene **41** and 4-acetylphenylboronic acid. Purification by automated medium-pressure flash chromatography (hexane/EtOAc = 100/0 to 80/20) afforded the product **50** as a white solid (117 mg, 85 %).

^{1}H NMR (400 MHz, $CDCl_3$) δ 7.94 – 7.87 (m, 2H; 2x C(3')-H), 7.32 – 7.25 (m, 2H; 2x C(2')-H), 3.58 (p, *J* = 9.1 Hz, 1H; C(2)-H), 3.47 – 3.39 (m, 2H; 2x C(6)-H/C(8)-H), 3.34 – 3.27 (m, 2H; 2x C(6)-H/C(8)-H), 2.58 (s, 3H; CH_3), 2.39 – 2.28 (m, 2H; 1x C(1)-H, 1x C(3)-H), 1.98 – 1.87 (m, 2H; 1x C(1)-H, 1x C(3)–H), 1.76 – 1.68 (m, 2H; 2x C(5)-H/C(9)-H), 1.57 – 1.49 (m, 2H; 2x C(5)-H/C(9)-H), 1.47 (s, 9H; $C(CH_3)_3$).

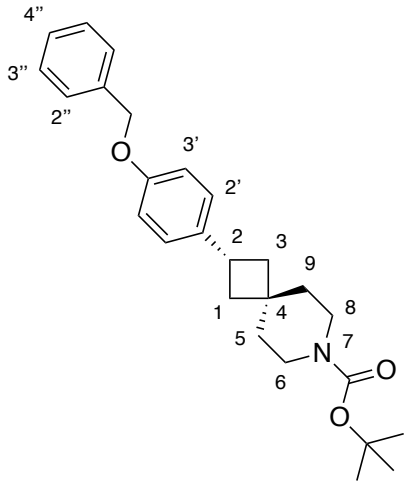
^{13}C NMR (101 MHz, $CDCl_3$) δ 197.8 ((*C*=O)CH_3), 155.0 (C=O), 151.8 (C(1')), 135.1 (C(4')), 128.6 (2x C(3')), 126.6 (2x C(2')), 79.4 (*C*$(CH_3)_3$), 41.0 (C(6)/C(8)), 40.7 (C(6)/C(8)), 39.2 (C(5)/C(9)), 39.0 (C(1), C(3)), 35.9 (C(5)/C(9)), 34.1 (C(4)), 33.6 (C(2)), 28.5 (3x CH_3), 26.6 (CH_3)

IR ($CHCl_3$ film): 2923 (w), 2851 (w), 1680 (s), 1605, 1421, 1364, 1268, 1243, 1175, 1146, 1111, 976 (w), 820 (w), 769 (w), 638 (w) cm^{-1}.

HRMS (ESI): m/z calcd for $C_{21}H_{29}NNaO_3^+$ $[M + Na]^+$ 366.2040 found 366.2040.

m.p.: 79 – 81 °C

Synthesis of **51**



This experiment was performed by F.W.G. The corresponding compound was prepared following general procedure 11 using cyclobutene **41** and 4-benzyloxyphenylboronic acid. Purification by automated medium-pressure flash chromatography (hexane/EtOAc = 100/0 to 80/20) afforded the product **51** as a white solid (60 mg, 37 %).

^{1}H NMR (400 MHz, $CDCl_3$) δ 7.47 – 7.42 (m, 2H; 2x C(2'')-H), 7.41 – 7.36 (m, 2H; 2x C(3'')-H), 7.35 – 7.29 (m, 1H; (4'')-H), 7.18 – 7.07 (m, 2H; 2x C(2')-H), 7.04 – 6.84 (m, 2H; 2x C(3')-H), 5.05 (s, 2H, OCH_2Ph), 3.48 (p, *J* = 9.1 Hz, 1H; C(2)-H), 3.42 (dd, *J* = 6.7, 4.6 Hz, 2H; 2x C(6)-H/C(8)-H), 3.36 – 3.25 (m, 2H; 2x C(6)-H/C(8)-H), 2.27 (ddt, *J* = 10.4, 8.8, 1.5 Hz, 2H; 1x C(1)-H, 1x C(3)-H), 1.86 (td, *J* = 9.5, 2.5 Hz, 2H; 1x C(1)-H, 1x C(3)-H), 1.70 (t, *J* = 5.7 Hz, 2H; 2x C(5)-H/C(9)-H), 1.51 (dd, *J* = 6.5, 4.6 Hz, 2H; 2x C(5)-H/C(9)-H), 1.47 (s, 9H; $C(CH_3)_3$).

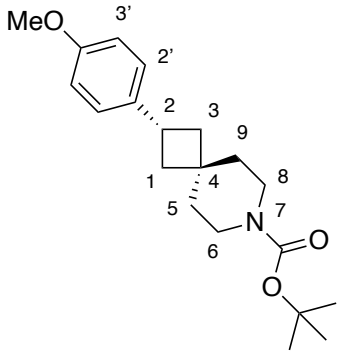
^{13}C NMR (101 MHz, $CDCl_3$) δ 157.1 (C(4')), 155.1 (C=O), 138.6 (C(1')), 137.3 (C(1'')), 128.7 (C(3'')), 128.0 (C(4'')), 127.6, 127.5 (2x C(2') and 2x C(2'')), 114.8 (2x C(3')), 79.3 ($C(CH_3)_3$), 70.2 (OCH_2Ph), 41.0 (rot.; C(6), C(8)), 39.5 (C(1), C(3)), 39.4 (C(5)/C(9)), 36.0 (C(5)/C(9)), 33.8 (C(4)), 32.9 (C(2)), 28.6 ($C(CH_3)_3$).

IR ($CHCl_3$ film): 2911 (w), 2852 (w), 1677 (s), 1609 (w), 1511, 1467 (w), 1454 (w), 1424, 1387 (w), 1270, 1243 (s), 1178, 1148, 1021 (w), 866 (w), 820 (w), 760 (w), 709 (w) cm^{-1}.

HRMS (ESI): m/z calcd for $C_{26}H_{33}O_3NNa^+$ $[M + Na]^+$ 430.2353 found 430.2352.

m.p.: 152 – 154 °C.

Synthesis of **52**



The corresponding compound was prepared following general procedure 11 using cyclobutene **41** and (4-methoxyphenyl)boronic acid. Purification by automated medium-pressure flash chromatography (hexane/EtOAc = 100/0 to 70/30) afforded the product **52** as a white solid (41 mg, 29 %).

^{1}H NMR (400 MHz, $CDCl_3$) δ 7.17 – 7.09 (m, 2H; 2x C(2')-H), 6.90 – 6.78 (m, 2H; 2x C(3')-H), 3.79 (s, 3H; O(CH_3)), 3.53 – 3.38 (m, 3H; 1x C(2)-H, 2x C(6)-H/C(8)-H), 3.33 – 3.26 (m, 2H; 2x C(6)-H/C(8)-H), 2.32 – 2.21 (m, 2H; 1x C(1)-H, 1x C(3)-H), 1.85 (td, *J* = 9.5, 2.6 Hz, 2H; 1x C(1)-H, 1x C(3)-H), 1.73 – 1.64 (m, 2H; 2x C(5)-H/C(9)-H), 1.53 – 1.48 (m, 2H; 2x C(5)-H/C(9)-H), 1.46 (s, 9H; $C(CH_3)_3$).

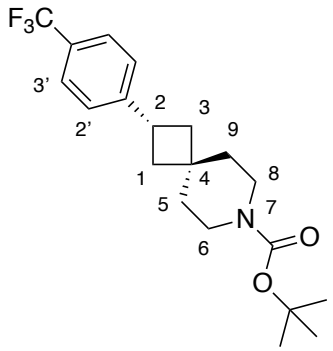
^{13}C NMR (101 MHz, $CDCl_3$) δ 157.9 (C(4')), 155.2 (C=O), 138.3 (C(1')), 127.5 (2x C(2')), 113.9 (2x C(3')), 79.4 ($C(CH_3)_3$), 55.4 (OCH_3), 40.0 (C(6)/C(8)), 40.8 (C(6)/C(8)), 39.5 (C(1), C(3)), 39.4 (C(5)/C(9)), 36.0 (C(5)/C(9)), 33.9 (C(4)), 32.9 (C(2)), 28.6 ($C(CH_3)_3$).

IR ($CHCl_3$ film): 2921.6 (w), 2842.3 (w), 1688.6 (s), 1611.2 (w), 1512.7 (w), 1420.6 (w), 1364.9 (w), 1244.0 (s), 1175.6 (w), 1146.6 (s), 1109.9, (w), 1037.4 (w), 820.95 (w), 769.2 (w) cm^{-1}.

HRMS (ESI): m/z calcd for $C_{20}H_{29}O_3NNa^+$ $[M + Na]^+$ 354.2040 found 354.2039.

m.p.: 80 – 82 °C.

Synthesis of **53**



The corresponding compound was prepared following general procedure 11 using cyclobutene **41** and (4-(trifluoromethyl)phenyl)boronic acid. Purification by automated medium-pressure flash chromatography (hexane/EtOAc = 100/0 to 80/20) afforded the product **53** as a white solid (124 mg, 84 %).

^{1}H NMR (400 MHz, $CDCl_3$) δ 7.58 – 7.50 (m, 2H; 2x C(3')-H), 7.33 – 7.26 (m, 2H; 2x C(2')-H), 3.57 (p, *J* = 9.1 Hz, 1H; C(2)-H), 3.46 – 3.40 (m, 2H; 2x C(6)-H/C(8)-H), 3.34 – 3.26 (m, 2H; 2x C(6)-H/C(8)-H), 2.38 – 2.27 (m, 2H; 1x C(1)-H, 1x C(3)-H), 1.98 – 1.83 (m, 2H; 1x C(1)-H, 1x C(3)-H), 1.75 – 1.65 (m, 2H; 2x C(5)-H/C(9)-H), 1.53 – 1.47 (m, 2H; 2x C(5)-H/C(9)-H), 1.46 (s, 9H; $C(CH_3)_3$).

^{13}C NMR (101 MHz, $CDCl_3$) δ 155.1 (C=O), 150.2 (C(1')), 128.2 (q, *J* = 31.9; C(4')) 126.8 (2x C(2')), 125.4 (q, *J* = 3.8; 2x C(3')) 124.5 (q, *J* = 271.4; CF_3), 79.5 ($C(CH_3)_3$), 41.1 (C(6)/C(8)), 40.7 (C(6)/C(8)), 39.3 (C(5)/C(9)), 39.1 (C(1), C(3)), 36.0 (C(5)/C(9)), 34.2 (C(4)), 33.4 (C(2)), 28.6 ($C(CH_3)_3$).

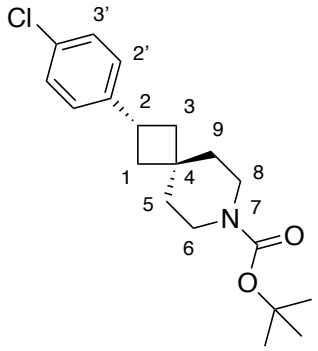
^{19}F NMR (377 MHz, $CDCl_3$) δ -62.29 (s; CF_3).

IR ($CHCl_3$ film): 2926 (w), 2855 (w), 1682 (s), 1424, 1365, 1322, 1244 (w), 1151, 1111 (s), 1064, 977 (w), 860 (w), 825 (w), 768 (w) cm^{-1}.

HRMS (ESI): m/z calcd for $C_{15}H_{19}F_3N^+$ $[M + H - CO_2 - CH_2{=}C(CH_3)_2]^+$ 270.1464 found 270.1465.

m.p.: 88 – 90 °C.

Synthesis of **54**



The corresponding compound was prepared following general procedure 11 using cyclobutene **41** and 4-chlorophenylboronic acid. Purification by automated medium-pressure flash chromatography (hexane/EtOAc = 100/0 to 80/20) afforded the product **54** as a white solid (114 mg, 85 %).

^{1}H NMR (400 MHz, $CDCl_3$) δ 7.32 – 7.22 (m, 2H; 2x C(3')-H), 7.16 – 7.10 (m, 2H; 2x C(2')-H), 3.48 (p, *J* = 9.1 Hz, 1H; C(2)-H), 3.45 – 3.39 (m, 2H; 2x C(6)-H/C(8)-H), 3.34 – 3.28 (m, 2H; 2x C(6)-H/C(8)-H), 2.37 – 2.23 (m, 2H; 1x C(1)-H, 1x C(3)-H), 1.86 (td, *J* = 9.5, 2.5 Hz, 2H; 1x C(1)-H, 1x C(3)-H), 1.77 – 1.66 (m, 2H; 2x C(5)-H/C(9)-H)), 1.55 – 1.49 (m, 2H; 2x C(5)-H/C(9)-H), 1.46 (s, 9H; $C(CH_3)_3$).

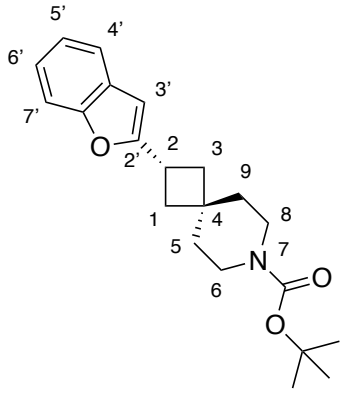
^{13}C NMR (101 MHz, $CDCl_3$) δ 155.1 (C=O), 144.6 (C(1')), 131.5 (C(4')), 128.4 (2x C(3')), 127.9 (2x C(2')), 79.4 ($C(CH_3)_3$), 41.0 (C(6)/C(8)), 40.7 (C(6)/C(8)), 39.3 (C(5)/C(9)), 39.2 (C(1), C(3)), 35.9 (C(5)/C(9)), 34.0 (C(4)), 33.0 (C(2)), 28.6 ($C(CH_3)_3$).

IR ($CHCl_3$ film): 2973(w), 2923 (w), 12851 (w), 1680 (s), 1491 (w), 1420, 1365, 1270, 1243, 1174, 1147 (s), 1090, 1034 (w), 976 (w), 908 (w), 814 (w) 731 cm^{-1}.

HRMS (ESI): m/z calcd for $C_{14}H_{19}{}^{35}ClN^+$ $[M + H - CO_2 - CH_2{=}C(CH_3)_2]^+$ 236.1201 found 236.1202.

m.p.: 112 – 114 °C.

Synthesis of **55**



This experiment was performed by F.W.G. The corresponding compound was prepared following general procedure 11 using cyclobutene **41** and 2-benzofuranylboronic acid. Purification by automated medium-pressure flash chromatography (hexane/EtOAc = 100/0 to

80/20) afforded the product **55** as a pale-yellow solid (117 mg, 86 %). Note: The product was contaminated with a small amount (~5 %) of an impurity which is likely the minor regioisomeric 1,1',2-substituted cyclobutane.

^{1}H NMR (400 MHz, $CDCl_3$) δ 7.55 – 7.44 (m, 1H; C(4')-H), 7.45 – 7.38 (m, 1H; C(7')-H), 7.24 – 7.19 (m, 1H; C(6')-H), 7.19 – 7.15 (m, 1H; C(5')-H), 6.39 (t, *J* = 0.8 Hz, 1H; C(3')-H), 3.62 (p, *J* = 8.7 Hz, 1H; C(2)-H), 3.45 – 3.37 (m, 2H; 2x C(6)-H/C(8)-H), 3.37 – 3.20 (m, 2H; 2x C(6)-H/C(8)-H), 2.40 – 2.19 (m, 2H; 1x C(1)-H, 1x C(3)-H), 2.19 – 2.06 (m, 2H; 1x C(1)-H, 1x C(3)-H), 1.71 – 1.66 (m, 2H; 2x C(5)-H/C(9)-H), 1.60 (td, *J* = 5.6, 5.0, 2.4 Hz, 2H; 2x C(5)-H/C(9)-H), 1.47 (s, 9H; $C(CH_3)_3$).

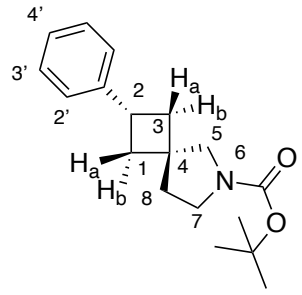
^{13}C NMR (101 MHz, $CDCl_3$) δ 162.2 (C(2')), 155.1 (C=O), 154.9 (C(7a')), 129.0 (C(3a')), 123.4 (C(6')), 122.6 (C(5')), 120.4 (C(4')), 110.9 (C(7')), 101.0 (C(3')), 79.4 ($C(CH_3)_3$), 40.9 (rot.; C(6) and C(8)), 38.9 (C(5)/C(9)), 37.2 (C(1), C(3)), 36.3 (C(5)/C(9)), 34.6 (C(4)), 28.6 ($C(CH_3)_3$), 27.4 (C(2)).

IR ($CHCl_3$ film): 2968 (w), 2927 (w), 2849 (w), 1689 (s), 1599 (w), 1455, 1421, 1365, 1270, 1243 (s), 1174, 1146 (s), 1115 (w), 890 (w), 863 (w), 795 (w), 751 cm^{-1}.

HRMS (ESI): m/z calcd for $C_{21}H_{27}O_3NNa^+$ [M + Na]+ 364.1883 found 364.1884.

m.p.: 59 – 61 °C.

Synthesis of **57**



The corresponding compound was prepared following general procedure 11 using cyclobutene **56** and phenylboronic acid. Purification by automated medium-pressure flash chromatography (hexane/EtOAc = 100/0 to 80/20) afforded the product **57** in a 4:1 diastereomeric ratio as a colourless oil (75 mg, 65 %).

^{1}H NMR (400 MHz, $CDCl_3$; major diastereomer) δ 7.36 – 7.28 (m, 2H; 2x C(3')-H), 7.23 – 7.10 (m, 3H; 2x C(2')-H, C(4')-H), 3.59 – 3.46 (m, 1H; C(2)-H), 3.41 (t, *J* = 6.8 Hz, 2H; C(7)-H_2), 3.26 (s, 2H; C(5)-H_2), 2.38 – 2.26 (m, 2H; C(1)-H_a, C(3)-H_a), 2.24 – 2.14 (m, 2H; C(1)-H_b, C(3)-H_b), 2.02 (t, *J* = 6.8 Hz, 1H; C(8)-H_2), 1.46 (s, 9H; C(CH_3)$_3$).

^{13}C NMR (101 MHz, $CDCl_3$; major diastereomer) δ 154.7 (C=O), 145.4 (C(1')), 128.4 (2x C(3')), 126.4 (2x C(2')), 126.1 (C(4')), 79.2 (*C*(CH_3)$_3$), 57.7 (C(5)), 44.8 (C(7)), 39.0 (C(3)), 36.8 (C(8)), 34.1 (C(4)), 28.7 (C(*C*H_3)$_3$).

IR ($CHCl_3$ film): 2974 (w), 2924 (w), 2866 (w), 1697 (s), 1476 (w), 1401 (s), 1365 (w), 1298 (w), 1255 (w), 1164, 1102, 974 (w), 934 (w), 879 (w), 772 (w) cm^{-1}.

HRMS (ESI): m/z calcd for $C_{18}H_{25}NNaO_2$+ [M + Na]+ 310.1778 found 310.1778.

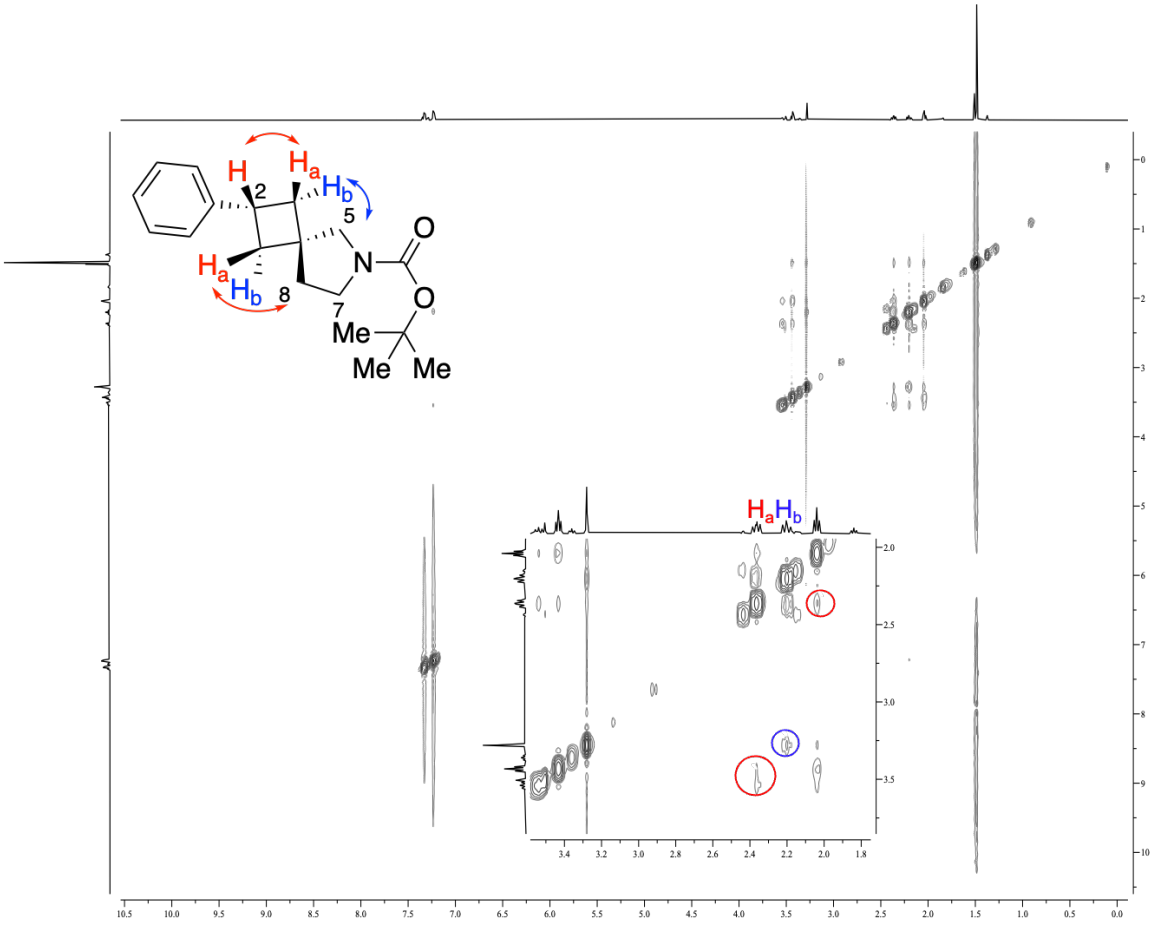
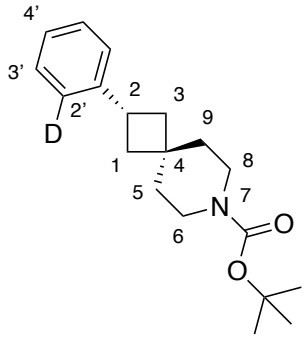


Figure S11. NOESY NMR (500 MHz, $CDCl_3$) spectrum of **57** recorded at 298 K.

4.3 Deuterium Labelling Study

Synthesis of **42-C2'-d**



The corresponding compound was prepared following general procedure 11 using cyclobutene **41** and phenylboronic acid with D_2O (0.40 mL) instead of H_2O and a solution of $CsOH{\cdot}H_2O$ in D_2O (70 µL; 0.4 mmol, 1.0 equiv.). Purification by automated medium-pressure flash chromatography (hexane/EtOAc = 100/0 to 80/20) afforded the product **42-C2'-*d*** as a white solid (65 mg, 54 %) with 80 % D incorporation at the C(2') position.

^{1}H NMR (400 MHz, $CDCl_3$; quantitative) δ 7.35 – 7.27 (m, 2H; 2x C(3')-H), 7.25 – 7.14 (m, 2.20 H; 2x C(2')-H, C(4')-H), 3.53 (p, *J* = 9.1 Hz, 1H; C(2)-H), 3.47 – 3.39 (m, 2H; 2x C(6)-H/C(8)-H), 3.35 – 3.25 (m, 2H; 2x C(6)-H/C(8)-H), 2.37 – 2.23 (m, 2H 1x C(1)-H, 1x C(3)–H), 1.97 – 1.84 (m, 2H; 1x C(1)-H, 1x C(3)-H), 1.76 – 1.67 (m, 2H), 1.55 – 1.49 (m, 2H; 2x C(5)-H/C(9)-H), 1.48 (s, 9H; $C(CH_3)_3$).

HRMS (ESI): m/z calcd for $C_{19}H_{26}DNNaO_2^+$ $[M + Na]^+$ 325.1997 found 325.1997.

References

1 Roughley, S. D. & Jordan, A. M. The Medicinal Chemist's Toolbox: An Analysis of Reactions Used in the Pursuit of Drug Candidates. *J. Med. Chem.* **54**, 3451-3479, (2011).

2 Cooper, T. W. J., Campbell, I. B. & Macdonald, S. J. F. Factors Determining the Selection of Organic Reactions by Medicinal Chemists and the Use of These Reactions in Arrays (Small Focused Libraries). *Angew. Chem. Int. Ed.* **49**, 8082-8091, (2010).

3 Lennox, A. J. J. & Lloyd-Jones, G. C. Selection of boron reagents for Suzuki–Miyaura coupling. *Chem. Soc. Rev.* **43**, 412-443, (2014).

4 Johansson Seechurn, C. C. C., Kitching, M. O., Colacot, T. J. & Snieckus, V. Palladium-Catalyzed Cross-Coupling: A Historical Contextual Perspective to the 2010 Nobel Prize. *Angew. Chem. Int. Ed.* **51**, 5062-5085, (2012).

5 Brown, D. G. & Boström, J. Analysis of Past and Present Synthetic Methodologies on Medicinal Chemistry: Where Have All the New Reactions Gone? *J. Med. Chem.* **59**, 4443-4458, (2016).

6 Lovering, F., Bikker, J. & Humblet, C. Escape from flatland: Increasing saturation as an approach to improving clinical success. *J. Med. Chem.* **52**, 6752-6756, (2009).

7 Lovering, F. Escape from Flatland 2: Complexity and promiscuity. *Med. Chem. Comm.* **4**, 515-519, (2013).

8 Goetzke, F. W., van Dijk, L. & Fletcher, S. P. in *PATAI'S Chemistry of Functional Groups*, (Wiley, 2019).

9 Rygus, J. P. G. & Crudden, C. M. Enantiospecific and Iterative Suzuki-Miyaura Cross-Couplings. *J. Am. Chem. Soc.* **139**, 18124-18137, (2017).

10 Leonori, D. & Aggarwal, V. K. Stereospecific Couplings of Secondary and Tertiary Boronic Esters. *Angew. Chem. Int. Ed.* **54**, 1082-1096, (2015).

11 Cammidge, A. N. & Crépy, K. V. L. The first asymmetric Suzuki cross-coupling reaction. *Chem. Commun.*, 1723-1724, (2000).

12 Yin, J. & Buchwald, S. L. A Catalytic Asymmetric Suzuki Coupling for the Synthesis of Axially Chiral Biaryl Compounds. *J. Am. Chem. Soc.* **122**, 12051-12052, (2000).

13 Zhang, D. & Wang, Q. Palladium catalyzed asymmetric Suzuki–Miyaura coupling reactions to axially chiral biaryl compounds: Chiral ligands and recent advances. *Coord. Chem. Rev.* **286**, 1-16, (2015).

14 Xu, G., Fu, W., Liu, G., Senanayake, C. H. & Tang, W. Efficient Syntheses of Korupensamines A, B and Michellamine B by Asymmetric Suzuki-Miyaura Coupling Reactions. *J. Am. Chem. Soc.* **136**, 570-573, (2014).

15 Ji, W., Wu, H.-h. & Zhang, J. Axially Chiral Biaryl Monophosphine Oxides Enabled by Palladium/WJ-Phos-Catalyzed Asymmetric Suzuki–Miyaura Cross-coupling. *ACS Catal.* **10**, 1548-1554, (2020).

16 Blakemore, D. in *Synthetic Methods in Drug Discovery: Volume 1* Vol. 1 1-69 (The Royal Society of Chemistry, 2016).

17 Shen, X., Jones, G. O., Watson, D. A., Bhayana, B. & Buchwald, S. L. Enantioselective Synthesis of Axially Chiral Biaryls by the Pd-Catalyzed Suzuki−Miyaura Reaction: Substrate Scope and Quantum Mechanical Investigations. *J. Am. Chem. Soc.* **132**, 11278-11287, (2010).

18 Steinreiber, J., Faber, K. & Griengl, H. De-racemization of enantiomers versus de-epimerization of diastereomers-classification of dynamic kinetic asymmetric transformations (DYKAT). *Chem. Eur. J.* **14**, 8060-8072, (2008).

19 Ros, A. *et al.* Dynamic Kinetic Cross-Coupling Strategy for the Asymmetric Synthesis of Axially Chiral Heterobiaryls. *J. Am. Chem. Soc.* **135**, 15730-15733, (2013).

20 Willis, M. C., Powell, L. H. W., Claverie, C. K. & Watson, S. J. Enantioselective Suzuki reactions: Catalytic asymmetric synthesis of compounds containing quaternary carbon centers. *Angew. Chem. Int. Ed.* **43**, 1249-1251, (2004).
21 Netherton, M. R., Dai, C., Neuschütz, K. & Fu, G. C. Room-Temperature Alkyl−Alkyl Suzuki Cross-Coupling of Alkyl Bromides that Possess β Hydrogens. *J. Am. Chem. Soc.* **123**, 10099-10100, (2001).
22 Yamamoto, Y., Takada, S. & Miyaura, N. Asymmetric Cross-coupling of Potassium 2-Butenyltrifluoroborates with Aryl and 1-Alkenyl Bromides Catalyzed by a Pd(OAc)2/Josiphos Complex. *Chem. Lett.* **35**, 1368-1369, (2006).
23 Yamamoto, Y., Takada, S., Miyaura, N., Iyama, T. & Tachikawa, H. γ-Selective cross-coupling reactions of potassium allyltrifluoroborates with haloarenes catalyzed by a Pd(0)/D-t-BPF or Pd(0)/Josiphos ((R,S)-CyPF-t-Bu) complex: Mechanistic studies on transmetalation and enantioselection. *Organometallics* **28**, 152-160, (2009).
24 Schuster, C. H., Coombs, J. R., Kasun, Z. A. & Morken, J. P. Enantioselective carbocycle formation through intramolecular Pd-catalyzed allyl-aryl cross-coupling. *Org. Lett.* **16**, 4420-4423, (2014).
25 Sun, C., Potter, B. & Morken, J. P. A Catalytic Enantiotopic-Group-Selective Suzuki Reaction for the Construction of Chiral Organoboronates. *J. Am. Chem. Soc.* **136**, 6534-6537, (2014).
26 Potter, B., Szymaniak, A. A., Edelstein, E. K. & Morken, J. P. Nonracemic allylic boronates through enantiotopic-group-selective cross-coupling of geminal bis(boronates) and vinyl halides. *J. Am. Chem. Soc.* **136**, 17918-17921, (2014).
27 Liu, X., Sun, C., Mlynarski, S. & Morken, J. P. Synthesis and Stereochemical Assignment of Arenolide. *Org. Lett.* **20**, 1898-1901, (2018).
28 Li, B., Li, T., Aliyu, M. A., Li, Z. H. & Tang, W. Enantioselective Palladium-Catalyzed Cross-Coupling of α-Bromo Carboxamides and Aryl Boronic Acids. *Angew. Chem. Int. Ed.* **58**, 11355-11359, (2019).
29 Li, B. *et al.* General Synthesis of Chiral α,α-Diaryl Carboxamides by Enantioselective Palladium-Catalyzed Cross-Coupling. *Org. Lett.* **22**, 4974-4978, (2020).
30 Zhang, P., Brozek, L. A. & Morken, J. P. Pd-catalyzed enantioselective allyl-allyl cross-coupling. *J. Am. Chem. Soc.* **132**, 10686-10688, (2010).
31 Zhang, P., Le, H., Kyne, R. E. & Morken, J. P. Enantioselective Construction of All-Carbon Quaternary Centers by. *J. Am. Chem. Soc.* **133**, 9716-9719, (2011).
32 Han, F. S. Transition-metal-catalyzed Suzuki-Miyaura cross-coupling reactions: A remarkable advance from palladium to nickel catalysts. *Chem. Soc. Rev.* **42**, 5270-5298, (2013).
33 Chung, K. G., Miyake, Y. & Uemura, S. Nickel(0)-catalyzed asymmetric cross-coupling reactions of allylic compounds with arylboronic acids. *J. Chem. Soc., Perkin Trans. 1*, 15-18, (2000).
34 Shields, J. D., Ahneman, D. T., Graham, T. J. A. & Doyle, A. G. Enantioselective, Nickel-Catalyzed Suzuki Cross-Coupling of Quinolinium Ions. *Org. Lett.* **16**, 142-145, (2014).
35 Huang, W., Wan, X. & Shen, Q. Enantioselective Construction of Trifluoromethoxylated Stereogenic Centers by a Nickel-Catalyzed Asymmetric Suzuki–Miyaura Coupling of Secondary Benzyl Bromides. *Angew. Chem. Int. Ed.* **56**, 11986-11989, (2017).
36 Lundin, P. M. & Fu, G. C. Asymmetric Suzuki Cross-Couplings of Activated Secondary Alkyl Electrophiles: Arylations of Racemic α-Chloroamides. *J. Am. Chem. Soc.***132**, 11027-11029, (2010).
37 Cong, H. & Fu, G. C. Catalytic enantioselective cyclization/cross-coupling with alkyl electrophiles. *J. Am. Chem. Soc.* **136**, 3788-3791, (2014).

38 Saito, B. & Fu, G. C. Enantioselective Alkyl−Alkyl Suzuki Cross-Couplings of Unactivated Homobenzylic Halides. *J. Am. Chem. Soc.***130**, 6694-6695, (2008).
39 Jiang, X., Sakthivel, S., Kulbitski, K., Nisnevich, G. & Gandelman, M. Efficient Synthesis of Secondary Alkyl Fluorides via Suzuki Cross- Coupling Reaction of 1-Halo-1- fluoroalkanes. *J. Am. Chem. Soc.***136**, 9548-9551, (2014).
40 Jiang, X. & Gandelman, M. Enantioselective Suzuki cross-couplings of unactivated 1-fluoro-1-haloalkanes: Synthesis of chiral β-, γ-, δ-, and ε-fluoroalkanes. *J. Am. Chem. Soc.* **137**, 2542-2547, (2015).
41 Wilsily, A., Tramutola, F., Owston, N. A. & Fu, G. C. New directing groups for metal-catalyzed asymmetric carbon-carbon bond-forming processes: Stereoconvergent alkyl-alkyl suzuki cross-couplings of unactivated electrophiles. *J. Am. Chem. Soc.***134**, 5794-5797, (2012).
42 Owston, N. A. & Fu, G. C. Asymmetric Alkyl-Alkyl Cross-Couplings of Unactivated Secondary Alkyl Electrophiles: Stereoconvergent Suzuki Reactions of Racemic Acylated Halohydrins. *J. Am. Chem. Soc.***132**, 11908-11909, (2010).
43 Zultanski, S. L. & Fu, G. C. Catalytic Asymmetric γ-Alkylation of Carbonyl Compounds via Stereoconvergent Suzuki Cross-Couplings. *J. Am. Chem. Soc.***133**, 15362-15364, (2011).
44 Lu, Z., Wilsily, A. & Fu, G. C. Stereoconvergent amine-directed alkyl-alkyl Suzuki reactions of unactivated secondary alkyl chlorides. *J. Am. Chem. Soc.* **133**, 8154-8157, (2011).
45 Tellis, J. C., Primer, D. N. & Molander, G. A. Single-electron transmetalation in organoboron cross-coupling by photoredox/nickel dual catalysis. *Science* **345**, 433, (2014).
46 Gutierrez, O., Tellis, J. C., Primer, D. N., Molander, G. A. & Kozlowski, M. C. Nickel-Catalyzed Cross-Coupling of Photoredox-Generated Radicals: Uncovering a General Manifold for Stereoconvergence in Nickel-Catalyzed Cross-Couplings. *J. Am. Chem. Soc.* **137**, 4896-4899, (2015).
47 Menard, F., Chapman, T. M., Dockendorff, C. & Lautens, M. Rhodium-catalyzed asymmetric allylic substitution with boronic acid nucleophiles. *Org. Lett.* **8**, 4569-4572, (2006).
48 Menard, F., Perez, D., Sustac Roman, D., Chapman, T. M. & Lautens, M. Ligand-controlled selectivity in the desymmetrization of meso cyclopenten-1,4-diols via rhodium(I)-Catalyzed addition of arylboronic acids. *J. Org. Chem.* **75**, 4056-4068, (2010).
49 Jacques, R., Hell, A. M. L., Pullin, R. D. C. & Fletcher, S. P. Desymmetrization of meso-bisphosphates via rhodium catalyzed asymmetric allylic arylation. *Tetrahedron* **75**, 130560-130560, (2019).
50 Yu, B., Menard, F., Isono, N. & Lautens, M. Synthesis of homoallylic alcohols via lewis acid assisted enantioselective desymmetrization. *Synthesis*, 853-859, (2009).
51 Miura, T., Takahashi, Y. & Murakami, M. Rhodium-catalysed substitutive arylation of cis-allylic diols with arylboroxines. *Chem. Commun.*, 595-597, (2007).
52 Kiuchi, H., Takahashi, D., Funaki, K., Sato, T. & Oi, S. Rhodium-Catalyzed Asymmetric Coupling Reaction of Allylic Ethers with Arylboronic Acids. *Org. Lett.* **14**, 4502-4505, (2012).
53 Sidera, M. & Fletcher, S. P. Rhodium-catalysed asymmetric allylic arylation of racemic halides with arylboronic acids. *Nat. Chem.* **7**, 935-939, (2015).
54 Schafer, P., Palacin, T., Sidera, M. & Fletcher, S. P. Asymmetric Suzuki-Miyaura coupling of heterocycles via Rhodium-catalysed allylic arylation of racemates. *Nat. Commun.* **8**, 15762-15762, (2017).

55 Almond-Thynne, J., Blakemore, D. C., Pryde, D. C. & Spivey, A. C. Site-selective Suzuki–Miyaura coupling of heteroaryl halides – understanding the trends for pharmaceutically important classes. *Chemical Science* **8**, 40-62, (2017).
56 Goetzke, F. W., Mortimore, M. & Fletcher, S. P. Enantio- and Diastereoselective Suzuki-Miyaura Coupling with Racemic Bicycles. *Angew. Chem. Int. Ed.* **58**, 12128-12132, (2019).
57 Wallace, D. J. *et al.* Development of a Fit-for-Purpose Large-Scale Synthesis of an Oral PARP Inhibitor. *Organic Process Research & Development* **15**, 831-840, (2011).
58 González, J., van Dijk, L., Goetzke, F. W. & Fletcher, S. P. Highly enantioselective rhodium-catalyzed cross-coupling of boronic acids and racemic allyl halides. *Nat. Protoc.* **14**, 2972-2985., (2019).
59 Kučera, R., Goetzke, F. W. & Fletcher, S. P. An Asymmetric Suzuki–Miyaura Approach to Prostaglandins: Synthesis of Tafluprost. *Org. Lett.* **22**, 2991-2994, (2020).
60 Cheng, Q. *et al.* Iridium-Catalyzed Asymmetric Allylic Substitution Reactions. *Chem. Rev.*, (2018).
61 Hamilton, J. Y., Sarlah, D. & Carreira, E. M. Iridium-catalyzed enantioselective allylic alkynylation. *Angew. Chem. Int. Ed.* **52**, 7532-7535, (2013).
62 Hamilton, J. Y., Sarlah, D. & Carreira, E. M. Iridium-Catalyzed Enantioselective Allylic Vinylation. *J. Am. Chem. Soc* **135**, 994-997, (2013).
63 Rossler, S. L., Krautwald, S. & Carreira, E. M. Study of Intermediates in Iridium-(Phosphoramidite,Olefin)-Catalyzed Enantioselective Allylic Substitution. *J. Am. Chem. Soc.* **139**, 3603-3606, (2017).
64 Zhan, M. *et al.* Silver-Assisted, Iridium-Catalyzed Allylation of Bis[(pinacolato)boryl]methane Allows the Synthesis of Enantioenriched Homoallylic Organoboronic Esters. *ACS Catal.* **6**, 3381-3386, (2016).
65 Shido, Y., Yoshida, M., Tanabe, M., Ohmiya, H. & Sawamura, M. Copper-Catalyzed Enantioselective Allylic Substitution with Alkylboranes. *J. Am. Chem. Soc.* **134**, 18573-18576, (2012).
66 Hojoh, K., Shido, Y., Ohmiya, H. & Sawamura, M. Copper-Catalyzed Enantioselective Intramolecular Alkylboron Allylic Alkylation Copper - Catalyzed Enantioselective Intramolecular Alkylboron Allylic Alkylation. *Chem. Lett.* **47**, 632-635, (2018).
67 Shintani, R., Takatsu, K., Takeda, M. & Hayashi, T. Copper-catalyzed asymmetric allylic substitution of allyl phosphates with aryl- and alkenylboronates. *Angew. Chem. Int. Ed.* **50**, 8656-8659, (2011).
68 Gao, F., Carr, J. L. & Hoveyda, A. H. Copper-catalyzed enantioselective allylic substitution with readily accessible carbonyl- and acetal-containing vinylboron reagents. *Angew. Chem. Int. Ed.* **51**, 6613-6617, (2012).
69 Jung, B. & Hoveyda, A. H. Site- and enantioselective formation of allene-bearing tertiary or quaternary carbon stereogenic centers through NHC-Cu-catalyzed allylic substitution. *J. Am. Chem. Soc.* **134**, 1490-1493, (2012).
70 Takeda, M., Takatsu, K., Shintani, R. & Hayashi, T. Synthesis of Quaternary Carbon Stereocenters by Copper-Catalyzed Asymmetric Allylic Substitution of Allyl Phosphates with Arylboronates. *J. Org. Chem.* **79**, 2354-2367, (2014).
71 Shi, Y. & Hoveyda, A. H. Catalytic SN2′- and Enantioselective Allylic Substitution with a Diborylmethane Reagent and Application in Synthesis. *Angew. Chem. Int. Ed.***55**, 3455-3458, (2016).
72 Jiang, S.-P. *et al.* Copper-Catalyzed Enantioconvergent Radical Suzuki–Miyaura C(sp3)–C(sp2) Cross-Coupling. *J. Am. Chem. Soc.* **142**, 19652-19659, (2020).
73 Iwamoto, T., Okuzono, C., Adak, L., Jin, M. & Nakamura, M. Iron-catalysed enantioselective Suzuki-Miyaura coupling of racemic alkyl bromides. *Chem. Commun.* **55**, 1128-1131, (2019).

74 Tyrol, C. C., Yone, N. S., Gallin, C. F. & Byers, J. A. Iron-catalysed enantioconvergent Suzuki–Miyaura cross-coupling to afford enantioenriched 1,1-diarylalkanes. *Chem. Commun.* **56**, 14661-14664, (2020).
75 Huang, W., Wan, X. & Shen, Q. Cobalt-Catalyzed Asymmetric Cross-Coupling Reaction of Fluorinated Secondary Benzyl Bromides with Lithium Aryl Boronates/ZnBr2. *Org. Lett.* **22**, 4327-4332, (2020).
76 Veber, D. F. *et al.* Molecular Properties That Influence the Oral Bioavailability of Drug Candidates. *J. Med. Chem.* **45**, 2615-2623, (2002).
77 Hayashi, T., Takahashi, M., Takaya, Y. & Ogasawara, M. Catalytic Cycle of Rhodium-Catalyzed Asymmetric 1,4-Addition of Organoboronic Acids. Arylrhodium, Oxa-π-allylrhodium, and Hydroxorhodium Intermediates. *J. Am. Chem. Soc.* **124**, 5052-5058, (2002).
78 Kina, A., Iwamura, H. & Hayashi, T. A Kinetic Study on Rh/Binap-Catalyzed 1,4-Addition of Phenylboronic Acid to Enones: Negative Nonlinear Effect Caused by Predominant Homochiral Dimer Contribution. *J. Am. Chem. Soc.* **128**, 3904-3905, (2006).
79 Bhat, V., Welin, E. R., Guo, X. & Stoltz, B. M. Advances in Stereoconvergent Catalysis from 2005 to 2015: Transition-Metal-Mediated Stereoablative Reactions, Dynamic Kinetic Resolutions, and Dynamic Kinetic Asymmetric Transformations. *Chem. Rev.* **117**, 4528-4561, (2017).
80 Pfaltz, A. L., M.; Jacobsen, E. N.; Pfaltz, A.; Yamamoto, H. *Comprehensive Asymmetric Catalysis.*, Vol. 2 (Springer, 1999).
81 Trost, B. M. & Thaisrivongs, D. A. Palladium-Catalyzed Regio-, Diastereo-, and Enantioselective Benzylic Allylation of 2-Substituted Pyridines. *J. Am. Chem. Soc.***131**, 12056-12057, (2009).
82 Xu, W.-B., Ghorai, S., Huang, W. & Li, C. Rh(I)/Bisoxazolinephosphine-Catalyzed Regio- and Enantioselective Allylic Substitutions. *ACS Catal.* **10**, 4491-4496, (2020).
83 You, H., Rideau, E., Sidera, M. & Fletcher, S. P. Non-stabilized nucleophiles in Cu-catalysed dynamic kinetic asymmetric allylic alkylation. *Nature* **517**, 351-355, (2015).
84 Rideau, E., You, H., Sidera, M., Claridge, T. D. W. & Fletcher, S. P. Mechanistic Studies on a Cu-Catalyzed Asymmetric Allylic Alkylation with Cyclic Racemic Starting Materials. *J. Am. Chem. Soc.***139**, 5614-5624, (2017).
85 Langlois, J.-B., Emery, D., Mareda, J. & Alexakis, A. Mechanistic identification and improvement of a direct enantioconvergent transformation in copper-catalyzed asymmetric allylic alkylation. *Chem. Sci.* **3**, 1062-1069, (2012).
86 Ito, H., Kunii, S. & Sawamura, M. Direct enantio-convergent transformation of racemic substrates without racemization or symmetrization. *Nat. Chem.* **2**, 972-976, (2010).
87 Turnbull, B. W. H. & Evans, P. A. Asymmetric Rhodium-Catalyzed Allylic Substitution Reactions: Discovery, Development and Applications to Target-Directed Synthesis. *J. Org. Chem.* **83**, 11463-11479, (2018).
88 Tsui, G. C., Menard, F. & Lautens, M. Regioselective Rhodium(I)-Catalyzed Hydroarylation of Protected Allylic Amines with Arylboronic Acids. *Org. Lett.* **12**, 2456-2459, (2010).
89 Yang, Q., Wang, Y., Luo, S. & Wang, J. Kinetic Resolution and Dynamic Kinetic Resolution of Chromene via Rh-Catalyzed Asymmetric Hydroarylation. *Angew. Chem. Int. Ed.*, (2019).
90 Yang, X.-H. *et al.* Catalytic Hydrothiolation: Counterion-Controlled Regioselectivity. *J. Am. Chem. Soc.* **141**, 3006-3013, (2019).
91 Meißner, A. *et al.* In Situ Synthesis of Neutral Dinuclear Rhodium Diphosphine Complexes [{Rh(diphosphine)(μ2-X)}2]: Systematic Investigations. *ChemPlusChem* **80**, 169-180, (2015).

92 Evans, P. A., Oliver, S. & Chae, J. Rhodium-Catalyzed Allylic Substitution with an Acyl Anion Equivalent: Stereospecific Construction of Acyclic Quaternary Carbon Stereogenic Centers. *J. Am. Chem. Soc.* **134**, 19314-19317, (2012).
93 Blackmond, D. G. Kinetic Aspects of Nonlinear Effects in Asymmetric Catalysis. *Acc. Chem. Res.* **33**, 402-411, (2000).
94 Yang, Q., Wang, Y., Luo, S. & Wang, J. Kinetic Resolution and Dynamic Kinetic Resolution of Chromene by Rhodium-Catalyzed Asymmetric Hydroarylation. *Angew. Chem. Int. Ed.* **58**, 5343-5347, (2019).
95 Singleton, D. A. & Thomas, A. A. High-Precision Simultaneous Determination of Multiple Small Kinetic Isotope Effects at Natural Abundance. *J. Am. Chem. Soc.* **117**, 9357-9358, (1995).
96 Frantz, D. E., Singleton, D. A. & Snyder, J. P. 13C Kinetic Isotope Effects for the Addition of Lithium Dibutylcuprate to Cyclohexenone. Reductive Elimination Is Rate-Determining. *J. Am. Chem. Soc.* **119**, 3383-3384, (1997).
97 Li, J. *et al.* Catalytic Asymmetric Cascade Vinylogous Mukaiyama 1,6-Michael/Michael Addition of 2-Silyloxyfurans with Azoalkenes: Direct Approach to Fused Butyrolactones. *J. Am. Chem. Soc.* **137**, 10124-10127, (2015).
98 Colletto, C., Islam, S., Juliá-Hernández, F. & Larrosa, I. Room-Temperature Direct β-Arylation of Thiophenes and Benzo[b]thiophenes and Kinetic Evidence for a Heck-type Pathway. *J. Am. Chem. Soc.* **138**, 1677-1683, (2016).
99 Smith, J. R. *et al.* Enantioselective Rhodium(III)-Catalyzed Markovnikov Hydroboration of Unactivated Terminal Alkenes. *J. Am. Chem. Soc.* **139**, 9148-9151, (2017).
100 Rathbun, C. M. & Johnson, J. B. Rhodium-Catalyzed Acylation with Quinolinyl Ketones: Carbon−Carbon Single Bond Activation as the Turnover-Limiting Step of Catalysis. *J. Am. Chem. Soc.* **133**, 2031-2033, (2011).
101 Moore, J. L., Silvestri, A. P., de Alaniz, J. R., DiRocco, D. A. & Rovis, T. Mechanistic Investigation of the Enantioselective Intramolecular Stetter Reaction: Proton Transfer Is the First Irreversible Step. *Org. Lett.* **13**, 1742-1745, (2011).
102 Lee, D.-H., Kwon, K.-H. & Yi, C. S. Selective Catalytic C–H Alkylation of Alkenes with Alcohols. *Science* **333**, 1613, (2011).
103 Vo, L. K. & Singleton, D. A. Isotope Effects and the Nature of Stereo- and Regioselectivity in Hydroaminations of Vinylarenes Catalyzed by Palladium(II)−Diphosphine Complexes. *Org. Lett.* **6**, 2469-2472, (2004).
104 Roytman, V. A., Karugu, R. W., Hong, Y., Hirschi, J. S. & Vetticatt, M. J. 13C Kinetic Isotope Effects as a Quantitative Probe To Distinguish between Enol and Enamine Mechanisms in Aminocatalysis. *Chem. Eur. J.* **24**, 8098-8102, (2018).
105 Simmons, E. M. & Hartwig, J. F. On the Interpretation of Deuterium Kinetic Isotope Effects in C-H Bond Functionalizations by Transition-Metal Complexes. *Angew. Chem. Int. Ed.* **51**, 3066-3072, (2012).
106 Deb, A., Hazra, A., Peng, Q., Paton, R. S. & Maiti, D. Detailed Mechanistic Studies on Palladium-Catalyzed Selective C–H Olefination with Aliphatic Alkenes: A Significant Influence of Proton Shuttling. *J. Am. Chem. Soc.* **139**, 763-775, (2017).
107 Mekareeya, A. *et al.* Mechanistic Insight into Palladium-Catalyzed Cycloisomerization: A Combined Experimental and Theoretical Study. *J. Am. Chem. Soc.* **139**, 10104-10114, (2017).
108 McDaniel, D. H. & Brown, H. C. An Extended Table of Hammett Substitutent Constants Based on the Ionization of Substituted Benzoic Acids. *J. Org. Chem.* **23**, 420-427, (1958).
109 Corrie, T. J. A., Ball, L. T., Russell, C. A. & Lloyd-Jones, G. C. Au-Catalyzed Biaryl Coupling To Generate 5- to 9-Membered Rings: Turnover-Limiting Reductive Elimination versus π-Complexation. *J. Am. Chem. Soc.* **139**, 245-254, (2017).

110 Shulgin, A. T. & Baker, A. W. Determination of Hammett Sigma Constants by Intramolecular Hydrogen Bonding. *Nature* **182**, 1299-1299, (1958).
111 Tian, P., Dong, H.-Q. & Lin, G.-Q. Rhodium-Catalyzed Asymmetric Arylation. *ACS Catal.* **2**, 95-119, (2012).
112 Lennox, A. J. J. & Lloyd-Jones, G. C. Transmetalation in the Suzuki-Miyaura Coupling: The Fork in the Trail. *Angew. Chem. Int. Ed.* **52**, 7362-7370, (2013).
113 Thomas, A. A. & Denmark, S. E. Pre-transmetalation intermediates in the Suzuki-Miyaura reaction revealed: The missing link. *Science* **352**, 329-332, (2016).
114 Yaman, T. & Harvey, J. N. Suzuki–Miyaura coupling revisited: an integrated computational study. *Faraday Discuss.* **220**, 425-442, (2019).
115 Straker, R. N., Peng, Q., Mekareeya, A., Paton, R. S. & Anderson, E. A. Computational ligand design in enantio- and diastereoselective ynamide [5+2] cycloisomerization. *Nat. Commun.* **7**, 10109, (2016).
116 Pareek, M. & Sunoj, R. B. Energetics of Dynamic Kinetic Asymmetric Transformation in Suzuki-Miyaura Coupling. *ACS Catal*. (2020).
117 Peng, Q., Duarte, F. & Paton, R. S. Computing organic stereoselectivity – from concepts to quantitative calculations and predictions. *Chem. Soc. Rev.* **45**, 6093-6107, (2016).
118 Falivene, L. *et al.* Towards the online computer-aided design of catalytic pockets. *Nat. Chem.* **11**, 872-879, (2019).
119 Blackmond, D. G. Reaction Progress Kinetic Analysis: A Powerful Methodology for Mechanistic Studies of Complex Catalytic Reactions. *Angew. Chem. Int. Ed.* **44**, 4302-4320, (2005).
120 Nielsen, C. D. T. & Burés, J. Visual kinetic analysis. *Chem. Sci.* **10**, 348-353, (2019).
121 Burés, J. A Simple Graphical Method to Determine the Order in Catalyst. *Angew. Chem. Int. Ed.* **55**, 2028-2031, (2016).
122 Karabiyikoglu, S., Brethomé, A. V., Palacin, T., Paton, R. S. & Fletcher, S. P. Enantiomerically enriched tetrahydropyridine allyl chlorides. *Chem. Sci.* **11**, 4125-4130, (2020).
123 Mackenzie, P. B., Whelan, J. & Bosnich, B. Asymmetric synthesis. Mechanism of asymmetric catalytic allylation. *J. Am. Chem. Soc.* **107**, 2046-2054, (1985).
124 Lloyd-Jones, G. C. & Stephen, S. C. Memory Effects in Pd-Catalysed Allylic Alkylation: Stereochemical Labelling through Isotopic Desymmetrization. *Chem. Eur. J.* **4**, 2539-2549, (1998).
125 Lloyd-Jones, G. C. *et al.* Conclusive Evidence for a Retention−Retention Pathway for the Molybdenum-Catalyzed Asymmetric Alkylation. *J. Am. Chem. Soc.* **126**, 702-703, (2004).
126 Madrahimov, S. T. & Hartwig, J. F. Origins of Enantioselectivity during Allylic Substitution Reactions Catalyzed by Metallacyclic Iridium Complexes. *J. Am. Chem. Soc.* **134**, 8136-8147, (2012).
127 Granberg, K. L. & Baeckvall, J. E. Isomerization of (.pi.-allyl)palladium complexes via nucleophilic displacement by palladium(0). A common mechanism in palladium(0)-catalyzed allylic substitution. *J. Am. Chem. Soc.* **114**, 6858-6863, (1992).
128 Büschleb, M. *et al.* Synthetic Strategies toward Natural Products Containing Contiguous Stereogenic Quaternary Carbon Atoms. *Angew. Chem. Int. Ed.* **55**, 4156-4186, (2016).
129 Li, C., Ragab, S. S., Liu, G. & Tang, W. Enantioselective formation of quaternary carbon stereocenters in natural product synthesis: a recent update. *Nat. Prod. Rep.*, (2020).
130 Liu, Y., Han, S.-J., Liu, W.-B. & Stoltz, B. M. Catalytic Enantioselective Construction of Quaternary Stereocenters: Assembly of Key Building Blocks for the Synthesis of Biologically Active Molecules. *Acc. Chem. Res.* **48**, 740-751, (2015).

131 Quasdorf, K. W. & Overman, L. E. Catalytic enantioselective synthesis of quaternary carbon stereocentres. *Nature* **516**, 181-191, (2014).
132 Das, J. P. & Marek, I. Enantioselective synthesis of all-carbon quaternary stereogenic centers in acyclic systems. *Chem. Commun.* **47**, 4593, (2011).
133 Regueira, J. L. L. F., Silva, L. F. & Pilli, R. A. Total Synthesis of (+)-Raputindole A: An Iridium-Catalyzed Cyclization Approach. *Org. Lett.* **22**, 6262-6266, (2020).
134 Jacques, R., Hell, A. M. L., Pullin, R. D. C. & Fletcher, S. P. Desymmetrization of meso-bisphosphates via rhodium catalyzed asymmetric allylic arylation. *Tetrahedron* **75**, 130560, (2019).
135 Douglas, C. J. & Overman, L. E. Catalytic asymmetric synthesis of all-carbon quaternary stereocenters. *Proceedings of the National Academy of Sciences of the United States of America* **101**, 5363, (2004).
136 Schafroth, M. A., Sarlah, D., Krautwald, S. & Carreira, E. M. Iridium-Catalyzed Enantioselective Polyene Cyclization. *J. Am. Chem. Soc.* **134**, 20276-20278, (2012).
137 Jeker, O. F., Kravina, A. G. & Carreira, E. M. Total Synthesis of (+)-Asperolide C by Iridium-Catalyzed Enantioselective Polyene Cyclization. *Angew. Chem. Int. Ed.* **52**, 12166-12169, (2013).
138 Sidera, M., Roth, P. M. C., Maksymowicz, R. M. & Fletcher, S. P. Formation of Quaternary Centers by Copper-Catalyzed Asymmetric Conjugate Addition of Alkylzirconium Reagents. *Angew. Chem. Int. Ed.* **52**, 7995-7999, (2013).
139 Ardkhean, R., Mortimore, M., Paton, R. S. & Fletcher, S. P. Formation of quaternary centres by copper catalysed asymmetric conjugate addition to β-substituted cyclopentenones with the aid of a quantitative structure–selectivity relationship. *Chem. Sci.* **9**, 2628-2632, (2018).
140 Müller, D. & Alexakis, A. Formation of Quaternary Stereogenic Centers by Copper-Catalyzed Asymmetric Conjugate Addition Reactions of Alkenylaluminums to Trisubstituted Enones. *Chem. Eur. J.***19**, 15226-15239, (2013).
141 Holder, J. C. *et al.* Mechanism and Enantioselectivity in Palladium-Catalyzed Conjugate Addition of Arylboronic Acids to β-Substituted Cyclic Enones: Insights from Computation and Experiment. *J. Am. Chem. Soc.* **135**, 14996-15007, (2013).
142 Shintani, R., Tsutsumi, Y., Nagaosa, M., Nishimura, T. & Hayashi, T. Sodium Tetraarylborates as Effective Nucleophiles in Rhodium/Diene-Catalyzed 1,4-Addition to β,β-Disubstituted α,β-Unsaturated Ketones: Catalytic Asymmetric Construction of Quaternary Carbon Stereocenters. *J. Am. Chem. Soc.* **131**, 13588-13589, (2009).
143 Lu, Z. & Ma, S. Metal-Catalyzed Enantioselective Allylation in Asymmetric Synthesis. *Angew. Chem. Int. Ed.* **47**, 258-297, (2008).
144 Jiang, R., Ding, L., Zheng, C. & You, S.-L. Iridium-catalyzed Z-retentive asymmetric allylic substitution reactions. *Science* **371**, 380, (2021).
145 Trost, B. M. & Schroeder, G. M. Palladium-Catalyzed Asymmetric Alkylation of Ketone Enolates. *J. Am. Chem. Soc.* **121**, 6759-6760, (1999).
146 Trost, B. M., Schroeder, G. M. & Kristensen, J. Palladium-Catalyzed Asymmetric Allylic Alkylation of α-Aryl Ketones. *Angew. Chem. Int. Ed.* **41**, 3492-3495, (2002).
147 Hong, A. Y. & Stoltz, B. M. The Construction of All-Carbon Quaternary Stereocenters by Use of Pd-Catalyzed Asymmetric Allylic Alkylation Reactions in Total Synthesis. *Eur. J. Org. Chem.* **2013**, 2745-2759, (2013).
148 Trost, B. M. & Crawley, M. L. Asymmetric Transition-Metal-Catalyzed Allylic Alkylations: Applications in Total Synthesis. *Chem. Rev.* **103**, 2921-2944, (2003).
149 Liao, X., Stanley, L. M. & Hartwig, J. F. Enantioselective Total Syntheses of (−)-Taiwaniaquinone H and (−)-Taiwaniaquinol B by Iridium-Catalyzed Borylation and Palladium-Catalyzed Asymmetric α-Arylation. *J. Am. Chem. Soc.* **133**, 2088-2091, (2011).

150 Rao, X. *et al.* Efficient Synthesis of (−)-Corynoline by Enantioselective Palladium-Catalyzed α-Arylation with Sterically Hindered Substrates. *Angew. Chem. Int. Ed.* **57**, 12328-12332, (2018).
151 Wang, J., Boyarskikh, V. & Rainier, J. D. Vinyl Diazophosphonates as Precursors to Quaternary Substituted Indolines and Cyclopentenes. *Org. Lett.* **13**, 700-702, (2011).
152 Chen, Z.-S., Huang, X.-Y., Gao, J.-M. & Ji, K. Relay Rh(II)/Pd(0) Dual Catalysis: Selective Construction of Cyclic All-Quaternary Carbon Centers. *Org. Lett.* **18**, 5876-5879, (2016).
153 Davies, H. M. L. & Beckwith, R. E. J. Catalytic Enantioselective C−H Activation by Means of Metal−Carbenoid-Induced C−H Insertion. *Chem. Rev.* **103**, 2861-2904, (2003).
154 Gonzalez, J., van Dijk, L., Goetzke, F. W. & Fletcher, S. P. Highly enantioselective rhodium-catalyzed cross-coupling of boronic acids and racemic allyl halides. *Nat Protoc* **14**, 2972-2985, (2019).
155 Kagan, H. B. Various aspects of the reaction of a chiral catalyst or reagent with a racemic or enantiopure substrate. *Tetrahedron* **57**, 2449-2468, (2001).
156 Lauer, A. M., Mahmud, F. & Wu, J. Cu(I)-Catalyzed, α-Selective, Allylic Alkylation Reactions between Phosphorothioate Esters and Organomagnesium Reagents. *J. Am. Chem. Soc.* **133**, 9119-9123, (2011).
157 Breit, B., Demel, P. & Studte, C. Stereospecific and Stereodivergent Construction of Quaternary Carbon Centers through Switchable Directed/Nondirected Allylic Substitution. *Angew. Chem. Int. Ed.* **43**, 3786-3789, (2004).
158 Webster, R., Boeing, C. & Lautens, M. Reagent-Controlled Regiodivergent Resolution of Unsymmetrical Oxabicyclic Alkenes Using a Cationic Rhodium Catalyst. *J. Am. Chem. Soc.* **131**, 444-445, (2009).
159 St. John, P., Guan, Y., Kim, Y., Kim, S. & Paton, R. *Prediction of Homolytic Bond Dissociation Enthalpies for Organic Molecules at near Chemical Accuracy with Sub-Second Computational Cost Nat. Commun.* **11**, 2328-2339, (2019).
160 Yale, H. L. The Trifluoromethyl Group in Medical Chemistry. *J. Med. Chem.***1**, 121-133, (1959).
161 Rideau, E. & Fletcher, S. P. Copper-catalysed asymmetric allylic alkylation of alkylzirconocenes to racemic 3,6-dihydro-2 H -pyrans. *Beilstein J. Org. Chem.* **11**, 2435-2443, (2015).
162 Eames, J. Parallel Kinetic Resolutions. *Angew. Chem. Int. Ed.* **39**, 885-888, (2000).
163 Miller, L. C. & Sarpong, R. Divergent reactions on racemic mixtures. *Chem. Soc. Rev.* **40**, 4550-4562, (2011).
164 Doyle, M. P. *et al.* Highly selective enantiomer differentiation in intramolecular cyclopropanation reactions of racemic secondary allylic diazoacetates. *J. Am. Chem. Soc.* **117**, 11021-11022, (1995).
165 Funken, N., Zhang, Y.-Q. & Gansäuer, A. Regiodivergent Catalysis: A Powerful Tool for Selective Catalysis. *Chem. Eur. J.* **23**, 19-32, (2017).
166 Kamlet, A. S., Préville, C., Farley, K. A. & Piotrowski, D. W. Regioselective Hydroarylations and Parallel Kinetic Resolution of Vince Lactam. *Angew. Chem. Int. Ed.* **52**, 10607-10610, (2013).
167 Wu, B., Parquette, J. R. & RajanBabu, T. V. Regiodivergent Ring Opening of Chiral Aziridines. *Science* **326**, 1662, (2009).
168 Yang, H. & Zheng, W.-H. Parallel Kinetic Resolution of Unsymmetrical Acyclic Aliphatic syn-1,3-Diols. *Org. Lett.* **21**, 5197-5200, (2019).
169 Lee, T., Wilson, T. W., Berg, R., Ryberg, P. & Hartwig, J. F. Rhodium-Catalyzed Enantioselective Silylation of Arene C–H Bonds: Desymmetrization of Diarylmethanols. *J. Am. Chem. Soc.* **137**, 6742-6745, (2015).

170 Noyori, R. & Hashiguchi, S. Asymmetric Transfer Hydrogenation Catalyzed by Chiral Ruthenium Complexes. *Acc. Chem. Res.* **30**, 97-102, (1997).
171 Shende, V. S., Singh, P. & Bhanage, B. M. Recent trends in organocatalyzed asymmetric reduction of prochiral ketones. *Catal. Sci. Technol.* **8**, 955-969, (2018).
172 Chen, B.-S. & Ribeiro de Souza, F. Z. Enzymatic synthesis of enantiopure alcohols: current state and perspectives. *RSC Advances* **9**, 2102-2115, (2019).
173 ter Halle, R. *et al.* Development of a Practical Multikilogram Production of (R)-Seudenol by Enzymatic Resolution. *Org. Process Res. Dev.* **8**, 283-286, (2004).
174 Wang, X.-T., Han, W.-B., Chen, H.-J., Zha, Q. & Wu, Y. Regio- and Stereoselective Addition of HO/OOH to Allylic Alcohols. *J. Org. Chem.* **85**, 10007-10021, (2020).
175 Ohmiya, H., Yokokawa, N. & Sawamura, M. Copper-Catalyzed γ-Selective and Stereospecific Allyl−Aryl Coupling between (Z)-Acyclic and Cyclic Allylic Phosphates and Arylboronates. *Org. Lett.* **12**, 2438-2440, (2010).
176 Webster, R., Boyer, A., Fleming, M. J. & Lautens, M. Practical Asymmetric Synthesis of Bioactive Aminotetralins from a Racemic Precursor Using a Regiodivergent Resolution. *Org. Lett.* **12**, 5418-5421, (2010).
177 Xu, Y., Kaneko, K., Kanai, M., Shibasaki, M. & Matsunaga, S. Regiodivergent Kinetic Resolution of Terminal and Internal rac-Aziridines with Malonates under Dinuclear Schiff Base Catalysis. *J. Am. Chem. Soc.* **136**, 9190-9194, (2014).
178 Rodrigo, J. M., Zhao, Y., Hoveyda, A. H. & Snapper, M. L. Regiodivergent Reactions through Catalytic Enantioselective Silylation of Chiral Diols. Synthesis of Sapinofuranone A. *Org. Lett.* **13**, 3778-3781, (2011).
179 Galloway, W. R. J. D., Isidro-Llobet, A. & Spring, D. R. Diversity-oriented synthesis as a tool for the discovery of novel biologically active small molecules. *Nat. Commun.s* **1**, 80, (2010).
180 Goel, P. *et al.* Recent advancement of piperidine moiety in treatment of cancer- A review. *Eur. J. Med. Chem.* **157**, 480-502, (2018).
181 Schmid, M., Grossmann, A. S., Wurst, K. & Magauer, T. Total Synthesis of Salimabromide: A Tetracyclic Polyketide from a Marine Myxobacterium. *J. Am. Chem. Soc.* **140**, 8444-8447, (2018).
182 Kock, M. & Lindel, T. Diastereoselective Total Synthesis of Raputindole A. *Org. Lett.* **20**, 5444-5447, (2018).
183 Lv, J., Wang, B., Yuan, K., Wang, Y. & Jia, Y. Regioselective Direct C-4 Functionalization of Indole: Total Syntheses of (−)-Agroclavine and (−)-Elymoclavine. *Org. Lett.* **19**, 3664-3667, (2017).
184 Evans, P. A. & Uraguchi, D. Regio- and Enantiospecific Rhodium-Catalyzed Arylation of Unsymmetrical Fluorinated Acyclic Allylic Carbonates: Inversion of Absolute Configuration. *J. Am. Chem. Soc.* **125**, 7158-7159, (2003).
185 Bing Yu, F. M., Naohiro Isono, Mark Lautens. Synthesis of Homoallylic Alcohols via Lewis Acid Assisted Enantioselective Desymmetrization. *Synthesis*, 853-859, (2009).
186 Li, C. & Breit, B. Rhodium-Catalyzed Dynamic Kinetic Asymmetric Allylation of Phenols and 2-Hydroxypyridines. *Chem. Eur. J.* **22**, 14655-14663, (2016).
187 Arnold, J. S. & Nguyen, H. M. Rhodium-Catalyzed Dynamic Kinetic Asymmetric Transformations of Racemic Tertiary Allylic Trichloroacetimidates with Anilines. *J. Am. Chem. Soc.* **134**, 8380-8383, (2012).
188 Li, C. *et al.* Pd-catalyzed regioselective and stereospecific Suzuki-Miyaura coupling of allylic carbonates with arylboronic acids. *Org. Lett.* **14**, 390-393, (2012).
189 Khan, S., Shah, B. H., Khan, I., Li, M. & Zhang, Y. J. Pd-Catalyzed regio- and enantioselective allylic substitution with 2-pyridones. *Chem. Commun.* **55**, 13168-13171, (2019).
190 Trost, B. M., Osipov, M. & Dong, G. Palladium-Catalyzed Dynamic Kinetic Asymmetric Transformations of Vinyl Aziridines with Nitrogen Heterocycles: Rapid

Access to Biologically Active Pyrroles and Indoles. *J. Am. Chem. Soc.* **132**, 15800-15807, (2010).
191 Trost, B. M., Bunt, R. C., Lemoine, R. C. & Calkins, T. L. Dynamic Kinetic Asymmetric Transformation of Diene Monoepoxides: A Practical Asymmetric Synthesis of Vinylglycinol, Vigabatrin, and Ethambutol. *J. Am. Chem. Soc.* **122**, 5968-5976, (2000).
192 Fagnou, K. & Lautens, M. Rhodium-Catalyzed Ring Opening of Vinyl Epoxides with Alcohols and Aromatic Amines. *Org. Lett.* **2**, 2319-2321, (2000).
193 Zhang, Q. & Nguyen, H. M. Rhodium-catalyzed regioselective opening of vinyl epoxides with Et3N·3HF reagent-formation of allylic fluorohydrins. *Chem. Sci.* **5**, 291-296, (2014).
194 Wang, M. & Lu, P. Catalytic approaches to assemble cyclobutane motifs in natural product synthesis. *Organic Chemistry Frontiers* **5**, 254-259, (2018).
195 Dembitsky, V. M. Bioactive cyclobutane-containing alkaloids. *J. Nat. Med.* **62**, 1-33, (2008).
196 Carreira, E. M. & Fessard, T. C. Four-Membered Ring-Containing Spirocycles: Synthetic Strategies and Opportunities. *Chem. Rev.* **114**, 8257-8322, (2014).
197 Seiser, T., Saget, T., Tran, D. N. & Cramer, N. Cyclobutanes in Catalysis. *Angew. Chem. Int. Ed.* **50**, 7740-7752, (2011).
198 Namyslo, J. C. & Kaufmann, D. E. The Application of Cyclobutane Derivatives in Organic Synthesis. *Chem. Rev.* **103**, 1485-1538, (2003).
199 Poplata, S., Tröster, A., Zou, Y.-Q. & Bach, T. Recent Advances in the Synthesis of Cyclobutanes by Olefin [2 + 2] Photocycloaddition Reactions. *Chem. Rev.* **116**, 9748-9815, (2016).
200 Xu, Y., Conner, M. L. & Brown, M. K. Cyclobutane and Cyclobutene Synthesis: Catalytic Enantioselective [2+2] Cycloadditions. *Angew. Chem. Int. Ed.* **54**, 11918-11928, (2015).
201 Lee-Ruff, E. & Mladenova, G. Enantiomerically Pure Cyclobutane Derivatives and Their Use in Organic Synthesis. *Chem. Rev.* **103**, 1449-1484, (2003).
202 Meyers, A. I. & Fleming, S. A. Efficient asymmetric (2 + 2) photocycloaddition leading to chiral cyclobutanes. Application to the total synthesis of (-)-grandisol. *J. Am. Chem. Soc.* **108**, 306-307, (1986).
203 Han, Y. T. *et al.* A versatile synthetic approach to grandisol monoterpene pheromone. *Arch. Pharmacal Res.* **34**, 1437, (2011).
204 Pagar, V. V. & RajanBabu, T. V. Tandem catalysis for asymmetric coupling of ethylene and enynes to functionalized cyclobutanes. *Science* **361**, 68-72, (2018).
205 Brimioulle, R. & Bach, T. Enantioselective Lewis acid catalysis of intramolecular enone [2+2] photocycloaddition reactions. *Science* **342**, 840-843, (2013).
206 García-Morales, C. *et al.* Enantioselective synthesis of cyclobutenes by intermolecular [2+2] cycloaddition with non-c2 symmetric digold catalysts. *J. Am. Chem. Soc.* **139**, 13628-13631, (2017).
207 Du, J., Skubi, K. L., Schultz, D. M. & Yoon, T. P. A Dual-Catalysis Approach to Enantioselective [2 + 2] Photocycloadditions Using Visible Light. *Science* **344**, 392, (2014).
208 Wang, Y.-M., Bruno, N. C., Placeres, Á. L., Zhu, S. & Buchwald, S. L. Enantioselective Synthesis of Carbo- and Heterocycles through a CuH-Catalyzed Hydroalkylation Approach. *J. Am. Chem. Soc.* **137**, 10524-10527, (2015).
209 Kim, D. K., Riedel, J., Kim, R. S. & Dong, V. M. Cobalt Catalysis for Enantioselective Cyclobutanone Construction. *J. Am. Chem. Soc.* **139**, 10208-10211, (2017).
210 Zhong, C. *et al.* Enantioselective Synthesis of 3-Substituted Cyclobutenes by Catalytic Conjugate Addition/Trapping Strategies. *Angew. Chem. Int. Ed.*, 1-6, (2020).

211 Chen, Y. J., Hu, T. J., Feng, C. G. & Lin, G. Q. Synthesis of chiral cyclobutanes via rhodium/diene-catalyzed asymmetric 1,4-addition: A dramatic ligand effect on the diastereoselectivity. *Chem. Commun.* **51**, 8773-8776, (2015).
212 Audisio, D. *et al.* Palladium-Catalyzed Allylic Substitution at Four-Membered-Ring Systems: Formation of η1-Allyl Complexes and Electrocyclic Ring Opening. *Angew. Chem. Int. Ed.* **52**, 6313-6316, (2013).
213 Xiao, K.-J. *et al.* Palladium(II)-Catalyzed Enantioselective C(sp3)–H Activation Using a Chiral Hydroxamic Acid Ligand. *J. Am. Chem. Soc.* **136**, 8138-8142, (2014).
214 Guisán-Ceinos, M., Parra, A., Martín-Heras, V. & Tortosa, M. Enantioselective Synthesis of Cyclobutylboronates via a Copper-Catalyzed Desymmetrization Approach. *Angew. Chem. Int. Ed.* **55**, 6969-6972, (2016).
215 Feng, S., Hao, H., Liu, P. & Buchwald, S. L. Diastereo- and Enantioselective CuH-Catalyzed Hydroamination of Strained Trisubstituted Alkenes. *ACS Catal.* **10**, 282-291, (2020).
216 Roy, S. R., Eijsberg, H., Bruffaerts, J. & Marek, I. Zirconocene catalyzed diastereoselective carbometalation of cyclobutenes. *Chem. Sci.* **8**, 334-339, (2016).
217 Dian, L. & Marek, I. Rhodium-Catalyzed Arylation of Cyclopropenes Based on Asymmetric Direct Functionalization of Three-Membered Carbocycles. *Angew. Chem. Int. Ed.* **57**, 3682-3686, (2018).
218 Menard, F. & Lautens, M. Chemodivergence in enantioselective desymmetrization of diazabicycles: Ring-opening versus reductive arylation. *Angew. Chem. Int. Ed.* **47**, 2085-2088, (2008).
219 Bexrud, J. & Lautens, M. A rhodium IBiox[(-)-menthyl] complex as a highly selective catalyst for the asymmetric hydroarylation of azabicyles: An alternative route to epibatidine. *Org. Lett.* **12**, 3160-3163, (2010).
220 Wiberg, K. B. The Concept of Strain in Organic Chemistry. *Angew. Chem. Int. Ed.* **25**, 312-322, (1986).
221 So, C. M., Kume, S. & Hayashi, T. Rhodium-Catalyzed Asymmetric Hydroarylation of 3-Pyrrolines Giving 3-Arylpyrrolidines: Protonation as a Key Step. *J. Am. Chem. Soc.* **135**, 10990-10993, (2013).
222 Sommer, H., Juliá-Hernández, F., Martin, R. & Marek, I. Walking Metals for Remote Functionalization. *ACS Cent. Sci.*, (2018).
223 Zheng, Y., Tice, C. M. & Singh, S. B. The use of spirocyclic scaffolds in drug discovery. *Bioorg. Med. Chem. Lett.* **24**, 3673-3682, (2014).
224 Bassindale, M. J., Hamley, P. & Harrity, J. P. A. Employment of a cyclobutene ring-opening metathesis reaction towards a concise synthesis of (±)-sporochnol A. *Tetrahedron Lett.* **42**, 9055-9057, (2001).
225 Buter, J., Moezelaar, R. & Minnaard, A. J. Enantioselective palladium catalyzed conjugate additions of ortho-substituted arylboronic acids to β,β-disubstituted cyclic enones: Total synthesis of herbertenediol, enokipodin A and enokipodin B. *Org. Biomol. Chem.***12**, 5883-5890, (2014).
226 Meyers, M. J. *et al.* Discovery of novel spirocyclic inhibitors of fatty acid amide hydrolase (FAAH). Part 2. Discovery of 7-azaspiro[3.5]nonane urea PF-04862853, an orally efficacious inhibitor of fatty acid amide hydrolase (FAAH) for pain. *Bioorg. Med. Chem. Lett.* **21**, 6545-6553, (2011).
227 Wortley, M. A. *et al.* Targeting fatty acid amide hydrolase as a therapeutic strategy for antitussive therapy. *Eur. Respir. J.* **50**, (2017).
228 Oguma, K., Miura, M., Satoh, T. & Nomura, M. Merry-go-round multiple alkylation on aromatic rings via rhodium catalysis. *J. Am. Chem. Soc.***122**, 10464-10465, (2000).
229 Antermite, D., Degennaro, L. & Luisi, R. Recent advances in the chemistry of metallated azetidines. *Org. Biomol. Chem.* **15**, 34-50, (2017).

230 Didier, D., Baumann, A. N. & Eisold, M. Unsaturated four-membered N-heterocycles: From synthesis to applications. *Tetrahedron Lett.* **59**, 3975-3987, (2018).
231 Fawcett, A., Murtaza, A., Gregson, C. H. U. & Aggarwal, V. K. Strain-Release-Driven Homologation of Boronic Esters: Application to the Modular Synthesis of Azetidines. *J. Am. Chem. Soc.***141**, 4573-4578, (2019).
232 Gianatassio, R. *et al.* Strain-release amination. *Science* **351**, 241, (2016).
233 Han, S. & Zard, S. Z. Modular Approach to Substituted Boc-Protected 4-(Aminomethyl)pyrroles. *Org. Lett.* **16**, 1992-1995, (2014).
234 Bosset, C. *et al.* Minisci-Photoredox-Mediated α-Heteroarylation of N-Protected Secondary Amines: Remarkable Selectivity of Azetidines. *Org. Lett.* **20**, 6003-6006, (2018).
235 Burkhard, J. A., Wuitschik, G., Rogers-Evans, M., Müller, K. & Carreira, E. M. Oxetanes as Versatile Elements in Drug Discovery and Synthesis. *Angew. Chem. Int. Ed.* **49**, 9052-9067, (2010).
236 Wuitschik, G. *et al.* Oxetanes in Drug Discovery: Structural and Synthetic Insights. *J. Med. Chem.* **53**, 3227-3246, (2010).
237 Dean, C. *et al.* Synthesis of sp3-rich chemical libraries based upon 1,2-diazetidines. *Tetrahedron* **79**, 131836, (2021).
238 Yang, J., Wu, B. & Hu, L. A General and Practical Synthesis of Chiral 1,2-Oxazetidines. *Asian J. Org. Chem.* **9**, 197-201, (2020).
239 Kwan, E. E., Park, Y., Besser, H. A., Anderson, T. L. & Jacobsen, E. N. Sensitive and Accurate 13C Kinetic Isotope Effect Measurements Enabled by Polarization Transfer. *J. Am. Chem. Soc.***139**, 43-46, (2017).
240 Katcher, M. H. & Doyle, A. G. Palladium-Catalyzed Asymmetric Synthesis of Allylic Fluorides. *J. Am. Chem. Soc.* **132**, 17402-17404, (2010).
241 Chai, J.-D. & Head-Gordon, M. Long-range corrected hybrid density functionals with damped atom–atom dispersion corrections. *Phys. Chem. Chem.***10**, 6615-6620, (2008).
242 Hay, P. J. & Wadt, W. R. Ab initio effective core potentials for molecular calculations. Potentials for the transition metal atoms Sc to Hg. *J. Chem. Phys.* **82**, 270-283, (1985).
243 Roy, L. E., Hay, P. J. & Martin, R. L. Revised Basis Sets for the LANL Effective Core Potentials. *J. Chem. Theory Comput.* **4**, 1029-1031, (2008).
244 Xu, W., Zhou, Y., Wang, R., Wu, G. & Chen, P. Lithium amidoborane, a highly chemoselective reagent for the reduction of α,β-unsaturated ketones to allylic alcohols. *Org. Biomol. Chem.* **10**, 367-371, (2012).
245 Prakash, G. K. S., Tongco, E. C., Mathew, T., Vankar, Y. D. & Olah, G. A. Preparation of 3-trifluoromethyl-2-cycloalkenones by the oxidative rearrangement of trifluoromethylated tertiary allylic alcohols with pyridinium chlorochromate. *J. Fluorine Chem.* **101**, 199-202, (2000).
246 Brown, M. K., Degrado, S. J. & Hoveyda, A. H. Highly Enantioselective Cu-Catalyzed Conjugate Additions of Dialkylzinc Reagents to Unsaturated Furanones and Pyranones: Preparation of Air-Stable and Catalytically Active Cu–Peptide Complexes. *Angew. Chem. Int. Ed.* **44**, 5306-5310, (2005).
247 Carrillo-Marquez, T. *et al.* New routes to β-cycloalkylalanine derivatives using serine-derived organozinc reagents. *Org. Biomol. Chem.***3**, 4117-4123, (2005).
248 Grimme, S. Supramolecular Binding Thermodynamics by Dispersion-Corrected Density Functional Theory. *Chem. Eur. J.* **18**, 9955-9964, (2012).